

**Structural and functional
analyses of the QacA
multidrug resistance efflux
protein from
*Staphylococcus aureus***

By

Abolfazl Dashtbani-Roozbehani

Thesis

Submitted to Flinders University

for the degree of

Doctor of Philosophy

College of Science and Engineering

October 2021

TABLE OF CONTENTS

TABLE OF CONTENTS	i
LIST OF FIGURES	vi
LIST OF TABLES	ix
THESIS SUMMARY	x
DECLARATION	xii
ACKNOWLEDGEMENTS	xiii
CHAPTER 1 INTRODUCTION	1
1.1 Antimicrobial resistance in bacteria: A worldwide crisis.....	2
1.2 Infections caused by <i>Staphylococcus aureus</i> : A growing public health problem	4
1.3 Development and dissemination of multidrug resistance in <i>S. aureus</i>	4
1.4 Molecular mechanisms of antimicrobial resistance in <i>S. aureus</i>	6
1.5 Efflux mediated antimicrobial resistance in <i>S. aureus</i> : clinical implications	8
1.6 Classification of bacterial efflux pumps.....	10
1.7 Prototypical characterised efflux pumps in <i>S. aureus</i>	13
1.8 The major facilitator superfamily	17
1.8.1 Major structural features of MFS transporters.....	18
1.8.1.1 Conservation of structures across MFS transporters.....	18
1.8.1.2 Evolutionary conserved motifs in MFS.....	22
1.8.2 Transport mechanisms in MFS transporters.....	24
1.8.3 MdfA: a paradigm of 12 TMS multidrug-sensing MFS antiporters	27
1.9 Key MFS efflux pumps in antimicrobial resistance of <i>S. aureus</i>	29
1.9.1 NorA, NorB and NorC efflux proteins.....	29
1.9.2 TetA(K) and Tet38 efflux pumps.....	31
1.9.3 QacA multidrug efflux protein.....	32
1.9.3.1 Structure-function properties of QacA.....	34
1.9.3.2 Substrate profile of QacA.....	37
1.9.3.3 Regulation of <i>qacA</i> expression.....	40
1.9.3.4 Prevalence of <i>qacA</i> in clinical isolates of <i>S. aureus</i>	41
1.9.3.5 QacB.....	42
1.10 QacC: Another important member of Qac efflux system in <i>S. aureus</i>	43
1.11 MepA: The only MATE efflux system encoded on the <i>S. aureus</i> chromosome.....	44

1.12	The role of <i>S. aureus</i> efflux pumps in biocide resistance	45
1.13	Cross-resistance of biocides and antibiotics mediated by multidrug efflux pumps	48
1.14	Modulation (inhibition) of <i>S. aureus</i> efflux pumps	49
1.15	Scope of this thesis	50
CHAPTER 2 MATERIALS AND METHODS.....		53
2.1	Chemicals, solutions and buffers.....	54
2.2	Bacterial strains and plasmids	54
2.3	Bacterial culture media, growth conditions and storage.....	54
2.4	Transformation of <i>E. coli</i>	62
2.4.1	Preparation of chemically competent <i>E. coli</i> cells	62
2.4.2	Transformation of competent <i>E. coli</i> cells	62
2.5	DNA procedures.....	63
2.5.1	Small-scale purification of plasmid DNA.....	63
2.5.2	Restriction endonuclease digestion	64
2.5.3	Agarose gel electrophoresis	64
2.5.4	Purification of DNA fragments from agarose gel slices.....	65
2.5.5	DNA sequencing	65
2.6	Recombinant DNA procedures	66
2.6.1	Polymerase chain reaction	66
2.6.2	Site-directed mutagenesis.....	66
2.6.3	DNA ligation.....	70
2.7	Protein overexpression and purification	70
2.7.1	Overexpression of QacA and TetA(K) from pBAD-based vectors	70
2.7.2	Preparation of membrane vesicles	71
2.7.3	Purification of His-tagged QacA/TetA(K) proteins by affinity chromatography	71
2.8	Protein detection.....	72
2.8.1	Protein quantification	72
2.8.2	Sodium dodecyl-sulphate polyacrylamide gel electrophoresis	73
2.8.3	Coomassie staining.....	73
2.8.4	Western blot analysis	73
2.8.4.1	Protein transfer to polyvinylidene fluoride membrane.....	73
2.8.4.2	Immunological detection of transferred proteins.....	74
2.9	Fluorescein maleimide reactivity assay.....	74
2.9.1	Effect of substrate preincubation on maleimide reactivity	75
2.10	Minimum inhibitory concentration assay	76
2.11	Whole-cell fluorometric transport assays	76

2.11.1	Effect of maleimide treatment on efflux of ethidium and DAPI	79
2.12	Determination of kinetic parameters of transport.....	79
2.13	Bioinformatic analyses.....	80
2.13.1	Computer software employed	80
2.13.2	Amino acids sequence alignments	80
2.13.3	Homology modelling of the QacA structure	81
2.13.4	Molecular docking	81
Chapter 3	FUNCTIONAL ANALYSIS OF RESIDUES WITHIN AND SURROUNDING TMS 12 OF QACA	84
3.1	Introduction	85
3.2	Results and Discussion.....	88
3.2.1	QacA variants generated by site-directed mutagenesis	88
3.2.2	Expression of QacA mutants	91
3.2.3	Resistance profile of QacA mutants	93
3.2.4	Evaluating the causal role of A157G and A378V mutations in increased chlorhexidine resistance of QacA	96
3.2.5	Ethidium transport activity.....	97
3.2.6	Solvent accessibility profile of residues	102
3.2.7	Assessment of residue conservation in a multiple sequence alignment.....	103
3.3	Conclusions	106
Chapter 4	DETAILED ASSESSMENT OF THE ROLE OF IDENTIFIED QACA RESIDUES CRITICAL IN SUBSTRATE INTERACTIONS	111
4.1	Introduction	112
4.2	Results and Discussion.....	117
4.2.1	DAPI MIC analysis	117
4.2.2	Fluorometric transport assay of DAPI	117
4.2.3	Influence of substrate binding on solvent accessibility	119
4.2.4	Effect of NEM treatment on the efflux of DAPI	123
4.2.5	Determination of kinetics of substrate transport by selected QacA mutants.....	127
4.2.6	Overexpression and purification of QacA and TetA(K) proteins from a pBAD expression vector.....	132
4.2.7	Generation of expression construct for QacA S387C.....	136
4.2.8	Overexpression and purification of QacA S387C mutant protein.....	138
4.3	Conclusions	140

Chapter 5	STRUCTURAL MODELLING OF QACA AND IDENTIFICATION OF PUTATIVE SUBSTRATE-BINDING POCKETS.....	144
5.1	Introduction	145
5.2	Results and discussion	148
5.2.1	Homology modelling	148
5.2.2	QacA orientation in the membrane	152
5.2.3	Hotspot regions in QacA for interaction with chlorhexidine identified from mutagenesis experiments.....	155
5.2.4	Identification of the chlorhexidine binding pocket in QacA by molecular docking in conjunction with mutagenesis data	159
5.2.5	Hotspot regions in QacA that interact with benzalkonium identified from mutagenesis experiments.....	164
5.2.6	Identification of the benzalkonium binding pocket in QacA by molecular docking in conjunction with mutagenesis data	164
5.2.7	Identification of binding pockets in QacA for ethidium, rhodamine 6G, dequalinium, pentamidine and DAPI by molecular docking	170
5.2.8	TMS 7 and TMS 8 constitute a lateral cavity as a second possible binding site for some substrates	173
5.3	Conclusion.....	179
Chapter 6	GENERAL DISCUSSION AND CONCLUSIONS.....	186
6.1	3D model of QacA as a framework for integrating and interpreting mutagenesis data	191
6.2	Helix packing of the QacA transporter	192
6.3	Refinement of QacA topology model	195
6.4	Solvent-accessible surface areas within the QacA central cavity.....	200
6.5	Architecture of the QacA multidrug binding site	204
6.5.1	Comparison of binding sites of QacA with other multidrug-binding proteins	209
6.5.2	Possible structural underpinning for competitive and non-competitive substrate binding in QacA	214
6.6	Functional and structural assessment of identified important residues within and around TMS 12.....	215
6.6.1	G361 as a hinge point for the extracellular loop flanking the TMS 12.....	215
6.6.2	G379 as an intramembrane conserved glycine residue for TMS 12 helical flexibility.....	217
6.6.3	S387 as a kink site in TMS 12.....	218
6.7	Future research: Towards developing QacA inhibitors	219
6.8	Conclusions	222

Chapter 7	APPENDICES.....	224
7.1	Appendix 1 – The nucleotide and amino acid sequence of QacA	225
7.2	Appendix 2 – AutoDock Vina input configuration file used in docking.....	227
7.3	Appendix 3 – Protein expression, resistance profile and ethidium efflux activity of A157G and A378V substitutions.....	228
7.4	Appendix 4 – Ethidium efflux curves of QacA mutants obtained in this study	230
7.5	Appendix 5 – Amino acid sequence alignment of QacA with MFS DHA1 and DHA2 family members	237
7.6	Appendix 6 – QacA topology generated by Protter webserver	241
7.7	Appendix 7 – Codes and chemical properties of the 20 standard amino acids found in proteins.....	242
7.8	Appendix 8 – List of abbreviations	243
7.9	Appendix 9 – Conference contributions and publications	248
CHAPTER 8	REFERENCES.....	250

LIST OF FIGURES

Figure 1.1 Schematic representation of the seven families/superfamilies of multidrug transporters.....	12
Figure 1.2 Canonical structural fold of MFS proteins.	20
Figure 1.3 Schematic diagram of the alternating access mechanism for MFS transporters.....	25
Figure 1.4 Schematic representation of the topology of the QacA protein.	33
Figure 1.5 Substrates of multidrug efflux protein QacA.	38
Figure 3.1 Overview of QacA mutants.	90
Figure 3.2 Western blot analysis of QacA mutants examined in this study.	92
Figure 3.3 Effect of A157G and A378V substitutions on QacA resistance to CH.....	98
Figure 3.4 Representative ethidium efflux curves of wild-type QacA and mutant derivatives.	100
Figure 3.5 Ethidium transport activity of QacA mutants examined in this study.....	101
Figure 3.6 Solvent accessibility profile of QacA residues examined in this study.....	104
Figure 3.7 Refined membrane topology model of TMS 12 of QacA protein based on solvent accessibility results.	105
Figure 3.8 Amino acid sequence alignment of QacA in the region targeted in this study with related MFS DHA1 and DHA2 drug efflux proteins. ...	107
Figure 4.1 DAPI resistance capacity of G361C, G379C and S387C QacA mutants...	118
Figure 4.2 Fluorometric transport assays of DAPI.	120

Figure 4.3 Labelling reactivity of G361C, G379C and S387C QacA mutants with fluorescein maleimide in the presence of selected substrates.	122
Figure 4.4 DAPI transport activity of QacA and selected cysteine mutants in the absence and presence of NEM.	126
Figure 4.5 Michaelis–Menten curves depicting kinetics of substrate transport by wild-type QacA.	128
Figure 4.6 Purification of wild-type QacA protein overexpressed in <i>E. coli</i> TOP10 cells.	134
Figure 4.7 Purification of TetA(K) protein overexpressed in <i>E. coli</i> TOP10 cells.	135
Figure 4.8 Subcloning of QacA mutants into the pBAD vector.	137
Figure 4.9 Purification of QacA S387C mutant protein overexpressed in <i>E. coli</i> TOP10 cells.	139
Figure 5.1 Homology model of QacA showing structural arrangement of the 14 TMS.	151
Figure 5.2 Structural superimposition of modelled QacA against the YePEPT crystal structure.	154
Figure 5.3 Spatial orientation of QacA within the lipid membrane as obtained by PPM modelling.	156
Figure 5.4 Hotspot regions in QacA for interaction with chlorhexidine assigned based on extensive mutagenesis studies.	160
Figure 5.5 Docking of chlorhexidine to QacA.	161
Figure 5.6 Depiction of intermolecular interactions in the binding site of QacA with its substrate chlorhexidine.	163
Figure 5.7 Hotspot regions in QacA for interaction with benzalkonium assigned based on extensive mutagenesis studies.	166

Figure 5.8 Docking of benzalkonium to QacA.....	168
Figure 5.9 Depiction of intermolecular interactions in the binding site of QacA with its substrate benzalkonium.	169
Figure 5.10 Putative substrate-binding sites of QacA for ethidium, rhodamine 6G, dequalinium, pentamidine, and DAPI, identified by molecular docking analysis.....	172
Figure 5.11 Lateral cavity in QacA made up by TMS 7 and TMS 8 as an additional possible substrate-binding site.	177
Figure 6.1 Spatial arrangement of 14 TMS in the inward-open model structure of QacA.....	193
Figure 6.2 QacA embedded into a bilayer membrane.....	197
Figure 6.3 Refined 2D QacA topology model.....	198
Figure 6.4 Solvent-accessible regions in the QacA central cavity.....	202
Figure 6.5 Architecture of the expansive central multidrug-binding pocket of QacA.....	207
Figure 6.6 Structural alignment of QacA homology model and MdfA structure.....	211
Figure 6.7 Spatial orientation of functionally important residues identified within and around TMS 12.....	220

LIST OF TABLES

Table 1.1 Characterised drug efflux pumps in <i>S. aureus</i>	14
Table 1.2 Key findings of amino acid substitutions in QacA reported in previous studies.	35
Table 2.1 Buffers and solutions.....	55
Table 2.2 Bacterial strains used in this study.....	57
Table 2.3 Plasmids used in this study	58
Table 2.4 Primers used in the present study.	67
Table 2.5 Compounds used for MIC analysis	77
Table 3.1 Resistance profile to six representative antimicrobial compounds by <i>E. coli</i> expressing QacA and mutant derivatives	94
Table 4.1 Comparative kinetic data of ethidium resistance-defective mutants	130
Table 4.2 Comparative kinetic data of DAPI resistance-defective mutants	131
Table 5.1 List of the 57 residues important for chlorhexidine resistance as taken from QacA mutational analyses.....	158
Table 5.2 List of the 48 residues important for benzalkonium resistance as taken from QacA mutational analyses.....	165
Table 5.3 Binding energy, number of H-bond and hydrophobic interactions between substrates with QacA predicted by molecular docking.....	174
Table 6.1 Comparison of the predicted extents of TMS regions in QacA.....	196
Table 6.2 Comparison of binding site residues of QacA and MdfA.	212

THESIS SUMMARY

The increasing emergence of multidrug resistant bacteria is a major health threat worldwide. Among the most serious human pathogens is *Staphylococcus aureus*, which is responsible for burgeoning multidrug resistant hospital- or community-acquired infections with significant morbidity and mortality globally. *S. aureus* utilises a number of mechanisms to circumvent the effects of antimicrobials. One of these is the export of antimicrobial agents through the activity of membrane-embedded multidrug efflux pump proteins. QacA is one such protein that mediates resistance to a diverse array of cationic and lipophilic antimicrobial compounds, including many commonly used antiseptics and disinfectants such as benzalkonium and chlorhexidine.

The proton motive force-driven efflux pump QacA belongs to the major facilitator superfamily of transporter proteins. QacA comprises 514 amino acids which are organised into 14 transmembrane-spanning (TMS) regions. Being plasmid-borne allows QacA to rapidly spread among staphylococci in clinical and natural environments and challenge our modern lifestyle by causing not just biocide resistance but also cross-resistance with antibiotics. Thus, a detailed understanding of the structural and functional features of QacA is a required step in finding a strategy to overcome its efflux activity and thus breaking QacA-mediated resistance. The main aim of this thesis was to analyse QacA and the architectural features of its substrate-binding pockets by performing a blend of microbiological, biochemical and bioinformatic analyses.

To interact specifically with each antimicrobial substrate QacA employs distinct subsets of amino acid residues. TMS 12 of QacA is postulated to be involved in interactions with substrates due to being one of the helices that directly contribute to forming the QacA internal cavity, which is purported to be the central location of substrate-binding and transport. To further understand the importance of TMS 12 in the structure and function of QacA, 38 amino acid residues in the putative TMS 12 and its flanking regions were replaced individually with cysteine using site-directed mutagenesis. These mutants were subsequently analysed to determine the impact of the introduced mutation on protein expression and QacA activity (Chapter 3).

Minimum inhibitory concentration analysis for representative monovalent and bivalent cationic antimicrobial substrates and fluorimetric transport assays identified a number of functionally important amino acid residues. Moreover, accessibility analysis of cysteine-substituted mutants with fluorescein maleimide found that TMS 12 is amphipathic and identified its termini which allowed for refinement of the QacA topology model.

The roles of the identified functionally important residues in QacA substrate-binding and transport pathway were further examined by a suite of biochemical assays (Chapter 4). DAPI fluorescent transport assays, together with results obtained from the effects of substrate preincubation on maleimide reactivity and maleimide pre-treatment on QacA-mediated DAPI efflux, demonstrated that the residues G361 and S387 directly partake in the DAPI transport pathway and perhaps that for other bivalent cationic substrates. Moreover, the solvent accessible residue, S387 at the cytoplasmic end of TMS 12, was found to be directly involved in or located in close vicinity to the substrate-binding site and translocation pathway of chlorhexidine and DAPI. Importantly, the conserved residue G379 in TMS 12 appeared to be structurally important in QacA for transport of bivalent substrates, commensurate with the role of glycine residues in helical flexibility and inter-helical interactions.

A high resolution structure of QacA still remains unresolved. Therefore, a QacA model structure was generated based on homology modelling with the available high resolution structure of a 14 TMS major facilitator superfamily (MFS) protein as a template (Chapter 5). The residues important for QacA mediated resistance to benzalkonium and chlorhexidine were overlaid onto the 3D QacA model. This identified regions lining the QacA central cavity as potentially critical interaction sites for such biocides. Molecular docking analysis revealed the putative substrate-binding pockets for the six antimicrobials used in the functional analyses.

Overall, the work described in thesis makes an original contribution to basic and applied understanding of the structure-function of QacA and provides new insights into the architecture of its drug binding pockets. More generally, the findings can be used in complementing the high-resolution structural data when they are available and also for rational development of efflux pump inhibitor.

DECLARATION

I certify that this thesis does not incorporate without acknowledgment any material previously submitted for a degree or diploma in any university; and that to the best of my knowledge and belief it does not contain any material previously published or written by another person except where due reference is made in the text.

Abolfazl Dashtbani-Roozbehani

ACKNOWLEDGEMENTS

First and foremost, I would like to express my sincere utmost gratitude to my supervisor Professor Melissa Brown for welcoming me into her laboratory and giving me the opportunity to undertake my PhD project. I am very grateful for her great advice, knowledge, patience, optimism, encouragement and support throughout my journey that allowed me to complete this thesis. I am thankful to Melissa for opening my eyes to the world of multidrug efflux pump proteins and giving me the opportunities and autonomy to develop my confidence as a researcher and scientist.

I would also like to thank my co-supervisor Dr Sunita Ramesh for sharing her research experience and her welcoming manner. I would also like to thank my thesis advisory panel, Professor Catherine Abbott and Associate Professor Rietie Venter, for overseeing my progress and providing thoughtful insights and feedback that no doubt improved my research work. I would like to acknowledge the financial support I have received from Flinders University through the Australian Government Research Training Program Scholarship.

I would also like to thank many past and present members of the Brown Lab, especially Mohsen, Sylvia, Felise, Jenny and Sarah for helping me along the way and making it a great research environment. I am particularly appreciative of Mohsen for invaluable discussions, technical advice and mentorship. My thanks are also extended to members of the Leterme Lab (past and present): Sophie, Tamar, Elise, Marie and Anna. I appreciate all their kindness, friendship, assistance and sharing the joy and laughter during the time of my candidature, particularly in the COVID-19 year. I will fondly remember all these wonderful people.

Last but not least, I am immensely grateful and thankful to my family in my home country for understanding the heavy work commitment of a PhD research, constant encouragement and moral support over the past few years.

CHAPTER 1 INTRODUCTION

1.1 Antimicrobial resistance in bacteria: A worldwide crisis

The term 'antimicrobial' encompasses all antibiotics and biocides (antiseptics, disinfectants and preservatives) which are used to kill or inhibit the growth of microorganisms. After the serendipitous discovery of penicillin by Alexander Fleming in the late 1920's, antimicrobials have been a vital medication for the control of bacterial infections. Antimicrobials, however, have progressively failed to kill or inhibit various bacterial pathogens due to the emergence of antimicrobial resistance (AMR) among bacteria (Martens and Demain, 2017; Frieri *et al.*, 2017). Extensive application of antimicrobials in human and veterinary medicine imposes selective pressures on bacteria, which are incredibly adaptable to their environments. Consequently, antimicrobials eliminate the susceptible population and the resistant bacterial cells that have developed ways to survive, can grow and propagate in the presence of these compounds (Venter *et al.*, 2017; Yen and Papin, 2017; Henderson *et al.*, 2021). Resistant bacteria can rapidly spread causing a growing and worrying threat to public health worldwide. According to World Health Organisation (WHO) (WHO, 2018), we are heading for a post-antibiotic era, where common infections and small injuries may again be fatal if we fail to act urgently against the rapid spread of AMR. Of particular concern is AMR in the "ESKAPE" pathogens which are the leading cause of nosocomial infections globally (Santajit and Indrawattana, 2016; Renner *et al.*, 2017). ESKAPE is an acronym for the panel of bacteria, comprised of *Enterococcus faecium*, *Staphylococcus aureus*, *Klebsiella pneumoniae*, *Acinetobacter baumannii*, *Pseudomonas aeruginosa*, and *Enterobacter* species, that have the capacity to "escape" the effects of routine antimicrobial regimes (Santajit and Indrawattana, 2016). A horrendous situation is when bacteria exhibit non-susceptibility to three or

more agents from different antimicrobial classes which are then defined as multidrug resistant (MDR) bacteria (Nikaido, 2009; Magiorakos *et al.*, 2012; Exner *et al.*, 2017). As an example, MDR *S. aureus* strains have gained resistance to multiple antibiotics such as chloramphenicol, aminoglycosides, lincosamide, macrolides, fluoroquinolones, streptomycin, sulphonamides and tetracycline (Jang, 2016). Because infections caused by MDR bacteria are becoming significantly harder to treat, they result in increases in the length of stay in hospitals, in addition to economic and social costs and mortality (Xia *et al.*, 2016; Collignon, 2015).

Apart from a colossal threat to global health, AMR incurs considerable economic costs to society. In Europe, it is estimated that 25,000 people die annually from MDR bacterial infections with the associated cost of €1.5 billion (Blair *et al.*, 2015). In the U.S., MDR bacteria infect more than 2 million people per year with 23,000 deaths at a cost of \$20 billion (Hampton, 2013). Moreover, AMR is estimated to cause 10 million deaths per year globally by 2050, with a loss of up to \$100 trillion (£64 trillion) (Munita and Arias, 2016; de Kraker *et al.*, 2016; Venter *et al.*, 2017). Indeed, our arsenal of new antimicrobial medicines for humans and animals is being depleted by the rapid increase in AMR. It is important to consider that antibiotics not only save patients' lives, they play a pivotal role in modern medicine and surgery. Without effective antibiotics, prevention or treatment of bacterial infections associated with cancer chemotherapy, organ transplantation or major surgeries would not be possible (Lewis, 2020). The public-health crisis caused by AMR cannot be solved unless we invest in research to understand the underlying mechanisms *per se* (Wu *et al.*, 2020).

1.2 Infections caused by *Staphylococcus aureus*: A growing public health problem

Staphylococci are Gram-positive spherical bacteria consisting of more than 70 species and subspecies (Prax *et al.*, 2013). They are typically non-motile, non-spore forming, facultative anaerobic, catalase-positive bacteria with grape-like growth characteristics (Becker *et al.*, 2014). The most prominent member of the staphylococcal genus is *S. aureus* (DeLeo *et al.*, 2010), which colonises 20–80% of the human population either transiently or permanently (Brown *et al.*, 2014; Spaulding *et al.*, 2013). It is found on the skin (predominantly on the chest, hands and abdomen) (Otto, 2010) or in the anterior part of the nasal cavity (Weidenmaier *et al.*, 2012). *S. aureus* is an opportunistic pathogen that causes a wide spectrum of infections ranging from minor skin and soft tissue abscesses to major fatal necrotising pneumonia, meningitis, infective endocarditis, sepsis, osteomyelitis, and toxic shock syndrome (Tong *et al.*, 2015; Snell *et al.*, 2021). Moreover, *S. aureus* is a significant contributor to foodborne diseases and outbreaks (Scallan *et al.*, 2011; Andersen *et al.*, 2015).

1.3 Development and dissemination of multidrug resistance in *S. aureus*

S. aureus represents the most notorious superbug among Gram-positive bacteria due to its extraordinary ability to rapidly develop resistance to a broad range of antimicrobial compounds (Schito, 2006; Bagnoli *et al.*, 2018). Historically, penicillin was used to treat *S. aureus* infections. However, by the mid-1940's, penicillin resistant *S. aureus* strains began to appear in hospitals only a few years after its introduction into clinical practice. Within a decade, penicillin-resistant strains spread to the community and reached pandemic levels (Chambers and Deleo, 2009;

MacIntyre and Bui, 2017). Resistance to penicillin emerged through the acquisition of the *blaZ* gene. This gene encodes β -lactamase, which hydrolyses the β -lactam ring of penicillin and thus inactivates its antimicrobial activity (Kong *et al.*, 2010; Miragaia, 2018). To circumvent the problems associated with penicillin resistance, second generation semi-synthetic penicillins, which include methicillin and oxacillin, were introduced in 1959. However, resistance to methicillin was first reported in the UK in 1961, giving rise to methicillin-resistant *S. aureus* (MRSA) (Fishovitz *et al.*, 2014; Venter *et al.*, 2017). This resistance phenotype was 20 years later identified to be due to the acquisition of a *mecA* gene that encodes the low affinity penicillin binding protein (PBP) 2a enabling the bacterium to maintain cell-wall synthesis while other PBPs are inhibited by β -lactam antibiotics (Chambers and Deleo, 2009).

S. aureus is highlighted as a globally pervasive pathogen associated with rising AMR (Wernli *et al.*, 2017; Sirijatuphat *et al.*, 2018). Infections caused by MDR bacteria are difficult to treat due to limited treatment options (Li and Webster, 2018). Furthermore, this 'superbug' has garnered substantial attention from public health researchers and health policy makers in particular due to significant morbidity and mortality caused by MDR *S. aureus* infections in the hospitals or in the community settings globally (Senn *et al.*, 2016; Lee *et al.*, 2017; Hassoun *et al.*, 2017). For example, MRSA strains, which are resistant to all β -lactam antibiotics, were once largely confined to hospitals but recently have been increasingly isolated from community infections (David and Daum, 2010; Agostino *et al.*, 2017; Choo, 2017). These so-called community-associated MRSA (CA-MRSA) strains have been rapidly spreading in diverse communities throughout the world since the 1990s with reports of outbreaks in several countries (Kong *et al.*, 2016; Uehara *et al.*, 2019). In Australia,

high prevalence of CA-MRSA has been reported from skin and soft tissue infections among indigenous communities in the Northern Territory (McDonald *et al.*, 2006; Ng *et al.*, 2009). In addition to its dissemination, CA-MRSA can cause complicated infections such as infective endocarditis and sepsis, whose incidence was rare before the emergence of CA-MRSA (McDougal *et al.*, 2010; Hassoun *et al.*, 2017).

In addition to β -lactam antibiotics, *S. aureus* has also developed resistance to numerous other antibiotics such as vancomycin, erythromycin, gentamicin, and oxacillin. This has resulted in increasingly limited antibiotic choices for the treatment of cognate infections (McDougal *et al.*, 2010; Hassoun *et al.*, 2017; Garoy *et al.*, 2019). A notable example of this phenomenon is the development of vancomycin resistance in *S. aureus*. Vancomycin, a glycopeptide antibiotic that inhibits cell wall biosynthesis, has been used as the drug of choice for the treatment of MRSA infections since the 1980s; however, *S. aureus* strains exhibiting decreased susceptibility to vancomycin, known as vancomycin-intermediate and vancomycin-resistant MRSA (VISA and VRSA, respectively) have emerged and are now compromising successful therapy (Choo and Chambers, 2016; Sarkar *et al.*, 2017; McGuinness *et al.*, 2017; Wang *et al.*, 2018). The biochemistry behind the development of resistance in this pathogen is discussed in the following section.

1.4 Molecular mechanisms of antimicrobial resistance in *S. aureus*

Technical advances have gradually unveiled the molecular mechanisms of bacterial AMR. Bacterial resistance can emerge via two major genetic pathways: i) spontaneous mutations/deletions in the bacterial chromosome which independently result in resistance to some antimicrobials (e.g., *S. aureus* resistance to quinolones, linezolid and daptomycin) (Pantosti *et al.*, 2007; Touati *et al.*, 2021); and ii) acquisition

of foreign DNA, referred to as 'mobile genetic elements' (MGEs), through either horizontal or vertical gene transfer. MGEs include plasmids, transposons, bacteriophages, insertion sequences, integrons, pathogenicity islands, and chromosomal cassettes that can disseminate a variety of pre-existing antimicrobial resistance determinants across bacterial genomes (Malachowa and DeLeo, 2010; Haaber *et al.*, 2017; Bukowski *et al.*, 2019; Sargison and Fitzgerald, 2020). While plasmids are mostly extrachromosomal, other MGEs have the ability to integrate into the host DNA (Haaber *et al.*, 2017; Jamrozny *et al.*, 2017). MGEs contribute to the high-level emergence of MDR strains which can rapidly spread in both community and healthcare environments worldwide (Malachowa and DeLeo, 2010; Lewis, 2020). For example, *S. aureus* resistance to methicillin and vancomycin was developed through the acquisition of the Staphylococcal Chromosomal Cassette *mec* harbouring the *mecA* gene (Earls *et al.*, 2017) and the Enterococcal *vanA* operon residing on a conjugal plasmid (Weigel *et al.*, 2003; Qureshi *et al.*, 2014), respectively.

AMR can be mediated by the following biochemical mechanisms: (i) enzymatic modification of the antimicrobial binding site to decrease the affinity for the antimicrobial (e.g. resistance to methicillin by penicillin-binding protein 2a); (ii) enzymatic inactivation/modification of the antimicrobial (e.g. resistance to β -lactam antibiotics by production of β -lactamases); (iii) bypassing the metabolic pathway to avoid antimicrobial action (e.g. resistance to trimethoprim-sulphamethoxazole by production of an insensitive dihydrofolate reductase); (iv) sequestration of the antimicrobial to protect the target (e.g. resistance against host defence antimicrobial peptides such as α -defensins by secretion of staphylokinase); and (v) increased expression of efflux pumps to extrude antimicrobial molecules (e.g. resistance to

tetracycline by the TetA(K) efflux pump) (Foster, 2017; Xia *et al.*, 2016; Munita and Arias, 2016; Nawrocki *et al.*, 2014; Peacock and Paterson, 2015). Central to the resistance mechanisms is the expression of efflux pumps, which has gained significant traction in recent years as a widespread underlying mechanism of MDR *S. aureus* infections (Jang, 2016), and is discussed in the following sections.

1.5 Efflux mediated antimicrobial resistance in *S. aureus*: clinical implications

Efflux pumps are ubiquitous transport proteins which are distributed in the cytoplasmic membrane of bacteria, archaea and eukaryotes (Tanaka *et al.*, 2013). Efflux-mediated drug resistance has increasingly continued to challenge the chemotherapy of bacterial infections and human cancers (Hughes and Andersson, 2015; Melander and Melander, 2017). Bacteria essentially utilise efflux pumps as a natural defence mechanism by virtue of their ability to expel a wide variety of toxic compounds in the environment which lowers their concentration inside the cell to sub-toxic levels (Venter *et al.*, 2017; Henderson *et al.*, 2021). Drug efflux pumps are considered as an effective resistance mechanism in bacterial pathogens including *S. aureus* to cope with the diverse range of antimicrobials used clinically to treat infections or as antiseptics and disinfectants to reduce bacterial load (Blanco *et al.*, 2016). Efflux proteins actively efflux the antimicrobial molecules from within the cell to the outside environment before they reach their targets. Some bacterial efflux pumps are substrate-specific since they recognise and expel a single substrate or its closely-related derivatives (e.g., tetracycline-specific pumps), whereas MDR efflux pumps recognise and export a broad spectrum of structurally-unrelated substrates (Poole, 2002). In other words, substrate polyspecificity (or promiscuity toward

substrates) is the characteristic feature of MDR efflux proteins (Ramaswamy *et al.*, 2017). MDR efflux proteins are major contributors to the development and maintenance of AMR (Du *et al.*, 2018). They enable bacterial survival for a longer period of time increasing the probability of spontaneous mutations which cause high-level resistance to specific antimicrobials. Thus, the activity of efflux pumps can contribute to acquisition of other resistance mechanisms (Piddock, 2006a; Ebbensgaard *et al.*, 2020).

In addition to antimicrobial resistance, efflux pumps in bacteria play numerous vital physiological roles including extrusion of endogenous noxious metabolites, host-derived antimicrobials and virulence factors, suggesting that the synthetic antimicrobials could be “accidental substrates” of these membrane transport proteins (Piddock, 2006b; Hassan *et al.*, 2019; Short *et al.*, 2020). There is growing evidence from many studies that highlight the contribution of bacterial efflux pumps towards bacterial biofilm formation (Du *et al.*, 2018), particularly in several important pathogenic species of bacteria such as *S. aureus*, *A. baumannii*, *E. coli*, and *P. aeruginosa*. These bacteria can form biofilms on medical devices and cause biofilm infections, which constitute clinical challenges (Alav *et al.*, 2018; Schilcher and Horswill, 2020).

Chromosomal drug efflux genes are appreciated as having additional housekeeping function unrelated to antimicrobial export and resistance (Poole 2007). The expression levels of these genes are low under ordinary environmental conditions due to strict control of multiple regulators (Sun *et al.* 2014). Notably, hospital-associated bacteria that use efflux pumps for antimicrobial resistance often express such pumps constitutively at higher levels as a result of regulatory mutations, either

in the promoter region of the efflux pump or in its regulator gene (Webber and Piddock, 2003; Poole, 2004; Henderson *et al.*, 2021). This provides a piece of evidence in favour of the proposition that efflux pumps have primordial physiological functions distinct from antimicrobial resistance but have been fortuitously exploited for antimicrobial resistance roles in bacterial pathogens under intense antimicrobial selective pressures in hospital environments.

1.6 Classification of bacterial efflux pumps

Bacterial efflux pumps are currently classified into seven membrane protein families based on a number of properties including protein sequence homology, structural conformation of the protein (the number of transmembrane-spanning [TMS] regions they possess), the energy source used (ATP hydrolysis or the ion electrochemical gradient), and substrate specificity (Figure 1.1). These families are: (1) the ATP-binding cassette (ABC) family; (2) the major facilitator superfamily (MFS); (3) the small multidrug resistance (SMR) family; (4) the proteobacterial antimicrobial compound efflux (PACE) family; (5) the multidrug and toxic compound extrusion (MATE) family; (6) the resistance-nodulation division (RND) family; and (7) the *p*-aminobenzoyl-glutamate transporter (AbgT) family (Chitsaz and Brown, 2017). While ABC transporters utilise the energy produced by ATP hydrolysis, other transporters depend on the electrochemical energy stored in the ion gradient, typically the proton motive force (pmf), as the driving force for the extrusion of their substrates. MATE family proteins can also use the sodium membrane gradient as the source of energy (Kumar and Schweizer, 2005). Multidrug efflux pumps identified in *S. aureus* belong to the ABC, MFS, MATE or SMR superfamilies/families of membrane proteins and are discussed in the following sections. Interestingly, a new RND type efflux pump, FarE,

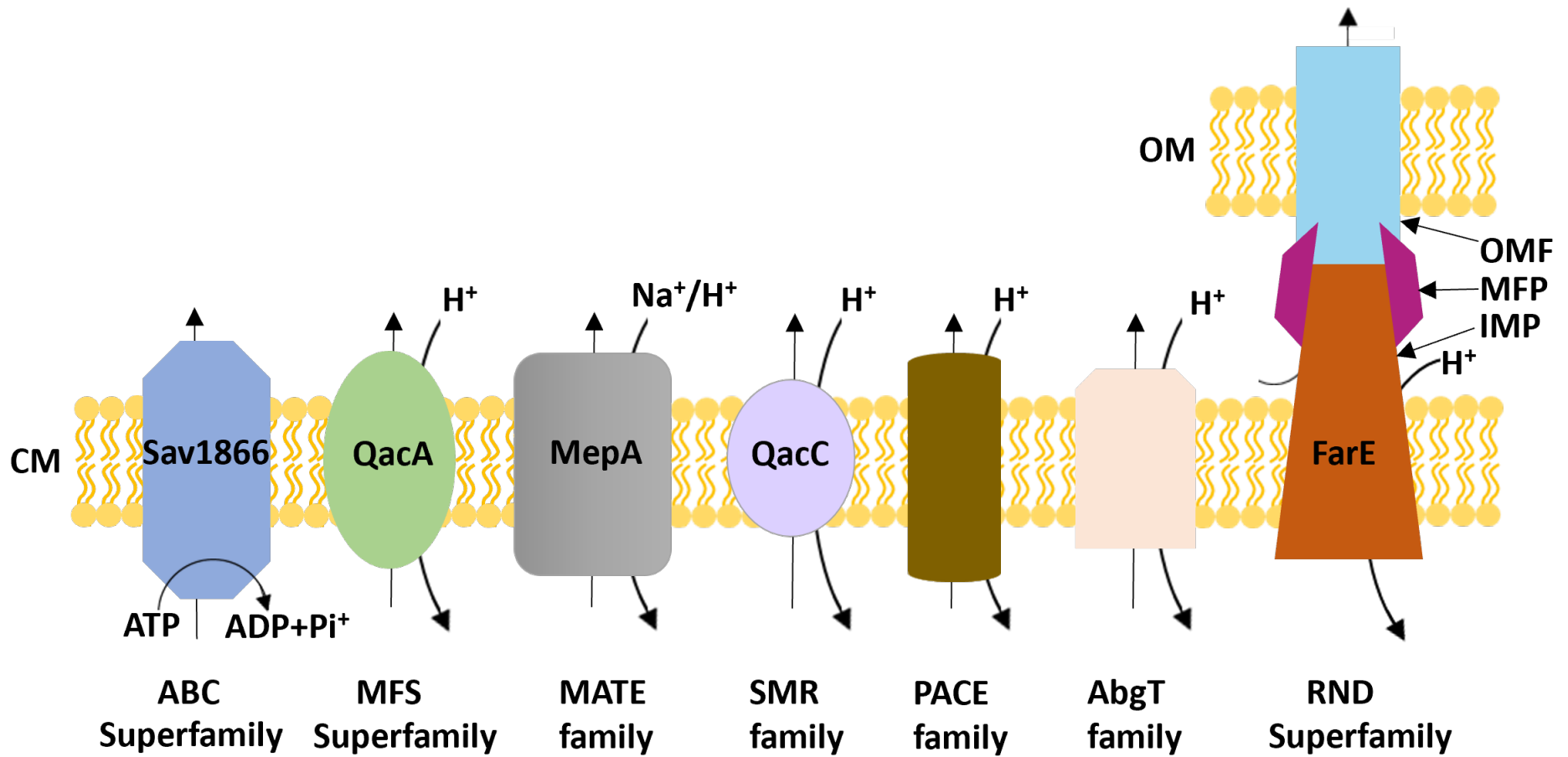


Figure 1.1 Schematic representation of the seven families/superfamilies of multidrug transporters.

Each transport system is depicted as a distinct shape and colour along with the energy source for driving substrate export (i.e., ATP hydrolysis for the ABC superfamily and electrochemical energy stored in ion gradient $[H^+/Na^+]$ for the others). The transporters classified within the ATP-binding cassette (ABC), major facilitator superfamily (MFS), multidrug and toxic compound extrusion (MATE), proteobacterial antimicrobial compound efflux (PACE), small multidrug resistance (SMR), and *p*-aminobenzoyl-glutamate transporter (AbgT) families commonly expel their substrates across the cytoplasmic membrane (CM). In Gram-negative bacteria, resistance-nodulation division (RND) transporters typically form tripartite systems containing an inner membrane protein (IMP), membrane fusion protein (MFP), and outer membrane factor (OMF) (Daury *et al.*, 2016). Such tripartite RND efflux pumps facilitate the extrusion of substrates across both the CM and outer membrane (OM) of Gram-negative bacteria, as illustrated. Examples of *S. aureus* transporters, where applicable, are included.

from *S. aureus* has been identified to transport antimicrobial fatty acids found on the skin and nasal secretions (Alnaseri *et al.*, 2015). Efflux systems that belong to the RND family are composed of three proteins (see Figure 1.1). However, here FarE seems to be the only identified component of the efflux system in the staphylococcal cell envelope and may not form a tripartite assembly with partner proteins due to lack of the outer membrane.

1.7 Prototypical characterised efflux pumps in *S. aureus*

Efflux pumps play a key role in antimicrobial resistance in *S. aureus* (Lekshmi *et al.*, 2018). Recent technological advances in genome analysis and bioinformatics have identified a large number of genes encoding putative efflux pumps in bacteria (<http://www.membranetransport.org/>). However, the majority of these remain experimentally uncharacterised. More than 10 efflux pumps have been described in *S. aureus* thus far. These efflux pumps are encoded either on the chromosome or on plasmids (Costa *et al.*, 2013; Lekshmi *et al.*, 2018). In combination, these drug transporters potentiate resistance to a wide spectrum of unrelated antibiotics, such as tetracyclines, macrolides, and quinolones, as well as a vast array of biocides, including quaternary ammonium compounds (QACs), biguanidines and diamidines. Table 1.1 summarises the information of the prototypical efflux pumps within *S. aureus*.

The SMR transporters, as implied by their name, are smaller than other efflux pump proteins and are approximately 100–130 amino acids in length. They only consist of four TMS and are carried on plasmids. The *S. aureus* SMR exporter identified thus far is QacC (also known as QacD or Ebr) (Littlejohn *et al.*, 1991; Sasatsu *et al.*, 1989; Henderson *et al.*, 2021). Proteins of the MATE family range from 400 to 550 amino

Table 1.1 Characterised drug efflux pumps in *S. aureus*

Family	Transporter	TMS	Gene Location	Prominent substrates	Reference(s)
ABC	AbcA	12	Chromosome	Hydrophobic β -lactams	(Villet <i>et al.</i> , 2014)
	MsrA	12	Plasmid	Macrolides, type B streptogramins, erythromycin	(Le Bouter <i>et al.</i> , 2011; Wang <i>et al.</i> , 2019)
	Sav1866	12	Chromosome	Vinblastine, doxorubicin, Dyes (ethidium, Hoechst 33342)	(Dawson and Locher, 2007; Velamakanni <i>et al.</i> , 2008)
	VgaA	12	Plasmid	Lincosamides, streptogramin A, pleuromutilins	(Allignet <i>et al.</i> , 1992; Vimberg <i>et al.</i> , 2020)
	VgaB	12	Plasmid	Pristinamycin, streptogramin A, streptogramin B virginiamycin, mikamycin, synergistin, dalfopristin	(Allignet and El Solh, 1997; Chesneau <i>et al.</i> , 2005)
MATE	MepA	12	Chromosome	Fluoroquinolones (norfloxacin, ciprofloxacin, moxifloxacin), Glycylcyclines (tigecycline), QACs (benzalkonium, cetrimide), Dyes (ethidium)	(Kaatz <i>et al.</i> , 2005; McAleese <i>et al.</i> , 2005; de Morais Oliveira-Tintino <i>et al.</i> , 2021)
MFS	FexA	14	Transposon	All phenicols	(Kehrenberg and Schwarz, 2005; Lekshmi <i>et al.</i> , 2018)
	LmrS	14	Chromosome	Lincomycin, Oxazolidinone (linezolid), Phenicols (chloramphenicol), QACs (tetraphenylphosphonium), Dyes (ethidium)	(Floyd <i>et al.</i> , 2010; Nava <i>et al.</i> , 2020)

(Continued on next page)

Table 1.1 (continued)

Family	Transporter	TMS	Gene Location	Prominent substrates	Reference(s)
	MdeA	14	Chromosome	Fluoroquinolones (norfloxacin, ciprofloxacin), QACs (benzalkonium, dequalinium), Dyes (ethidium)	(Huang <i>et al.</i> , 2004; Yamada <i>et al.</i> , 2006b; Alav <i>et al.</i> , 2018)
	NorA	12	Chromosome	Fluoroquinolones (norfloxacin, ciprofloxacin), QACs (benzalkonium), Dyes (ethidium, rhodamine)	(Yu <i>et al.</i> , 2002; Costa <i>et al.</i> , 2019)
	NorB	14	Chromosome	Fluoroquinolones (norfloxacin, ciprofloxacin, moxifloxacin), QACs (cetrimide), Dyes (ethidium)	(Truong-Bolduc and Hooper, 2010; Rajabi <i>et al.</i> , 2020)
	NorC	14	Chromosome	Fluoroquinolones (ciprofloxacin, moxifloxacin), Dyes (rhodamine)	(Truong-Bolduc <i>et al.</i> , 2006; Kumar <i>et al.</i> , 2020b)
	QacA	14	Plasmid	QACs (benzalkonium, dequalinium), Diamidines (pentamidine), Biguanidines (chlorhexidine), Dyes (ethidium, rhodamine, acriflavine)	(Paulsen <i>et al.</i> , 1996a; Mitchell <i>et al.</i> , 1998) (Majumder <i>et al.</i> , 2019; LaBreck <i>et al.</i> , 2020)
	QacB	14	Plasmid	QACs (benzalkonium), Dyes (ethidium, rhodamine 6G, acriflavine)	(Paulsen <i>et al.</i> , 1996a; Hassanzadeh <i>et al.</i> , 2020)
	SdrM	14	Chromosome	Fluoroquinolones (norfloxacin), Dyes (ethidium, acriflavine)	(Yamada <i>et al.</i> , 2006a) (Costa <i>et al.</i> , 2013; Lekshmi <i>et al.</i> , 2018)
	TetA(K)	14	Plasmid	Tetracyclines	(Ginn <i>et al.</i> , 2000; Costa <i>et al.</i> , 2019)

(Continued on next page)

Table 1.1 (continued)

Family	Transporter	TMS	Gene Location	Prominent substrates	Reference(s)
	Tet38	14	Chromosome	Tetracyclines, certain unsaturated fatty acids fosfomycin	(Truong-Bolduc <i>et al.</i> , 2018)
SMR	QacC	4	Plasmid	QACs (benzalkonium, cetrimide), Dyes (ethidium)	(Littlejohn <i>et al.</i> , 1991; Sasatsu <i>et al.</i> , 1989; Scherf <i>et al.</i> , 2020)
	QacJ	4	Plasmid	QACs (benzalkonium, cetyltrimethylammonium bromide)	(Bjorland <i>et al.</i> , 2003)
	SepA	4	Plasmid	benzalkonium, chlorhexidine, acriflavine	(Narui <i>et al.</i> , 2002; Schindler and Kaatz, 2016)

acid residues. MATE transporters possess 12 TMS and are chromosomally-encoded (Omote *et al.*, 2006; Henderson *et al.*, 2021). MepA is the only MDR transporter from *S. aureus* which is classified as a MATE protein (Kaatz *et al.*, 2006; McAleese *et al.*, 2005; Kaatz *et al.*, 2005). Transporters of the ABC family have a structure that consists of four domains; two transmembrane domains and two highly conserved nucleotide-binding domains (Rees *et al.*, 2009). The multidrug ABC exporters Sav1866 and AbcA from *S. aureus* are chromosomally encoded and contain a transmembrane and nucleotide-binding domain fused together that dimerise to form the complete transporter (Dawson and Locher, 2007; Schrader-Fischer and Berger-Bachi, 2001). *S. aureus* Sav1866 is a homologue of the human ABC transporter P-glycoprotein that causes MDR in cancer cells (Dawson and Locher, 2006; Velamakanni *et al.*, 2008). Sav1866 protein is one of the best-studied bacterial multidrug ABC transporters, whose three-dimensional crystal structure was determined at 3.0 Å resolution (Dawson and Locher, 2006). The Sav1866 structure revealed a homodimeric protein of 12 TMS where nucleotide-binding domains exhibited a 'head-to-tail' arrangement with a shared interface forming two ATP-binding and hydrolysis sites (Dawson and Locher, 2006; Dawson and Locher, 2007). The plasmid-encoded MsrA efflux pump of *S. aureus* contains 488 residues with two putative ATP-binding domains but no hydrophobic membrane spanning domains (Reynolds *et al.*, 2003). Similar to MsrA, plasmid-mediated Vga proteins from *S. aureus* are ABC transporters that have been characterised with no transmembrane domains (Chesneau *et al.*, 2005).

1.8 The major facilitator superfamily

The MFS represents the largest and most diverse family of membrane transporters found ubiquitously in all domains of living organisms. Considering the mode of

transport, MFS transporters are grouped into uniporters (that transport a single substrate across the membrane without any coupling ions), symporters (that co-transport a substrate with a coupling ion in the same direction) and antiporters (that co-transport a substrate with a coupling ion in opposite directions) (Quistgaard *et al.*, 2016; Du *et al.*, 2018).

The MFS superfamily encompasses over 15,000 proteins which is currently classified into more than 105 families according to the Transporter Classification Database (TCDB; <http://www.tcdb.org>) (Wang *et al.*, 2020b; Saier Jr *et al.*, 2021). Each family within the MFS superfamily usually performs transport across the membranes of a certain set of related substrates that includes monosaccharides, oligosaccharides, amino acids, peptides, nucleosides, nucleotides, vitamins, enzyme cofactors, drugs, organic and inorganic anions and cations (Reddy *et al.*, 2012; Varela *et al.*, 2017). A large number of MFS proteins have medical significance, as MFS transporters in bacteria can function as drug efflux pumps thereby conferring antimicrobial resistance and in humans, the glucose transporters Glut4 and G6PT when impaired causes type II diabetes and glycogen storage disease, respectively (Bai *et al.*, 2017).

1.8.1 Major structural features of MFS transporters

1.8.1.1 Conservation of structures across MFS transporters

Proteins of the MFS family are generally highly hydrophobic and range from 350 to 600 amino acid residues predicted to comprise α -helical TMS connected by relatively short loops (Henderson *et al.*, 2021). MFS transporters commonly possess 12 or 14 TMS (Lekshmi *et al.*, 2018). To date, a handful of crystallographically solved high-resolution structures of bacterial MFS transporters exist. These resolved MFS protein crystal structures include the glycerol-3-phosphate transporter (GlpT) (Huang *et al.*,

2003), lactose permease (LacY) (Abramson *et al.*, 2003b), fucose transporter (FucP) (Dang *et al.*, 2010), xylose transporter (XylE) (Quistgaard *et al.*, 2013), nitrate/nitrite transporters NarK (Zheng *et al.*, 2013) and NarU (Yan *et al.*, 2013), peptide transporter (YbgH) (Zhao *et al.*, 2014), organic anion transporter (DgoT) (Leano *et al.*, 2019), the multidrug transporters YajR (Jiang *et al.*, 2013), EmrD (Yin *et al.*, 2006) and MdfA (Heng *et al.*, 2015) from *E. coli*, the oligopeptide-H⁺ symporter (PepT_{So}) from *Shewanella oneidensis* (Newstead *et al.*, 2011), phosphate transporter (PiPT) from *Piriformospora indica* (Pedersen *et al.*, 2013), melibiose permease (MelB) from *Salmonella typhimurium* (Ethayathulla *et al.*, 2014), glucose transporter (GlcP_{Se}) from *Staphylococcus epidermidis* (Iancu *et al.*, 2013), and the multidrug transporter LmrP from *Lactococcus lactis* (Debruycker *et al.*, 2020). It should be noted that the majority, if not all, of the currently available 14-TMS MFS structures such as YbgH and PepT_{So} peptide transporters belong to the proton-dependent oligopeptide transporter (POT) family and are in inward-open conformations (Daniel *et al.*, 2006; Quistgaard *et al.*, 2017).

Analysis of the known high-resolution structures of MFS proteins revealed that these transporters regardless of their various substrate specificities, different transport modes and low sequence identity share a similar structural core (Vardy *et al.*, 2004; Varela *et al.*, 2017; Quistgaard *et al.*, 2016). The MFS structural core consists of twelve TMS (TMS 1–TMS 12) that is organised into two pseudo-symmetrical 6-TMS domains, the N-domain (TMS 1–TMS 6) and the C-domain (TMS 7–TMS 12), each consisting of two inverted three-helix units (Figure 1.2) (Madej *et al.*, 2013; Yan, 2013; Quistgaard *et al.*, 2016; Drew *et al.*, 2021). It has been shown that the two domains (also known as halves) of the modern MFS transporters have arisen from a common ancestor

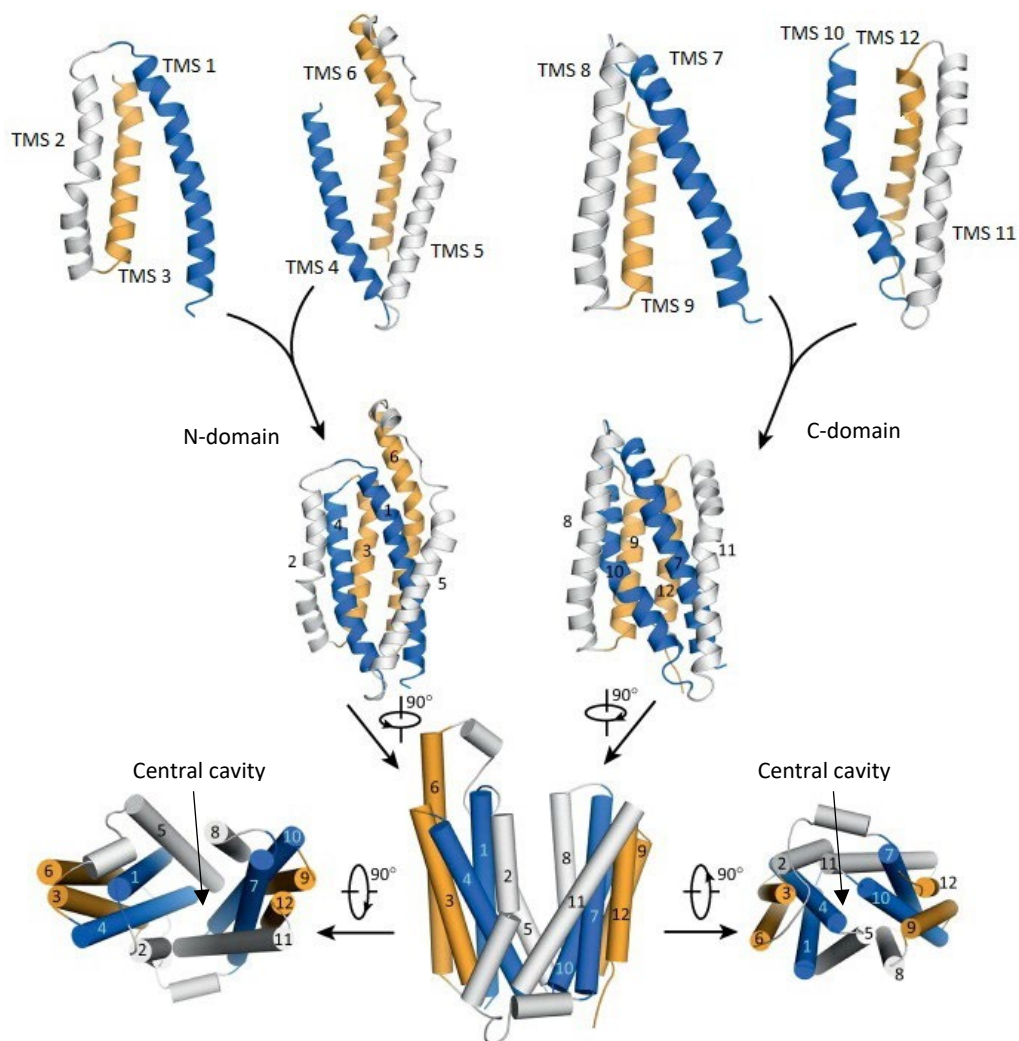


Figure 1.2 Canonical structural fold of MFS proteins.

A typical 12-TMS MFS fold is comprised of four 3-TMS units (top row). Two inverted 3-TMS units make up one distinctive domain (middle row). The two domains (N-domain and C-domain) are connected with approximately 180° rotation around an axis perpendicular to the membrane plane (bottom row). The corresponding TMS in each of the 3-TMS repeats have the same colour. Figure modified from Yan (2013).

through an internal gene duplication event which resulted in a repeat of four triple-helix units (Griffith *et al.*, 1992; Madej *et al.*, 2013). The 14-TMS MFS members presumably have evolved via the subsequent insertion of a central loop in 12-TMS precursors to form two extra TMS helices or the substitution of the central loop region for two TMS helices (Saier, 2003; Henderson *et al.*, 2021).

Another apparently common feature of the structural core of the MFS proteins is the presence of a large aqueous cavity in the centre of the transporter (Figure 1.2). The central cavity is formed between the two domains, the N-domain and the C-domain (Quistgaard *et al.*, 2016; Drew *et al.*, 2021). The central cavity serves as both the binding site and transport path for the substrates. TMS 1, 4, 7, and 10 (the first helix in each triple-helix repeat) are directly involved in the formation of the central cavity (each referred to as a 'cavity helix'). TMS 2, 5, 8 and 11 (the second helix in each triple-helix repeat) form the sidewalls of the central cavity (referred to as rocker helices). These helices are usually long, curved and banana shaped. The rocker helices contribute to inter-domain conformational changes. TMS 3, 6, 9, and 12 (the third helix in each triple-helix repeat) are located at the rim of the longest dimension of the transmembrane core (referred to as supporting helices). These helices are most hydrophobic TMS which usually do not directly contribute to the formation of the central cavity. However, they are involved in hydrophobic interactions with the surrounding lipid membrane (Jiang *et al.*, 2013; Yan, 2015; Lee *et al.*, 2016). The supporting helices are generally about one-turn shorter than the other two groups of helices (Zhang *et al.*, 2015). Thus, during a major conformational change, supporting helices would presumably move less than the other two groups of helices do (Heng *et al.*, 2015).

Within the MFS transporters, antiporters that function as drug and multidrug efflux pumps can be sub-grouped into three well characterised drug:H⁺ antiporter (DHA) families, namely DHA1, DHA2 and DHA3 (Saier *et al.*, 2014; Chitsaz and Brown, 2017; Henderson *et al.*, 2021). However, of note, the “unknown major facilitator family-2” has recently been renamed as the DHA4 family, owing to phylogenetic and functional characterisation of efflux protein BC3310 from *Bacillus cereus* (Kroeger *et al.*, 2015; Henderson *et al.*, 2021). The DHA4 sub-group remains to be further investigated experimentally. DHA1 and DHA3 families have been shown experimentally to have 12 TMS (Reddy *et al.*, 2012; Chitsaz and Brown, 2017), whereas DHA2 family exporters such as QacA, QacB, and TetA(K) from *S. aureus* (Paulsen *et al.*, 1996a; Paulsen *et al.*, 1996b), TetA(L) from *Bacillus subtilis* (Jin *et al.*, 2001), EmrB from *E. coli* (Tanabe *et al.*, 2009), and LfrA from *Mycobacterium smegmatis* (Li *et al.*, 2004), have been shown to have a 14-TMS topology. Nonetheless, evolutionary studies suggested that DHA2 transporters have evolved from a 12-TMS precursor where the extra two central TMS are localised between TMS 6 and 7 (Saier, 2003; Hassan *et al.*, 2007a; Reddy *et al.*, 2012). Sequence similarities suggested that TMS 5 and 6 duplicated to produce TMS 7 and 8 in DHA2 family members (Reddy *et al.*, 2012).

1.8.1.2 Evolutionary conserved motifs in MFS

In addition to the conservation of the 12-TMS overall structure, extensive primary amino acid sequence comparative studies have found that MFS transporters often contain several highly conserved amino acid sequence motifs (Paulsen and Skurray, 1993; Zhang *et al.*, 2015). High conservation of these motifs within the MFS members indicate that they are likely to be essential for common structural or functional attributes of these transporters (Griffith *et al.*, 1992; Andersen *et al.*, 2015). These

motifs are either common throughout the superfamily, such as motifs A and B, or family-specific, such as motif C, which is found exclusively in the DHA families (Paulsen *et al.*, 1996b; Ginn *et al.*, 2000).

Motif A, located in the intracellular loop connecting TMS 2 and 3, is known as the MFS-specific motif. Motif A is also called an MFS signature motif since it is the most conserved motif in MFS transporters (Paulsen *et al.*, 1996b; Zhang *et al.*, 2015). Site-directed mutagenesis studies have repeatedly shown that motif A is vital for the transport activity in many MFS transporters (Yamaguchi *et al.*, 1992; Jessen-Marshall *et al.*, 1995; Zhang *et al.*, 2015). Crystal structure of the MFS transporter YjaR from *E. coli* has demonstrated the functional role of motif A in stabilising the outward conformation (also known as the C_{Out} state) of the MFS transporters (Jiang *et al.*, 2013). This study implied that the charge-relay system associated with motif A participates in regulation of protonation inside the central cavity which is important for the transport function of pmf-driven MFS transporters. Moreover, recently, the crystal structure of LmrP bound to Hoechst 33342 showed that highly conserved D68 in motif A interacts with the bottom of TMS 11 to stabilise the outward-open/inward-closed state (Debruycker *et al.*, 2020).

Motif B, located in TMS 4, is present in many MFS proteins (Paulsen *et al.*, 1996b), including a number of MFS MDR transporters (Fluman and Bibi, 2009). Motif B contains an essential, membrane-embedded basic residue (Zhang *et al.*, 2015), such as R112 in MdfA (Fluman and Bibi, 2009; Nagarathinam *et al.*, 2018). Mutagenesis analyses have shown that changes in motif B abolished transport activity in several MFS transporters (Kimura *et al.*, 1998; Sigal *et al.*, 2005; Pascual *et al.*, 2008; Kapoor *et al.*, 2009; Heng *et al.*, 2015). Such data imply that motif B plays an important

functional role in motif B-containing MFS proteins. Motif C, located in TMS 5, was initially thought to be specific for DHA antiporters of the MFS, and was therefore known as the “antiporter motif” (Varela *et al.*, 1995). However, an extensive multiple sequence comparative analysis discovered that Motif C is also found in the symporters and uniporters of the MFS (Yaffe *et al.*, 2013). The main feature of motif C is a high glycine content. It has been postulated that motif C is important for the transport-associated conformational change (Yaffe *et al.*, 2013). This speculation is consonant with the abundance of glycine residues which could confer conformational flexibility to a TMS (Brown and Skurray, 2001). It has been recently demonstrated in the crystal structure of MdfA antiporter in the outward-open state that TMS 5 conformation exhibits a profound kink and twist to facilitate relative rotation of the N-terminal and C-terminal domains upon antiporter switching. In this regard, the presence of a two-proline-containing motif C (MFS-antiporter motif C), which is absent in symporters and uniporters, plays a central role in TMS 5 in order to be able to adopt such conformation (Nagarathinam *et al.*, 2018).

1.8.2 Transport mechanisms in MFS transporters

Based on the available high-resolution structures and other biophysical analyses, MFS transporters, despite having differences in substrate specificities and in transport mode, have repeatedly been found to exhibit similar structural folds and, hence, possess a common transport mechanism (Shi, 2013; Andersen *et al.*, 2015; Calabrese *et al.*, 2017). The current model for generally describing the substrate transport mechanism in MFS proteins is termed alternating access, whereby binding sites for substrates are alternately exposed to either side of the cell membrane (Huang *et al.*, 2003; Zhang *et al.*, 2015; Bisignano *et al.*, 2020). According to this model (Figure 1.3),

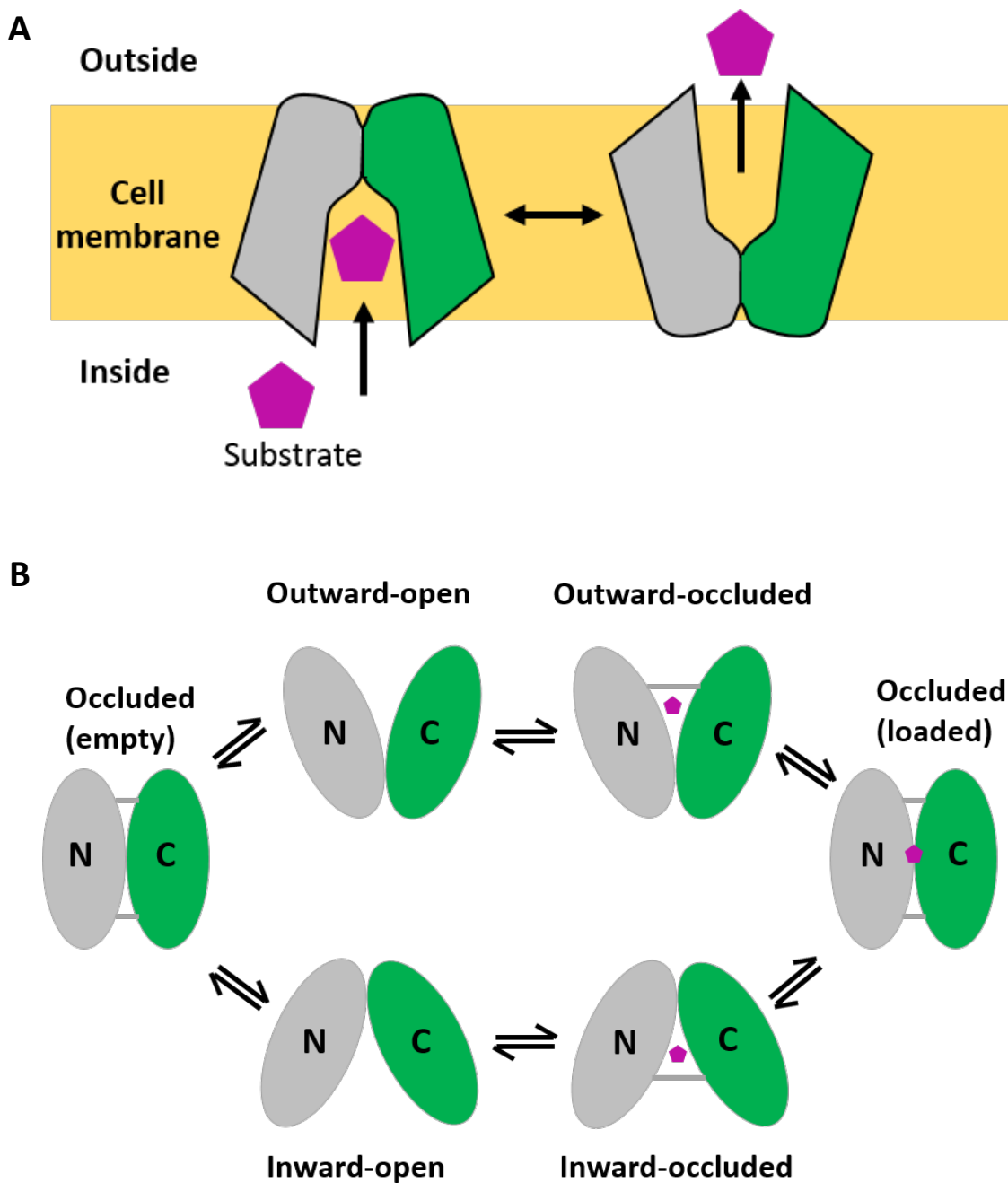


Figure 1.3 Schematic diagram of the alternating access mechanism for MFS transporters.

(A) The diagram depicts the proposed alternating access mechanism with a rocker switch type of movement that MFS transporters undergo during transport cycle. The inward-open and outward-open conformations are depicted on the left and right, respectively. The binding of a substrate (purple pentagon) results in a conformational change to the outward-open conformation. The release of the substrate to the outside causes a further conformational change, back to the inward-facing state. **(B)** The schematic illustrates the six major conformations in the transport cycle of an MFS transporter: outward-open, outward-occluded with bound substrate, occluded with substrate, inward-occluded with substrate, inward-open and occluded without substrate. N-terminal (grey) and C-terminal (green) domains are shown. Figure modified from Drew (2021).

a substrate can access the substrate-binding site from one side of the membrane when the MFS transporter is in an inward-open conformation. The transporter then undergoes a conformational change to an outward-open state, such that the binding site becomes inaccessible from the substrate entry side but accessible from the other side of the membrane, thereby allowing the substrate to cross the membrane (Deng *et al.*, 2015; Quistgaard *et al.*, 2016; Harris *et al.*, 2017; Nagarathinam *et al.*, 2018). A “rocker switch”-like conformational change was proposed to represent the mechanism underlying the alternating access model where the two halves of the protein move back and forth against each other during a transport cycle (Zhang *et al.*, 2015; Wang *et al.*, 2020b). It has been shown that the outward-open and inward-open conformations are further connected by formation of an “O”-shaped intermediate state, which is called the “occluded conformation” (Drew *et al.*, 2021). In the occluded state, the intracellular and extracellular sides of the MFS transporter are simultaneously constricted. It should be stressed, however, that in a more recent model, six distinct major structural conformations have been described for the transport cycle of an MFS transporter: outward-open, outward-occluded with bound substrate, occluded with substrate, inward-occluded with substrate, inward-open and occluded with no substrate (Drew *et al.*, 2021) (Figure 1.3B). Additionally, it should be noted that a recent study on conformational dynamics of MdfA in membrane environment has proposed a modified model for transport of lipophilic substrates in this protein and presumably other multidrug MFS transporters (Yardeni *et al.*, 2020). This model suggests that MdfA in its ‘resting state’ is laterally open to the inner leaflet of the membrane while both the cytoplasmic and periplasmic sides are relatively closed. This mechanism, which deviates from the classical alternating

access, enables recruitment of lipophilic drugs into central substrate binding pocket from the inner leaflet of the membrane.

1.8.3 MdfA: a paradigm of 12 TMS multidrug-sensing MFS antiporters

The *E. coli* MdfA efflux pump is one of the most extensively characterised MFS MDR transporters (Bibi *et al.*, 2001; Fluman and Bibi, 2009) that serves as a model system for understanding molecular mechanisms of DHA-family members such as QacA, even though the number of TMS differ (Nagarathinam *et al.*, 2018). MdfA consists of 410 amino acid residues, organised in 12 TMS, with N- and C-terminal tails located in the cytoplasm (Adler and Bibi, 2002). Notably, MdfA is a remarkably promiscuous antiporter, being able to recognise and transport a broad spectrum of lipophilic, cationic, neutral, and zwitterionic substrates (Adler and Bibi, 2005; Yardeni *et al.*, 2018). The broad substrate specificity of MdfA is attributed to its large hydrophobic substrate-binding pocket which can interact with multiple substrates either individually or simultaneously (Lewinson and Bibi, 2001; Heng *et al.*, 2015). Furthermore, regardless of the chemical nature, size, charge and hydrophobicity of a variety of dissimilar substrates, their binding to the recognition pocket of MdfA, can promiscuously induce similar conformational changes in the transporter to drive translocation across the cell membrane (Fluman *et al.*, 2009; Yardeni *et al.*, 2018). This indicates that the binding pocket of MdfA is conformationally sensitive, as a prerequisite for MDR transport.

The membrane-embedded residue D34 serves as the protonation site in MdfA (Fluman *et al.*, 2012). MdfA works with a stoichiometry of one proton per drug (Edgar and Bibi, 1997; Lewinson *et al.*, 2003; Fluman *et al.*, 2012). This stoichiometry renders MdfA inactive in export of bivalent cationic substrates, which require exchange of

two protons per transport cycle (Tirosh *et al.*, 2012). However, it has been shown that MdfA mutants harbouring an additional acidic residue at specific membrane-embedded positions are capable of exchanging two protons per drug and hence able to export bivalent cationic substrates (Tirosh *et al.*, 2012; Fluman *et al.*, 2014). It was demonstrated that surprisingly, wild-type MdfA can also pump out certain bivalent cationic substrates, whose two charged moieties are separated by a long linker. A processive transport mechanism has been proposed for these substrates, meaning that MdfA exports each charged moiety as if it were a separate substrate (Fluman *et al.*, 2014).

The crystal structure of MdfA in complex with chloramphenicol in an inward-facing conformation showed that the substrate-binding site is located within the central cavity formed between N- and C-terminal domains (Heng *et al.*, 2015) consistent with earlier biochemical analyses (Fluman *et al.*, 2009; Fluman *et al.*, 2012). The recently acquired outward-facing structure of MdfA shed light on the conformational changes during transitions between the inward-facing and outward-facing states (Nagarathinam *et al.*, 2018). In sharp contrast to wild-type MdfA, which cannot pump out short bivalent cationic compounds such as DAPI and methyl viologen (Fluman *et al.*, 2014), the MdfA mutant I239T/G354E can export both monovalent and short bivalent drugs, in addition to other known MdfA substrates (Tirosh *et al.*, 2012). The crystal structures of this MdfA I239T/G354E variant bound with electrically different substrates identified that these mutations broaden the substrate recognition spectrum of MdfA by altering the transporter-substrate interactions (Wu *et al.*, 2019). In general, structural and biochemical studies of MdfA provide a conceptual framework for understanding how mutation of specific key residues can even expand

the already broad substrate profile of the DHA-family transporters, which may lead to clinical consequences such as new antimicrobial resistance. Reflecting the similar structural folds of DHA-family transporters and their common alternating-access transport mechanism via a rocker-switch type of movement, the information on molecular recognition of substrates by MdfA offers new clues for potent therapeutics to be designed to evade extrusion by any DHA-family transporters such as QacA.

1.9 Key MFS efflux pumps in antimicrobial resistance of *S. aureus*

Antimicrobial expulsion by efflux pumps is one of the major resistance mechanisms in *S. aureus*. Most of the efflux pumps found in *S. aureus* are members of the MFS (Table 1.1). The genes encoding QacA, QacB and TetA(K) are primarily carried on plasmids whereas those encoding other MFS transporters are present in the chromosome (Table 1.1). The following sections provide an overview of well-characterised *S. aureus* MFS efflux pumps, focusing on their structural and functional aspects as well as clinical implications.

1.9.1 NorA, NorB and NorC efflux proteins

NorA, together with QacA, represent the best studied MFS efflux pumps from *S. aureus* (Lekshmi *et al.*, 2018). NorA was the first chromosomally-encoded efflux pump to be characterised in *S. aureus* (Yoshida *et al.*, 1990; Palazzotti *et al.*, 2019). Besides hydrophilic fluoroquinolones antibiotics (e.g. norfloxacin and ciprofloxacin; treatment options against *S. aureus* infections), NorA was found to be a MDR efflux pump (Neyfakh *et al.*, 1993) conferring resistance to a broad range of structurally different compounds including biocides (e.g. cetrimide, benzalkonium [BK]), dyes (e.g. ethidium, rhodamines), puromycin and chloramphenicol (Buonerba *et al.*, 2017; Zimmermann *et al.*, 2017). Therefore, NorA is of huge clinical importance. NorA is an

endogenous efflux pump (chromosomally-encoded) possessing 12 TMS with 388 amino acids and a molecular weight of 42.2 kDa (Lekshmi *et al.*, 2018). It has been shown to have modest homology (20–25% sequence identity) with plasmid-encoded tetracycline-specific efflux proteins of Gram-negative bacteria such as TetA, TetB, and TetC. Despite this homology, NorA does not confer resistance to tetracycline (Neyfakh, 1992; Schindler and Kaatz, 2016). NorA has a close bacterial homologue, Bmr efflux pump of *Bacillus subtilis*, with which it shares 44% amino acid sequence identity (Neyfakh, 1992; Piddock, 2006a). NorA has been a well-established target to develop potent efflux pump inhibitors (EPI) for the reversion of MDR in Gram-positive bacteria (Brincat *et al.*, 2011; Felicetti *et al.*, 2018; Palazzotti *et al.*, 2019). However, due to lack of a crystal structure for NorA, chemical approaches and *in silico* analyses (molecular docking studies) have been implemented to discover novel NorA efflux pump inhibitors (Costa *et al.*, 2016; Buonerba *et al.*, 2017; Felicetti *et al.*, 2017; Singh *et al.*, 2017).

NorB and NorC are other chromosomally-encoded efflux pumps in *S. aureus* which confer resistance to quinolones. NorA confers resistance to hydrophilic quinolones such as ciprofloxacin and norfloxacin, whereas NorB and NorC also confer resistance to hydrophobic quinolones such as moxifloxacin and sparfloxacin (Truong-Bolduc *et al.*, 2005; Truong-Bolduc *et al.*, 2006). These three pumps, collectively known as 'Nor efflux pumps', have broad substrate profiles that include not only quinolones but also other antimicrobials, disinfectants, and dyes (Ding *et al.*, 2008; Hooper and Jacoby, 2015). The efflux pump NorB has amino acid sequence identity with *B. subtilis* Bmr (30%) as well as *S. aureus* NorA (30%) and QacA (39%) (Truong-Bolduc *et al.*, 2006; Costa *et al.*, 2013). NorB and NorC are composed of 464 and 462 amino acid residues,

respectively (Lekshmi *et al.*, 2018) and they share 61% amino acid identity (Truong-Bolduc *et al.*, 2006; Ding *et al.*, 2008). Expression of the Nor efflux pumps in *S. aureus* is regulated by the global regulator MgrA (multiple gene regulator). MgrA appears to act as a positive regulator (activator) of *norA* expression but as a negative regulator (repressor) of *norB* and *norC* expression (Truong-Bolduc and Hooper, 2010; Truong-Bolduc *et al.*, 2012; Briaud *et al.*, 2019). Increased expression of *norB* in a mouse subcutaneous abscess model showed that NorB was important for *S. aureus* survival in abscesses, suggesting a contribution of NorB in staphylococcal pathogenesis (Truong-Bolduc *et al.*, 2014; Pasqua *et al.*, 2019).

1.9.2 TetA(K) and Tet38 efflux pumps

In *S. aureus* TetA(K) is a key drug efflux pump which is able to confer high levels of resistance to the tetracycline antibiotics (Guay and Rothstein, 1993; Ginn *et al.*, 2000). TetA(K) has 14 TMS (Guay *et al.*, 1993; Ginn *et al.*, 1997) and is closely related to chromosome-encoded TetA(L) protein of *B. subtilis* (Jin *et al.*, 2002) and Tet38 of *S. aureus* (Truong-Bolduc *et al.*, 2005). The TetA(K) and TetA(L) proteins were found to be multifunctional antiporters because they transport the cations Na⁺ and K⁺ across the membrane along with tetracycline and H⁺. This indicates that these efflux pumps play physiological functions in salt and alkali tolerance in addition to antimicrobial resistance (Wang *et al.*, 2000; Krulwich *et al.*, 2001).

Tet38 is a chromosomally encoded MFS efflux transporter that shares 46% identity with the TetA(K) protein. Tet38 mediates resistance to tetracyclines, certain fatty acids (Truong-Bolduc *et al.*, 2005) and can export fosfomycin (Truong-Bolduc *et al.*, 2018; Truong-Bolduc *et al.*, 2019), a clinically used antibiotic to target the MurA protein involved in bacterial cell wall synthesis (Fu *et al.*, 2016). The Tet38 efflux

pump contributes to *S. aureus* colonisation of skin and survival in the environment of an abscess (Truong-Bolduc *et al.*, 2014; Truong-Bolduc *et al.*, 2015). Moreover, it has recently been demonstrated that this protein is involved in the attachment and internalisation of staphylococci into host cells via interaction with host cell receptors CD36 and Toll-Like Receptor 2 (TLR-2) (Truong-Bolduc *et al.*, 2019; Truong-Bolduc *et al.*, 2021).

1.9.3 QacA multidrug efflux protein

The QacA transporter is classified within the DHA2 subfamily of MFS proteins (Paulsen *et al.*, 1996b) (www.tcdb.org). Similar to other MFS efflux pumps, QacA uses the pmf to energise the translocation of antimicrobial compounds across the cell membrane via a processive mechanism involving the exchange of two protons per a single substrate molecule (Mitchell *et al.*, 1999; Fluman *et al.*, 2014). QacA comprises 514 amino acids that have been shown to be organised into 14 TMS (Figure 1.4) based on hydrophathy studies (Rouch *et al.*, 1990) and membrane topological analyses using alkaline phosphate and β -galactosidase fusions (Paulsen *et al.*, 1996a). As noted earlier, the QacA efflux pump remains the most prevalent plasmid-encoded QAC-resistance mechanism among Gram-positive bacteria. QacA is encoded by the *qacA* gene which was the first bacterial MDR gene to be reported (Tennent *et al.*, 1985; Paulsen *et al.*, 1996b; Brown and Skurray, 2001). The *qacA* gene is carried by transmissible plasmids (Paulsen *et al.*, 1998) including multiresistance plasmids such as the β -lactamase and heavy-metal resistance plasmid pSK57 (Gillespie *et al.*, 1986) as well as pSK1-family plasmids (Lyon and Skurray, 1987; Eto *et al.*, 2019; Baines *et al.*, 2019).

While *qacA* is usually found in clinical isolates of *S. aureus* (Hassan *et al.*, 2007a; Paulsen *et al.*, 1996a; Hassan *et al.*, 2009) and coagulase-negative staphylococci such as *Staphylococcus epidermidis*, *Staphylococcus saprophyticus*, and *Staphylococcus hominis* (Leelaporn *et al.*, 1994; Teixeira *et al.*, 2010; Zhang *et al.*, 2011; Jennings *et al.*, 2015b), it has also been identified in *Enterococcus faecalis* that showed increased chlorhexidine (CH) resistance (Bischoff *et al.*, 2012). This suggests that the plasmid-born *qacA* gene can spread across bacterial genera (Wassenaar *et al.*, 2015).

1.9.3.1 Structure-function properties of QacA

Although there has been an increase in the number of X-ray structural data for 12-TMS MFS transporters, there is currently no high resolution structure available for any DHA2 member protein, including QacA, as they appear to be inherently difficult for crystallographic studies due to their extreme hydrophobicity and defiance to high-level protein overexpression and purification (Hassan *et al.*, 2009; Carpenter *et al.*, 2008; Xu *et al.*, 2006). Alternatively, structure-function analyses mainly by cysteine-scanning mutagenesis and chemical labelling techniques have been used to determine the functional importance of key amino acid residues in the recognition and transport of substrates by QacA (Hassan *et al.*, 2007a). Table 1.2 summarises the salient results of published studies that have investigated the structure-function relationships in QacA. Such studies have demonstrated that the residues in QacA are not equally important. As evidenced, specific residues have been found to be essential for either binding or transport functions of the QacA, since their substitutions with cysteine and/or other amino acids have impacted the antimicrobial resistance profile and/or efflux capacity as compared to the wild-type QacA.

Table 1.2 Key findings of amino acid substitutions in QacA reported in previous studies.

Target residues	Location	Substitutions	Findings	Ref.
Three residues in putative TMS 10 and its surrounding regions	A291T, D323A, M380T	altered to corresponding residues in QacB	An acidic residue at position 323 (D323) within TMS 10 of QacA was shown to play a critical role in conferring resistance to bivalent cations. Neutralising D323 by mutagenesis interrupted the activity of QacA against bivalent cations while retaining active efflux of monovalent cations.	(Paulsen <i>et al.</i> , 1996a)
10 prolines residues located in membrane	P73, P126, P161, P182, P211, P240, P318, P328, P331, P344	glycine, alanine, or serine	Substitution of TMS-bound proline residues in QacA, even those at conserved positions between MFS-related transporters, did not result in a profound disruption in protein expression or resistance to representative substrates tested. This indicated that such residues are not important for the structure and function of QacA.	(Hassan <i>et al.</i> , 2006a)
35 amino acid residues in putative TMS 10 and its surrounding regions	S308 to V342	cysteine	Cysteine-substitution generally did not have a remarkable effect on the expression of the mutant proteins. However, K311C, R336C, and K340C showed protein expression below or equivalent to 50% of that of the QacA wild-type level, suggesting that these basic residues may be important for protein expression, stability, and/or insertion in the cell membrane. TMS 10 was shown to extend from P309 to A334 and contain a 20-amino-acid hydrophobic core from P310 to I329. Additionally, TMS 10 was suggested to form an integral part of the bivalent substrate-binding pocket of QacA, with residues D323 and M319 directly involved in the efflux of bivalent substrates whereas only G313 was identified to be essential for the efflux of both monovalent and bivalent cations.	(Xu <i>et al.</i> , 2006)

(Continued on next page)

Table 1.2 (continued)

Target residues	Location	Substitutions	Findings	Ref.
One acidic residue in TMS 10 and a residue in TMS 12	D323, G377	cysteine, glutamic acid, aspartic acid, glutamine	Acidic substitutions for G377 restored the capacity for bivalent cation resistance to the D323C QacA mutant protein, implying that position 377 in TMS 12 participate in the binding site for bivalent cations.	(Hassan <i>et al.</i> , 2007b)
Seven tyrosine residues in QacA	Y63, Y315, Y358, Y366, Y410, Y429, Y501	alanine, phenylalanine, serine, or valine	The tyrosine residues in QacA were shown to be easily replaceable with phenylalanine, insinuating that the hydroxyl moiety of the tyrosine side-chains was not crucial for transport activity of QacA. However, a hydroxyl group at position 410 appeared to be essential for recognition of the monovalent dyes ethidium and pyronin Y. The aromaticity of residues at three positions 63, 410 and 429, was found to be functionally important for QacA-mediated transport and resistance to most representative substrates tested, indicating that these side-chains may function mechanistically in a QacA-mediated transport common to QacA substrates.	(Wu <i>et al.</i> , 2008)
Nine tryptophan residues located in membrane or within loop regions	W18, W58, W81, W149, W173, W208, W225, W241, W300	alanine, phenylalanine	Substitution of tryptophan residues in QacA did not seriously compromise QacA protein expression. Mutation of W58 to A abolished all detectable QacA-mediated resistance and transport function. Second-site suppressor mutations found four amino acid substitutions (D79N, M391I, G400D, A403T) that restored resistance and transport function of W58A mutant, indicating a conformational association between distal loops 2-3 and 12-13.	(Hassan <i>et al.</i> , 2008)
Six acidic residues in the vestibule of QacA	D34, D61, D323, E406, E407, D411	asparagine, glutamine, cysteine	The roles of six protonatable residues lining the QacA vestibule as observed by homology modelling were analysed. D34 (TMS 1) was found to be essential for recognition and transport of tetraphenylphosphonium, dequalinium and pentamidine. E407 (TMS 13) was identified to act as a protonation site in QacA needed for tetraphenylphosphonium and pentamidine transport. Furthermore, E407 was shown to be crucial as a recognition site for the transport of dequalinium.	(Majumder <i>et al.</i> , 2019)

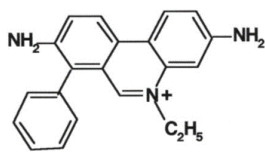
1.9.3.2 Substrate profile of QacA

QacA is able to mediate resistance to a diverse range of cationic lipophilic antimicrobial compounds belonging to different chemical classes. The one common feature of these compounds is that they are aromatic and contain a positive charge, being monovalent or bivalent cations (Figure 1.5). Monovalent cations include QACs (e.g., BK and cetrимide) and intercalating dyes (e.g., ethidium [Et] and acriflavine). Bivalent cations include diamidines (e.g., pentamidine [PE], 4',6-diamidino-2-phenylindole [DAPI]) and the biguanidines (e.g., Ch) (Mitchell *et al.*, 1998; Chitsaz and Brown, 2017). It is worth noting that QACs (from which the QacA efflux protein takes its name) account for the most prominent QacA substrates. Examples of QACs are cetrимide, BK and dequalinium (DQ), which are commonly used as antiseptics and disinfectants (Mitchell *et al.*, 1998; Xu *et al.*, 2006). Nevertheless, studies have shown that QacA does not mediate resistance to trivalent cations, neutral or anionic compounds (Mitchell *et al.*, 1998; Mitchell *et al.*, 1999; Brown and Skurray, 2001).

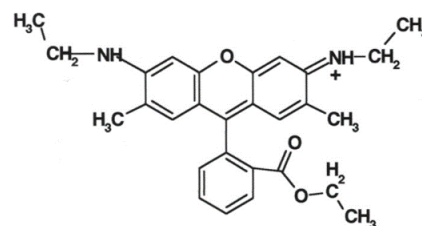
QacA exhibits significantly higher levels of resistance for a wide range of bivalent cationic substrates such as diamidines and biguanidines as opposed to its close homologue QacB. MIC analysis of diamidine compounds with structural variations indicated that QacA protein interacts with bivalent cationic substrates irrespective of the interamidine linkage, side-chain alterations, or the placement of the amidine group on the aromatic ring (Mitchell *et al.*, 1998). Previous fractional inhibitory concentration analysis (FIC) of various combinations of two QacA substrates indicated that QacA confers resistance to structurally dissimilar cationic compounds

Monovalent cations**Dyes**

Acridine yellow
 Acriflavine
 Crystal violet
 DiOC3
 Ethidium
 Proflavine
 Pyronin Y
 Quinaldine red
 Rhodamine 6G
 Safranin O



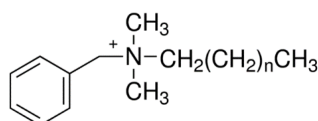
Ethidium



Rhodamine 6G

Quaternary ammonium compounds

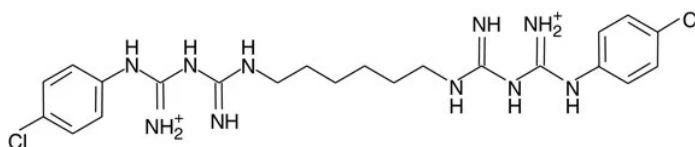
Benzalkonium
 Cetylpyridinium
 Cetyltrimethylammonium
 Dimethylaminostyryl-1-ethylpyridinium
 Tetraphenylarsonium
 Tetraphenylphosphonium
 TMA-DPH
 Triphenylmethylphosphonium



Benzalkonium

Bivalent cations**Biguanidines**

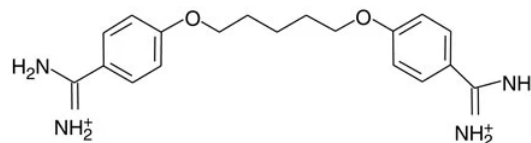
Chlorhexidine



Chlorhexidine

Diamidines

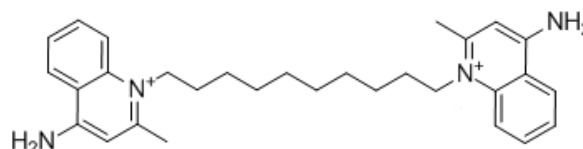
Amicarbalide
 DAPI
 Dibromopropamide
 Diamidinodiphenylamine
 Diminazene
 Hexamidine
 Pentamidine
 Phenamidine
 Propamidine
 Stilbamidine



Pentamidine

Guanylhyaones

1 i-39/JC-1-134
 1 a-62/JC-1-127



Dequalinium

Quaternary ammonium compounds

Dequalinium

Figure 1.5 Substrates of multidrug efflux protein QacA.

QacA confers resistance to more than 30 structurally diverse substrates which can be categorised as monovalent or bivalent cations. Chemical structures for the representative QacA substrates that were used in this study are presented. Figure modified from Brown and Skurray (2001).

via the same antiport mechanism (Mitchell *et al.*, 1998). Transport kinetic analyses of monovalent and bivalent fluorescent substrates revealed that QacA has a high affinity binding mechanism for the recognition of bivalent cationic substrates while QacB lacks such characteristics (Mitchell *et al.*, 1999). The broad substrate specificity of the QacA, like other MDR transport proteins, raises the question whether this protein has a common binding site or multiple unique binding sites for individual substrates. Previous studies have shown that QacA-mediated efflux of the monovalent cation Et is competitively inhibited by other monovalent cations and non-competitively inhibited by bivalent cations (Mitchell *et al.*, 1999). This suggests that monovalent substrates of QacA are likely to either share a common binding site or have overlapping binding sites, whereas bivalent substrates bind at a distinct site(s) (Brown and Skurray, 2001). In addition to cationic antimicrobials, QacA was shown to provide resistance to thrombin-induced platelet microbicidal protein-1 (tPMP-1), a rabbit-derived cationic antimicrobial peptide (Yeaman *et al.*, 1997; Kupferwasser *et al.*, 1999). QacA-dependent tPMP-1 resistant *S. aureus* strains were found to survive and proliferate within rabbit model of endocarditis. Moreover, tPMP resistance was shown to be an important *S. aureus* virulence factor correlated with endocarditis in humans (Kupferwasser *et al.*, 1999; Bayer *et al.*, 1998; Nawrocki *et al.*, 2014). Of note, the presence of QacA transporter in the cell membrane of *S. aureus* strains has been found to be linked to increased membrane fluidity in comparison to parental strain or strains containing QacB or QacC (Bayer *et al.*, 2000; Bayer *et al.*, 2006; Kohler *et al.*, 2019).

1.9.3.3 Regulation of *qacA* expression

The expression of *qacA* has been shown to be inducible *in vivo* by the addition of QacA substrates. These substrates have been demonstrated to directly bind to a regulatory protein known as QacR, which represses expression of *qacA* (Grkovic *et al.*, 1998). QacR belongs to the TetR family of transcriptional regulators. The *qacR* gene is located upstream of *qacA*, and is divergently transcribed to *qacA*. QacR acts as a repressor of *qacA* expression by specific binding to the 28-base pair inverted repeat 1 (IR1) operator which overlaps the *qacA* promoter site, thereby preventing *qacA* transcription (Grkovic *et al.*, 2001). Induction of *qacA* expression occurs when QacA substrates bind to QacR, inducing a conformational change in the protein such that QacR releases from the promoter region allowing transcription of *qacA* to proceed (Grkovic *et al.*, 1998; Brown and Skurray, 2001; Schumacher *et al.*, 2002). QacR was the first crystallised multidrug-binding protein in complex with multiple structurally different substrates which are also QacA substrates (Schumacher *et al.*, 2001). Crystal structures for QacR have shown that this protein has a single extended and multifaceted drug-binding pocket which contains two separate but overlapping binding sites referred to as “rhodamine 6G binding pocket” and the “ethidium pocket”. A remarkable feature of the QacR substrate-binding pocket is the existence of several ‘mini-pockets’ within the larger substrate-binding site, which is also anticipated for other multidrug-binding proteins including QacA (Schumacher *et al.*, 2001; Schumacher *et al.*, 2004).

The drug-binding pocket of QacR is comprised of four acidic (E57, E58, E90, and E120) and multiple aromatic and polar residues that can accommodate a wide range of hydrophobic cations (Murray *et al.*, 2004; Schumacher *et al.*, 2001; Grkovic *et al.*,

2003; Peters *et al.*, 2011). The presence of acidic residues serve to neutralise the positive charges of substrates (Schumacher *et al.*, 2001; Schumacher *et al.*, 2004). Furthermore, structures of the glutamine-substituted QacR E90 and E120 mutant proteins in complex with structurally dissimilar substrates have indicated that the role of the binding pocket acidic residues of QacR is primarily to attract and steer cationic substrates into the best available positions within the binding pocket (Peters *et al.*, 2011). Moreover, the redundancy of glutamates in the QacR multidrug-binding pocket allows the loss of anyone of them with little effect on function, underscoring the plasticity and promiscuity of the multidrug-binding pocket as a common feature in multidrug-binding proteins (Peters *et al.*, 2008; Peters *et al.*, 2011) such as QacA.

1.9.3.4 Prevalence of *qacA* in clinical isolates of *S. aureus*

In clinical practice, disinfectants (for disinfection of inanimate surfaces) and antiseptics (for disinfection of living tissues such as hand washing and skin decolonisation prior to invasive procedures) are extensively used in hospitals to prevent spread of nosocomial pathogens (Wang *et al.*, 2008a; Gebel *et al.*, 2013). Studies have investigated the frequency of disinfectant and antiseptic resistance genes carried by *S. aureus* isolated from clinical settings in different regions of the world. Prevalence of *qacA* among *S. aureus* clinical isolates fluctuates depending on the geographic location, varying from 10 to 80% (Zaki *et al.*, 2019). Carriage of *qacA* has been reported to be as high as 73.9% in Australia (Baines *et al.*, 2019), 63% in Europe (Mayer *et al.*, 2001), 8.3%–26.3% in the UK (Smith *et al.*, 2008; Vali *et al.*, 2008), and 33%–61% in Asia (Wang *et al.*, 2008b; Sheng *et al.*, 2009; Wang *et al.*, 2008a). An increasing trend in *qacA* prevalence has been observed in the U.S. and Asian countries (LaBreck *et al.*, 2020), establishing the relevance of this resistance

determinant. Varying *qacA* prevalence across studies is due to different factors, including the number of isolates screened in each study or the type of biocides used regularly, exerting different selective pressures on *S. aureus* isolates in each region (Smith *et al.*, 2008). As evidenced in these studies and others (Jennings *et al.*, 2015b), increasing use of disinfectants and antiseptics has raised concerns about the emergence of resistance to biocides in *S. aureus* at a quite alarming rate both in medical settings and in the community (Zhang *et al.*, 2011; Jennings *et al.*, 2015b).

1.9.3.5 QacB

QacB is a closely related paralog of QacA (Paulsen *et al.*, 1996a). Similar to *qacA*, expression of the *qacB* gene is regulated by QacR (Grkovic *et al.*, 2001). However, whereas QacA mediates resistance to both monovalent and bivalent cationic compounds, QacB only confers resistance to monovalent cations. It has been postulated that *qacA* evolved from *qacB* in response to the extensive use of bivalent cations such as CH in hospital environments (Paulsen *et al.*, 1998). Sequence analysis found that the *qacA* and *qacB* genes differ by only seven nucleotides (Paulsen *et al.*, 1996a; Mitchell *et al.*, 1999). Mutagenesis studies provided evidence that the wider substrate specificity of QacA in comparison to QacB is due primarily to the presence of an acidic residue (aspartic acid) at position 323 within TMS 10 of QacA (Table 1.2), while an uncharged alanine residue is available at the same position in QacB. D323 is critically required for conveying resistance to bivalent cations which implies that this residue may form part of the binding site(s) for bivalent cations in QacA (Paulsen *et al.*, 1996a; Majumder *et al.*, 2019).

1.10 QacC: Another important member of Qac efflux system in *S. aureus*

Apart from QacA and QacB proteins, the QacC efflux pump system also mediates QAC resistance in clinical isolates of *S. aureus* and other staphylococci (Leelaporn *et al.*, 1994; Paulsen *et al.*, 1996c; Bay *et al.*, 2008). Unlike QacA/B, QacC belongs to the SMR family of transporter proteins (Lyon and Skurray, 1987; Wassenaar *et al.*, 2015). The *S. aureus* QacC multidrug transporter was the first SMR transporter to be identified and characterised in Gram-positive bacteria (Littlejohn *et al.*, 1991; Paulsen *et al.*, 1995). QacC (107 amino acids) is composed of four TMS (Paulsen *et al.*, 1995) and forms dimers in the bacterial membrane (Littlejohn *et al.*, 1991; Poget *et al.*, 2010). Similar to the prototypical SMR protein EmrE from *E. coli*, QacC has been proposed to function as a homo-oligomer (Paulsen *et al.*, 1996b; Putman *et al.*, 2000; Bay and Turner, 2016). QacC expression is not modulated by a transcriptional regulator (Wassenaar *et al.*, 2015). There is no high-resolution structure yet available for QacC. Mutagenesis and functional assessments have shown that E13 residue in TMS 1 of QacC, is essential for resistance to BK. This residue, which is highly conserved in SMR members, is part of the both substrate and proton binding site of QacC (Grinius and Goldberg, 1994). In addition, highly conserved residues Y59 and W62 in TMS 3 were found to be functionally important as substitutions resulted in a significant reduction in the ability of QacC to confer resistance to BK and other compounds (Paulsen *et al.*, 1995).

The *qacC* gene (also known as *smr*) (Bay *et al.*, 2008; LaBreck *et al.*, 2020), can be carried on small rolling-circle replicating plasmids present in both *S. aureus* and coagulase-negative *Staphylococcus* species (Leelaporn *et al.*, 1995; Wassenaar *et al.*,

2016). In addition, *qacC* is found on large low-copy-number multiresistance plasmids and its promoter is known to differ between these plasmids and rolling-circle replicating plasmids (LaBreck *et al.*, 2020). Similar to *qacA*, *qacC* confers high resistance to some of the QACs (BK and ceftrimide) in staphylococcal strains (Littlejohn *et al.*, 1992; Paulsen *et al.*, 1995), but it does not provide resistance against CH (Horner *et al.*, 2012; Baines *et al.*, 2019). It has been shown that *S. aureus* isolates carrying both *qacA* and *qacC* have the potential to survive exposure to a higher dose of QACs compared to those carrying only *qacA* (Leelaporn *et al.*, 1994; Smith *et al.*, 2008). Such *S. aureus* strains with elevated resistance to QACs can lead to infections in the hospital necessitating infection control measures to prevent their transmission (Smith *et al.*, 2008).

1.11 MepA: The only MATE efflux system encoded on the *S. aureus* chromosome

The efflux pump MepA belongs to the MATE family of transport proteins. It is the first and the only MATE transporter found in the chromosome of *S. aureus*. MepA (451 amino acids) has 12 TMS and presents 21% amino acid identity to the MATE transporter NorM from *Vibrio parahaemolyticus* (Kaatz *et al.*, 2005; Costa *et al.*, 2013; Schindler *et al.*, 2013b). MepA is associated with a MDR phenotype in clinical *S. aureus* isolates, mediating low-level resistance to several monovalent and bivalent biocides and dyes (Huet *et al.*, 2008), as well as to tigecycline (Fang *et al.*, 2020), a glycylicycline antibiotic. Like NorA, MepA is an important fluoroquinolone efflux system in *S. aureus* that expels hydrophilic fluoroquinolone antibiotics such as norfloxacin and ciprofloxacin. Nonetheless, these antibiotic compounds are weak substrates of MepA but strong substrates for NorA (Kaatz *et al.*, 2005; McAleese *et*

al., 2005; Schindler *et al.*, 2013b). *In silico* modelling of MepA has revealed a probable expansive central binding cavity that represents a substrate translocation pathway similar to other multidrug binding proteins, such as AcrB and QacR. Site-directed mutagenesis studies have shown that residues S81, E156, A161, D183, M291, and A302 within the cavity are functionally important (Schindler *et al.*, 2013b).

Expression of *mepA* is regulated by MepR, a member of MarR family of transcriptional repressors encoded immediately upstream of *mepA*. MepR dimers binds to inverted repeats contained within operator regions upstream of *mepR* and *mepA*. The *mepR* operator contains one inverted repeat, whereas the *mepA* operator contains two such MepR binding sites. Thus, MepR reveals higher affinity binding towards the *mepA* operator site (Kaatz *et al.*, 2006). MepR is substrate responsive and represses both *mepA* and its own gene *mepR*. In the presence of MepA substrates, MepR binding to each of the *mepA* and *mepR* operator sites is essentially abrogated in a different manner as a result of conformational change in MepR, with a markedly reduced binding affinity for the *mepA* operator site (Kaatz *et al.*, 2005; Kaatz *et al.*, 2006; Birukou *et al.*, 2014).

1.12 The role of *S. aureus* efflux pumps in biocide resistance

Biocides are widely used as disinfectants, antiseptics and preservatives in healthcare settings, industry (food and cosmetics) and agriculture to eliminate or inhibit the risk of infection or spoilage (Vijayakumar and Sandle, 2019; Weber *et al.*, 2019). The use of biocides, in particular as cleaning products, in homes and high-risk public spaces such as schools, workplaces, health care facilities and food service has even increased substantially during the ongoing COVID-19 pandemic. Such indiscriminate use of

biocides creates conditions to accelerate development of multidrug resistant bacteria and it is therefore anticipated to worsen the biocide resistance threat in the coming year (Zheng *et al.*, 2020; Mahoney *et al.*, 2021). Since biocides are not utilised for treating in-host infections, the regulations for the growing use of these antimicrobials are not as strict as those applied to antibiotics (Blanco *et al.*, 2016). Nonetheless, the excessive use of biocides has raised concerns as it can lead to selection of bacterial strains with an increased resistance to these compounds and potentially also to cross-resistance to antibiotics (Buffet-Bataillon *et al.*, 2012; Hardy *et al.*, 2018). QACs (e.g. BK) and CH are common biocides which are discussed subsequently.

QACs have been constantly used as the leading biocides in medical, industrial, agricultural, and household settings for nearly a century (Jennings *et al.*, 2015b). Although other alternative biocides such as hydrogen peroxide and bleach exist, their use for disinfection and sanitisation is limited due to their relatively short half-life and corrosive nature. QACs represent one of the most popular and effective disinfectants with robust chemical stability, simple preparation and versatile incorporation into consumer products. When adsorbed onto the bacterial cell membrane, the amphiphilic nature of QACs results in cell lysis and bacterial death (Jennings *et al.*, 2015a). It is estimated that approximately 500 000 tons of commercial QACs are used annually in a host of consumer products (Mitchell *et al.*, 2015). Therefore, QACs inevitably leach into the environment particularly soil and wastewater treatment facilities which host microbial communities with enormous biodiversity. Given their high stability, accumulation of QACs in the environment is of obvious concern. Unfortunately, repeated exposure of bacterial populations to diluted, sub-lethal doses of QACs in the environment can drive the development of resistance against

QACs (Jennings *et al.*, 2015b; Mulder *et al.*, 2018). In the past three decades the identification of bacterial isolates with QAC resistance genes has increased rapidly (Forman *et al.*, 2016). Although numerous molecular mechanisms, including physiological changes in bacterial lipid membrane can give rise to QAC resistance, the most prominent method of resistance originates from the production of efflux pumps which extrude various QAC structures from bacterial cells (Mitchell *et al.*, 2015). BK is a known QAC which is frequently used in broad-spectrum disinfectant solutions and as a preservative in personal care products (Pereira and Tagkopoulos, 2019; Lee *et al.*, 2020; Wang *et al.*, 2020a).

CH, a cationic bisbiguanide compound, is of high importance in preventing the spread of pathogens. It can exert an antimicrobial effect via damaging the bacterial plasma membrane and subsequent leakage of cytoplasmic material (Cieplik *et al.*, 2019). CH is widely used globally as antiseptic and disinfectant in the community and hospitals, with applications ranging from over-the-counter soaps and mouthwashes to pre-surgical skin decontamination (Hassan *et al.*, 2019; Zamudio *et al.*, 2019; LaBreck *et al.*, 2020). Notably, however, the use of CH has led to the emergence of bacterial strains, including *S. aureus*, that are resistant to CH (Kampf, 2016). Prevalence studies in staphylococci report the reduction of susceptibility to CH due to the increased presence of efflux-mediated resistance genes in particular *qacA* and its associated co-resistance to other antimicrobial agents (Horner *et al.*, 2012; do Vale *et al.*, 2019).

Among the various resistance mechanisms, efflux pumps contribute as a major mechanism for increased biocide tolerance of bacteria (Blanco *et al.*, 2016). Contrary to Gram-negative bacteria, Gram-positive bacteria such as *S. aureus* lack an outer membrane, making them markedly more susceptible to QACs that target the

bacterial cell membrane. However, efflux pumps act as the first-line of defence against QACs (Costa *et al.*, 2013; Jennings *et al.*, 2015b). As discussed above, in *S. aureus* the antiporter proteins NorA, QacA, QacC and MepA are known to impart increased resistance to a broad range of ubiquitously used biocides such as BK and CH. While NorA and MepA proteins are encoded by the chromosome of *S. aureus* and not easily donated to another bacteria (Schindler *et al.*, 2013b; Costa *et al.*, 2019), QacA and QacC proteins are encoded by a variety of conjugative and nonconjugative plasmids and are readily transmissible (Firth *et al.*, 1993; Berg *et al.*, 1998; LaBreck *et al.*, 2018). A recent study using a panel of isogenic *S. aureus* strains has shown that concomitant presence of NorA, QacA and QacC can give rise to the highest level of antiseptic resistance. Moreover, QacA alone could confer the highest level of resistance of an individual pump compared to NorA and QacC efflux pumps (LaBreck *et al.*, 2020).

1.13 Cross-resistance of biocides and antibiotics mediated by multidrug efflux pumps

Apart from biocide-tolerant strains, a matter of greater concern is that biocide resistance genes (*qacA* and *qacC*) are often co-localised with antibiotic resistance determinants on multidrug resistance plasmids (Laxminarayan, 2014; Jennings *et al.*, 2015b; Hong *et al.*, 2019). A number of studies provided evidence for the correlation between widespread use of biocides, particularly BK and CH, and cross-resistance to antibiotics in bacteria including *S. aureus* (Blanco *et al.*, 2016; Paul *et al.*, 2019; Lee *et al.*, 2020). For example, BK-resistant *S. aureus* isolates harbouring plasmids with *qacA* gene were found to be less sensitive to multiple antibiotics such as penicillin, oxacillin, cefazolin and ofloxacin compared to BK-sensitive ones (Pereira and

Tagkopoulos, 2019). Another study demonstrated that exposure of *S. aureus* to subinhibitory concentrations of CH could develop cross-resistance to cefepime and tetracycline (Wu *et al.*, 2016).

It has been shown that preexposure to BK could subsequently increase resistance to CH in *S. aureus* strains carrying *norA* and/or *qacA* (LaBreck *et al.*, 2020). Given that BK exists in many personal-care products such as shampoos, conditioners, soaps, lotions and makeup, it is no wonder that long-term use of such products can prime bacterial cells for enhanced tolerance to a CH preoperative surgical skin preparation. This could be a risk factor associated with surgical site infection (LaBreck *et al.*, 2020). Therefore, greater antiseptic stewardship is needed for addressing the issue of cross-resistance between biocides and antibiotics.

1.14 Modulation (inhibition) of *S. aureus* efflux pumps

The upsurge of MDR bacteria, in particular *S. aureus*, substantially diminishes the effectiveness of the existing antimicrobial arsenal and therefore increases the rate of failure in prevention and/or treatment of infections caused by such bacteria (Section 1.1). Active extrusion of antimicrobial agents via efflux pumps is a major mechanism of intrinsic and acquired bacterial resistance (Li *et al.*, 2015). There has been immense interest in developing EPIs to be used in conjunction with existing antimicrobials (adjuvant strategy) to restore their activity against MDR bacterial infection; thereby reducing the emergence of resistant mutant strains (Handzlik *et al.*, 2013; Opperman and Nguyen, 2015; Wright, 2016; Wang *et al.*, 2016).

Basically, EPIs are often designed to resemble substrates and have the ability to bind to the same site impairing the proper binding of substrates via a competitive

mechanism. Additionally, EPIs can bind at an allosteric site that precludes the efflux pump from undergoing the conformational changes required for transport (AlMatar *et al.*, 2020). The wide distribution of efflux pumps associated with high emergence of MDR (Handzlik *et al.*, 2013; Jang, 2016) has triggered considerable efforts in recent years to discover EPIs against *S. aureus* in particular focusing on natural and synthetic inhibitors of the clinically-important NorA efflux pump (Schindler *et al.*, 2013; Handzlik *et al.*, 2013; Jang, 2016; Wang *et al.*, 2016). However, the crystal structure of NorA and its precise mechanism of binding and transport of diverse compounds still remains unsolved (Section 1.9.1). This has hampered a structure-based approach to rationally design potent EPIs for this transporter (Durães *et al.*, 2018; Lamut *et al.*, 2019). Although several EPIs have been found to inhibit *S. aureus* efflux pumps, no EPI has been approved for clinical use to treat *S. aureus* infections mainly due to cytotoxicity in human cells (Seukep *et al.*, 2020).

Crystal structures and computational models, together with detailed biochemical and microbiological analyses, are able to provide valuable information about EPI molecules that can specifically interact with NorA and other MDR efflux pumps in *S. aureus*. This approach holds promise for development of clinically useful EPIs for improving the treatment of bacterial infections (Kourtesi *et al.*, 2013; AlMatar *et al.*, 2020). More information about EPIs will be discussed in Chapter 6.

1.15 Scope of this thesis

Alarming, widespread use of biocides such as BK and CH for infection prevention in hospitals and the community has led to appearance/maintenance of efflux-mediated resistance in bacteria including *S. aureus*. The QacA efflux pump is a major

contributor to biocide resistance and is quite widespread among clinical isolates of *S. aureus*, being easily transferred to other bacteria through transmissible plasmids. Furthermore, QacA plays a crucial role in antibiotic cross- and co-resistance in both community and healthcare environments which poses public health challenges worldwide.

Despite accumulating knowledge of MFS transport proteins, currently detailed understanding of the molecular structure and transport mechanisms operating within DHA2 members of the MFS transporters such as QacA is sorely lacking and required to help combat their efflux activity. Therefore, the broad aim of the studies presented in this thesis was to expand our knowledge about the structure and function in a DHA2 transporter by conducting a range of molecular, biochemical and computational analyses of the QacA multidrug transporter. Specifically, the thesis focused on determining the functional and/or structural importance of amino acid residues in TMS 12 and its flanking loops as well as the topology of this region of QacA. Moreover, it aimed to derive a structural model for QacA to identify its binding pockets for selected substrates by combining site-directed mutagenesis data and docking studies.

Mutagenic studies are extremely useful for analysing the activity of transport proteins. In particular, site-directed cysteine-scanning mutagenesis can provide details of the functional importance and solvent accessibility of each targeted amino acid residue. Although TMS 12 of QacA has previously been suggested to be connected with the recognition of bivalent antimicrobial substrates, detailed roles in substrate binding and transport played by individual residues within this TMS remain

unknown. Moreover, the exact boundaries of TMS 12 and the microenvironment of each residue within the QacA protein are elusive.

In the studies described in this thesis, 38 residues within or flanking the putative TMS 12 of QacA were individually replaced with cysteine. The constructed mutants were comprehensively analysed for their resistance profiles and transport activities against representative antimicrobial substrates. The results aided in identification of residues important for substrate binding and/or translocation of QacA. Furthermore, determination of the solvent accessibility of each amino acid position allowed for the refinement of the QacA topology.

Finally, the spatial arrangement of TMS 12 in QacA was evaluated by developing a full-length QacA 3D model guided by the structure of distantly-related 14-TMS MFS transporters of POT family members. By spatial overlaying of functionally important residues identified here, and in previous studies, onto the predicted QacA model, putative substrate interaction pockets for BK and CH were formulated. Additionally, molecular docking studies of QacA revealed the putative substrate-binding pockets of six selected antimicrobials.

Overall, the results presented in this study have advanced our understanding about structure-function relationships in QacA and provided new insights into the architectural features of substrate-binding pockets in this multidrug transporter. More generally, such information could be used in the rational design of efflux pump inhibitors to efficiently hamper the QacA efflux process.

CHAPTER 2
MATERIALS AND METHODS

2.1 Chemicals, solutions and buffers

Stock solutions of buffers and reagents used in this study are listed in Table 2.1. Final concentrations of reagents in solution are given. Unless otherwise noted, all chemicals were of reagent grade and purchased from Sigma. Sterile Milli-Q water was used to prepare all buffers and solutions. Powdered compounds were dissolved according to the manufacturers' instructions. Stock solution of carbonyl-cyanide *m*-chlorophenyl hydrazone (CCCP) was prepared at 1 mg/mL in ethanol. Solutions were sterilised, when needed, by either autoclaving at 121°C for 15 min or by passaging through a 0.22 µm filter unit (Sartorius Stedim, Germany).

2.2 Bacterial strains and plasmids

The bacterial strains used in the experiments, along with their relevant genetic characteristics, are listed in Table 2.2. The plasmids used in this study, along with their relevant properties and source descriptions, are listed in Table 2.3.

2.3 Bacterial culture media, growth conditions and storage

The *E. coli* strain DH5α was used as the host for plasmid propagation during routine genetic manipulations/cloning procedures and functional analyses. The *E. coli* strain TOP10 was used as the expression strain for overproduction of QacA. *E. coli* cells were grown in Luria-Bertani (LB) broth medium (tryptone, 10 g/L; yeast extract, 5 g/L; NaCl, 10 g/L, pH=7.5) at 37°C for 16 hours with shaking at 200 revolutions per minute (rpm). Ampicillin was added to the LB broth to a final concentration of 100 µg/mL for plasmid selection where required. Mueller-Hinton (MH) medium used in minimum inhibitory concentration (MIC) assays were prepared according to the manufacturer's instructions (Oxoid, UK).

Table 2.1 Buffers and solutions

Buffer/solution	Composition
Bead wash buffer	20 mM Tris HCl (pH 8.0), 10% (v/v) glycerol, 0.1% (w/v) n-dodecyl β -D-maltoside (DDM), 20 mM imidazole (pH 8.0)
Blocking buffer	10% (w/v) skim milk power in Tris-buffered saline with 0.1% Tween-20 (TTBS)
Coomassie staining solution	50% (v/v) methanol, 10% (v/v) glacial acetic acid, 15% (w/v) Coomassie Brilliant Blue R-250
Coomassie destaining solution	25% (v/v) methanol, 10% (v/v) glacial acetic acid
Crushing buffer	0.02 M Tris-HCl (pH 7), 10% (v/v) glycerol, 0.3 M NaCl
Elution buffer	20 mM Tris-HCl (pH 7.5), 10% (v/v) glycerol, 400 mM imidazole, 0.1 % (w/v) DDM
GelRed staining solution (3X)	Per 100 mL: 30 μ L of GelRed nucleic acid gel stain and 10 mL 1 M NaCl in Milli-Q water
HEPES buffer	1 M HEPES, pH 7.0 with NaOH
Membrane resuspension buffer	20 mM Tris-HCl (pH 7.5), 10% (v/v) glycerol, 1% (w/v) DDM
NEM-quenching buffer	50 mM Tris HCl (pH 8.0), 20 mM N-ethylmaleimide (NEM), 10% (v/v) glycerol
Resolving SDS-PAGE gel (10%)	3.8 mL of Milli-Q water, 3.4 mL of 30% (v/v), acrylamide mix, 2.6 mL of 1.5 M Tris HCl (pH 8.8), 100 μ l of 10% (v/v) sodium dodecyl sulphate (SDS), 100 μ l of 10% (v/v) ammonium persulphate, 10 μ l of N,N,N', N' – tetramethylethylene diamine (TEMED)

(Continued on next page)

Table 2.1 (continued)

Buffer/solution	Composition
SDS-PAGE running buffer (10X)	0.25 M Tris free base (pH 8.3), 1.92 M glycine, 1% (w/v) SDS
SDS-PAGE sample buffer (4X)	250 mM Tris-HCl (pH 6.8), 5% (v/v) β -mercaptoethanol, 10% (w/v) SDS, 40% (v/v) glycerol, 0.4% (w/v) bromophenol blue
Stacking SDS-PAGE gel (4%)	1.25 mL of 0.5 M Tris-HCl (pH 6.8), 650 μ l of 30% (v/v) acrylamide, 50 μ l of 10% (v/v) SDS, 50 μ l of 10% (v/v) ammonium persulphate, 5 μ l of TEMED and 3 mL of dH ₂ O
TAE buffer (50X)	24.2% (w/v) Tris free base, 5.71 (v/v) glacial acetic acid, 50 mM ethylenediamine-tetraacetic acid (EDTA)
Transfer buffer (10X)	25 mM Tris free base, 192 mM glycine, 20% (v/v) methanol
TBS (20X)	0.4 M Tris-HCl (pH 7.5), 3 M NaCl
TTBS	150 mM NaCl, 10 mM Tris-HCl (pH 7.5), 0.1% (v/v) tween
Transformation Buffer I	100 mM potassium chloride, 50 mM manganese(II) chloride tetrahydrate, 30 mM potassium acetate, 10 mM calcium chloride dihydrate, and 15% (v/v) glycerol (pH 5.8)
Transformation Buffer II	10 mM 4-morpholinepropanesulfonic acid (MOPS), 10 mM potassium chloride, 75 mM calcium chloride and 15% (v/v) glycerol (pH 6.5)

Table 2.2 Bacterial strains used in this study

Strain	Genotype	Reference/Source
<i>E. coli</i> DH5 α	<i>supE44</i> Δ <i>lacU169</i> (ϕ 80 <i>lacZ</i> Δ M15) <i>hsdR17</i> <i>recA1</i> <i>endA1</i> <i>gyrA96</i> <i>thi-1</i> <i>relA1</i>	(Hanahan, 1983)
<i>E. coli</i> TOP10	<i>mcrA</i> , Δ (<i>mrr-hsdRMS-mcrBC</i>), Δ <i>lacX74</i> , <i>deoR</i> , <i>recA1</i> , <i>araD139</i> Δ (<i>ara-leu</i>)7697, <i>galK</i> , <i>rpsL</i> , <i>endA1</i> , <i>nupG</i>	Invitrogen

Table 2.3 Plasmids used in this study

Plasmids	Relevant features ^a	References
pBluescript II SK (pBS)	pUC-based protein expression vector containing the <i>T7</i> promoter; Amp ^R	Stratagene
pBAD	pUC-based protein expression vector containing the <i>araBAD</i> promoter; Amp ^R	(Guzman <i>et al.</i> , 1995)
pSK7201 (pBSQacA)	pBluescript II SK containing codon optimised <i>qacA</i> cloned into the <i>EcoRI</i> and <i>PstI</i> restriction sites, carrying a C-terminal 6xHis-tag; Amp ^R	(Xu <i>et al.</i> , 2006)
pSK7128	pBAD containing codon optimised <i>qacA</i> cloned into the <i>NcoI</i> and <i>XbaI</i> restriction sites, carrying a C-terminal 6xHis-tag; Amp ^R	(Hassan <i>et al.</i> , 2009)
pSK7122	pBAD containing <i>tetA(K)</i> cloned into the <i>NcoI</i> and <i>XbaI</i> restriction sites, carrying a C-terminal His6 tag; Amp ^R	(Hassan <i>et al.</i> , 2009)
pSK7200	P309C <i>qacA</i> derivative of pSK7201, used as a control in fluorescein maleimide reactivity assays; Amp ^R	(Xu <i>et al.</i> , 2006)
pBSQacA/G361C	G361C <i>qacA</i> derivative of pSK7201; Amp ^R	This study
pBSQacA/H362C	H362C <i>qacA</i> derivative of pSK7201; Amp ^R	This study
pBSQacA/P363C	P363C <i>qacA</i> derivative of pSK7201; Amp ^R	This study

(Continued on next page)

Table 2.3 (continued)

Plasmids	Relevant features ^a	References
pBSQacA/L364C	L364C <i>qacA</i> derivative of pSK7201; Amp ^R	This study
pBSQacA/S365C	S365C <i>qacA</i> derivative of pSK7201; Amp ^R	This study
pBSQacA/Y366C	Y366C <i>qacA</i> derivative of pSK7201; Amp ^R	This study
pBSQacA/S367C	S367C <i>qacA</i> derivative of pSK7201; Amp ^R	This study
pBSQacA/T368C	T368C <i>qacA</i> derivative of pSK7201; Amp ^R	This study
pBSQacA/M369C	M369C <i>qacA</i> derivative of pSK7201; Amp ^R	This study
pBSQacA/A370C	A370C <i>qacA</i> derivative of pSK7201; Amp ^R	This study
pBSQacA/L371C	L371C <i>qacA</i> derivative of pSK7201; Amp ^R	This study
pBSQacA/A372C	A372C <i>qacA</i> derivative of pSK7201; Amp ^R	This study
pBSQacA/L373C	L373C <i>qacA</i> derivative of pSK7201; Amp ^R	This study
pBSQacA/I374C	I374C <i>qacA</i> derivative of pSK7201; Amp ^R	This study
pBSQacA/L375C	L375C <i>qacA</i> derivative of pSK7201; Amp ^R	This study
pBSQacA/V376C	V376C <i>qacA</i> derivative of pSK7201; Amp ^R	This study
pBSQacA/A378C	A378C <i>qacA</i> derivative of pSK7201; Amp ^R	This study
pBSQacA/A378V	A378V <i>qacA</i> derivative of pSK7201; Amp ^R	This study

(Continued on next page)

Table 2.3 (continued)

Plasmids	Relevant features ^a	References
pBSQacA/A378V-A157G	A378V-A157G <i>qacA</i> derivative of pSK7201; Amp ^R	This study
pBSQacA/G379C	G379C <i>qacA</i> derivative of pSK7201; Amp ^R	This study
pBSQacA/M380C	M380C <i>qacA</i> derivative of pSK7201; Amp ^R	This study
pBSQacA/A381C	A381C <i>qacA</i> derivative of pSK7201; Amp ^R	This study
pBSQacA/S382C	S382C <i>qacA</i> derivative of pSK7201; Amp ^R	This study
pBSQacA/L383C	L383C <i>qacA</i> derivative of pSK7201; Amp ^R	This study
pBSQacA/A384C	A384C <i>qacA</i> derivative of pSK7201; Amp ^R	This study
pBSQacA/V385C	V385C <i>qacA</i> derivative of pSK7201; Amp ^R	This study
pBSQacA/A386C	A386C <i>qacA</i> derivative of pSK7201; Amp ^R	This study
pBSQacA/S387C	S387C <i>qacA</i> derivative of pSK7201; Amp ^R	This study
pBADQacA/S387C	S387C <i>qacA</i> derivative of pSK7128; Amp ^R	This study
pBSQacA/A388C	A388C <i>qacA</i> derivative of pSK7201; Amp ^R	This study
pBSQacA/L389C	L389C <i>qacA</i> derivative of pSK7201; Amp ^R	This study
pBSQacA/I390C	I390C <i>qacA</i> derivative of pSK7201; Amp ^R	This study

(Continued on next page)

Table 2.3 (continued)

Plasmids	Relevant features ^a	References
pBSQacA/M391C	M391C <i>qacA</i> derivative of pSK7201; Amp ^R	^b
pBSQacA/L392C	L392C <i>qacA</i> derivative of pSK7201; Amp ^R	This study
pBSQacA/E393C	E393C <i>qacA</i> derivative of pSK7201; Amp ^R	^b
pBSQacA/T394C	T394C <i>qacA</i> derivative of pSK7201; Amp ^R	This study
pBSQacA/P395C	P395C <i>qacA</i> derivative of pSK7201; Amp ^R	This study
pBSQacA/T396C	T396C <i>qacA</i> derivative of pSK7201; Amp ^R	This study
pBSQacA/S397C	S397C <i>qacA</i> derivative of pSK7201; Amp ^R	This study
pBSQacA/K398C	K398C <i>qacA</i> derivative of pSK7201; Amp ^R	This study
pBSQacA/A399C	A399C <i>qacA</i> derivative of pSK7201; Amp ^R	This study
pBSQacA/N401	N401 <i>qacA</i> derivative of pSK7201; Amp ^R	This study
pBSQacA/A402	A402 <i>qacA</i> derivative of pSK7201; Amp ^R	This study
pBSQacA/A157G	A157G <i>qacA</i> derivative of pSK7201; Amp ^R	This study

^a Amp^R, ampicillin resistance

^b available in the laboratory, constructed by Angela Parker.

All growth media were sterilised by autoclaving at 121°C for 15 minutes (min). For short term storage and isolation of single colonies, bacteria were streaked out on LB agar plates supplemented with ampicillin (100 µg/mL) where required, incubated at 37°C overnight and stored at 4°C. For long term storage, overnight bacterial culture (16 hours), grown from a single fresh colony, was mixed with sterile 80% glycerol in a cryovial and stored at -80°C (Sambrook and Russell, 2006).

2.4 Transformation of *E. coli*

2.4.1 Preparation of chemically competent *E. coli* cells

Overnight cultures of *E. coli* strain DH5α were grown from single, well-isolated colonies in 10 mL of LB broth. These cultures were used to inoculate fresh LB broth at a 1:100 dilution. Cells were grown with shaking at 200 rpm until OD₆₀₀ = 0.6 and then placed on ice for 10 min. After that, the cells were pelleted by gentle centrifugation (2,800 x *g* for 5 min at 4°C), resuspended in 20 mL ice cold Transformation Buffer I (Table 2.1) and incubated on ice for 20 min. Cells were pelleted by centrifugation (2,800 x *g* for 10 min at 4°C), resuspended in 1 mL Transformation Buffer II (Table 2.1) and incubated on ice for 10 min (Green and Rogers, 2013). Single aliquots of competent cells (50 µL) were made in pre-chilled eppendorf tubes and stored at -80°C.

2.4.2 Transformation of competent *E. coli* cells

Aliquots of 50 µL of competent *E. coli* cells (Section 2.4.1) were thawed on ice prior to use (approximately 20 min). Typically, 100 ng of purified plasmid DNA (Section 2.5.1), or 20 µL of *DpnI*-digested polymerase chain reaction (PCR) product (Section 2.5.2), was added and the DNA-competent cells mixture incubated on ice for 30 min. The cells were then heat shocked by placing the tube into a 42°C water bath for 45

seconds and immediately putting the tube on ice for 2 min. Two hundred fifty microliters of LB broth without antibiotic was added to each transformation mixture and cells were incubated at 37°C for 1 hour with shaking. After that, the transformation mixture was plated onto pre-warm LB agar plates containing 100 µg/mL of ampicillin and spread via a sterile spreader. Plates were incubated overnight at 37°C and single, well-isolated colonies (then called transformant colonies) were purified for further analysis.

2.5 DNA procedures

2.5.1 Small-scale purification of plasmid DNA

Single, well isolated transformant colonies were used to inoculate 5 mL LB broth containing 100 µg/mL of ampicillin in 15 mL culture tubes and cultures were incubated at a tilted position overnight at 37°C with shaking at 200 rpm. Cultures were pelleted by centrifugation (11,000 x *g* for 5 min at room temperature). Plasmid DNA was isolated and purified using the Isolate II Plasmid Mini Kit (Bioline) according to the manufacturer's instructions. Briefly, cell pellets were resuspended in 250 µL of Resuspension Buffer P1. Cells were lysed by the addition of 250 µL of Lysis Buffer P2 with gentle mixing by inverting the tubes. After 5 min of incubation at room temperature, the lysate was neutralised by the addition of 300 µL of Neutralisation Buffer P3 and mixed thoroughly by gently inverting tubes. Cellular debris was removed by centrifugation (11,000 x *g* for 5 min at room temperature) and the supernatant passed through an Isolate II Plasmid Mini Spin column via centrifugation (11,000 x *g* for 1 min at room temperature). Columns were first washed with 500 µL Wash Buffer PW1 preheated to 50°C, followed by 600 µL of Wash buffer PW2 (supplemented with ethanol) and further centrifugation (11,000 x *g* for 1 min at room

temperature). Columns with bound DNA were dried by centrifugation (11,000 x *g* for 2 min at room temperature) and placed in new 1.5 mL microfuge tubes. The DNA was eluted by the addition of 50 μ L of Elution buffer P followed by 1 min incubation at room temperature and centrifugation (11,000 x *g* for 1 min at room temperature). Concentration and purity of the extracted DNA plasmids were measured using a NanoDrop One Spectrophotometer (Thermo Fischer Scientific). Plasmids were stored at -20°C till further use.

2.5.2 Restriction endonuclease digestion

DNA samples were digested using restriction endonucleases as per manufacturer's instructions (New England Biolabs, UK). Where double digestion was required, the recommended buffer compatibility information from the manufacturer was used. For double digestion with the enzymes whose buffer requirements were different, DNA fragments were purified between single digestions as described in Section 2.5.4. Digested DNA fragments to be used in cloning were excised from a gel and column purified (Section 2.5.4) before performing the ligation.

For *DpnI* digestion of the amplification products, each amplification reaction mixture was treated with 1 μ L of *DpnI* restriction enzyme (New England Biolabs) and incubated at 37°C for 1 hour. The *DpnI* digests the methylated DNA (unmodified template plasmid) but not the newly replicated plasmid which is unmethylated.

2.5.3 Agarose gel electrophoresis

Agarose gels were made by dissolving agarose (Bioline) in 0.5X TAE buffer (Table 2.1) at a concentration of 1% for resolution of DNA fragments greater than 500 bp and 2% for fragments less than 500 bp. DNA samples were mixed with 5X DNA

electrophoresis loading dye (Bioline) and electrophoresed at 100 V until the front line dye (bromophenol blue) reached approximately three quarters of the length of the gel. As a molecular weight standard, 1 kb DNA ladder, Hyperladder I (Bioline), was used for estimation of band size. The gels were stained with 3X GelRed staining solution (Biotium), prepared as in Table 2.1, for approximately 20 min. Stained DNA bands were visualised and imaged using a Gel Doc EZ Imager (Bio-Rad).

2.5.4 Purification of DNA fragments from agarose gel slices

DNA fragments to be extracted were first electrophoresed on an agarose gel and stained as explained in Section 2.5.3. DNA bands were then visualised on a UV transilluminator. Fragments of interest were excised from the gel using a sterile scalpel blade and placed into a sterile 1.5 mL microfuge tube. DNA purification was performed using a Wizard SV Gel and PCR Clean-Up System (Promega, USA), according to the manufacturer's protocol. Briefly, Membrane Binding Solution was added to the agarose gel slice at a ratio of 10 μ L per 10 mg of gel and incubated at 65°C for 10 min. DNA fragments were then bound to a SV Minicolumn, washed with 700 μ L of Membrane Wash Solution, and eluted in 50 μ L of Nuclease-Free Water.

2.5.5 DNA sequencing

Plasmid DNA was prepared using the Isolate II Plasmid Mini Kit (Bioline) as described in Section 2.5.1. Sequencing samples were prepared by mixing 500 ng of plasmid DNA with 10 pmol (equates to 1 μ L of a 10 μ M primer stock solution) of an appropriate sequencing primer (Table 2.4) in a 12 μ L volume. DNA sequencing reactions were performed by the Australian Genome Research Facility (AGRF) using Sanger sequencing. The sequencing results were analysed as described in Section 2.13.

2.6 Recombinant DNA procedures

2.6.1 Polymerase chain reaction

Each PCR was performed in separate thin-walled 0.5 mL tubes. The following reaction components and conditions were used: 100 ng of the plasmid DNA template, 0.4 mM dNTPs (Sigma-Aldrich), 1 U Velocity™ DNA polymerase (Bioline), 1 x Velocity™ Buffer (Bioline) and 200 nM of each primer. Thermal cycling conditions included initial denaturation for 5 min at 95°C, followed by 35 cycles of 30 seconds denaturation step at 95°C, 1 min annealing step at 55°C, 6 min extension at 72°C and 10 min final extension step at 72°C. While annealing temperature was mostly 55°C, different annealing temperatures using gradient PCR was used for optimisation when required. Amplified products were visualised by agarose electrophoresis (Section 2.5.3).

2.6.2 Site-directed mutagenesis

Site-directed *qacA* mutants were constructed via the QuickChange™ site-directed mutagenesis method (Stratagene) utilising high fidelity Velocity™ DNA polymerase (Bioline). Initially, pairs of complementary oligonucleotide primers were designed (Table 2.4) to incorporate a cysteine or other amino acid substitution into the desired position within the wild-type *qacA* sequence (see Appendix 1). The following considerations were made for an efficient mutagenic primer design: a primer length between 25-45 nucleotides with the nucleotide change as close to the centre of the primer as possible flanked by 10-15 nucleotides on each side, a melting temperature in the range of 70–85 °C, a primer ending in C or G to promote stronger binding and a G+C content of at least 40%. To screen rapidly for a plasmid containing the desired mutation, a silent mutation (where possible) was also introduced in the primer sequence in parallel to the desired mutation. The additional silent mutation did not

Table 2.4 Primers used in the present study.

Primer ^a	Nucleotide sequence (5'→3') ^{b,c}	Restriction enzyme ^d
QacA mutagenic primers		
G361C_F	GTTTATTATGTATTTCTTTGTCATCCCTTAAGTTATTCTACAATGGCTT	<i>Afl</i> III
H362C_F	GTATTTCTTTGGTTGTCCCTTAAGTTATTCTACAATGGCTTTAG	<i>Afl</i> III
P363C_F	GTATTTCTTTGGCCATTGTTTATCATATTCTACAATGGC	<i>Msc</i> I
L364C_F	GTATTTCTTTGGCCATCCATGTTTATCATATTCTACAATGGC	<i>Msc</i> I
S365C_F	GGTCATCCATTATGTTATTCTACAATGGCGCTAGCATTAAATTTAG	<i>Nhe</i> I
Y366C_F	CTTTGGTCATCCCTTAAGTTGTTCTACAATGGCTTTAGC	<i>Afl</i> III
S367C_F	CCATTATCATATTGTACAATGGCTTTAGC	<i>Bsr</i> GI
T368C_F	CCATTATCATATTCTGTATGGCGCTAGCATTAAATTTAGTTG	<i>Nhe</i> I
M369C_F	CCATTATCATATTCTACATGTGCGCTAGCATTAAATTTAGTTGGAGC	<i>Nhe</i> I
A370C_F	CTTTGGTCATCCCTTAAGTTATTCTACAATGTGCTTAGCATTAAATTTA GTTGG	<i>Afl</i> III
L371C_F	CATATTCTACAATGGCATGCGCATTAAATTTAGTTGGAGC	<i>Sph</i> I
A372C_F	CCATTATCATATTCTACCATGGCTTTATGCTTAATTTAGTTGGAGC	<i>Nco</i> I
L373C_F	CAATGGCTTTAGCATGCATTTTAGTTGGAGCTGG	<i>Nsi</i> I
I374C_F	GGCTTTAGCATTATGTTTAGTTGGAGCTGGGATGGCTTCACTAGC	<i>Bse</i> YI
L375C_F	GGCTTTAGCATTAAATTTGCGTTGGAGCTGGGATGGCTTCACTAGC	<i>Bse</i> YI

(Continued on next page)

Table 2.4 (continued)

Primer ^a	Nucleotide sequence (5'→3') ^{b,c}	Restriction enzyme ^d
QacA mutagenic primers		
V376C_F	GCATTAATTTTATGTGGAGCTGGGATGGCTTCACTAGC	<i>Bse</i> YI
A378C_F	GCATTAATTTTAGTTGGATGCGGAATGGCTTCACTAGC	<i>Xmn</i> I
G379C_F	GCATTAATTTTAGTTGGAGCTTGATGGCTTCGCTAGCAGTTGC	<i>Nhe</i> I
M380C_F	GTTGGAGCTGGTTCGCTTCGCTAGCAGTTGC	<i>Nhe</i> I
A381C_F	GGAGCTGGTATGTGTTTCGCTAGCAGTTGCATCTGC	<i>Nhe</i> I
S382C_F	GTTGGAGCTGGGATGGCTTCCTAGCAGTTGCATCTGC	<i>Bse</i> YI
L383C_F	GTTGGAGCTGGAAATGGCTTCATGCGCAGTTGCATCTGC	<i>Xmn</i> I
A384C_F	GTTGGAGCTGGGATGGCTTCACTATGCGTTGCATCTGC	<i>Bse</i> YI
V385C_F	GCTGGTATGGCTTCGCTAGCATGCGCATCTGCTCTAATAATG	<i>Nhe</i> I
A386C_F	GGTATGGCTTCGCTAGCAGTTGCTCTGCTCTAATAATG	<i>Nhe</i> I
S387C_F	GGCTTCACTAGCAGTTGCATGCGCTCTAATAATGTTAGAAACACC	<i>Sph</i> I
A388C_F	GCTTCACTAGCAGTTGCATCTGTCTTATAATGTTAGAAACACC	<i>Psi</i> I
L389C_F	GGCTTCACTAGCAGTTGCATCTGCATGCATAATGTTAGAAACACC	<i>Nsi</i> I
I390C_F	GCAGTTGCATCTGCTCTATGCATGTTAGAAACACC	<i>Nsi</i> I
L392C_F	GCAGTTGCATCTGCTCTTATAATGTGCGAAACACCTACATCAAAGC	<i>Psi</i> I
T394C_F	GCTCTAATAATGTTAGAATGCCCTACATCAAAGC	<i>Bsm</i> I

(Continued on next page)

Table 2.4 (continued)

Primer ^a	Nucleotide sequence (5'→3') ^{b,c}	Restriction enzyme ^d
QacA mutagenic primers		
P395C_F	GCTCTAATAATGTTAGAAACAT <u>TG</u> TACATCAAAAGCAGG	<i>PciI</i>
T396C_F	GCATCTGCTCT <u>T</u> TATAATGTTAGAAACACCT <u>TG</u> CTCAAAAGCAGG	<i>PsiI</i>
S397C_F	GCTCTAATAATGTTAGAAACACCTACAT <u>GT</u> AAAGCAGGTAATGC	<i>PciI</i>
K398C_F	GAAACACCTACATCAT <u>TGT</u> G <u>CAGG</u> TAATGCAGC	<i>BsgI</i>
A399C_F	CCTACATCAAAAT <u>TGC</u> <u>GG</u> AATGCAGCTGC	<i>BsmI</i>
N401C_F	CCTACATCAAAAGCAGGTT <u>TGT</u> G <u>CAG</u> CTGCTGTTG	<i>BsgI</i>
A402C_F	CAAAAGCAGGTAATT <u>TGC</u> <u>GCTGC</u> AGTTGAAGAGTC	<i>PstI</i>
A157G_F	GCTTCAT <u>CGAT</u> <u>C</u> GGT <u>G</u> TGTTTTGGACCAATTATCG	<i>PvuI</i>
A378V_F	GCATTAATTTTAGTTGGAGT <u>TGG</u> A <u>TGG</u> CTTCACTAGC	<i>XmnI</i>
Sequencing primers		
M13_F	TGTAAAACGACGGCCAGT	
M13_R	CAGGAAACAGCTATGACC	
pBAD_F	ATGCCATAGCATTTTTATCC	
pBAD_R	GATTTAATCTGTATCAGG	

^a Each primer is presented by the one-letter amino acid code and its corresponding position number in the QacA amino acid sequence (see Appendix 1) followed by the second letter representing the new generated amino acid.

^b Primers are presented in a 5' to 3' direction. Two primers were used to create each mutation. Only forward (_F) mutagenic primers are listed. The reverse (_R) primers are the reverse and complement of the forward primer sequence.

^c The nucleotide change(s) leading to the new amino acid replacement are in red. The nucleotide change(s) that created a silent restriction site mutation are indicated in green and the restriction sites are underlined.

^d Enzymes used for restriction digestions to screen for desired mutations prior to sequence verification.

cause a change in the QacA amino acid but results in the addition or removal of restriction site to assist in differentiating mutant plasmid from the wild-type parent plasmid by a simple restriction digest (Section 2.5.2).

Reactions typically contained 100 ng of the plasmid DNA template, 0.4 mM dNTPs (Sigma-Aldrich), 1 U Velocity™ DNA polymerase (Bioline), 1 x Velocity™ Buffer (Bioline) and 200 nM of each primer. Thermal cycling conditions included initial denaturation for 5 min at 95°C, followed by 35 cycles of 30 seconds denaturation step at 95°C, 1 min annealing step at 55°C, 6 min extension at 72°C and 10 min final extension step at 72°C. PCR products were treated with *DpnI* (Section 2.5.2) prior to transformation into competent *E. coli* cells (Section 2.4.2).

2.6.3 DNA ligation

Ligation reactions were performed in a 10 µL volume containing T4 DNA Ligase and Ligase Buffer as per the manufacturer's protocol (New England Biolabs, UK) with a 1:3 molar ratio of vector to insert. The reaction mixture was incubated overnight at 4°C. T4 DNA ligase was inactivated by heat at 65°C for 10 min before being used for transformation into competent *E. coli* (Section 2.4.2).

2.7 Protein overexpression and purification

2.7.1 Overexpression of QacA and TetA(K) from pBAD-based vectors

Overnight cultures of *E. coli* TOP10 cells carrying plasmids pSK7128 or pSK7122 (Table 2.3) were inoculated at 1:50 dilution into 1 L fresh LB broth containing 100 µg/mL ampicillin and grown with shaking at 200 rpm until $OD_{600} = 0.8$. Cultures were induced with L-arabinose at a final concentration of 0.002% (w/v) for QacA and 0.0005% (w/v) for TetA(K) and grown for a further 4 to 21 hours at 37°C. Cells were then harvested

by centrifugation (5,000 x *g* for 20 min at 4°C) and either kept at -80°C until later protein extractions or immediately used in QacA protein purification (Section 2.7.2 and 2.7.3).

2.7.2 Preparation of membrane vesicles

Harvested *E. coli* TOP10 cells (Section 2.7.1) or *E. coli* DH5α harbouring the plasmids of interest (Table 2.3) were resuspended in 30 mL of crushing buffer (Table 2.1) and disrupted using a high-pressure cell disrupter device (Constant Systems) at 30,000 pounds per square inch (psi). After removal of cell debris by centrifugation (27,000 x *g* for 30 min at 4°C), the membrane fraction was separated by ultracentrifugation (134,000 x *g* for 1 hour at 4°C) and resuspended in 250 μL of membrane resuspension buffer (Table 2.1). Membrane protein samples were stored at -80°C until used in sodium dodecyl-sulphate polyacrylamide gel electrophoresis (SDS-PAGE) for detection of protein expression by Western blot (Section 2.8.4), or for labelling of QacA cysteine residues by fluorescein-5-maleimide (FM) (Section 2.9).

2.7.3 Purification of His-tagged QacA/TetA(K) proteins by affinity chromatography

Membrane fractions of *E. coli* TOP10 cells containing the transport protein of interest were prepared as described in Section 2.7.2. Isolated membrane proteins were solubilised for 1 hour at 4°C with slow rotation in membrane resuspension buffer (Table 2.1) to a final total protein concentration of approximately 5 mg/mL. Insoluble material was removed by centrifugation (16,000 x *g* for 20 min at 4°C). Batch method purification at microcentrifuge tube scale was performed as follows. One-fifth volume of 50% slurry ProBond™ Nickel-Chelating Resin (Life Technologies), equilibrated in bead wash buffer (Table 2.1), was added to solubilised membranes,

and incubated at 4°C for 1 hour with slow rotation. Nickel-resin was pelleted by centrifugation (3,000 x *g* for 3 min at 4°C) and washed four times with four resin volumes of bead wash buffer (Table 2.1). His-tagged proteins were then eluted from the resin by adding five resin volumes of elution buffer (Table 2.1). The eluate fractions were analysed by SDS-PAGE and Coomassie staining (Section 2.8.3) and Western blotting (Section 2.8.4). The eluate fractions containing purified proteins were dialysed twice against 2 litres of buffer containing 20 mM Tris-HCl (pH 7.5) and 10% (v/v) glycerol at 4°C. The protein samples were concentrated using Amicon® Ultra-15 centrifugal filter units (Merck Millipore) with the nominal molecular weight limit of 30 kDa as per manufacturer's instructions. The protein concentration was determined as explained in Section 2.8.1. The protein was stored at -80 °C.

2.8 Protein detection

2.8.1 Protein quantification

The protein concentration of total membrane fractions (Section 2.7.2) or purified proteins (Section 2.7.3) was quantified using a detergent compatible (DC) bicinchoninic acid (BCA) protein assay (Bio-Rad), which is a modified version of the Lowry assay. The reagents were used according to the manufacturer's instructions. This colorimetric assay was performed in a 96 well microtitre plate and solutions of bovine serum albumin (BSA; New England Biolabs) at known concentrations (0 to 5 mg/mL) were used to produce a standard curve. The microtitre plate was read at 595 nm using a Multiskan spectrophotometer (Labsystems Multiskan EX). Protein concentrations were determined by comparison to the standard curve obtained from the BSA reference.

2.8.2 Sodium dodecyl-sulphate polyacrylamide gel electrophoresis

Total membrane protein samples in membrane resuspension buffer (Section 2.7.2) were mixed with 2X SDS-PAGE sample buffer (Table 2.1) in a 1:1 ratio and incubated at 37°C for 30 min before loading onto 10% polyacrylamide gels (Table 2.1). Protein electrophoresis was performed using the Bio-Rad Mini-PROTEAN™ gel system. Equal amounts (100 µg) of total membrane proteins were loaded onto the gels and electrophoresis performed at 120 V until the front line dye ran off the bottom of the gel. Pre-stained Precision Plus Protein Standards™ (Bio-Rad) were used to estimate protein molecular mass. Gels were stained with Coomassie blue (Section 2.8.3) to reveal the protein profile, or the protein content of the gel was transferred to a membrane for protein detection by Western blot as described in Sections 2.8.4.1 and 2.8.4.2, respectively.

2.8.3 Coomassie staining

Polyacrylamide gels (Section 2.8.2) were removed from the electrophoresis tank and stained for at least 1 hour in Coomassie staining solution (Table 2.1). Coomassie-stained gels were placed in destaining solution (Table 2.1) for at least 2 hours until the background was clear and protein bands appeared visible. Gels were scanned using a BioRad Gel Doc™ EZ imager.

2.8.4 Western blot analysis

2.8.4.1 Protein transfer to polyvinylidene fluoride membrane

After SDS-PAGE (Section 2.8.2), the separated proteins were electro-transferred from gels onto polyvinylidene difluoride (PVDF) membranes (Amersham Hybond-P™, GE Healthcare) at 30 mA overnight using a wet transfer system (Bio-Rad) filled with transfer buffer (Table 2.1).

2.8.4.2 Immunological detection of transferred proteins

After transferring proteins from gels onto PVDF membranes (Section 2.8.4.1), the PVDF membranes with the bound proteins were soaked in 1X TTBS buffer (Table 2.1) for 5 min, then incubated in 50 mL of Blocking Buffer (Table 2.1) at room temperature for 1 hour with gentle agitation. The membranes were washed once in 1X TTBS buffer for 5 min and then incubated with primary antibody, rabbit anti-6xHis antibody (Rockland Immunochemicals) with a 1:5,000 dilution in 1X TTBS, at room temperature on a rocking shaker for 2 hours. After that, membranes were washed three times for 10 min each in 1X TTBS on an orbital shaker and incubated with secondary antibody, goat-anti-rabbit IgG conjugated to horseradish peroxidase (BioRad) with a 1:10,000 dilution in 1X TTBS, at room temperature on a rocking shaker for 1 hour. Membranes were washed six times for 5 min each in 1X TTBS on an orbital shaker. Membranes were then covered with chemiluminescence detection reagents A and B (Bio-Rad) mixed in a 1:1 ratio and imaged using a ChemiDoc™ MP Imaging System (Bio-Rad). Detected bands from QacA variants were quantified by densitometry using ImageLab software (Bio-Rad), and all bands were normalised to the wild-type QacA band used as a reference in order to determine the relative amount of QacA protein present in each mutant.

2.9 Fluorescein maleimide reactivity assay

E. coli DH5 α cells carrying a pSK7201-derived plasmid expressing a cysteine-substituted QacA mutant protein (Table 2.3) were harvested from overnight cultures by centrifugation (5,000 x *g* for 5 min at 4°C). Membrane fractions were prepared after cell disruption as explained in Section 2.7.2 and were used for FM reactivity analysis as previously described with slight modification (Xu *et al.*, 2006; Hassan *et*

al., 2008). FM was added to 250 μg of membrane vesicles to a final concentration of 0.25 mM, and incubated on a rotator at room temperature for 10 min. The labelling reaction was stopped by adding 850 μL of NEM-quenching buffer (Table 2.1). QacA protein was solubilised by adding 100 μL of 10% DDM. Following 1 hour incubation on a rocker mixer at 4°C, samples were centrifuged (5,000 $\times g$ for 20 min at 4°C) to remove debris. QacA and QacA variant proteins were then purified by adding 100 μL of 50% slurry ProBond™ Nickel-Chelating Resin (Life Technologies), equilibrated in bead wash buffer (Table 2.1), and incubated mixing on an end-over-end rotator at 4°C for 1 hour. The resin was washed four times with 750 μL of bead wash buffer and purified QacA proteins were eluted by adding 40 μL of 2X SDS-PAGE sample buffer (Table 2.1). Equal amounts (20 μL) of eluted proteins were resolved on 10% SDS-polyacrylamide gels (Table 2.1) which were scanned using a Gel-Doc system (Bio-Rad) to detect the associated fluorescein labels. The gels were also stained with Coomassie blue (Section 2.8.3) to visualise purified QacA protein. All images were analysed using ImageLab software (Bio-Rad) and fluorescence intensity of labelled QacA bands were quantified and normalised to the intensity of corresponding Coomassie-stained QacA bands. The previously constructed P309C QacA mutant having a high reactivity with FM (Xu *et al.*, 2006), was used as a control to which the level of labelling intensity of each newly constructed cysteine-substituted mutant was compared.

2.9.1 Effect of substrate preincubation on maleimide reactivity

To determine the effect (if any) of substrate binding on the FM labelling profile of the QacA cysteine mutant proteins, membrane vesicles (Section 2.7.2) containing QacA mutant proteins were first incubated in the absence or presence of different concentrations of a QacA substrate (0.5-10 mM) at room temperature for 5 min. Then

maleimide labelling of QacA mutant proteins was performed as described in Section 2.9.

2.10 Minimum inhibitory concentration assay

MIC analysis of QacA variants to representative antimicrobial compounds, was conducted using an agar plate method as previously described (Xu *et al.*, 2006; Hassan *et al.*, 2008). Overnight cultures of freshly transformed *E. coli* DH5 α cells carrying the pBluescript II SK-based QacA and its variants (Table 2.3) were inoculated at 1:50 dilution into 10 mL fresh LB broth containing 100 μ g/mL ampicillin and grown at 37°C with shaking at 200 rpm till the OD₆₀₀=0.6. Then the cells were diluted 1:100 in MH broth (Section 2.3) and replica plated onto MH agar plates containing a range of concentrations of the antimicrobial compounds under examination (Table 2.5) using a microplate replicator. Plates were incubated at 37°C and colony growth was checked at 24 and 48 hours. The MIC was defined as the lowest concentration of each substrate that inhibited the visible growth of bacteria within 48 hour incubation. Three independent biological replicates of the experiment (each containing technical replicates) were conducted to obtain a representative set of MIC data from one experiment, chosen based on reproducibility of results. The MIC data of QacA mutants was normalised to the wild-type QacA level and shown as a comparison percentage of wild-type levels.

2.11 Whole-cell fluorometric transport assays

QacA-mediated efflux of Et and DAPI in live bacterial cells was conducted essentially using a previously described protocol (Xu *et al.*, 2006; Wu *et al.*, 2008). A single colony from freshly transformed *E. coli* DH5 α cells carrying the plasmids of interest

Table 2.5 Compounds used for MIC analysis

Compound	Concentration range ($\mu\text{g/mL}$)	Increment ($\mu\text{g/mL}$)
Monovalent dyes		
Ethidium bromide	50-1200	50
Rhodamine 6G	50-1200	50
Monovalent QACs		
Benzalkonium	10-100	10
Bivalent QACs		
Dequalinium	25-350	25
Biguanidines		
Chlorhexidine	1-12	1
Diamidines		
Pentamidine	25-400	25
DAPI	5-60	5

(Table 2.3) was picked and grown overnight in 10 mL of LB broth containing 100 $\mu\text{g}/\text{mL}$ ampicillin. Cells were diluted 1:50 with fresh LB broth with 100 $\mu\text{g}/\text{mL}$ ampicillin and grown at 37°C till the $\text{OD}_{600}=0.6$ before 5 mL of culture was harvested by centrifugation (3,000 $\times g$ for 5 min at 4 °C). The collected cells were washed twice with ice-cold 20 mM HEPES buffer (Table 2.1), resuspended in 5 mL of the same buffer and kept on ice. Aliquots (1 mL) of cells in 1.5 mL microfuge tubes were loaded with either 15 μM Et or 10 μM DAPI in the presence of 10 μM CCCP. Tubes were wrapped with aluminium foil and incubated at 37°C for 90 min with gentle agitation. Cells were pelleted at 3,000 $\times g$ for 3 min at room temperature and washed three times with 1 mL of 20 mM HEPES buffer (Table 2.1) and resuspended in the same buffer. Cells were warmed to 37°C, transferred into a quartz cuvette for fluorimetric analysis in a fluorescence spectrometer (LS 55, Perkin-Elmer) using FL WinLab software. Sodium formate (125 mM final concentration) was added at 10 second time point to Et-loaded cells to energise the system. The fluorescence spectra were recorded for 5 min with excitation and emission wavelengths of 530 nm and 590 nm, respectively for Et. It should be noted that for optimal DAPI fluorimetric analysis (yielding decent resolution and avoiding signal saturation), diluted DAPI-loaded cells (mixed 1:20 with 20 mM HEPES buffer) were used. The fluorescence spectra were recorded for 15 min with excitation and emission wavelengths of 364 nm and 454 nm, respectively. Sodium formate (500 mM final concentration) was added at the 10 second time point to DAPI-loaded cells to energise the efflux pumps. The maximum fluorescence data recorded over 5 min (for Et) or 15 min (for DAPI) of mutants were normalised to the maximum fluorescence data of the wild-type QacA (100%). Fluorimetric measurements data were analysed and plotted by Microsoft Office Excel 2013.

2.11.1 Effect of maleimide treatment on efflux of ethidium and DAPI

To determine the effect of maleimide modification on QacA-mediated efflux of Et or DAPI, aliquots of bacterial cells expressing cysteine-substituted QacA mutants (Table 2.3) prepared as explained in Section 2.11 were pre-incubated in the presence or absence of 5 mM NEM, a sulphhydryl-binding compound, for 20 min at 37°C. Cells were then washed with 20 mM HEPES (pH 7.0) to remove NEM prior to conducting the Et efflux assay or DAPI efflux assay.

2.12 Determination of kinetic parameters of transport

Transport assays with a series of Et or DAPI concentrations were used to estimate the kinetic parameters of transport (K_m and V_{max}) of QacA-mediated drug efflux in *E. coli* DH5 α cells. Aliquots of cells (1 mL) were prepared as described in Section 2.11 and loaded with Et at concentrations ranging from 0.3-25 μ M or DAPI at concentrations ranging from 0.3-20 μ M. Each range contained 10 substrate concentrations selected to be equally spread above and below the predicted K_m . The concentrations were 0.3, 0.5, 1, 3, 5, 7, 10, 15, 20 and 25 μ M for Et and 0.3, 0.5, 1, 3, 5, 7, 10, 12, 15, 20 μ M for DAPI. From these concentrations, a series of efflux curves were generated and the initial transport velocity was calculated by averaging the linear portion of each curve, identified by visual examination. Then the efflux transport data in fluorescence unit per second (FU/S) were plotted against increasing substrate concentrations [S] using GraphPad Prism version 8 (GraphPad Software Inc., USA). The nonlinear least square regression analysis was used to fit the data to a Michaelis-Menten equation to obtain estimates of K_m and V_{max} values as previously described (Mitchell *et al.*, 1999; Xu *et al.*, 2006).

2.13 Bioinformatic analyses

2.13.1 Computer software employed

DNA sequence alignments and manipulation for plasmid construction and cloning were performed with Sequencher™ 4.9 software (GeneCodes). SnapGene software (GSL Biotech; <https://www.snapgene.com>) was used in complement with Sequencher™ software to create plasmid maps and plan cloning steps. The *qacA* gene (UniProtKB/Swiss-Prot accession number: P0A0J8) was used as the reference sequence to ensure the presence of desired mutations in the constructed plasmids (Table 2.3). Protein data bank (PDB) files were visualised and analysed using Chimera 1.11.2 software (Pettersen *et al.*, 2004) and PyMOL molecular graphics system (Molecular Graphics System, Version 1.71 Schrödinger, LLC). Structural analysis and preparation of protein 3D figures were performed using PyMOL.

2.13.2 Amino acids sequence alignments

Multiple sequence alignments of protein sequences were performed using the on-line version of Clustal Omega (Sievers *et al.*, 2011). Accession number (UniProtKB/Swiss-Prot) for alignments in Figure 3.8 were as follows: *S. aureus* QacA (P0A0J8); *Mycobacterium smegmatis* LfrA (A0R5K5); *K. pneumoniae* KmrA (W9BGM8); *Salmonella typhimurium* SmvA (D0ZXQ3); *A. baumannii* AmvA (C4PAW9); *Listeria monocytogenes* MdrM (I0J098); *S. aureus* LmrS (A0A4T9Z2L7); *Listeria monocytogenes* MdrT (I0J094); *Neisseria gonorrhoeae* FarB (Q9RQ29); *S. aureus* NorB (Q7A5M0); *S. aureus* NorC (A0A0E1ACG1) *Vibrio cholerae* VceB (O51919); *Bacillus subtilis* TetA(L) (P23054); *E. coli* EmrB (P0AEJ0); *S. aureus* TetA(K) (P02983); *S. aureus* Tet38 (Q5PU79); *S. aureus* MdeA (A0A660A2M0); *Bacillus subtilis* Bmr (P33449); *E. coli* MdfA (P0AEY8); *E. coli* TetA(B) (P02980); *E. coli* TetA(C)

(P02981); *Pseudomonas aeruginosa* CmlA (P32482); *E. coli* EmrD (P31442); *E. coli* MdtM (P39386); *S. aureus* NorA (POA0J4); *Lactococcus lactis* LmrP (Q48658).

2.13.3 Homology modelling of the QacA structure

The FASTA formatted QacA (both full-length and truncated lacking the big loop between TMS 13 and 14) were submitted to SWISS-MODEL (<http://swissmodel.expasy.org>) (Biasini *et al.*, 2014), Phyre2 (<http://www.sbg.bio.ic.ac.uk/phyre2>) (Kelley *et al.*, 2015) and I-TASSER (<http://zhanglab.ccmb.med.umich.edu/I-TASSER/>) (Zhang, 2008; Roy *et al.*, 2010; Yang *et al.*, 2015) web servers. Additionally, structures of MdfA and LmrP (QacA homologous proteins with 12 TMS having 17.20% and 12.16% amino acid sequence identity with QacA, respectively) as well as different POT family transporters (14 TMS) which have the highest sequence identity with QacA were provided as templates for I-TASSER to be used as restraints for guiding the modelling simulations (Yang and Zhang, 2015). The generated models were visualised using Chimera and PyMOL searching for a model in which all 14 TMS were modelled without any gaps and disordered loops.

The mutant forms of QacA were generated individually using the PyMOL program. The QacA model structures were submitted to ModRefiner Server (<http://zhanglab.ccmb.med.umich.edu/ModRefiner>) to apply atomic-level structure refinement and energy minimisation (Xu and Zhang, 2011) before executing the molecular docking.

2.13.4 Molecular docking

Each compound (a substrate of QacA or a putative inhibitor) was docked to the modelled QacA using the open-source molecular docking software AutoDock Vina

1.1.2 (<http://vina.scripps.edu/>) (Trott and Olson, 2010). The 3D structure of each compound was obtained from PubChem database (<http://pubchem.ncbi.nlm.nih.gov/>). Prior to docking, the protein and compound were prepared according to AutoDock Tools (<http://autodock.scripps.edu>) (Morris *et al.*, 2009) instructions, which adds polar hydrogen atoms and Gasteiger charges. Moreover, each substrate was automatically considered conformationally flexible with its rotatable bonds and torsions defined by AutoDock Tools according to their chemical features. The prepared structures of protein and ligand were saved as pdbqt format and used as input files for docking.

A blind docking approach was performed since the binding pocket of QacA was unknown. The size of the docking grid box was set as 90 Å (x, y, z), while the grid box centre was set to 70.901, 73.681, and 75.257 for the x, y and z coordinates, respectively. The adjusted box size was large enough to enclose the whole central cavity as well as the identified important amino acids across the cavity-lining helices (TMS 1, 2, 4, 5, 9, 10, 12, and 13) in QacA. These setting parameters along with the default docking settings, e.g. exhaustiveness of the search algorithm, were stored in a configuration file (Appendix 2) and retained throughout the docking studies in order to remove the bias. For each docking run, nine different docked poses were generated in the Vina output file. The docking results were ranked according to the default energy scoring function in AutoDock Vina, wherein the first pose represents the highest binding affinity and hence the most stable docked pose with the lowest binding energy value (kcal/mol). All substrate poses resulting from docking were visually inspected by PyMOL to select the best-docked pose based on the following criteria: lowest-energy pose, proper orientation inside the central cavity of QacA

(which is assumed as the major binding site of QacA similar to other MFS proteins), and highest agreement with the experimental data (i.e. the most overlap between the binding residues found by docking and the functionally-important residues identified by mutagenesis studies). In some instances, substrate was found to be on the outside of the protein which is not biologically relevant. Thus, such poses were discarded from analyses. Subsequently, the interactions of the selected docking poses were further analysed using Poseview (<http://poseview.zbh.uni-hamburg.de/>) (Stierand and Rarey, 2010) which calculates for all types of interactions including hydrogen bonds, hydrophobic and π interactions.

CHAPTER 3
FUNCTIONAL ANALYSIS OF RESIDUES
WITHIN AND SURROUNDING TMS 12 OF
QACA

3.1 Introduction

Even though high-resolution structural information of different 12-TMS DHA antiporters such as EmrD (Yin *et al.*, 2006), YajR (Jiang *et al.*, 2013), MdfA (Heng *et al.*, 2015; Nagarathinam *et al.*, 2018) and LmrP (Debruycker *et al.*, 2020) are publicly available, unfortunately there is neither a structure of QacA nor any of its close homologues due to inherent difficulties in obtaining sufficient amounts of quality proteins (Xu *et al.*, 2006; Hassan *et al.*, 2009). In spite of the recent advances in the field of protein structural biology, technical difficulties for determination of realistic high-quality atomic resolution structures of membrane proteins still remain to be overcome. The main challenges are low protein yield and structural integrity if membrane proteins are separated from their natural lipid environment (Birch *et al.*, 2020). In lieu of continued attempts to solve high-resolution structures, molecular and biochemical approaches have been employed to investigate the structural and functional properties of difficult to crystallise membrane proteins such as QacA.

Site-directed mutagenesis is a fundamental and widely used technique for revealing functionally important positions in proteins and can be used to identify substrate binding and transport sites (Alegre *et al.*, 2016; Kinana *et al.*, 2016). Single amino acid scanning mutagenesis, in which residues in a target position of a protein are systematically substituted for one particular amino acid, continues to be used for detecting amino acid side chains important for protein function (Gray *et al.*, 2017). Various types of amino acid substitutions, including cysteine (Angelow and Yu, 2009; Zhu and Casey, 2007; Alexeyev *et al.*, 2004), alanine (Bian *et al.*, 2015; Tang and Fenton, 2017), glycine (Weinglass *et al.*, 2001), histidine (Starace and Bezanilla, 2001), methionine (Stoffregen *et al.*, 2012), tryptophan (Depriest *et al.*, 2011; Deacon *et al.*,

2014), and proline (Patel *et al.*, 2013) have been employed in scanning mutagenesis studies, depending on a specific hypothesis (*e.g.*, glycine for shortening the bulky side chains, alanine for hydrophobisation, and asparagine for charge neutralisation) (Quick *et al.*, 2001).

Cysteine-scanning mutagenesis has provided a wealth of data on the functionally and structurally important residues of membrane proteins embedded in their natural lipid membrane environments (Akabas, 2015). Such an approach has been employed in the study of drug efflux membrane proteins to make deductions regarding their binding and translocation regions, as demonstrated by structural and functional studies on AcrB from *E. coli* (Takatsuka and Nikaido, 2006), NorM from *N. gonorrhoea* (Radchenko *et al.*, 2016), LmrA from *L. lactis* (Jones and George, 2015) and QacA from *S. aureus* (Xu *et al.*, 2006), to name a few. Moreover, cysteine-scanning mutagenesis has provided valuable evidence for the study of structure in membrane proteins, as seen, for example, in the *E. coli* lactose permease LacY where the model built on cysteine-scanning mutagenesis showed to be highly consistent with the obtained corresponding high-resolution structure (Kaback *et al.*, 2001; Abramson *et al.*, 2003a). Furthermore, systematic cysteine-scanning mutagenesis of the entire residues in bacterial TetA(B) protein (Tamura *et al.*, 2001) and human P-glycoprotein (Loo and Clarke, 2000) provided a complete map of functionally or structurally important residues within these proteins as well as a complete picture of their topological model.

In this study, cysteine-scanning mutagenesis was used to study structure-function relationships in the QacA membrane transporter for the following reasons: (i) cysteine is a small and relatively hydrophobic residue and substitution of amino acids

with cysteine at most positions in a membrane protein appears to be well tolerated without a detrimental effect on protein structure (Bogdanov *et al.*, 2005; van Geest and Lolkema, 2000; Akabas, 2015); (ii) replacement of residues with cysteine allows evaluation of the influence of electrostatic interactions in the binding of cationic antimicrobials to QacA after neutralisation by cysteine substitution (Hassan *et al.*, 2007b); (iii) among the 20 major amino acids, cysteine has a unique reactivity with sulphhydryl reactive compounds which provided researchers with a myriad of data on the structure-function relationships in membrane proteins (Akabas, 2015). It is noteworthy that methionine, the other sulphur-containing amino acid, lacks such ability (Kim *et al.*, 2014). Even when a high-resolution 3D structure becomes available, a cysteine mutagenesis approach provides complementary information about the protein structure and dynamics (Bass *et al.*, 2007; Greene *et al.*, 2007).

Given that QacA lacks intrinsic cysteine residues, it is an ideal protein target for site-directed cysteine mutagenesis. This methodology has been extensively applied and Figure 3.1 summarises all of the QacA functionally important residues found to date (shown in red). The criteria for a residue being assigned as important was that its substitution with cysteine and/or other amino acids resulted in $\geq 50\%$ reduction of resistance capacity to at least one of the six representative compounds tested.

A previous study (Hassan *et al.*, 2007) identified that substitution of G377 in TMS 12 with aspartic acid or glutamic acid (acidic residues) compensated for the absence of an acidic residue at position 323 in TMS 10 which had been shown to be involved in resistance to bivalent cations (Section 1.9.3.1). Hence, TMS 12 has been postulated to be involved in binding to bivalent cationic substrates. However, the structural and functional role of TMS 12 region remains undefined. Against this backdrop, the

present study aimed to construct 38 individual cysteine mutants of the previously untargeted residues in TMS 12 and its flanking loops, then examine the impact of these mutations to provide details of the functional and/or structural importance of all the targeted amino acid residues as well as the topology of this region of QacA. The target area is highlighted in green in Figure 3.1.

3.2 Results and Discussion

3.2.1 QacA variants generated by site-directed mutagenesis

To evaluate the functional importance of the amino acid residues that form the extracellular loop 11-12 (aa 361 to 368), TMS 12 (aa 369 to 391) and cytoplasmic loop 12-13 (aa 392 to 410) within QacA as shown in Figure 3.1 (green coloured residues), each of these thirty-eight residues was individually mutated to cysteine using site-directed mutagenesis of the pBluescript II SK-based *qacA* plasmid (Section 2.6.2). The mutagenic primers used for amplification are listed in Table 2.4. The pBluescript II SK-based vector system in *E. coli* DH5 α cells provides constitutive low-level expression (leaky expression) of QacA protein which is at a level suitable for *in vivo* functional QacA analyses (Hassan *et al.*, 2009; Xu *et al.*, 2006; Hassan *et al.*, 2006a). The wild-type and mutant QacA proteins are designed to carry a C-terminal 6xHis-tag that facilitates the downstream detection and affinity purification of the proteins.

It should be mentioned that the residues in the target region of QacA that were not mutated in this study (red and black coloured residues), had already been analysed and their data were included for completeness. The constructed mutants were first sequenced and analysed to verify the presence of the desired mutation as well as the absence of spurious mutations within the DNA sequence. For some constructs that

Figure 3.1 Overview of QacA mutants.

Shown is the 2D topology model for QacA protein based on predictions from hydropathy, gene fusion studies and solvent accessibility analyses (Hassan *et al.*, 2007b; Paulsen *et al.*, 1996a) (www.tcdb.org). The cell membrane is shaded in light yellow and TMS are enclosed in purple boxes, numbered 1 to 14. Each residue is represented by its one-letter symbol. Residues analysed in published studies (Paulsen *et al.*, 1996a; Hassan *et al.*, 2006a; Xu *et al.*, 2006; Hassan *et al.*, 2007b; Wu *et al.*, 2008; Hassan *et al.*, 2008) and unpublished mutational dataset available in our laboratory, for which cysteine substitution resulted in a resistance capacity $\leq 50\%$ to ethidium, rhodamine 6G, BK, dequalinium, CH, or pentamidine compared to wild-type QacA are considered as functionally important and shown in red letters. Residues substituted with amino acids other than cysteine are indicated in the extended ellipses. Residues studied by site-directed mutational analysis in the present study are highlighted in green. Original figure courtesy of Prof. M. H. Brown.

did not initially produce the desired results, the mutagenesis steps were repeated after PCR optimisations with different annealing temperatures or with a redesigned mutagenic primer.

3.2.2 Expression of QacA mutants

To determine if the generated single-residue substitutions affected QacA protein expression, Western blot analysis (Section 2.8.4) on membrane fractions of *E. coli* DH5 α cells (Section 2.7.2) containing the pBluescript-based plasmids was performed. Using an anti-6xHis antibody (Section 2.8.4.2) for capturing the 6xHis-tag fused to the C-terminus of the QacA protein, a band between 37 kDa and 55 kDa corresponding to QacA was detected of the wild-type and mutant QacA proteins, but was absent from the negative control (Figure 3.2). It should be noted that wild-type QacA is predicted to have a molecular weight of 55 kDa but was observed to run faster relative to soluble molecular weight standards on SDS-PAGE due to its higher hydrophobicity and SDS binding capacity (Hassan *et al.*, 2009). Western blot results confirmed that QacA proteins were inserted into the cell membrane of *E. coli*. Furthermore, densitometric quantification after loading equal amounts (100 μ g) of membrane fractions (Section 2.8.2) demonstrated that the expression level of each of the QacA mutant proteins in *E. coli* cells was similar to that of wild-type QacA (Figure 3.2). This suggested that the cysteine substitution did not have an adverse impact on expression which is consistent with previous findings (Xu *et al.*, 2006). Moreover, any significant changes that would be observed in subsequent functional analyses of QacA mutants would not be attributable to a variation in production of the protein.

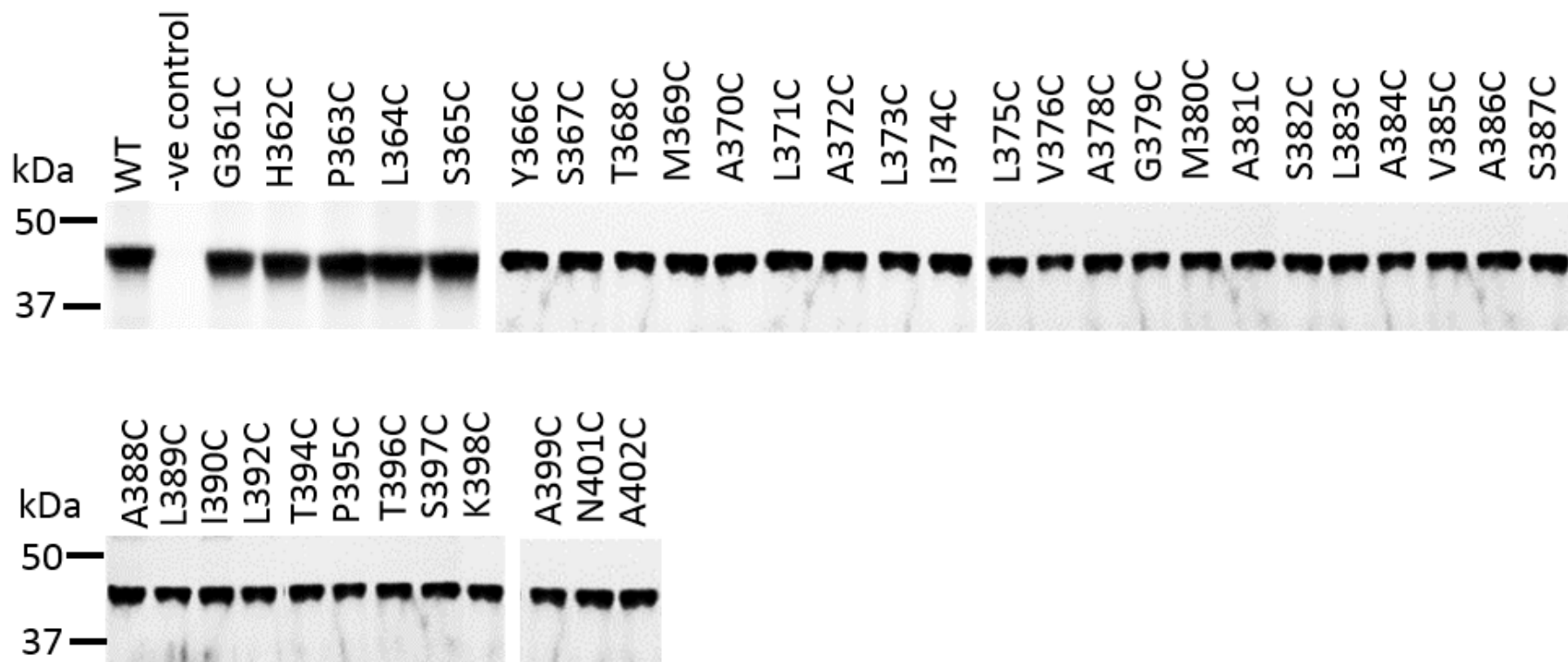


Figure 3.2 Western blot analysis of QacA mutants examined in this study.

Protein expression was analysed using membrane vesicles isolated from *E. coli* DH5 α expressing wild-type (WT) QacA and mutant derivatives. Equal amounts (100 μ g) of total membrane proteins were loaded onto 10% polyacrylamide gels (Section 2.8.2) and QacA proteins immunologically detected using a rabbit anti-6xHis antibody. The negative (-ve) control is pBluescript II SK vector which lacks the *qacA* gene. Positions of molecular weight markers are indicated and QacA bands are between 37 and 50 kDa.

3.2.3 Resistance profile of QacA mutants

MIC analyses (Section 2.10) were used to assess the functional importance of residues in the target region based on QacA-mediated resistance to a panel of six antimicrobial compounds, chosen as representatives of QacA substrates from different chemical classes. These include: monovalent dyes (Et and rhodamine 6G [R6G]); monovalent QACs (BK); bivalent QACs (DQ); biguanidines (CH); and diamidines (PE). These substrates have the common feature of being lipophilic, aromatic and positively-charged. Their structures are shown in Figure 1.5. The relative resistance levels conferred by each QacA mutant to the six representative antimicrobial substrates in comparison to wild-type QacA are presented as a percentage in Table 3.1. As can be seen, the majority of the mutants showed normal levels of resistance to each of the antimicrobials tested with resistance capacities similar or slightly reduced/increased in comparison with the wild-type QacA (indicative of 100% resistance activity). Remarkably, substitutions of G379 and S387 (TMS 12) resulted in $\geq 50\%$ reduction of resistance to all representative bivalent cations (Table 3.1, red). This suggests that residues at positions G379 and S387 within TMS 12 of QacA are functionally important, participating in an aspect of substrate binding and/or transport of these bivalent cationic substrates. Moreover, while substitution of the examined amino acid residues showed little or no effect on resistance to monovalent cations, QacA S387C was the only mutant that showed a substantial reduction of resistance to monovalent compound BK. Thus, S387 residue may play an important role in recognition and/or translocation of BK in addition to bivalent cations. As presented in Table 3.1, mutation of G361, present in the extracellular loop 11-12, impacted on resistance to bivalent substrate PE.

Table 3.1 Resistance profile to six representative antimicrobial compounds by *E. coli* expressing QacA and mutant derivatives

Mutation	Location of mutation ^a	Relative MICs of QacA mutants (% wild-type QacA) ^{b,c}					
		Monovalent substrates			Bivalent substrates		
		Et	R6G	BK	DQ	CH	PE
WT QacA ^d		100 (250)	100 (800)	100 (100)	100 (300)	100 (7)	100 (240)
No QacA		20	30	30	25	10	35
G361C	Loop 11-12	100	100	100	75	80	50
H362C	Loop 11-12	100	112	100	83	100	83
P363C	Loop 11-12	100	100	90	83	80	83
L364C	Loop 11-12	100	100	90	83	80	100
S365C	Loop 11-12	100	112	100	83	100	83
Y366C	Loop 11-12	100	112	100	125	100	83
S367C	Loop 11-12	100	112	100	125	100	83
T368C	Loop 11-12	100	112	90	100	100	83
M369C	TMS 12	100	100	80	100	100	87
A370C	TMS 12	100	100	100	125	100	83
L371C	TMS 12	100	100	100	100	100	100
A372C	TMS 12	100	100	100	100	82	100
L373C	TMS 12	83	100	100	114	82	100
I374C	TMS 12	75	100	100	100	100	100
L375C	TMS 12	100	100	100	83	91	86
V376C	TMS 12	100	100	100	100	82	100
A378C	TMS 12	83	100	100	100	100	100
G379C	TMS 12	83	100	100	50	50	40
M380C	TMS 12	100	100	100	100	82	86
A381C	TMS 12	83	100	100	100	100	100
S382C	TMS 12	100	100	87	100	100	100
L383C	TMS 12	100	100	100	100	100	127
A384C	TMS 12	100	116	100	100	112	127
V385C	TMS 12	100	100	100	140	100	118
A386C	TMS 12	100	116	100	120	100	118
S387C	TMS 12	70	80	50	40	45	50
A388C	TMS 12	100	100	100	100	100	118
L389C	TMS 12	100	100	87	80	100	100
I390C	TMS 12	100	100	100	80	100	100
L392C	Loop 12-13	100	107	87	100	125	107
T394C	Loop 12-13	83	107	95	119	100	100

(Continued on next page)

Table 3.1 (continued)

Mutation	Location of amino acid change ^a	Relative MICs of mutants (% wild-type QacA) ^{b,c}					
		Monovalent substrates			Bivalent substrates		
		Et	R6G	BK	DQ	CH	PE
P395C	Loop 12-13	95	115	95	124	119	100
T396C	Loop 12-13	103	145	105	119	131	107
S397C	Loop 12-13	100	134	110	115	136	107
K398C	Loop 12-13	131	144	115	124	135	107
A399C	Loop 12-13	66	108	95	100	97	76
N401C	Loop 12-13	100	92	100	108	100	133
A402C	Loop 12-13	140	134	110	124	125	133

^a Location of amino acid changes in QacA is based on the previously predicted QacA topology model (Figure 3.1).

^b Numbers indicate relative resistance level of the mutants in comparison to the wild-type QacA (indicative of 100% resistance activity). MIC values determined by a standard agar dilution method, where *E. coli* DH5 α cells expressing wild-type and mutant QacA proteins were grown on LB agar supplemented with different concentrations of individual compounds (Section 2.10). Red indicates $\leq 50\%$ MIC compared to wild-type QacA. MIC data are from one experiment that is a representative of three independent experiments. The MIC values of QacA mutants are presented as percentage value relative to wild-type QacA.

^c Et: ethidium; R6G: rhodamine 6G; BK: benzalkonium; DQ: dequalinium; CH: chlorhexidine; PE: pentamidine.

^d MIC value ($\mu\text{g mL}^{-1}$) for wild-type QacA against each substrate is shown in parentheses (first row).

A notable observation in the response of the mutants toward the six substrates was that T396C, K398C and A402C mutations in the loop between TMS 12 and TMS 13 uniformly displayed a slight to modest increase in resistance (101-149%) to all the substrates unlike other mutations whose MICs were rather variable (Table 3.1). This suggests that these loop mutants could potentiate QacA to provide better resistance toward all substrates, possibly allowing easier entrance of substrates to the binding pockets. A similar slight to modest increase in resistance has been observed for the QacA mutants P196C, S198C and K199C in the cytoplasmic loop between TMS 6 and TMS 7 (M. H. Brown, unpublished data).

Another noteworthy observation is that among the mutants tested, three mutants I374C, S387C and A399C, exhibited the lowest MICs to Et (Table 3.1) suggesting their partial involvement in interactions with this substrate. Therefore, together with above-mentioned results, it can be concluded that TMS 12 is involved in the interaction with both monovalent and bivalent cationic substrates similar to what has been found previously with TMS 10 (Xu *et al.*, 2006).

3.2.4 Evaluating the causal role of A157G and A378V mutations in increased chlorhexidine resistance of QacA

A recent study investigating the genetic basis of elevated resistance to CH within clinical *Staphylococcus* spp obtained from Seattle Children's Hospital identified a novel *qacA* nucleotide sequence variant (Addetia *et al.*, 2019). The published study hypothesised that two amino acid substitutions, namely A157G (in TMS 5) and A378V (in TMS 12) were associated with the observed increased MIC to CH ($\geq 4 \mu\text{g/mL}$). However, an appreciation of the structural and functional impact of these substitutions was not obtained. Therefore, the influence of each individual

substitution, together with the dual substitution was evaluated. To this end, site-directed mutagenesis (Section 2.6.2) was used to generate individual isogenic A157G and A378V substitutions and concomitant substitution of both (A157G-A378V double mutant) in the wild-type QacA template. The quantity of QacA protein, MICs of Et, R6G, BK, DQ and PE as well as Et efflux activity for cells expressing these substitutions were found to be equivalent to those of the wild-type QacA (Appendix 3). It should be noted that the resistance profile of the A378V substitution in TMS 12 showed little or no difference to that of the A378C QacA mutant described previously (see Table 3.1), suggesting that this position is not functionally important as either cysteine or valine replacement did not cause a difference. However, MIC measurements indicated that the QacA A157G and A157G-A378V double mutant conferred a 40% increase in the MIC of CH compared to wild-type QacA (Figure 3.3). These data provide evidence that the QacA variant with an A157G substitution in TMS 5 had the causal role in the enhanced CH resistance in the variant isolated from the Seattle hospital patient and indicates that TMS 5 could mediate interactions with CH.

3.2.5 Ethidium transport activity

The effects of residue substitutions on QacA-mediated Et transport were assayed in live intact *E. coli* cells. Et, a fluorescent dye, is a known monovalent cationic substrate of QacA. Upon intercalating intracellular nucleic acids, Et causes an increase in fluorescence intensity. Energy-depleted *E. coli* DH5 α cells (through the addition of CCCP) expressing each mutant, preloaded with 15 μ M Et, were energised by addition of sodium formate and changes in fluorescent intensity as a function of time were monitored fluorimetrically (Section 2.11).

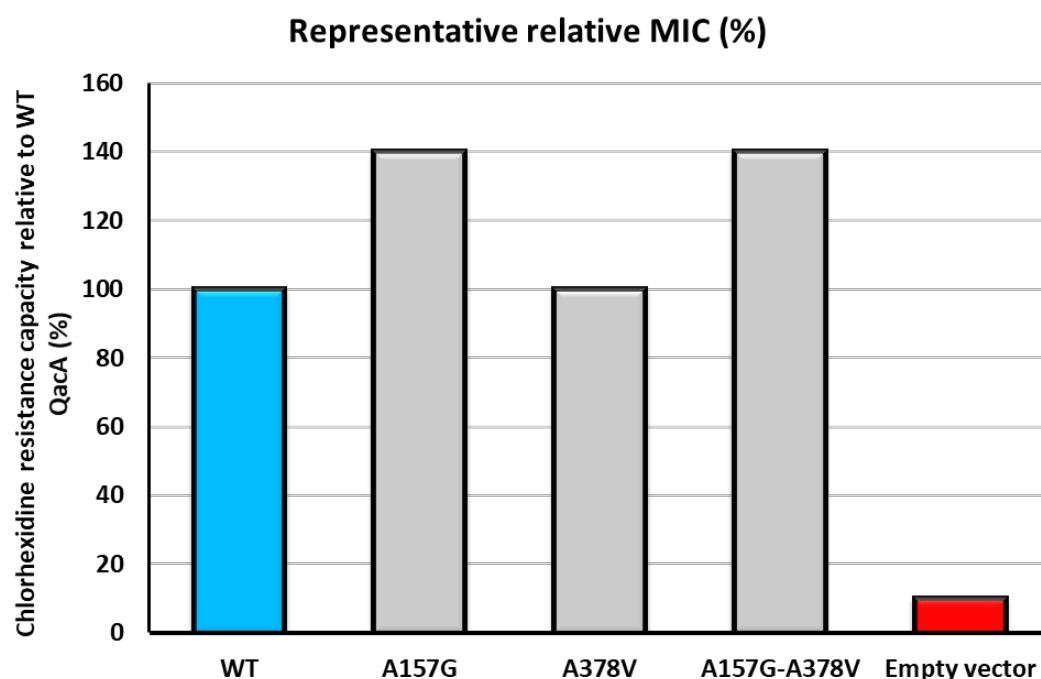


Figure 3.3 Effect of A157G and A378V substitutions on QacA resistance to CH.

MIC measurements were performed by a standard agar dilution method as described in Section 2.10. *E. coli* DH5 α cells expressing wild-type and mutant QacA proteins were grown on LB agar supplemented with CH with concentrations ranging from 1-20 $\mu\text{g}/\text{mL}$. Data are representative of at least three independent experiments. The MIC values of QacA mutants are shown as percentage value relative to wild-type QacA (blue). Cells carrying the empty vector (pBluescript II SK) are included as a negative control (red).

Et efflux was identified as a rapid decrease in fluorescent intensity (Figure 3.4). The I374C and S387C QacA mutants showed impaired efflux activity (approximately 40% reduced Et efflux activity compared to the parent cells) (Figure 3.4). This implies that I374 and S387 residues play a role in the QacA substrate translocation process. Efflux assays of cells expressing the remaining 36 QacA mutations had no discernible effect on transport activity (Appendix 4), indicating they are not essential for Et transport function of QacA.

Et transport capacity of QacA mutants are generally predictive of Et resistance activity, and vice versa. However, in some cases, the results obtained from MIC and fluorescence transport experiments may differ. For example, L389C and A399C QacA mutants had approximately 20% and 15% reduced Et transport capacity, respectively (Figure 3.5), whereas their Et MIC (Table 3.1) showed 0% and 34% reduction, respectively compared to the wild-type. Other studies also observed cases of discordance between the Et MIC and efflux data in some residues (Schindler *et al.*, 2013b; Kinana *et al.*, 2016). There are two main factors that may contribute to these observed discrepancies. Firstly, MIC analyses and efflux assays are tested under vastly different conditions which include their time courses, pre-exposing the cells with CCCP and Et loading for the efflux assay and the absence of such preconditioning in MIC testing (Schindler *et al.*, 2013b). Secondly, MICs are the outcome of interactions of multiple processes, including substrate influx, binding and efflux (Kinana *et al.*, 2016; Zomot *et al.*, 2018). Therefore, MICs may not be the direct yardstick of the efflux process alone.

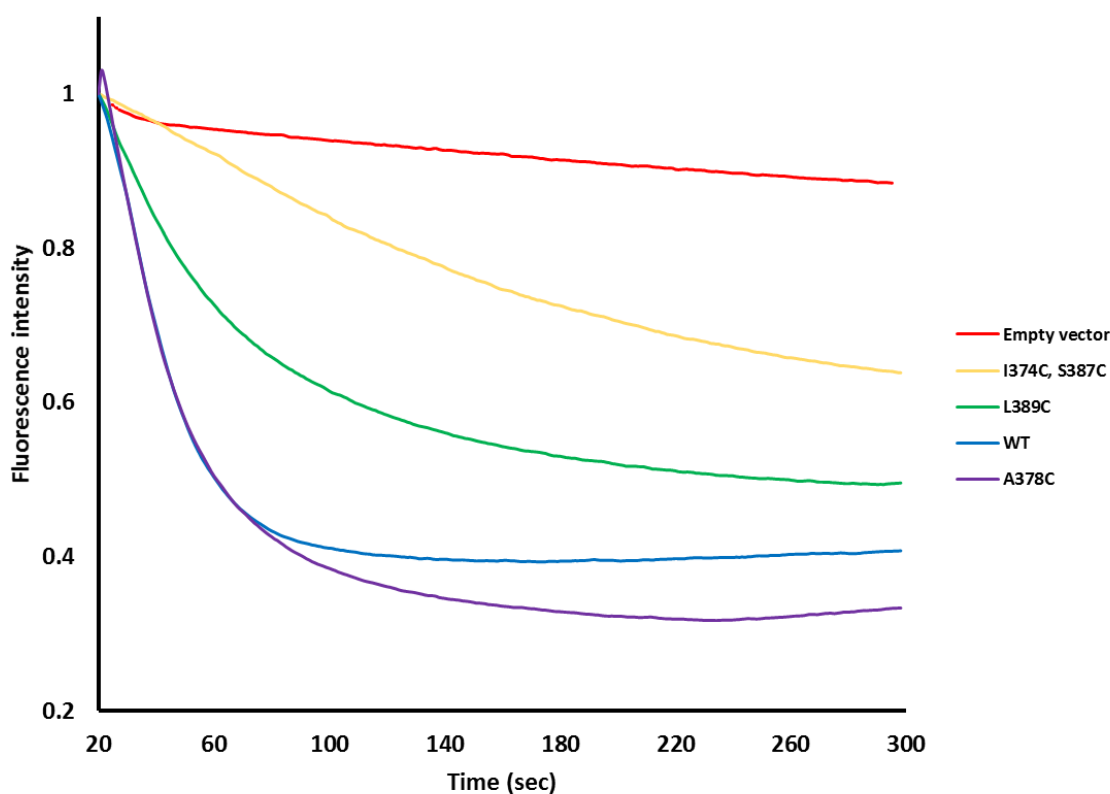


Figure 3.4 Representative ethidium efflux curves of wild-type QacA and mutant derivatives.

E. coli DH5 α cells carrying pBluescript II SK (empty vector), pSK7201 (wild-type [WT] QacA) and its derivatives were cultured and loaded with 15 μ M ethidium (Section 2.11). Sodium formate (final concentration, 125 mM) was added at the starting point to energise the energy-starved cells. Ethidium efflux is represented by a decrease in fluorescent intensity as a function of time. Here, representative ethidium efflux curves of WT, empty vector and four QacA mutants including I374C and S387C with lowest, L389C with moderate, and A378C with the highest efflux activities among the mutants examined in this study are shown. Other mutants had efflux curves that lie in the area between the green and purple curves (their individual efflux curves are displayed in Appendix 4).

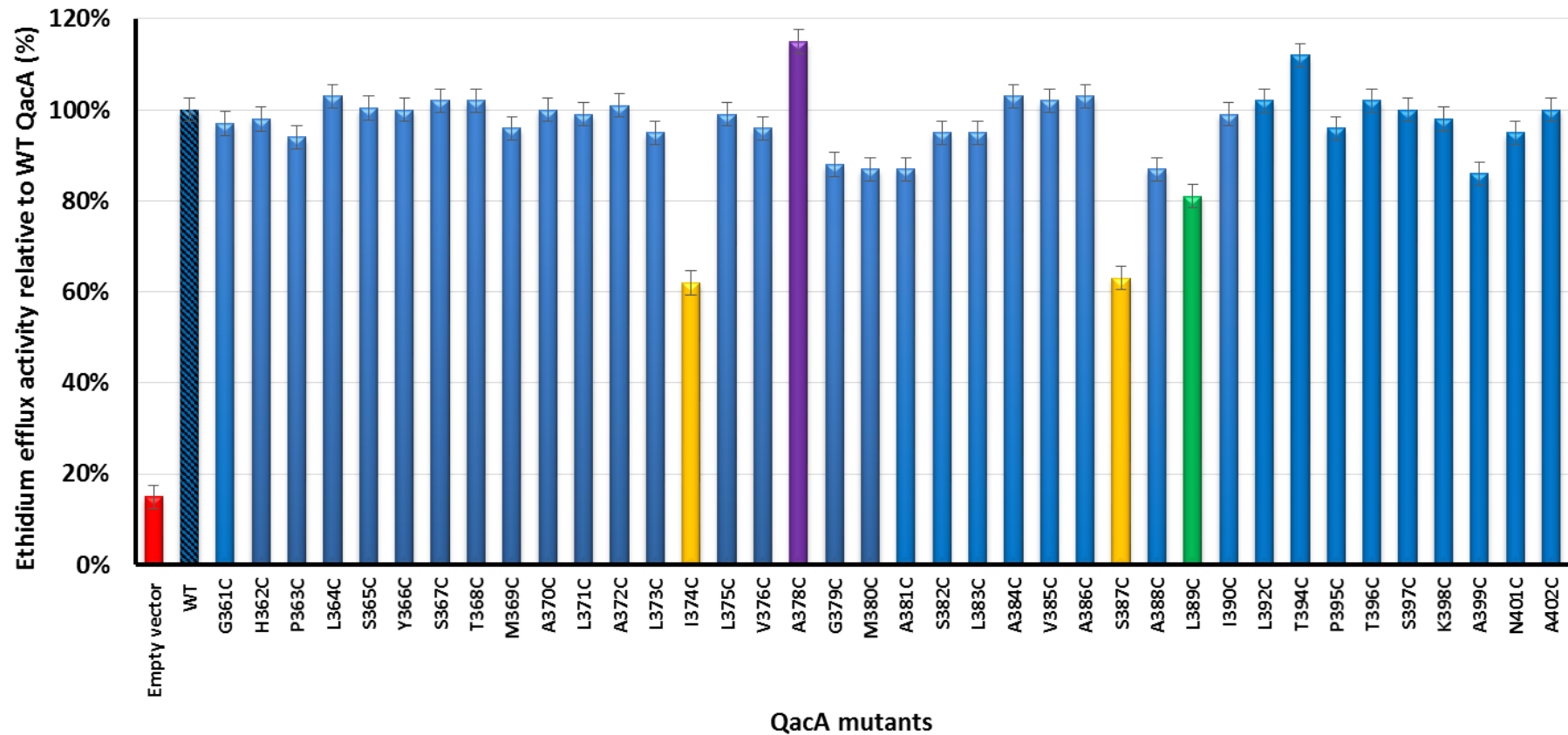


Figure 3.5 Ethidium transport activity of QacA mutants examined in this study.

Relative efflux values were calculated compared to WT QacA (the leftmost blue hatched bar), indicative of 100% efflux activity. Efflux values were taken at the end point of the efflux curves (300 second timepoint). Cells expressing the empty vector (pBluescript II SK) are included as a negative control (red bar). Yellow, purple and green bars correspond to the representative efflux curves of QacA mutants shown in Figure 3.4. Error bars represent SD of three biological replicates.

3.2.6 Solvent accessibility profile of residues

The rough boundaries of TMS 12 have been predicted in the initial QacA topology model (Figure 3.1), based on hydrophathy profile, gene fusion studies and solvent accessibility analyses. However, its precise termini remain to be experimentally validated. Labelling of cysteine mutants with sulphhydryl-reactive reagents such as polyethylene glycol-maleimide (PEG-Mal), methoxypolyethylene glycol maleimide (mPEG-Mal) or FM has been used to experimentally probe the solvent accessibility of residues in transporters such as LacY (Nie *et al.*, 2007), MdfA (Fluman *et al.*, 2012), P-glycoprotein (Rothnie *et al.*, 2004), QacA (Xu *et al.*, 2006; Majumder *et al.*, 2019) and TetA(K) (Hassan *et al.*, 2006b), to name a few. The FM (a fluorescent dye) is able to permeate through the membrane and react with (label) the ionised thiol of cysteine which is formed when cysteine is exposed to a water milieu but not embedded in a membrane (Bogdanov *et al.*, 2005; Belardinelli *et al.*, 2016). As such, maleimide reactivity is helpful to experimentally probe whether the cysteine residue is localised towards the hydrophobic core of the membrane bilayer (unreactive to labeling) or in a surface hydrophilic environment (able to be labelled) and therefore enabling the assignment of TMS in membrane proteins (Belardinelli *et al.*, 2016; Calabrese *et al.*, 2017).

In this study, solvent accessibility of cysteine-substituted QacA mutants was determined based on measuring their reactivity level with FM as described in Section 2.9. The FM reactivity levels of the cysteine-substituted QacA mutants were compared with that of a pre-existing QacA P309C mutant, which was shown to be highly reactive with FM (Xu *et al.*, 2006). Results of labelling reactivity of the cysteine-substituted QacA mutants with FM confirmed the location of residues G361, H362,

P363, L364 and S365 in the loop connecting TMS 11 and TMS 12 due to the observed high reactivity with FM (Figure 3.6). However, in contrast to the previously predicted QacA topology model (Figure 3.1) which depicted Y366, S367, T368 and M369 in the 11-12 loop, the solvent accessibility results (Figure 3.6) showed only a weak reactivity of these residues with FM, indicating their location more likely being inside the membrane bilayer. Thus, the solvent-accessibility analysis determined that Y366 and I390 make up the extracellular and cytosolic ends of TMS 12, respectively. As seen in Figure 3.6, uniform error rates for measurements of fluorescence across all mutants were obtained in the biological replicates, indicating the good consistency of the employed method. Further refinement of the QacA topology model was achieved by these experimental data (Figure 3.7), showing that TMS 12 is a rather long helix with 25 amino acid residues. Moreover, an interesting finding from the solvent-accessibility analysis was that A384, S387 and A388, although embedded in the TMS 12, somewhat strongly reacted with FM in contrast to other residues buried in the hydrophobic core of TMS 12 (Figure 3.6). This suggests that A384, S387 and A388 might be part of the substrate translocation pathway. Further discussion of these solvent-accessible residues together with those from other TMS in QacA as well as the length and tilt of TMS 12 in relation to other TMS are provided in Chapter 6.

3.2.7 Assessment of residue conservation in a multiple sequence alignment

TMS 12 in DHA2 14-TMS members, including QacA, is equivalent to TMS 10 of the DHA1 12-TMS transporters, according to the evolution model of 14-TMS MFS transporters (6+2+6) (Law *et al.*, 2008; Reddy *et al.*, 2012; Madej *et al.*, 2013). To determine the conservation of functionally important residues identified within and around the TMS 12, a multiple sequence alignment between QacA and a number of

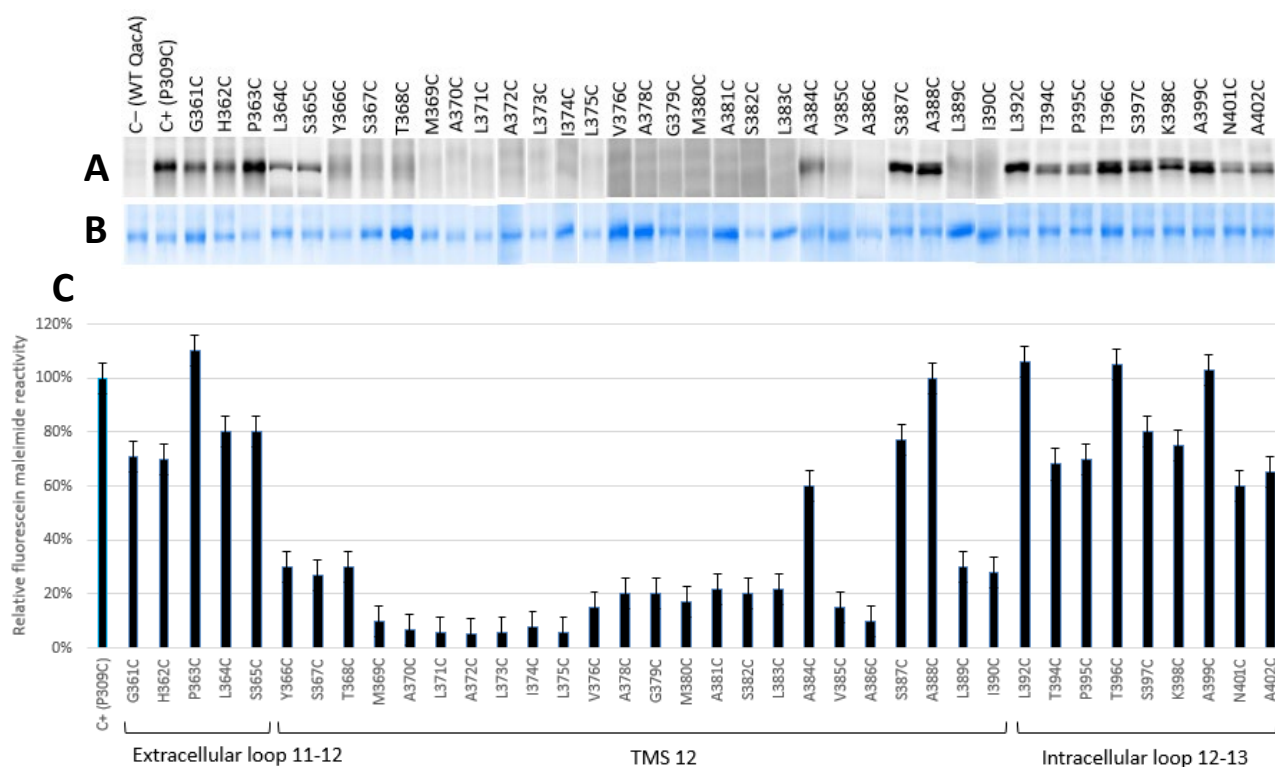


Figure 3.6 Solvent accessibility profile of QacA residues examined in this study.

Membrane vesicles containing single cysteine-substituted QacA mutant proteins were treated with FM and purified by nickel-chelation (Section 2.9). Purified QacA proteins were separated on 10 % SDS-PAGE gels. **(A)** Fluorescence images of labelled QacA proteins visualised with a Gel Doc EZ imager (Bio-Rad). **(B)** Coomassie Blue staining of SDS-PAGE gels to demonstrate protein amount on gels. **(C)** The level of fluorescence to the amount of protein for each mutant was quantified densitometrically using ImageLab software (Bio-Rad) and the FM reactivity levels relative to the highly reactive P309C QacA mutant (Xu *et al.*, 2006) are shown. Error bars represent SD of three biological replicates. Boundaries of TMS 12 are labelled underneath.

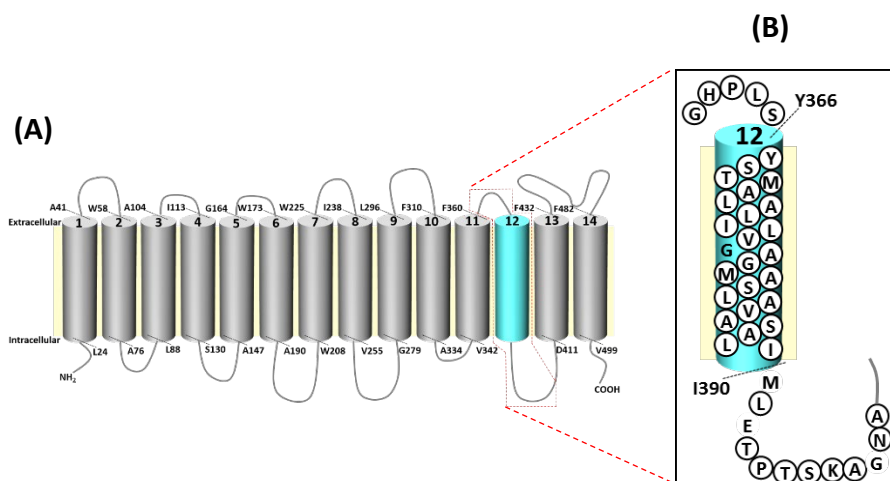


Figure 3.7 Refined membrane topology model of TMS 12 of QacA protein based on solvent accessibility results.

(A) Simplified topology model of QacA with its 14 TMS presented as cylinders labelled 1 through 14. One-letter residue names with their position numbers indicate the top and bottom extremities of TMS previously predicted by hydropathy and solvent accessibility analyses as shown in Figure 3.1. (B) Refined extents of TMS 12 determined based on analysis of solvent accessibility of cysteine residues inserted in this study (see text for details). Residues in circles were mutated in this study and others (G377, M391, E393 and G400) were analysed in previous studies (Hassan *et al.*, 2007b; Hassan *et al.*, 2008).

QacA-related multi- and single drug transporters from the DHA1 and DHA2 members of the MFS family was conducted as described in Section 2.13.2 with accession numbers listed therein. Interestingly, analysis of the multiple sequence alignment showed that the intramembranous glycine at position 379 is the only residue which is highly conserved (Figure 3.8). This suggests it is a key residue that probably plays a common important role in the structure or function of DHA-family transporters. However, to date, this glycine been mutated only in the DHA-1 transporter TetA(B) (at the corresponding position; G311C), where its replacement reduced tetracycline resistance (50% of the wild-type level) (Tamura *et al.*, 2001). Therefore, further structural and functional study is needed to evaluate the role of this residue across other different DHA transporters.

3.3 Conclusions

The efflux pump QacA is usually carried by clinical isolates of *S. aureus* and potentiates resistance to a wide range of lipophilic cationic antimicrobial compounds (Brown and Skurray, 2001; Hassan *et al.*, 2008; Costa *et al.*, 2013). Alarming, widespread use of antiseptics and disinfectants such as BK and CH for infection prevention in hospitals and the community has led to appearance of efflux-mediated antiseptic and disinfectant resistance in bacteria including *S. aureus* (LaBreck *et al.*, 2020). Given the highest contribution of QacA efflux pump to biocide resistance (Hardy *et al.*, 2018; Baines *et al.*, 2019), it is imperative to broaden our understanding of the structure function features of QacA including the role of key residues in QacA substrate binding and translocation.

Solvent accessibility experiments (Figure 3.6) helped to determine the extents of TMS 12 and refine its topology in the 2D model of QacA (Figure 3.7). Additionally, this

12

		GHPLSYSTMALALILV	GAGMASLAVAS	ALIMLE	TPTSKAGNA	402			
	QacA	GHPLSYSTMALALILV				GAGMASLAVAS	ALIMLE	TPTSKAGNA	402
	LfrA	RHNLTVAAIIASFVLEELGVGVSQTVSNDTIVASVPAAKSGA 400							
	KmrA	LDFSTQQWLAWGLMTLLGFSVASALLASSAIMAAAPKEKA 385							
	SmvA	MDFSTQQWQAWGLMALLGFSASALLASTSAIMAAAPAEGA 385							
	AmvA	QLNFSTDHFLAWTCMVFLGFSIEIALLASTAAIMSSVPPQKA 383							
	MdrM	DESTTLTFIIIVQTIIRSAGMAMVMMPLQTAALNSLPLKLASH 394							
DHA2	LmrS	HTDTSYTYLIVVYAIRMFVSLLMMPINTTGINSRNEEISH 393							
	MdrT	TMDTPLWYIVVFYAVRFFGISMAMMPVSTAGMNALPNHLIN 401							
	FarB	YADMIDIGNVIWPQFWQGVGVAMFFLPLTTITLSHMKGQIAA 395							
	NorB	PEILYVICCIIGYLFGLGLGIYATPSTDTAIANAPLEKGVV 396							
	NorC	PGIFYVISCVVGYLCFGLGLGIYATPSTDTAISNAPLDKGVV 392							
	VceB	TVDMTFSQISWPLFFQIGIMPLFFVPLTAIALGSKVPHEMES 401							
	TetA(L)	FIDAAPWIMTIIVIFVFGGLSFTKTVISTVSSSLKEKEAGA 384							
	EmrB	TFEPGMDFGASAWPQFIQGFVAVACFFMPLTTITLSGLPPERL 395							
	TetA(K)	FVEFSMWLTTFMFIFVMGGLSFTKTVISKIVSSSLSEEEVAS 384							
	Tet38	FAVGNHISIFVISMIFFAGSFALMYAPLLNEAIKTIDLNMTG 379							
	MdeA	DEQTSTIMLATVYAIRMVGIALGLIPVMHTMNQLKPEMNAH 388							

10

		TTVHSYVAILLVTVTVFVGFDLMPAVTTYLSKIAGNEQGFA				330		
	Bmr	TTVHSYVAILLVTVTVFVGFDLMPAVTTYLSKIAGNEQGFA				330		
	MdfA	ISSHAYLWMTAGLSIYAFGI LANAGLVRLTLFASDMSKGTV 349						
	TetA(B)	AFISEGWLVPVLILLAGGGIALPALQGVMSIQTKSHQQGAL 334						
	TetA(C)	AFATRGWMAFPIMILLASGGIGMPALQAMLSRQVDDDHQGQL 336						
DHA1	CmlA	WALQSVLGFIAPMWLVGIGVATAVSVAPNGALRGFDHVAGTV 343						
	EmrD	FGVMNVWTLVPAALFFFAGMLFPLATSGAMEPFPFLAGTA 335						
	MdtM	LSPHVWLSVLGTSLYAFGI GLIFPTLFRFTLFSNKLPKGTV 345						
	NorA	VFANGYWSIMLISFVVFIFGDMIRPAITNYFSNIAGERQGFA 327						
	LmrP	FLTTTFTPIFIAGIVYTLGEIVYTPSVQTLGADLMNPEKIGS 349						

Figure 3.8 Amino acid sequence alignment of QacA in the region targeted in this study with related MFS DHA1 and DHA2 drug efflux proteins.

Amino acid sequences of selected bacterial DHA1 and DHA2 drug transporters were aligned with QacA using Clustal Omega. Sequences were obtained from the UniProtKB/Swiss-Prot database with the accession numbers presented in Section 2.13.2. Only the portion of the alignment encompassing the region targeted in this study is shown (full sequence alignment is presented in Appendix 5). Sequence names are shown on left with their grouping into MFS DHA1 (12 TMS) or DHA2 (14 TMS) families. Numbers on the right refer to the position of the rightmost residue on each line. Residues targeted for mutagenesis (Figure 3.1) are highlighted in green shading and G361, G379 and S387 identified as functionally important residues in QacA (Section 3.2.3) are in red. Glycine residues conserved in positions corresponding to G379 residue in QacA are highlighted in grey. The location of the TMS 12 in QacA (as determined in Figure 3.7) and the approximate location of TMS 10 in DHA1 transporters are indicated by horizontal purple and orange bars above the alignment, respectively.

analysis showed that TMS 12 is an amphipathic helix that contains three accessible amino acid positions (namely 384, 387 and 388) near its cytoplasmic end. Therefore, the cytoplasmic end of TMS 12 appears to be orientated towards an internal aqueous environment in QacA. Similar patterns, in which three residues reactive with FM situated along with two non- or weakly reactive residues, have been observed at the ends of TMS 10 of QacA (Xu *et al.*, 2006) as well as several TMS of the tetracycline transporter TetA(B) from *E. coli* (Kimura-Someya *et al.*, 1998; Tamura *et al.*, 2001). Tight helix packing could create difficulties when trying to determine the exact extents of a TMS as the residues may not be accessible to maleimide.

This study evaluated the functional role of QacA residues within TMS 12 and its immediate flanking loop regions using cysteine-scanning mutagenesis. All cysteine substituted mutants were expressed in *E. coli* DH5 α at wild-type QacA levels verifying that individual substitutions of residues to cysteine were permissible, and the QacA protein was able to effectively locate in the cell membrane of the heterologous host *E. coli*. Resistance profiling of these QacA mutants revealed that the G361C mutant in the extracellular 11-12 loop had a significant reduction in resistance to PE, whereas the mutants G379C and S387C in TMS 12 displayed a significant reduction in resistance to all tested bivalent cationic compounds. Moreover, the S387C mutation caused a significant loss in QacA resistance activity towards BK and showed impaired Et efflux activity, suggesting partial involvement of this region of TMS 12 in the translocation pathway of monovalent cations. It can be concluded that G361, G379 and S387 appear to be essential for the ability of QacA protein to handle selective substrates and hence are likely to participate in substrate binding, translocation or conformational transitions during substrate flux. Unlike membrane-bound G379,

S387 is in a solvent accessible position. It is therefore conceivable that S387 may form part of a hydrophilic substrate binding pocket. The G377 is another residue located in TMS 12 of QacA that has been identified previously to be functionally important (Hassan *et al.*, 2007b). Our observation that TMS 12 also possesses two other residues G379 and S387 being critical for resistance activity against bivalent cations extends and confirms the role of TMS 12 of QacA in interactions with bivalent cations.

TMS 12 of 14-TMS DHA2 members, including QacA, corresponds to TMS 10 of 12-TMS MFS transporters (Section 3.2.7). A number of functionally significant residues in TMS 10 of DHA1 transporters have been reported. For example, V335 in MdfA was shown to be involved in interaction with its substrates chloramphenicol and tetraphenylphosphonium (Adler and Bibi, 2004; Adler and Bibi, 2005). Incidentally, this position in MdfA coincides with the position of S387 in TMS 12 of QacA (Figure 3.8). Furthermore, the crystal structure of MdfA has shown that R336 is part of the ligand-binding pocket (Nagarathinam *et al.*, 2018). Another example is TetA(B) which has been extensively analysed by mutagenesis. Three residues, L305, A317 and Q319 in putative TMS 10 of TetA(B), were identified as participating in tetracycline resistance (Tamura *et al.*, 2001). Similar to the DHA1 transporters, the general role of TMS 10 region in other 12-TMS MFS transporters such as Glu1 (Kasahara and Kasahara, 1998), Ga12 and Hxt2 sugar transporters (Kasahara *et al.*, 1996) has been implicated in substrate recognition.

Overall, the results of this study revealed that selected residues within TMS 12 and its immediate flanking loop regions are important for QacA-mediated export of some of the cationic compounds tested. Such residues can be combined and integrated

with previously identified important residues within different TMS to produce a fuller picture of regions of QacA protein that are involved in substrate binding and transport. The functionally important residues identified in this study are further investigated in detail for their role in substrate-binding and translocation pathway by biochemical studies presented in the following Chapter.

CHAPTER 4

DETAILED ASSESSMENT OF THE ROLE OF IDENTIFIED QACA RESIDUES CRITICAL IN SUBSTRATE INTERACTIONS

4.1 Introduction

A high resolution structure of QacA is not available to derive a clear-cut picture of specific amino acids forming the drug binding sites. There are myriad methods available to assess substrate binding interaction in transport proteins, but each method has pros and cons in terms of sample consumption, assay complexity, and degree of automation. Fluorescence anisotropy or polarisation (FP) is one of the commonly used substrate-binding methods. FP measures the changes in the intensity and polarisation of fluorescence that emanates from a fluorescent substrate upon binding to the protein. Some studies have successfully used FP binding assays to demonstrate the binding activities of purified MDR transporters such as human P-glycoprotein (Clay *et al.*, 2015), *S. aureus* MepA (Banchs *et al.*, 2014) and *P. aeruginosa* MexB (Welch *et al.*, 2010). Substrate-binding assays using R6G, a highly fluorescent substrate for QacA, have been suggested as a good indication to confirm whether purified QacA protein retains a functionally competent tertiary structure (Hassan *et al.*, 2009). The FP binding assays are fast, sensitive and quite inexpensive which can be conducted by commonly available and affordable instrumentation with relatively small amounts of purified protein. However, the accuracy of FP binding assays could suffer from light scattering as well as absorptive and autofluorescence interferences (Lea and Simeonov, 2011).

Calorimetric approaches such as isothermal titration calorimetry (ITC) allow the use of enthalpy changes to measure thermodynamic parameters from the binding interactions between a diverse array of ligands and proteins (Rajaratnam and Rosgen, 2014). For example, the binding affinity and stoichiometry of purified MDR exporters AcrB from *E. coli* and MexB and MexY from *P. aeruginosa* have been

measured by ITC studies (Nakashima *et al.*, 2013). ITC is a sensitive and robust technique. However, ITC has the biggest disadvantage of requiring large amounts of purified protein for substrate binding analysis. This is challenging for binding studies of membrane proteins which are difficult to purify in high amounts (Mowla *et al.*, 2018; Rajarathnam and Rosgen, 2014).

Microscale thermophoresis (MST) is a relatively recently developed technology that can rapidly and precisely measure binding affinity of ligand-protein interaction based on minute changes in size, charge, conformation, and hydration shell (Fisher *et al.*, 2017; Thurlow *et al.*, 2016). These parameters are typically affected upon binding of a ligand to the target protein during directed movement of molecules through a temperature gradient. Such a microscopic temperature gradient, which is referred to as thermophoresis, is produced by an infrared laser source. MST allows determination of binding affinity by utilisation of fluorescent ligands to a target protein or ligand binding to fluorescently labelled proteins (fluorescence-based method) without the need of large sample volumes and immobilisation to a surface (immobilisation-free method) (Jerabek-Willemsen *et al.*, 2011; Jerabek-Willemsen *et al.*, 2014). For example, MST has been used for detailed assessment of the interaction of purified human nicastrin, a component of multi-subunit integral membrane protease (Yu *et al.*, 2017). MST has also recently been shown to be a rapid tool for obtaining direct binding affinity measurements of substrates to purified QacA and its mutants which were labelled with a fluorescent dye in the C-terminus of the His-tag (Majumder *et al.*, 2019). Another study established a MST-based binding assay to characterise binding of ligands to the human solute carrier (SLC) membrane transport proteins without the need of prior protein purification and suggested that this

approach could be suitable in compound screening for drug discovery (Clemencon *et al.*, 2018). Moreover, MST can be performed in virtually any solution with buffer or detergent of choice or even in complex biological context such as cell lysis or blood serum (Wienken *et al.*, 2010; Seidel *et al.*, 2013). Reflecting the ability of MST in analysing the binding affinity of proteins in complex mixtures, the role of the lipid environment in modulating the substrate binding of multidrug efflux pumps can be assessed. This is particularly important since studies have shown that lipid environments influence structure and function of membrane proteins (Laganowsky *et al.*, 2014; Martens *et al.*, 2016) such as potassium channels (Long *et al.*, 2007) and MDR transporters e.g. P-glycoprotein (Sharom, 2014), AcrB (Ly *et al.*, 2014) and LmrP (Debruycker *et al.*, 2020).

Surface plasmon resonance (SPR) has emerged as a powerful method based on biosensing technology that allows real time monitoring of binding events between ligand and analyte without the need of fluorescence labelling of either protein or substrate (label-free method). In a typical SPR assay, a binding partner, e.g. a purified protein (termed “ligand”) is immobilised onto a sensor chip surface and the other binding partner, e.g. substrate or inhibitor (termed “analyte”) is free in solution and is injected over the surface. SPR can measure the binding kinetics and affinity of biomolecular interactions based on detecting the changes of accumulated mass on the sensor surface upon binding of analyte to ligand. Moreover, SPR requires small amounts of purified protein compared to other techniques (such as ITC), thus making SPR more affordable and accessible for binding kinetics of membrane proteins (Livnat Levanon *et al.*, 2014; Reinhard and Nurnberger, 2017; Su and Wang, 2018). Application of SPR for binding studies of purified proteins, including multidrug

binding proteins, has been reported in many studies, such as AcrB from *E. coli* (Mowla *et al.*, 2018), AceR protein, the transcriptional regulator of *aceI* MDR efflux pump gene in *A. baumannii* (Liu *et al.*, 2018), and the DevBCA efflux pump from the cyanobacterium *Anabaena* sp (Staron *et al.*, 2014).

According to above-mentioned information, MST and SPR seem to be better direct binding methods for QacA rather than FP and ITC. However, on the other hand, using conventional biochemical binding assays can also be useful as indirect binding methods to obtain insight into the binding of substrates to QacA. One important biochemical method to probe substrate binding sites in transport proteins is labelling introduced cysteine residues with maleimide derivatives in the presence of substrates (Lin *et al.*, 2019) and assessing the effects of NEM treatment on substrate efflux. This can provide clues whether residues form or are spatially juxtaposed to the substrate-binding site(s)/transport pathway (Xu *et al.*, 2006). It is worth noting that these biochemical methods enable the substrate binding to be studied whilst membrane proteins are maintained within their lipid bilayer environment. This is preferable because direct interactions with lipids as noted above, is a key determinant of the structure and function of membrane proteins. Therefore, these biochemical methods were used in this study to investigate whether the QacA residues identified as functionally important in Chapter 3 are located in the putative substrate-binding site(s)/transport pathway of QacA.

It should be pointed out that during the last few years, the use of styrene maleic acid (SMA) copolymers in lieu of detergents has gained popularity as a promising approach for structural and functional studies of membrane proteins (Brown *et al.*,

2021). Extraction, purification and solubilisation of membranes with such amphipathic copolymers produce SMA lipid particles (SMALPs), maintaining the membrane proteins in their native lipid bilayer environment and avoiding the detrimental effects due to the use of detergents (Fiori *et al.*, 2020). SMALPs, also referred to as native nanodiscs, have emerged as a revolutionary technology for preparing intact membrane:protein complexes (“memteins”) as fundamental functional units (Chen *et al.*, 2020; Brown *et al.*, 2021). Binding studies can be performed in nanodiscs to provide native-like affinities for binding of substrates and inhibitors (Lemieux and Overduin, 2020).

In Chapter 3, replacement of amino acid residues in TMS 12 and its flanking loops were investigated by cysteine-scanning mutagenesis and effects of mutations on antimicrobial activity and Et efflux capacity measured. MIC determination assays identified three single cysteine-substituted QacA mutants, namely G361C (Loop 11-12), G379C and S378 (TMS 12), that exhibited significantly reduced QacA resistance to selected substrates (PE in case of G361C; DQ, CH and PE in case of G379C; BK, DQ, CH and PE in case of S378). Furthermore, Et MIC and transport assays identified that QacA mutants I374C, S387C (TMS 12) and A399C (Loop 12-13) had impaired capacity for Et efflux. In this chapter, these seven residues were subjected to further examination using a suite of biochemical assays with the aim to: 1) determine whether they are crucial for QacA-mediated transport of bivalent cations; and 2) determine if they play a direct role in QacA substrate-binding site(s)/transport pathway. Additionally, initial steps towards establishing an SPR method for direct binding kinetics and affinity measurements of QacA were conducted by optimisation of protein purification methodology.

4.2 Results and Discussion

4.2.1 DAPI MIC analysis

The QacA mutants G361C, G379C and S387C, which conferred $\geq 50\%$ reduction of resistance to at least one of the tested bivalent substrates, were further examined to determine if they were capable of mediating resistance to DAPI, another representative of bivalent substrates. DAPI was chosen since it has previously been identified as a good bivalent substrate for QacA in *E. coli* cells able to show an increase in fluorescence intensity when bound to double-stranded DNA inside the cells (Mitchell *et al.*, 1999; Xu *et al.*, 2006; Hassan *et al.*, 2007). Therefore, DAPI efflux activities of cells expressing QacA and its variants can be measured by the detection of a decrease in the level of fluorescence over time. Prior to DAPI efflux assays, MIC tests with DAPI were first carried out using the standard agar dilution method (Section 2.10). These mutations were found to markedly decrease the ability of QacA to confer DAPI resistance (Figure 4.1). The most significant reduction in DAPI resistance capacity is seen with the S387C derivative, which only had 40% of the resistance level compared to the wild-type QacA protein. These results further revealed the importance of amino acid residues G361, G379 and S387 in resistance capacity of QacA against bivalent cations.

4.2.2 Fluorometric transport assay of DAPI

Compared to wild-type QacA the G361C, G379C and S387C mutants had a significantly reduced resistance to DAPI (Section 4.2.1) and at least one additional bivalent cation (Table 3.1). To determine if these substitutions affected bivalent substrate transport, fluorescent transport assays of QacA using DAPI were undertaken (Section 2.11). These DAPI transport assays were conducted in at least

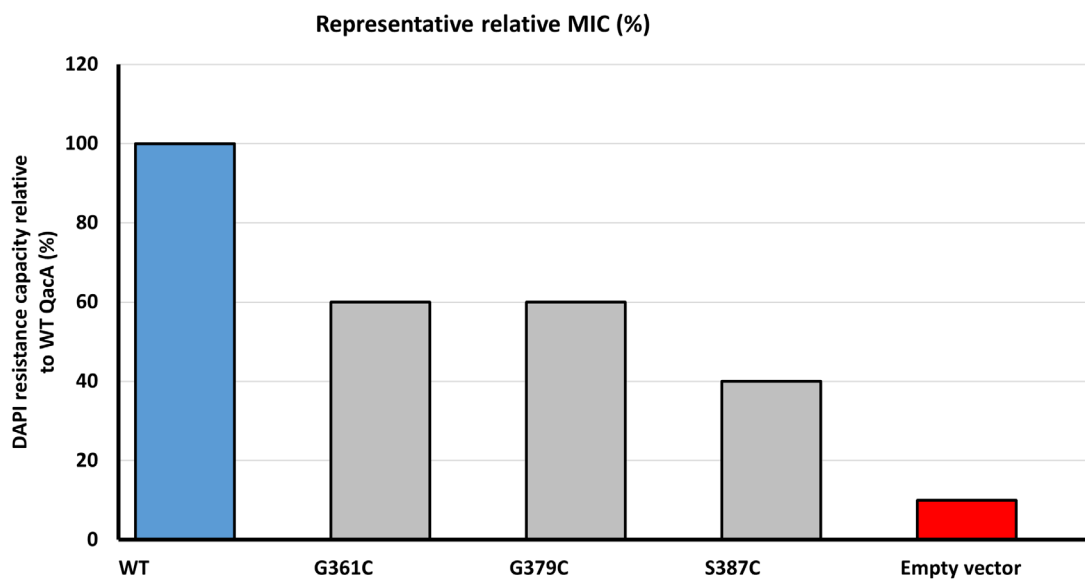


Figure 4.1 DAPI resistance capacity of G361C, G379C and S387C QacA mutants.

MICs were determined by a standard agar dilution method, where *E. coli* DH5 α cells expressing wild-type and mutant QacA proteins were grown on LB agar supplemented with 5-60 $\mu\text{g}/\text{mL}$ final concentration of DAPI as described in Section 2.10. Data are representative of at least three independent experiments. The MIC of QacA mutants are shown as percentages relative to the wild-type QacA control (blue). Cells expressing the empty vector (pBluescript II SK) are included as a negative control (red bar).

triplicate and representative DAPI efflux traces are shown in Figure 4.2. These transport studies demonstrated that G361C and G379C mutants had respectively 19% and 20% reduction in the DAPI transport activity compared to QacA wild-type level (Figure 4.2, A and B). This suggests that G361 and G379 are not essential for the transport of bivalent cations. Interestingly, the S387C mutation resulted in a significant reduction (70%) in DAPI transport activity (Figure 4.2, C) indicating that this residue plays an important role in the transport of bivalent substrates of QacA.

4.2.3 Influence of substrate binding on solvent accessibility

Cysteine labelling using maleimide derivatives after preincubation with varied concentration of substrates for membrane transport proteins has been employed previously as a biochemical methodology to probe the substrate-binding site and provide conformational insights (Krishnamoorthy *et al.*, 2013; Calabrese *et al.*, 2017). Basically, an introduced cysteine residue which is juxtaposed in close proximity to the substrate-binding site(s) would be allosterically protected from maleimide modification by the addition of substrates; or substrate-binding could lead to a conformational change in the protein, thereby making the cysteine residues more or less accessible to maleimide labelling (Xu *et al.*, 2006; Krishnamoorthy *et al.*, 2013). Against this backdrop, the effects of preincubation with selected QacA substrates on the labelling profile of the QacA G361C, G379C and S387C mutants were examined. The selection of substrates was based on MIC results where the mutants had a significant reduction of resistance against those substrates (Table 3.1 and Figure 4.1). Et was an exception, since no significant reduction was observed for the MIC for Et; therefore it was included as a control for all mutants. Membrane vesicles of

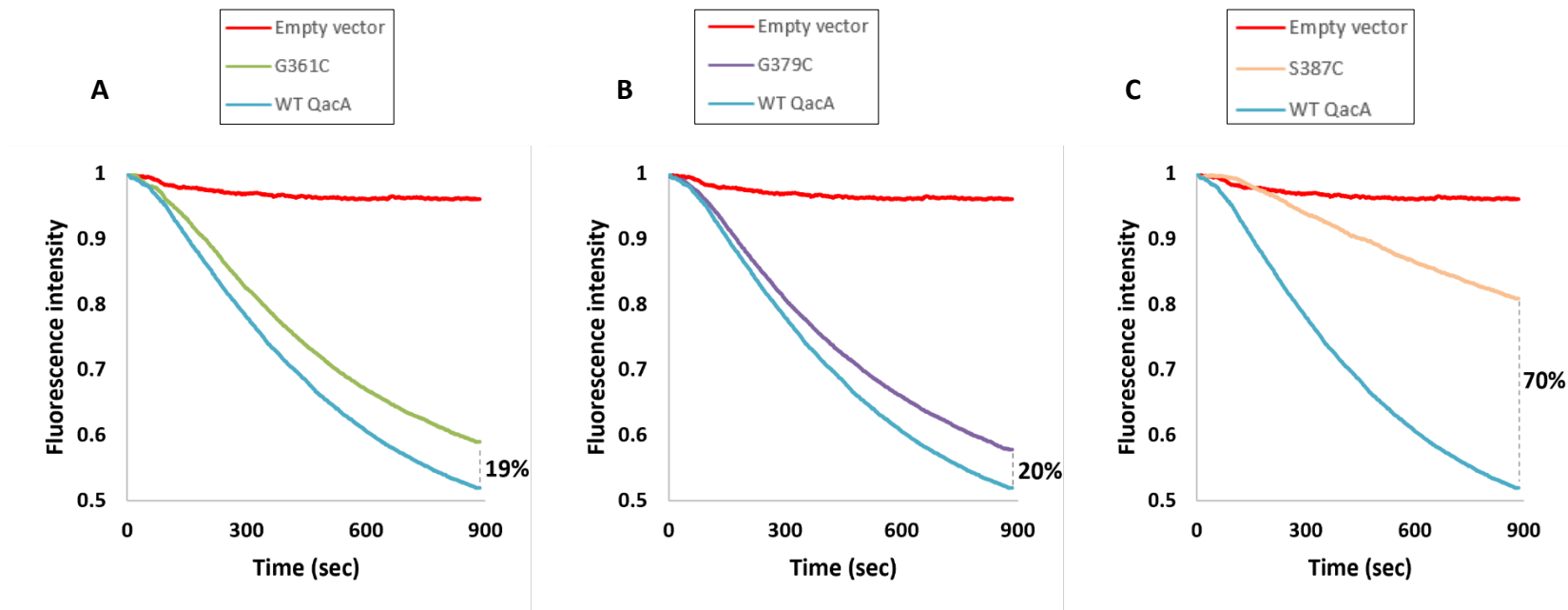


Figure 4.2 Fluorometric transport assays of DAPI.

E. coli DH5 α cells carrying the pBluescript II SK (empty vector, red), pSK7201 (wild-type QacA, cyan) and plasmids encoding **(A)** G361C, **(B)** G379C and **(C)** S387C QacA mutants (green, purple and yellow), were loaded with 10 μ M DAPI. Efflux of the bivalent QacA substrate DAPI from DAPI-loaded and energy-starved cells were measured fluorimetrically after energisation of transport with 500 mM sodium formate (Section 2.11) and plotted for each mutant as indicated above each graph. Transport assays were performed in at least triplicate and representative results are shown. The values next to the vertical dashed line denote the reduction in the DAPI transport activity of each mutant compared to QacA wild-type level as a percentage.

E. coli DH5 α cells expressing QacA G361C, G379C and S387C mutants were incubated at 37°C for 5 minutes in the absence or presence of each substrate before FM was added as described in Section 2.9.1. The mutant proteins were preincubated with different concentrations of each substrate ranging between 0.5 and 10 mM to find an optimal concentration and to ensure that unaffected maleimide labelling was not due to an incomplete reaction stoichiometry. High substrate concentration gave ambiguous results since little or no protein was detected on Coomassie Blue-stained SDS-PAGE gels, possibly due to an interference with purification step during FM reaction (Section 2.9). However, it was determined that consistent and reproducible results could be achieved with 2 mM of each substrate.

As can be seen from Figure 4.3, results showed that although preincubation with Et had no considerable effect on FM labelling of the QacA cysteine mutants, preincubation with DAPI (Figure 4.3, purple) produced a significant decrease in FM labelling of G361C and S387C, suggesting that these amino acid positions are likely to be either directly involved in or located in close vicinity to the DAPI substrate-binding site. Furthermore, the results showed that a significant proportion of QacA C387 protein was protected from maleimide modification in the presence of CH (Figure 4.3, green), possibly because of the direct involvement of S387 in binding to CH or that the location of this position is in close vicinity to the CH binding site. The addition of Et, BK, DQ and PE did not affect labelling profiles of the three QacA cysteine variants, suggesting that residues at positions 361, 379 and 387 may not be part of the binding pockets of these substrates nor located in close proximity of substrate-binding pockets for those drugs. It should be noted that unlike G361C and S387C that exhibited relatively high maleimide reactivity, G379C had essentially low reactivity

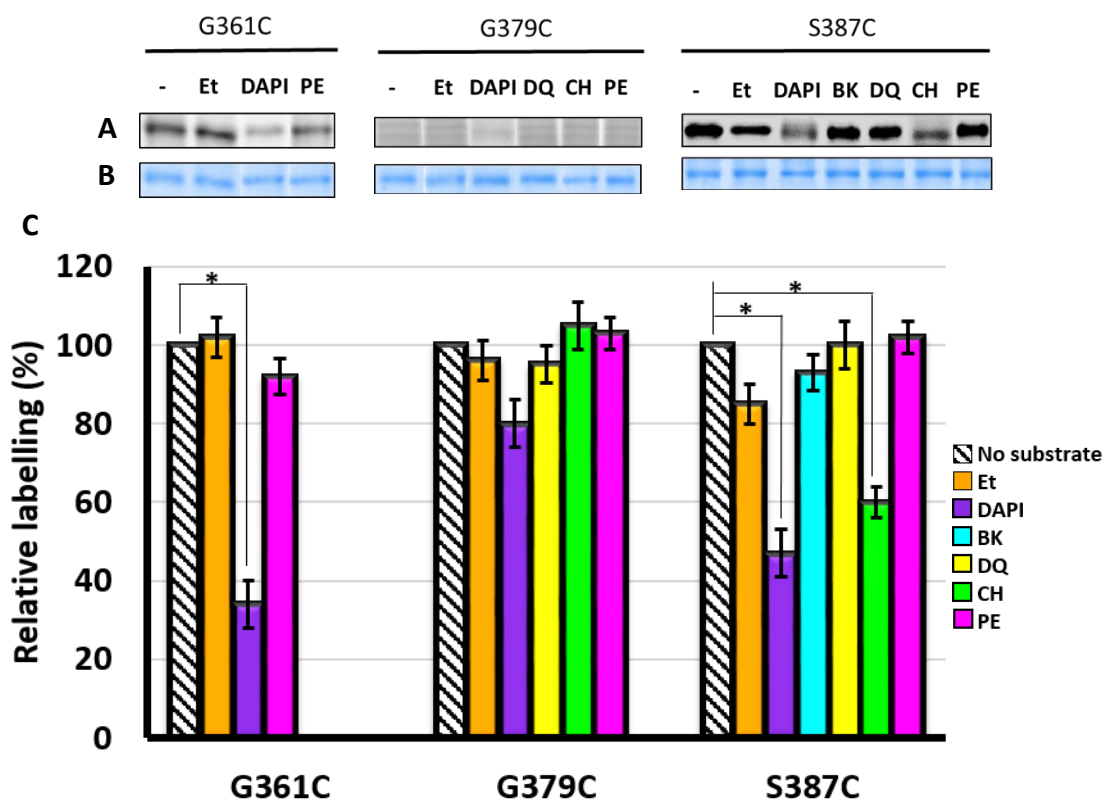


Figure 4.3 Labelling reactivity of G361C, G379C and S387C QacA mutants with fluorescein maleimide in the presence of selected substrates.

Membrane fractions of *E. coli* cells expressing the G361C, G379C and S387C QacA mutant proteins were preincubated with 2 mM of each QacA substrate individually for 5 min, then labelled with FM as described in Section 2.9.1. **(A)** Fluorescence of bands is directly related to accessibility/reactivity of cysteine with FM after substrate preincubation. – indicates the membrane fraction of each mutant labelled in the absence of substrate. Et: ethidium; DAPI: 4',6-diamidino-2-phenylindole; BK: benzalkonium; DQ: dequalinium; CH: chlorhexidine; PE: pentamidine. **(B)** Corresponding Coomassie Brilliant Blue-stained bands to demonstrate equal loading of QacA on SDS-polyacrylamide gels. **(C)** The percent labelling intensity of the substrate-treated protein relative to the untreated protein for each mutant is shown by the height of the bars coloured as indicated in the right-hand side legend for the ease of visual comparison. Error bars represent SD of three biological replicates. Statistical significance was determined by Student's t-test. Significance ($P < 0.05$) is indicated by an asterisk.

with FM indicating its solvent inaccessible position (Figure 3.6). Therefore, investigating whether or not such solvent inaccessible residues are involved in substrate-binding pockets through this approach seems challenging since significant reductions in their fluorescent labelling are difficult to be visually detected on SDS-polyacrylamide gels.

4.2.4 Effect of NEM treatment on the efflux of DAPI

Modification of single cysteine mutants by maleimide compounds such as NEM has widely been used to gain experimental insights into substrate-binding site and/or translocation pathway of membrane transport proteins (Xu *et al.*, 2006). For example, cysteine-modification using maleimide compounds has been reported to investigate the substrate binding specificity of the RND pump MexD (Mao *et al.*, 2002) and to map the substrate binding sites in the AcrB multidrug efflux pump of *E. coli* (Husain and Nikaido, 2010; Husain *et al.*, 2011). As another example, NEM alkylation of cysteine-substituted mutants in the LacY transporter provided a valuable strategy for studying mechanistic aspects of transport that were later supported by the X-ray crystal structure of LacY (Abramson *et al.*, 2003b). Fluorimetric assays in cells pre-treated with NEM (a non-fluorescent maleimide compound) were employed in previous studies exploring structure-function aspects of QacC (Paulsen *et al.*, 1995) and QacA (Xu *et al.*, 2006; Hassan *et al.*, 2008). To further assess whether thiol modification had an effect on transport function of the QacA mutants G361C, G379C and S387C, DAPI transport studies were undertaken after treatment of bacterial cells with 5 mM NEM as described in Section 2.11.1. It should be mentioned that during optimisation of this assay, there was no observable difference between various NEM concentrations (1-15 mM) as well as various time periods (10–60 min), ensuring that

if efflux was unaffected in the presence of 5 mM NEM this was not due to an incomplete reaction stoichiometry. Another point was that these QacA mutants were not evaluated for the effect of their NEM treatment on Et transport because functional assays revealed that the mutations had little-to-no significant effect on the resistance capacity to monovalent cation Et (Table 3.1).

As expected, NEM treatment did not impact on the rate of DAPI transport from cells carrying wild-type QacA, which inherently contains no cysteine residues (Figure 4.4 A). Additionally, NEM did not impact transport from cells expressing the QacA G379C mutant (Figure 4.4 C). However, treatment with NEM was seen to significantly reduce DAPI efflux in cells expressing the G361C and S387C QacA mutant proteins (Figure 4.4 B, D and E), indicating that these amino acid positions may interact with DAPI or the addition of the maleimide has altered the shape or architecture of the binding pocket. Indeed, binding of NEM at these positions presumably disrupts DAPI binding and/or the transport pathway due to steric hindrance between DAPI and the bulky maleimide group of NEM. Thus, these results together with those from the effects of DAPI binding on FM modification (Figure 4.3) strongly suggest that G361 and S387 are directly involved in the substrate binding site and/or translocation pathway used by DAPI.

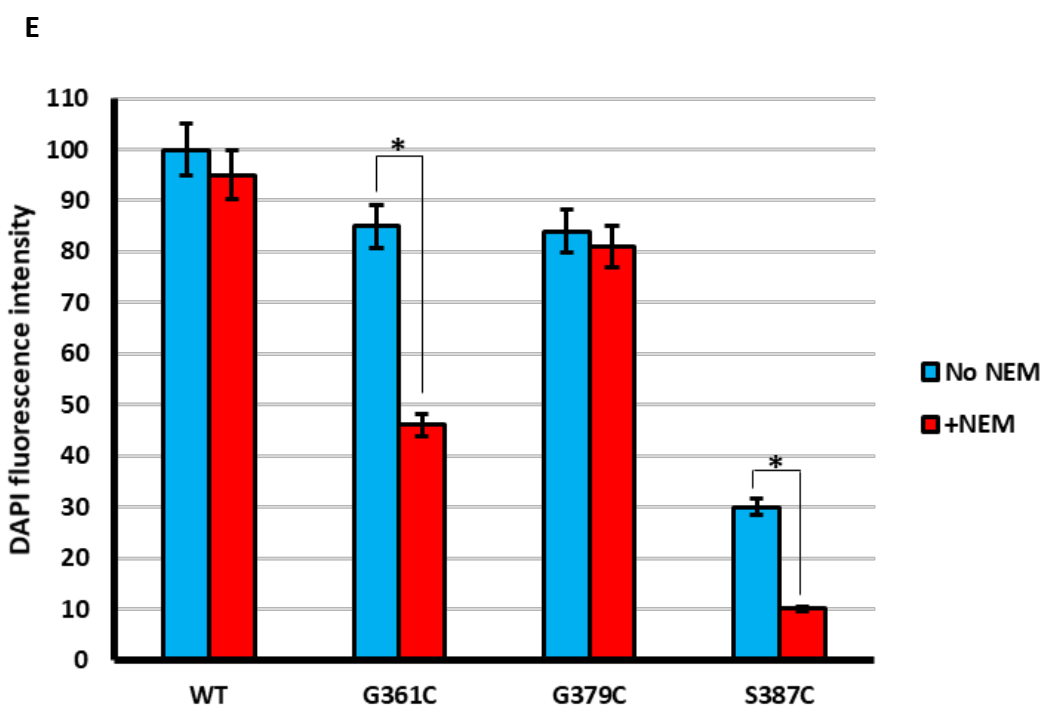
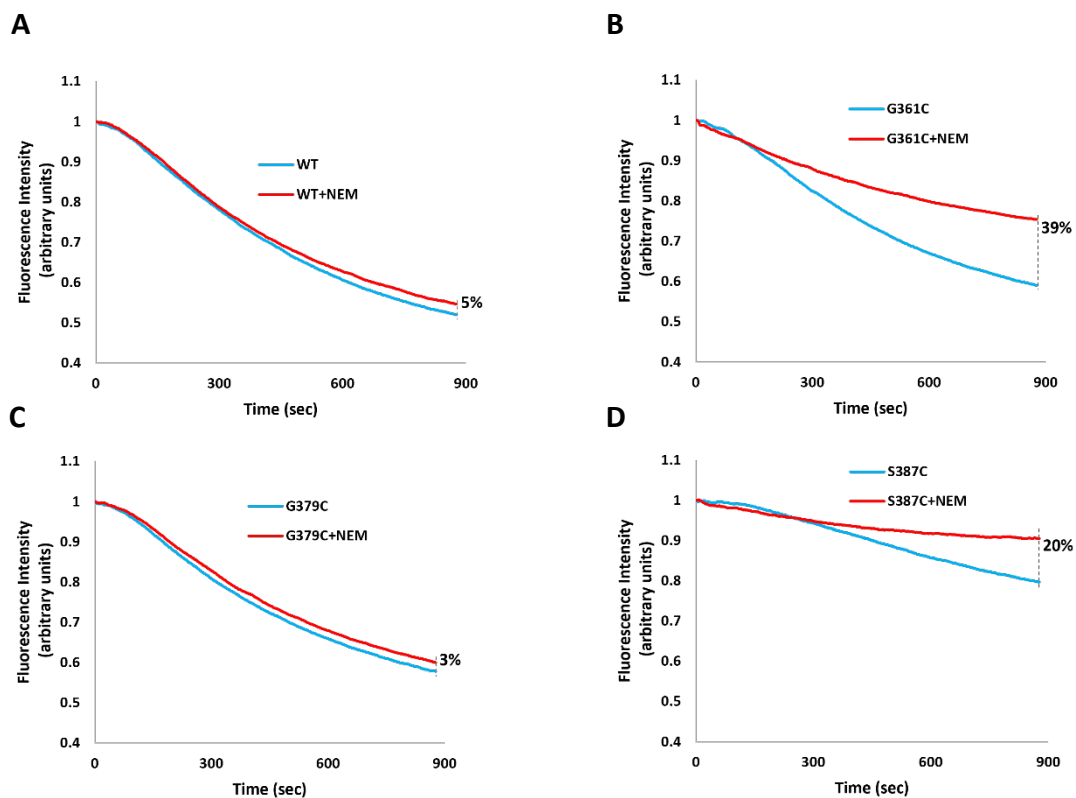


Figure 4.4 DAPI transport activity of QacA and selected cysteine mutants in the absence and presence of NEM.

To determine the effects of NEM binding on the capacity of QacA to efflux DAPI, *E. coli* DH5 α cells expressing pBluescript-based QacA variants were pre-treated with NEM (5 mM) prior to being loaded with 10 μ M DAPI (Section 2.11.1). Transport was energised by the addition of sodium formate (500 mM) at time point zero. **(A to D)** Each graph illustrates results of cells pre-treated with NEM (red) and those loaded with DAPI only (blue). Assays were performed in at least triplicate and representative results are presented above. The values next to the vertical dashed line denote the reduction in the DAPI transport activity of each sample after the addition of NEM as a percentage. **(E)** DAPI transport activities of NEM-treated cells (red) versus non-NEM-treated cells (blue). The height of the bars corresponds to the final efflux values shown as percentages. The final efflux value of the control (wild-type QacA without NEM) was set as 100%. Error bars represent SD of three biological replicates. Statistical significance was determined by Student's t-test. Significance ($P < 0.05$) is indicated by an asterisk.

4.2.5 Determination of kinetics of substrate transport by selected QacA mutants

Studying the kinetic behaviour of an efflux pump in intact cells can be used to determine the binding affinity of substrates (Nikaido, 2011). The rate of QacA-mediated transport of substrates has been shown to follow Michaelis-Menten kinetics (Mitchell *et al.*, 1999) whereby kinetic parameters of transport, V_{max} and K_m , can be derived. V_{max} is the maximum velocity of substrate transport and K_m (Michaelis constant) shows the substrate concentration required to reach half-maximal transport velocity. The K_m value therefore is an indication of the binding affinity of a transporter for its substrate (Vivian and Polli, 2014).

For kinetic analysis of transport, Et and DAPI were chosen as the two substrates to represent the monovalent and bivalent substrates of QacA, respectively and have been successfully used in our laboratory previously (Mitchell *et al.*, 1999; Xu *et al.*, 2006; Wu *et al.*, 2008). The kinetics of QacA-mediated efflux of Et and DAPI were measured in intact *E. coli* cells expressing QacA variants loaded with a range of 10 different concentrations of each substrate (Section 2.12). Representative Michaelis-Menten curves for wild-type QacA are presented in Figure 4.5. The K_m values derived for Et and DAPI transport were all less than 20 μM , consistent with previous results (Mitchell *et al.*, 1999; Xu *et al.*, 2006; Wu *et al.*, 2008).

Under the same conditions used for wild-type QacA, the K_m and V_{max} values of Et and DAPI transport for selected QacA mutants were determined. The selected mutants for Et transport kinetics included QacA I374C, S387C and A399C which displayed the lowest Et MIC among the mutants tested (Section 3.2.3) and for DAPI transport

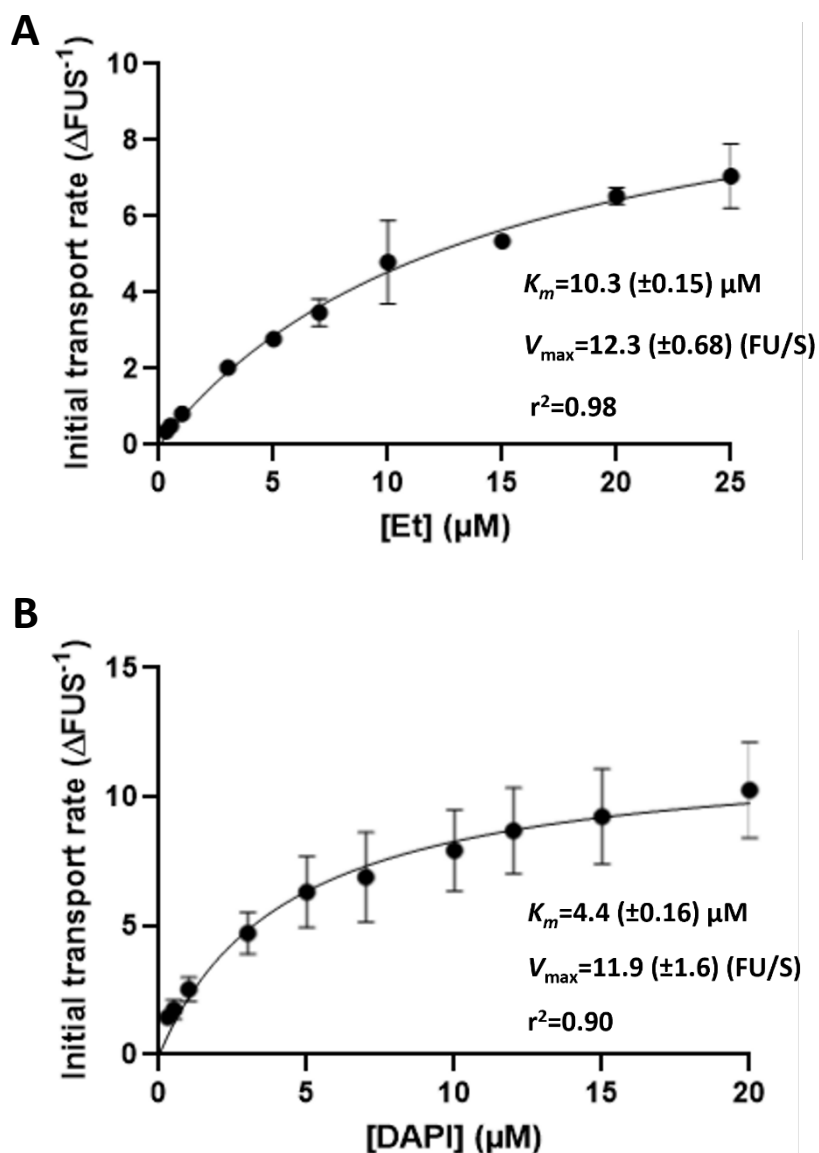


Figure 4.5 Michaelis–Menten curves depicting kinetics of substrate transport by wild-type QacA.

The initial transport velocity, represented by the change in fluorescent units per second ($\Delta\text{FU}\cdot\text{S}^{-1}$), of **(A)** ethidium and **(B)** DAPI was calculated in the presence of increasing concentrations of each substrate (Section 2.12). K_m and V_{\max} values were derived from the plots by fitting the data to a Michaelis-Menten equation with GraphPad Prism version 8 (GraphPad Software Inc., USA). Data are from three independent replicate experiments with r-squared values (r^2) of the goodness of fit ≥ 0.90 . Error bars show SEM.

kinetics the QacA G361C, G379C and S387C derivatives were selected as they showed significant reduction in MIC for at least one of the bivalent cations tested (Section 3.2.3) as well as impaired DAPI resistance activity (Section 4.2.1).

As shown in Table 4.1, QacA I374C, S387C and A399C (Et resistance-defective mutants) showed no significant difference in the K_m values for Et compared to wild-type QacA indicating that these residues do not directly bind Et. A similar lack of effect on substrate binding affinity was seen with mutation of some residues in the binding pocket of QacR due to flexibility of binding pockets in multidrug proteins (Peters *et al.*, 2011). Thus, their observed impaired Et resistance activity could be attributable to their role in other aspects rather than Et binding, perhaps in Et translocation.

The results shown in Table 4.2 revealed a non-statistically significant reduction in K_m for DAPI efflux by QacA mutants G361C, G379C and S387C (bivalent cation resistance-defective mutants) compared to wild-type QacA. Thus, a reliable conclusion about higher binding affinity between DAPI with G361C and S387C QacA mutant proteins (despite ~two-fold decrease in K_m compared to wild-type QacA) is difficult to draw due to low K_m values (~2-4 μM). Nevertheless, it lends itself to further analysis by using a direct and sensitive substrate binding assay to determine the dissociation constant (K_d) for specific binding of DAPI and other non-fluorescent bivalent substrates (DQ, CH and PE) to wild-type QacA and mutant derivatives. However, purified QacA protein is a prerequisite of such studies and these requirements are discussed in the next section.

Table 4.1 Comparative kinetic data of ethidium resistance-defective mutants

QacA	V_{\max} (FU/S) ^a	K_m (μ M) ^b
WT	12.3 (\pm 0.68)	10.3 (\pm 0.15)
I374C	12.7 (\pm 1.88)	14.3 (\pm 1.73)
S387C	10.4 (\pm 1.16)	16.5 (\pm 2.04)
A399C	11.8 (\pm 2.06)	14.7 (\pm 4.93)

^{a,b} V_{\max} indicates maximal transport capacity of QacA proteins, K_m indicates affinity of their binding sites for ethidium. The V_{\max} and K_m values for ethidium transport by the selected QacA mutants were measured under the same conditions used for wild-type QacA (WT) as shown in Figure 4.5, A. The results are the mean of three biological replicates \pm SEM. No significant difference was observed for the V_{\max} and K_m values ($P > 0.05$). Significance was calculated by Student's t-test.

Table 4.2 Comparative kinetic data of DAPI resistance-defective mutants

QacA	V_{\max} (FU/S)^a	K_m (μM)^b
WT	11.9 (\pm 1.56)	4.4 (\pm 0.16)
G361C	15.3 (\pm 1.75)	2.2 (\pm 0.13)
G379C	13.5 (\pm 1.17)	3.2 (\pm 0.15)
S387C	12.7 (\pm 1.52)	2.7 (\pm 0.10)

^{a,b} V_{\max} indicates maximal transport capacity of QacA proteins, K_m indicates affinity of their binding sites for DAPI. The V_{\max} and K_m values for DAPI transport by the selected QacA mutants were measured under the same conditions used for wild-type QacA as shown in Figure 4.5, B. The results are the mean of three biological replicates \pm SEM. No significant difference was observed for the V_{\max} and K_m values ($P > 0.05$). Significance was calculated by Student's t-test.

4.2.6 Overexpression and purification of QacA and TetA(K) proteins from a pBAD expression vector

The overexpression and downstream purification of membrane proteins such as QacA is prerequisite for *in vitro* binding studies. The pBluescript II SK-based vector system in *E. coli* provides constitutive low-level expression (leaky expression) of QacA protein which is at a level suitable for *in vivo* functional QacA analyses (Hassan *et al.*, 2006a; Xu *et al.*, 2006; Hassan *et al.*, 2009). However, using various growth and induction conditions to overexpress QacA from the pBluescript II SK-based expression plasmids resulted in relatively low protein yields. The *E. coli* pBAD expression system has been utilised successfully for the overexpression and purification of MFS transporters such as the GlpT (Auer *et al.*, 2001) and MdtM (Holdsworth and Law, 2013) proteins from *E. coli*. Additionally, QacA expression derived from several vector systems containing codon-optimised *qacA* (*co-qacA*) in *E. coli* TOP10 strain under various culture conditions has been performed and results suggested that the pBAD expression system is well suited for high-level QacA protein expression (Hassan *et al.*, 2009). Heterologous gene expression in pBAD-based expression vectors is driven under tight control of the promoter of the L-arabinose operon, pBAD (Guzman *et al.*, 1995).

Structural integrity of purified QacA protein obtained from this pBAD expression system has been previously tested by circular dichroism (CD) spectroscopy analysis. The CD results verified the expected secondary structure composition of purified QacA protein (Hassan *et al.*, 2009). Furthermore, substrate-binding assays using R6G, a highly fluorescent substrate for QacA, have shown that QacA protein retains its activity after purification (Hassan *et al.*, 2009). Therefore, in this study *E. coli* TOP10

and the pBAD expression system were used for their capacity to overproduce purified QacA proteins to be tested in a SPR binding assay.

In addition to wild-type QacA protein to be used as the positive control, a negative control is required for SPR binding assays to correct for non-specific binding. An appropriate negative control needs to have structural similarities such as similar hydrophobicity to the test protein but incapable of binding to the substrates tested (Mowla *et al.*, 2018). Against this backdrop, the staphylococcal TetA(K) protein (Hassan *et al.*, 2006) was selected as a negative control for SPR binding assays of QacA, because it contains 14 TMS similar to QacA. Unlike multidrug QacA, TetA(K) is a single-drug transporter (specific for tetracycline) and is incapable of binding to QacA substrates.

To overexpress wild-type QacA and TetA(K), *E. coli* TOP10 cells harbouring the plasmids pSK7128 and pSK7122 (Table 2.3), respectively, were cultured, induced with L-arabinose (Section 2.7.1), and whole membrane fractions isolated individually (Section 2.7.2). The C-terminal 6xHis-tagged QacA and TetA(K) proteins were purified by nickel affinity resins using the batch purification method (Section 2.7.3). To evaluate the purification efficiency, samples collected from each purification step were analysed on a SDS-PAGE gel stained with Coomassie blue (Figure 4.6 and Figure 4.7). The SDS-PAGE profile showed the expected proteins at the predicted molecular weight with high purity. QacA and TetA(K) have predicted sizes of 55 kDa and 51 kDa, respectively, but migrate faster on SDS-PAGE as previously described (Ginn *et al.*, 2000; Hassan *et al.*, 2009). Such discrepancy between the exact molecular weight and anomalous migration behaviour on SDS-PAGE is commonly seen in integral

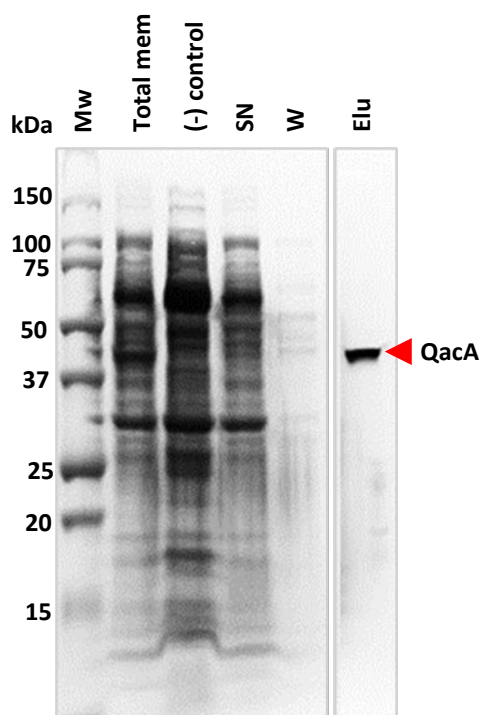


Figure 4.6 Purification of wild-type QacA protein overexpressed in *E. coli* TOP10 cells.

E. coli TOP10 cells harbouring pSK7128 were grown to $OD_{600}=0.8$ and induced with 0.002% (w/v) L-arabinose for 21 hours (Section 2.7.1). Isolated membrane fractions were subjected to batch purification with nickel affinity resins (Section 2.7.3). Equal quantities of fractions collected during purification stages of QacA were separated on a 10% SDS-PAGE gel (Section 2.8.2) and stained with Coomassie Blue (Section 2.8.3). The samples loaded in lanes are labelled as follows: MW, molecular weight marker (Precision Plus Protein™ Unstained Protein Standards, Bio-Rad); Total mem, total membrane proteins prepared from *E. coli* TOP10 cells expressing pSK7128 and solubilised; (-) control, total membrane proteins prepared from cells carrying the empty vector as negative control; SN, supernatant collected after centrifugation of nickel resin; W, sample of flow-through collected after first resin wash; Elu, sample of protein eluted from the nickel resin. The location of the purified QacA protein band is indicated by arrow at the side of the gel image.

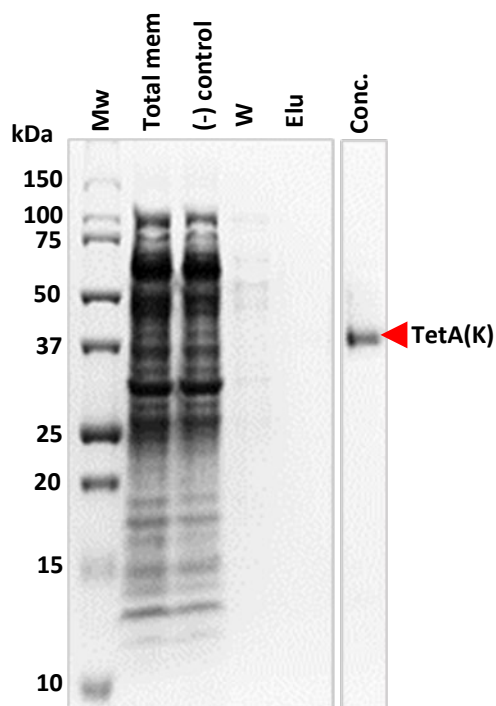


Figure 4.7 Purification of TetA(K) protein overexpressed in *E. coli* TOP10 cells.

E. coli TOP10 strain harbouring pSK7122 was grown to $OD_{600}=0.8$ and induced with 0.0005% (w/v) L-arabinose for 4 hours (Section 2.7.1). Isolated membrane fractions were subjected to batch purification with nickel affinity resins (Section 2.7.3). Equal quantities of fractions collected during purification stages of TetA(K) were separated on a 10% SDS-PAGE gel (Section 2.8.2) and stained with Coomassie Blue (Section 2.8.3). The samples loaded in lanes are labelled as follows: MW, molecular weight marker (Precision Plus Protein™ Unstained Protein Standards, Bio-Rad); Total mem, total membrane proteins prepared from *E. coli* TOP10 cells expressing pSK7122 and solubilised; (-) control, total membrane proteins prepared from cells carrying the empty vector as negative control; W, sample of flow-through collected after first resin wash; Elu, sample of protein eluted from the nickel resin. Conc., sample of a concentrated protein after eluting from the nickel resin. The location of the purified TetA(K) protein band is indicated by arrow at the side of the gel image.

membrane proteins (Mowla *et al.*, 2018). Under these conditions, QacA and TetA(K) could be purified with typical yields of approximately 1 mg of pure protein per litre of culture which is more than sufficient for SPR binding assays to be conducted. Purified proteins are usually concentrated to 0.5 mg/mL as these concentrations are commonly employed in SPR protocols (Polyak *et al.*, 2020). As can be seen from Figure 4.7, TetA(K) is hardly visible on Coomassie blue-stained SDS-PAGE gel after elution but it could be easily detected after elution fractions were concentrated on a centrifugal filter device (Section 2.7.3). This is because TetA(K) is difficult to overexpress as also previously observed (Hassan *et al.*, 2009).

4.2.7 Generation of expression construct for QacA S387C

The QacA S387C mutant was found to be directly involved in binding to DAPI and CH (Section 4.2.3). To determine the binding kinetics of this protein by SPR binding assays, purified protein is required. To this end, a subcloning protocol for the pBAD-based expression construct for QacA S387C was first designed using SnapGene (Figure 4.8). To generate the construct, plasmids pBSQacA/S387C (pBluescript II SK-based) and pSK7128 (pBAD-based) (Table 2.3) were digested with restriction endonucleases *KpnI* and *XbaI*. The resulting fragments containing the mutant *qacA* gene (1415 bp) and the pBAD vector backbone (4200 bp) as shown in Figure 4.8C were excised, gel purified (Section 2.5.4) and ligated together (Section 2.6.3). The ligation mixture was transformed into competent *E. coli* DH5 α cells. The desired transformants were screened by *KpnI* and *XbaI* restriction digestion. The recombinant plasmid was confirmed by sequencing and designated as pBADQacA/S387C before being transformed into *E. coli* TOP10 cells. This construct was used for overexpression of QacA S387C mutant protein (Section 4.2.8).

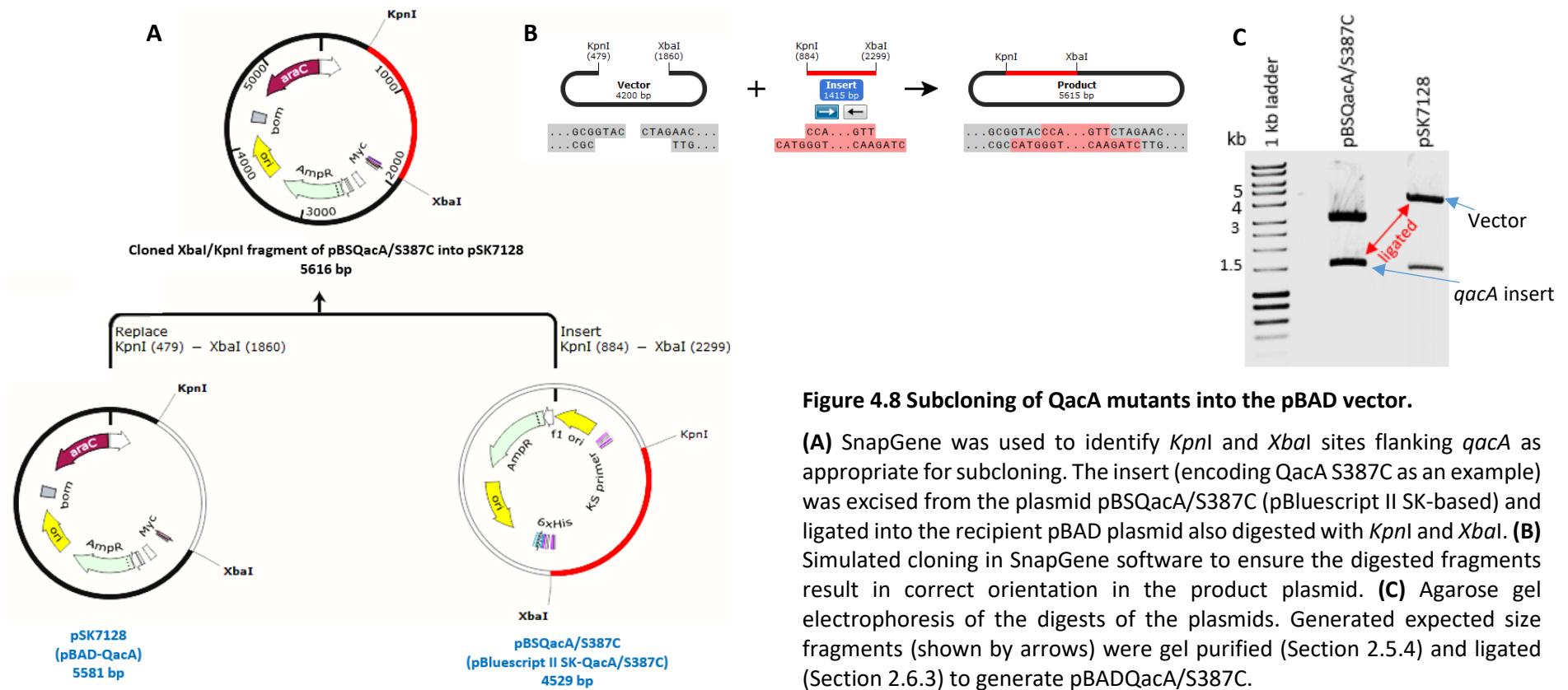


Figure 4.8 Subcloning of QacA mutants into the pBAD vector.

(A) SnapGene was used to identify *KpnI* and *XbaI* sites flanking *qacA* as appropriate for subcloning. The insert (encoding QacA S387C as an example) was excised from the plasmid pBSQacA/S387C (pBluescript II SK-based) and ligated into the recipient pBAD plasmid also digested with *KpnI* and *XbaI*. (B) Simulated cloning in SnapGene software to ensure the digested fragments result in correct orientation in the product plasmid. (C) Agarose gel electrophoresis of the digests of the plasmids. Generated expected size fragments (shown by arrows) were gel purified (Section 2.5.4) and ligated (Section 2.6.3) to generate pBADQacA/S387C.

4.2.8 Overexpression and purification of QacA S387C mutant protein

To overexpress the QacA S387C mutant protein, *E. coli* TOP10 cells harbouring pBADQacA/S387C (constructed in Section 4.2.7) were cultured and induced with 0.002% (w/v) L-arabinose for 21 hours (Section 2.7.1). Whole membrane fractions were isolated (Section 2.7.2) and subjected to batch purification using nickel affinity resin (Section 2.7.3). SDS-PAGE analysis of samples collected during purification steps of the QacA S387C mutant protein (Figure 4.9) showed the expected size protein band in the eluted fraction. The migration position is similar to that of the wild-type QacA protein on SDS-PAGE (Figure 4.6). A yield of approximately 1 mg of pure QacA S387C mutant protein per litre of culture was obtained.

Overexpression and purification of the wild-type and mutant QacA proteins as well as the TetA(K) protein by the above-mentioned experiments provided the starting protein material for SPR binding assay. Setting up a SPR assay for QacA was initially planned but unfortunately was not performed in view of COVID-19-related complexities and restrictions. Future SPR binding studies between these already-prepared proteins and non-fluorescent QacA substrates including BK, DQ, CH and PE should be conducted to obtain direct and specific measurements of their binding affinity.

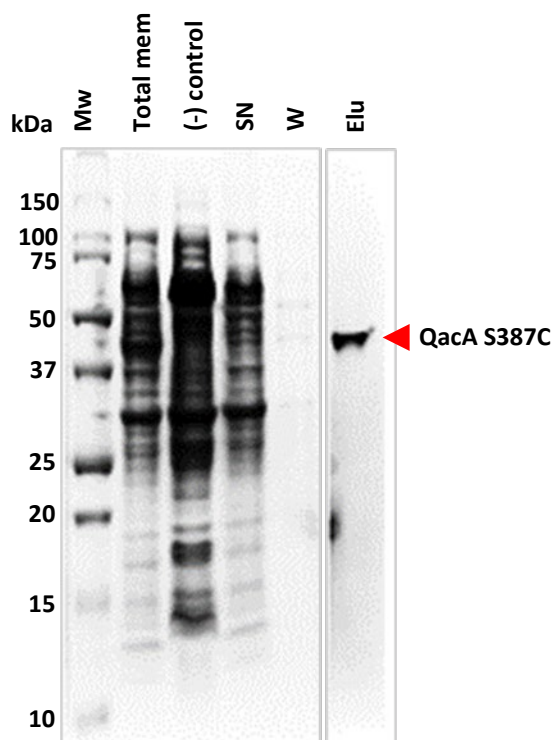


Figure 4.9 Purification of QacA S387C mutant protein overexpressed in *E. coli* TOP10 cells.

E. coli TOP10 cells carrying the constructed plasmid pBADQacA/S387C (Section 4.2.7) were grown to $OD_{600}=0.8$ and induced with 0.002% (w/v) L-arabinose for 21 hours (Section 2.7.1). Isolated membrane fractions were subjected to batch purification with nickel affinity resins (Section 2.7.3). Equal quantities of fractions collected during purification stages of QacA were separated on a 10% SDS-PAGE gel (Section 2.8.2) and stained with Coomassie Blue (Section 2.8.3). The samples loaded in lanes are labelled as follows: MW, molecular weight marker (Precision Plus Protein™ Unstained Protein Standards, Bio-Rad); Total mem, total membrane proteins prepared from *E. coli* TOP10 cells expressing pBADQacA/S387C and solubilised; (-) control, total membrane proteins prepared from cells carrying the empty vector as negative control; SN, supernatant collected after centrifugation of nickel resin; W, sample of flow-through collected after first resin wash; Elu, sample of protein eluted from the nickel resin. The location of the purified QacA S387C protein band is indicated by arrow at the side of the gel image.

4.3 Conclusions

High-resolution structures with and without bound substrate(s) are required to accurately determine how or where substrates interact with multidrug efflux pumps (Schindler *et al.*, 2013b; Schuller *et al.*, 2019). A growing understanding of multidrug efflux systems and their precise molecular determinants of interactions with antimicrobials has opened a new avenue in the development of novel antimicrobials less likely to be extruded, or inhibitors more efficient in hampering the efflux process (Atzori *et al.*, 2019b; Darzynkiewicz *et al.*, 2019). Details of the QacA substrate-recognition and transport mechanism remained largely unknown in part due to lack of high-resolution structural data for QacA. Molecular biological and biochemical methods can offer useful low-resolution structural information of membrane proteins, including characterisation of the substrate-binding site (Lin *et al.*, 2019). Cysteine-scanning mutagenesis and subsequent functional analyses identified that mutations of G361, G379 and S387 had deleterious effects on resistance capacity against some QacA substrates, in particular bivalent cationic substrates (Chapter 3). However, MIC observations are not discriminating the specific interactions between compounds and efflux protein. Prompted by these considerations, the focus of this chapter was to delineate the specific contributions of important residues in substrate binding and/or transport by employing a suite of molecular and biochemical assays.

The capacity of the QacA mutants G361C, G379C and S387C was first investigated to determine whether they impart resistance against DAPI, a bivalent cationic substrate of QacA and could efflux it out of the cell as it is a fluorescent dye. Resistance analysis showed all three mutants had a significantly impaired ability in resistance against DAPI (Section 4.2.1). DAPI transport assays revealed that mutation of G361 and G379

had only a modest effect on DAPI transport capacity while the S387C mutant exhibited significantly reduced DAPI export (Section 4.2.2). Overall, analysis of DAPI resistance and transport indicate that G361 and G379 seemed not to be directly involved in transport of DAPI, whereas S387 appeared to play a major role in transport of DAPI. Furthermore, residues G361, G379 and S387 did not completely abrogate QacA-mediated DAPI resistance and transport. They may be involved in DAPI binding or stabilising the DAPI binding site, as suggested by studies in other MFS multidrug efflux pumps such as MdfA (Schuller *et al.*, 2019) and LmrP (Schaedler and van Veen, 2010; Nair *et al.*, 2016) where mutations in binding-site residues did not completely abolish a substrate transport function.

Results of the effects of DAPI preincubation on labelling experiments of cysteine mutants with FM (Figure 4.3), concordant with the NEM treatment on DAPI efflux (Figure 4.4), demonstrated that G361 and S387 are directly involved in the DAPI substrate-binding site(s)/transport pathway. Furthermore, the level of FM reactivity observed for cysteine incorporated at position 387 was drastically reduced in the presence of CH (Figure 4.3) implying that S387 on helix 12 of QacA forms part of or is spatially juxtaposed to the CH binding site. It can also be inferred that CH and DAPI may share an overlapping binding pocket that involves TMS 12. In contrast to DAPI, preincubation of QacA mutants G361C, G379C and S387C with Et showed no appreciable effects on FM reactivity suggesting that TMS 12 does not play a major role in Et binding site. The results are in agreement with a previous study suggesting the involvement of TMS 12 of QacA in binding to bivalent cations (Hassan *et al.*, 2007b). It should be noted that similar substrate preincubation studies in MdfA have indicated the involvement of TMS 10 (corresponding to TMS 12 of QacA) in substrate

recognition pocket as maleimide labelling of V335 was appreciably inhibited by preincubation with chloramphenicol and tetraphenylphosphonium (Adler and Bibi, 2004; Adler and Bibi, 2005).

DAPI kinetic experiments were unable to provide clarity on the effect of cysteine replacement of the residues G361, G379 and S387 in DAPI binding affinity due to a non-statistically significant reduction in K_m values for DAPI transport (Table 4.2). Such a small difference in the binding affinity for DAPI may be because multidrug binding proteins (like QacA) have very low affinity interactions with the substrates to allow for the broad substrate specificity as seen for QacR (Peters *et al.*, 2011). Future studies using a more sensitive substrate binding assay such as SPR could be conducted on QacA mutants to directly determine the specific binding and K_d of DAPI and other bivalent substrates, namely DQ, CH and PE which are non-fluorescent. The purified QacA protein (carrying a C-terminal 6xHis-tag) can be directly captured on an NTA SPR sensor chip via Ni-mediated affinity capturing, which has been successfully used for the study of membrane proteins by SPR (Trahey *et al.*, 2015).

An important point that has to be considered is that glycine residues contribute greatly to TMS flexibility which is particularly important for the normal activity of efflux pumps (Costa *et al.*, 2019). In the 12-TMS MDR EmrD transporter from *E. coli*, MD simulation studies have shown that TMS 10 (equivalent to TMS 12 in 14-TMS MFS proteins) go through a large motion during the transport of substrate. This high mobility contributes to conformational fluctuations necessary for substrate translocation pathway. The presence of glycine residues can facilitate such helix flexibility (Baker *et al.*, 2012). It would be reasonable to suggest that in QacA,

alteration of glycine residues at position 361 and 379 disfavours the flexibility of helix 12 and therefore affects the substrate transport pathway. Similar speculation can also be made regarding the glycine residue at 377 in TMS 12 of QacA that has been identified previously to be important for resistance activity against bivalent cations (Hassan *et al.*, 2007b).

In summary, this study provided further knowledge about structural and functional roles of important amino acid residues within and around TMS 12 of QacA. Furthermore, this study helped to build on the pre-existing structure-function data of QacA and to arrive at a better understanding about the putative multidrug binding pocket of QacA. More generally, the results can be used in complementing the high-resolution structural data when they are available and also for rational development of inhibitor.

Chapter 5

STRUCTURAL MODELLING OF QACA AND IDENTIFICATION OF PUTATIVE SUBSTRATE-BINDING POCKETS

5.1 Introduction

The QacA efflux pump plays a significant role in development of multidrug resistance in *S. aureus* by the export of antimicrobial compounds particularly antiseptics and disinfectants (Section 1.13). The transport process used by multidrug binding proteins, including QacA, depends on distinct subsets of key residues that interact with each antimicrobial substrate, which in turn coordinate passage of substrates across the membrane (Mueckler and Makepeace, 2009).

Previously reported mutagenesis and downstream molecular and biochemical studies characterised a number of functionally-important residues in QacA (Section 1.9.3.1). Previous chapters of this thesis also built on the knowledge as to which specific residues in and around TMS 12 are potentially involved in the substrate-binding site and transport process. A holistic approach is now needed to integrate the so far identified functional residues in QacA to better understand the overall interactions of QacA with substrates.

An atomic-resolution structure is required to elucidate the molecular basis of substrate binding and transport in transporters (Ma *et al.*, 2019). Such a detailed understanding of structure-function relationships of the transport protein will allow the rational design and development of pharmacological procedures such as inhibitor compounds (Alford *et al.*, 2015; Almeida *et al.*, 2017). The combined use of an antimicrobial agent with an inhibitor holds promise for a successful strategy in curtailing the emerging crisis of efflux-mediated antimicrobial resistance (Anes *et al.*, 2015). The absence of an atomic-resolution structure for QacA has hampered rational inhibitor discovery efforts for this transporter.

Experimental structural determination of membrane proteins, unlike soluble proteins, is still difficult, slow and rather expensive when using common experimental methods, which include X-ray crystallography, nuclear magnetic resonance (NMR) or cryo-electron microscopy (Vénien-Bryan *et al.*, 2017). This is why despite their paramount biological importance, membrane protein structures constitute less than 2% of all protein structures deposited in the PDB as of January 2020 (Choy *et al.*, 2020). Technical experimental challenges in the structural characterisation of membrane proteins result mainly from their insertion in the lipid bilayer as a native environment (Moraes *et al.*, 2014). Not only structural characterisation of membrane proteins (Bogdanov *et al.*, 2008; Casares *et al.*, 2019) but also ligand discovery for these proteins is extremely challenging since they require to be situated in the natural environment of a cell membrane lipid bilayer to maintain protein structure and activity (Huang *et al.*, 2020). However, in the last few years, substantial headway has been made in solving structures of membrane proteins with the application of nanodiscs/SMALPs (Lemieux and Overduin, 2020; Brown *et al.*, 2021).

These challenges associated with experimental determination of membrane proteins structures have led to development of advanced computational algorithms to model their structure. Such powerful approaches are able to provide valuable insights into their structure (Venko *et al.*, 2017; Weinstein *et al.*, 2019). For example, various structural aspects of membrane proteins such as specific protein-lipid interactions, can be elucidated by molecular dynamics (MD) and machine-learning methods (Muller *et al.*, 2019; Marrink *et al.*, 2019). Homology modelling and molecular docking are two well-known computational methods routinely used in structural biology.

These methods play ever-growing roles in providing atomic level insights into the protein structure and substrate-binding interface with the ultimate goal of inhibitor discovery and development (Schlessinger *et al.*, 2018; Gulistan *et al.*, 2020).

Homology (or comparative) modelling, especially for membrane proteins, has matured into a useful and important technique in structural biology to build tertiary structural models of known protein sequences from experimentally determined structures as templates (Almeida *et al.*, 2017; Nikolaev *et al.*, 2018). The use of homology-driven structures for membrane proteins has substantially improved because of an increasing number of suitable template structures and recent advances in effective protein modelling methods (Koehler Leman *et al.*, 2015; Dokholyan, 2020). The homology modelling method is based upon the observation that tertiary structures are more preserved than the primary sequence of the protein during the course of evolution (Shatsky *et al.*, 2008; Siltberg-Liberles *et al.*, 2011). Thus, biological function of proteins and their binding interaction with other molecules are more influenced by their tertiary structure than primary (Breda *et al.*, 2007; Siltberg-Liberles *et al.*, 2011).

Molecular docking is a widely used computational method in structural molecular biology to predict at an atomic level the optimal binding mode (i.e., position and orientation) between a ligand and a protein when forming a stable complex (Schlessinger *et al.*, 2018; Atzori *et al.*, 2019a). These studies represent a rapid, powerful and economical alternative to time-consuming and expensive experimental techniques for studying protein-ligand binding interactions (Pereira *et al.*, 2016; De Siena *et al.*, 2020). In molecular docking, the ligand molecule (substrate or inhibitor) is docked to the protein structure which has either been experimentally determined

or modelled. Docking algorithms utilise a range of scoring functions on the basis of machine-learning, physics and statistics. The outcome is top-ranking docking conformations (poses) having low binding energy and good geometric fit (Akbal-Delibas *et al.*, 2015; Schlessinger *et al.*, 2018; Fu *et al.*, 2018). Mutagenesis studies of proteins can be informed by protein-ligand docking studies and vice versa (Türková and Zdrzil, 2019). Therefore, the approach of combining both mutagenesis and docking studies can provide accurate predictions of substrate binding sites in a transport protein.

Much-needed information at atomic scale can come from computational structure modelling and modelling of a substrate compound bound to QacA. Therefore, in this chapter, homology modelling and molecular docking studies were employed in combination with the experimental data in hand, with the aims being to: 1) derive a hypothetical 3D model for QacA as a framework to integrate and rationalise mutational data for expanded understanding of structure and function relationships in QacA; and 2) identify binding pockets in QacA for selected substrates by combining site-directed mutagenesis data and docking studies.

5.2 Results and discussion

5.2.1 Homology modelling

QacA is predicted to have 14 TMS based on hydropathy analysis (Figure 1.4). Homology modelling of QacA was performed as described in Section 2.13.3. After judicious inspection of numerous output models from SWISS-MODEL, Phyre2 and I-TASSER modelling servers based on the crystal structures of the 12-TMS transporters MdfA and LmrP and different 14-TMS transporters from the POT family, a QacA model using the I-TASSER webserver (Zhang, 2008; Roy *et al.*, 2010; Yang *et al.*, 2015)

was constructed. Modelled on PDB ID: 4W6V (the inward-facing crystal structure of YePEPT, a POT family transporter from *Yersinia enterocolitica*) (Boggavarapu *et al.*, 2015), it was chosen as the best-predicted model. This is based on: (1) it is a full-length QacA model with all 14 TMS and the big loop between TMS 13 and 14 modelled without any gaps within the TMS and disordered loops; (2) the extents of the modelled TMS generally align with the experimentally determined topology of QacA (see Table 6.1); (3) the C-score, which is a confidence score for evaluating the quality of a predicted model by I-TASSER, was -0.5 which fell well within the acceptable range [-5, 2] (Yang and Zhang, 2015); and (4) the estimated TM-score (template modelling score) and RMSD (root mean square deviation) of the model were 0.65 ± 0.13 and $8.5 \pm 4.5 \text{ \AA}$, respectively which were also in the accepted limits of estimation errors (Yang and Zhang, 2015). With the other produced models, it was identified, through visual inspection, that the 14 TMS of QacA were not modelled properly as they had gaps or distortions within TMS. Thus, these models were excluded from further considerations and although their C-score, TM-score and RMSD values were analysed and considered they are not included in this study.

As mentioned in Section 1.8.1, MFS proteins share a structural core which is organised into two six-TMS domains (N- and C-terminal domains) with the presence of a large cavity in the centre of the transporter (Madej *et al.*, 2013; Yan, 2013; Quistgaard *et al.*, 2016). The derived QacA model (Figure 5.1) features 14 TMS that generally conforms to the structural arrangement of 12-TMS MFS transporters. The two helices in QacA, TMS 7 and 8, which are in the centre of the topology model (Figure 1.4), are located on one side of the core in the 3D model of QacA (Figure 5.1) similar to the additional two TMS, termed H_A and H_B, in the crystal structures of POT

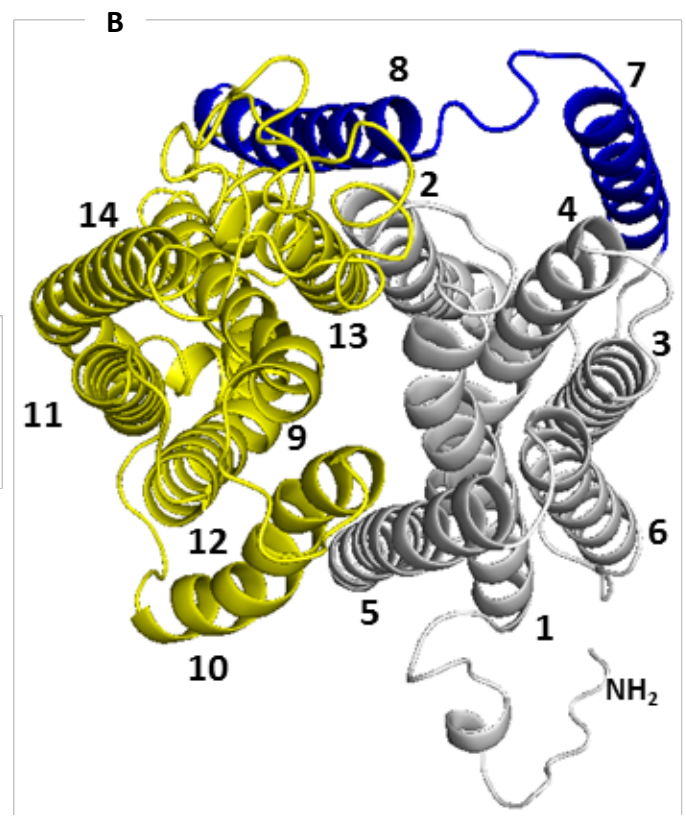
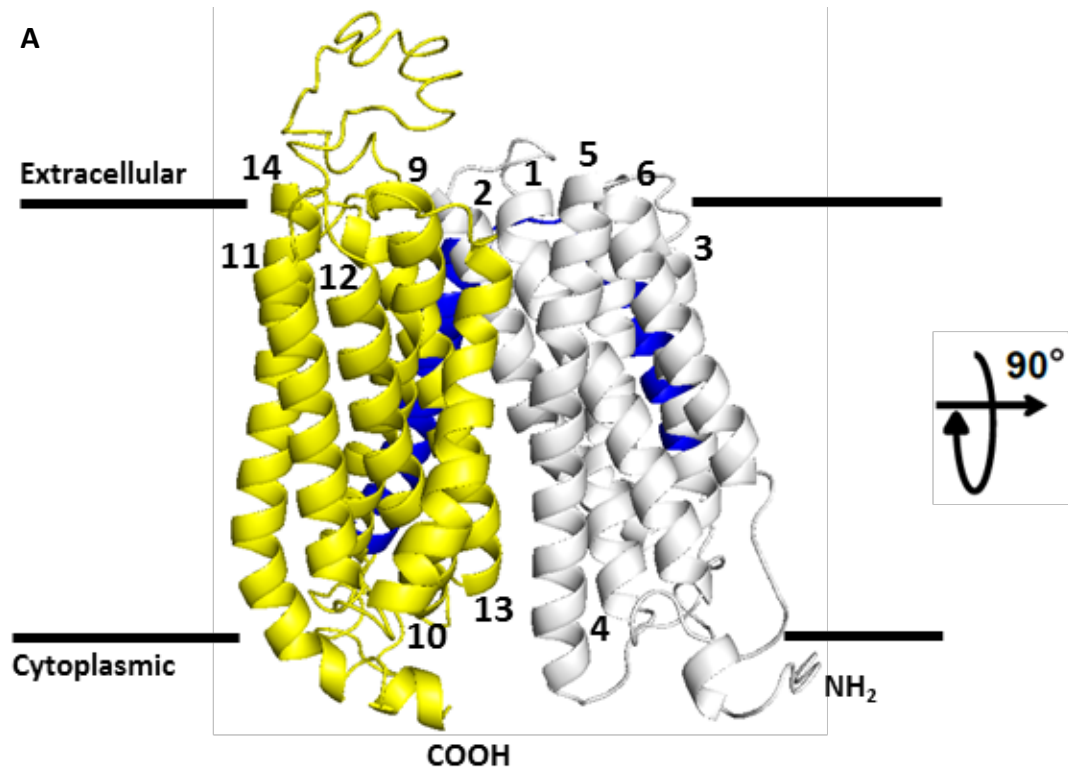


Figure 5.1 Homology model of QacA showing structural arrangement of the 14 TMS.

(A) Side-view ribbon representation of inward-facing QacA. The QacA model displays two-fold symmetrical domains as TMS 1-6 in the N-terminal domain (grey) and TMS 9-14 in the C-terminal domain (yellow) are connected by TMS 7 and 8 (blue). **(B)** Top-view showing the central cavity that leads into the cytoplasm. TMS 1, 2, 4, 5, 9, 10, 12 and 13 are directly lining the cavity while TMS 3, 6, 11 and 14 are farther away. TMS 7 and 8 which connect the N- and C-domains are situated at the side of the 12-TMS structural fold.

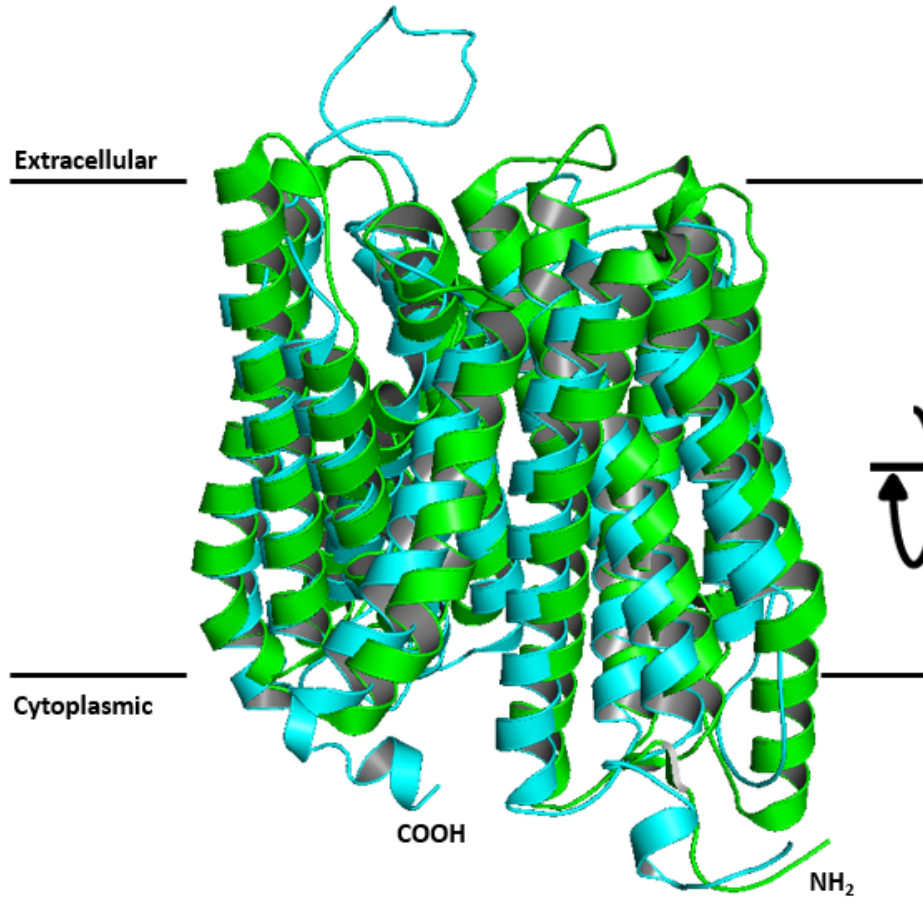
transporters (Solcan *et al.*, 2012; Zhao *et al.*, 2014). Similar to the YePEPT template, the obtained QacA model exhibits an inward-facing conformation, wherein the central cavity between its N- and C-domains is open to the inner leaflet of plasma membrane. As seen in Figure 5.2, the superposition of the experimental structure of YePEPT (template) and the model structure of QacA by using PyMOL indicates that their overall arrangement of the 14 transmembrane α -helices are similar.

In a recently published study that included QacA homology modelling (Majumder *et al.*, 2019), the QacA sequence that was used in the modelling procedure lacked the large extracellular loop between TMS 13 and 14. This derivative was modelled by the I-TASSER server based on the structure of the POT transporter GkPOT (PDB ID: 4IKV) followed by loop rebuilding to reincorporate the deleted region. In this study, using a different POT transporter template (PDB ID: 4W6V), full-length QacA was successfully modelled by I-TASSER, thereby bypassing the loop removal and remodelling. Moreover, the 4W6V template used here shared slightly higher sequence identity with QacA compared to the previously used 4IKV template (16.44% versus 14.59%).

5.2.2 QacA orientation in the membrane

The spatial positioning of membrane proteins in the lipid bilayer matrix is important in that it can affect the proper folding, biological activity, dynamic stability and binding with substrates (Lomize *et al.*, 2006a). Hence, the orientations of many proteins in membranes have been determined by experimental techniques such as chemical modification (Landreh and Robinson, 2015), atomic force microscopy (Carnally *et al.*, 2011), small-angle X-ray scattering (Chen and Hennig, 2018), NMR

A



B

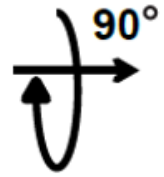
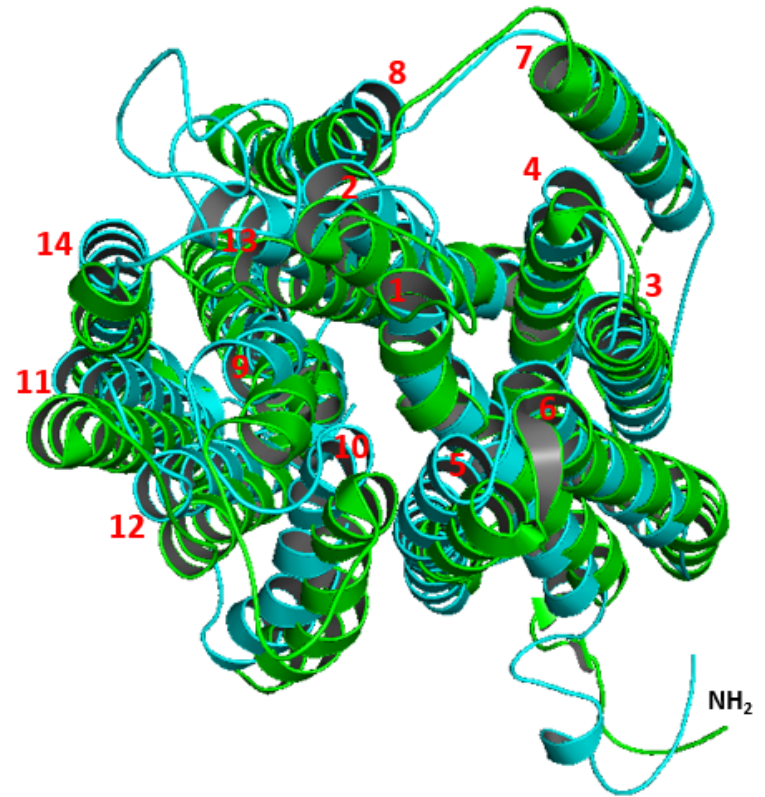


Figure 5.2 Structural superimposition of modelled QacA against the YePEPT crystal structure.

(A) side and **(B)** top views of structural alignment of the QacA homology model (cyan) and crystal structure of *Yersinia enterocolitica* YePEPT (PDB 4W6V) (green). The 14 helices and the amino terminus (NH₂) of QacA are labelled in the right panel.

(Purslow *et al.*, 2020) and spin labelling (Sahu and Lorigan, 2018) to just name a few. These studies have been complemented by development of reliable computational approaches that determine the spatial arrangement of expanding newly determined proteins structures in the PDB (Lomize *et al.*, 2006b).

The Orientations of Proteins in Membranes (OPM) database, available at <http://opm.phar.umich.edu>, is a curated online resource that provides spatial arrangements of PDB-deposited membrane protein structures in the lipid bilayer (Lomize *et al.*, 2012). The PPM server is a web tool found in the OPM database that can be used to investigate the spatial position and orientation of experimental structures or theoretical models of membrane proteins within the lipid bilayer membrane (Lomize *et al.*, 2012). Prompted by this, the modelled QacA structure (Section 5.2.1) was submitted to the PPM server. The predicted spatial orientation of the QacA protein in a theoretical membrane model is shown in Figure 5.3. The calculated hydrophobic thickness and tilt angle for QacA were $30.2 \pm 0.5 \text{ \AA}$ and $8.0 \pm 0.0^\circ$, respectively. The hydrophobic thicknesses of transmembrane proteins varies from 21.1 to 43.8 \AA depending on the type of membrane bilayer, while their tilt angles with respect to the membrane range from zero to 26° depending on symmetry of the membrane bilayer (Lomize *et al.*, 2006a). The predicted length and tilt of the TMS and correlation with experimental findings are further discussed in Section 6.3.

5.2.3 Hotspot regions in QacA for interaction with chlorhexidine identified from mutagenesis experiments

Revealing the exact location and design of binding sites within multidrug exporters is facilitated by the availability of substrate-bound structures (Blair and Piddock, 2016). For example, in substrate-bound crystal structures of the multidrug transporter MdfA

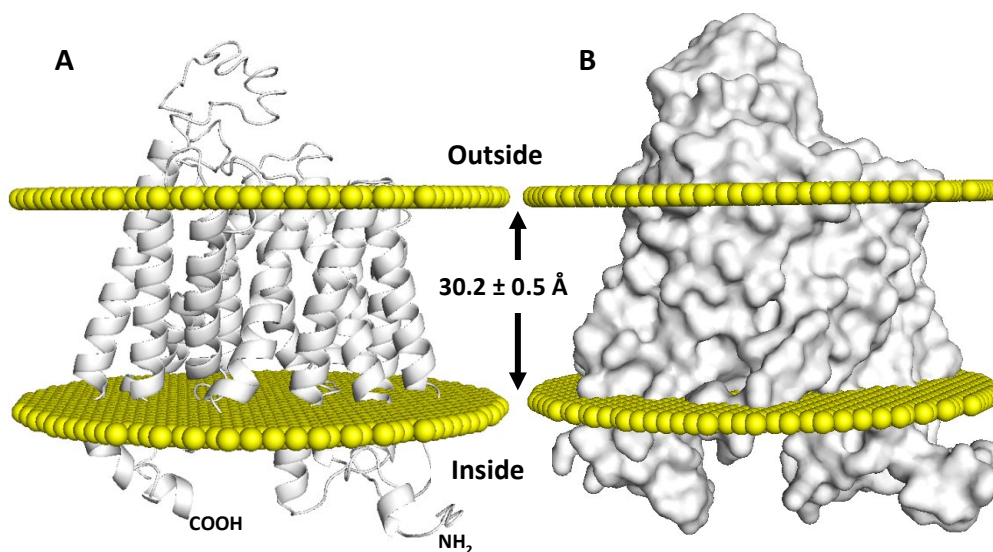


Figure 5.3 Spatial orientation of QacA within the lipid membrane as obtained by PPM modelling.

Embedding of the QacA model structure **(A)** ribbon representation and **(B)** surface view in a lipid bilayer membrane according to the PPM server calculations (Lomize *et al.*, 2012). The membrane boundaries are represented by yellow spheres. The local membrane thickness and N- and C-terminal ends of QacA are labelled.

from *E. coli* (Section 1.8.3), mutation of substrate-binding residues showed that some of these mutations significantly reduced the ability of MdfA to confer substrate resistance as confirmed by antimicrobial resistance assays (Wu *et al.*, 2019). This implies that functionally-important residues that lie along the length of TMS could be involved in substrate-binding. Thus far, site-directed mutagenesis studies have been conducted for more than two-third of the residues in the QacA efflux pump and the impact of these mutations on QacA resistance activity has been tested against a panel of substrates. Prompted by these data as well as the unavailability of substrate-bound crystallographic information for QacA, the analysis presented here focused on utilising hitherto identified important QacA residues for a substrate of interest in order to map out its potential binding pockets along the length of the protein.

CH is a widely used antiseptic and disinfectant in the community and hospitals and QacA is a major contributor to CH resistance (see Section 1.12). Therefore, it is of prime interest to determine an overall picture of “hotspot regions” for the interaction of QacA with CH so as to obtain clues for better rational development of potential anti-efflux strategies. Herein, “hotspot regions” refer to a cluster of functionally-important residues, the mutation of which significantly reduced the ability of QacA to confer resistance against a substrate (MIC \leq 50% compared to wild-type QacA).

Here, in an effort to identify hotspot regions for the interaction of CH with QacA, important residues that interact with this substrate were obtained from mutagenesis studies described in this thesis (Table 3.1) as well as those from previous publications and an unpublished mutational dataset in our laboratory (Figure 3.1). Numerous residues that interact with CH can be identified scattered within the TMS and adjoining loops of QacA (Table 5.1). To bring the ‘puzzle pieces’ together for a better

Table 5.1 List of the 57 residues important for chlorhexidine resistance as taken from QacA mutational analyses.

Location ^a	Residues ^b
L1	S3, F4, D10, M11, M12, K15, T19
H1	A20, A25, V26, S27, V30, D34, M35, T36
L1-2	L45, L49, G53
H2	L57, W58, Y63
H3	G90, F94, V97
L3-4	A107
H4	I113, R114, L117, G118, G121
H5	S153, S154, G156, G160
H6	W173
H9	L296
H10	G313, A320, G322, D323, P328, P331
H11	L343, G346, G353
H12	G377, G379, S387
H13	A403, E407, Y410, D411, G413, G417, L421
L13-14	Y429
H14	F482

^a The corresponding location of functionally-important residues for chlorhexidine in a H: helix or L: loop of QacA.

^b Important residues that interact with CH were obtained from mutagenesis studies undertaken and described in this thesis (Chapter 3) as well as those from previous publications and an unpublished mutational dataset in our laboratory (Figure 3.1).

understanding of the interaction of QacA with CH, all the identified residues that play a role in CH resistance (Table 5.1) were overlaid onto the 3D QacA model created in Section 5.2.1. This positioning enabled the identification of three hotspot regions for CH interactions inside the QacA interior cavity, shown as regions I, II, and III (Figure 5.4B), which appear to be located at different depths in the membrane. These regions are most likely to be critical for QacA interaction with CH, given that the interior cavity is purported to be the central location of substrate-binding and transport similar to other MFS transporters (Section 1.8.1.1).

5.2.4 Identification of the chlorhexidine binding pocket in QacA by molecular docking in conjunction with mutagenesis data

To pinpoint the specific residues within the central cavity of QacA involved in binding with CH, molecular docking of CH using the 3D model structure of QacA was performed by AutoDock Vina, which is an extensively optimised version in terms of accuracy of docking (Trott and Olson, 2010). As described in Section 2.13.4 regarding the criteria for the choice of best-docked pose for each substrate, one of the output docking poses for CH was selected for further analysis of substrate binding residues. The best-docked pose for CH (Figure 5.5) had the lowest-energy (-7.5 kcal/mol), proper orientation inside the central cavity of QacA, and most agreement with the experimental data (i.e. the most overlap between the binding residues found by docking and the functionally-important residues identified by mutagenesis studies).

To ensure the reliability of the CH docking, functional residues for CH identified by mutagenesis studies (Section 5.2.3) were overlaid onto the docking conformation (Figure 5.5A). Interestingly, the position of CH (Figure 5.5B) maps close to hotspot region II which was depicted in Figure 5.4. Analysis of the selected docking pose

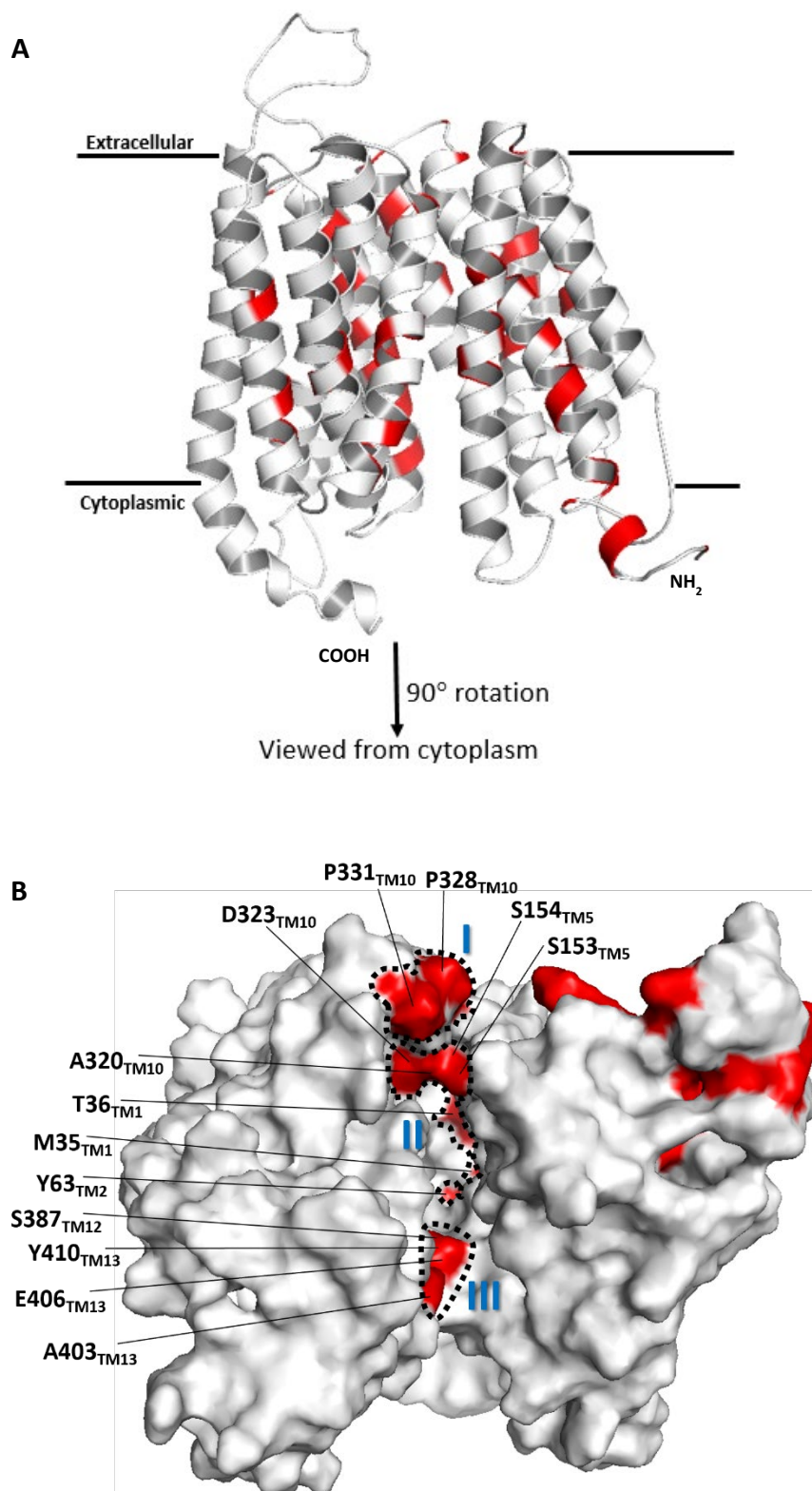


Figure 5.4 Hotspot regions in QacA for interaction with chlorhexidine assigned based on extensive mutagenesis studies.

(A) Shown in red are residues identified as important for chlorhexidine resistance (listed in Table 5.1) overlaid onto the QacA model. **(B)** Surface view model of QacA viewed from the cytoplasm. Residues that are located towards the central transmembrane cavity are labelled including their position in the protein. These residues clustered into three hotspot regions (I-III; blue) as indicated by dashed lines.

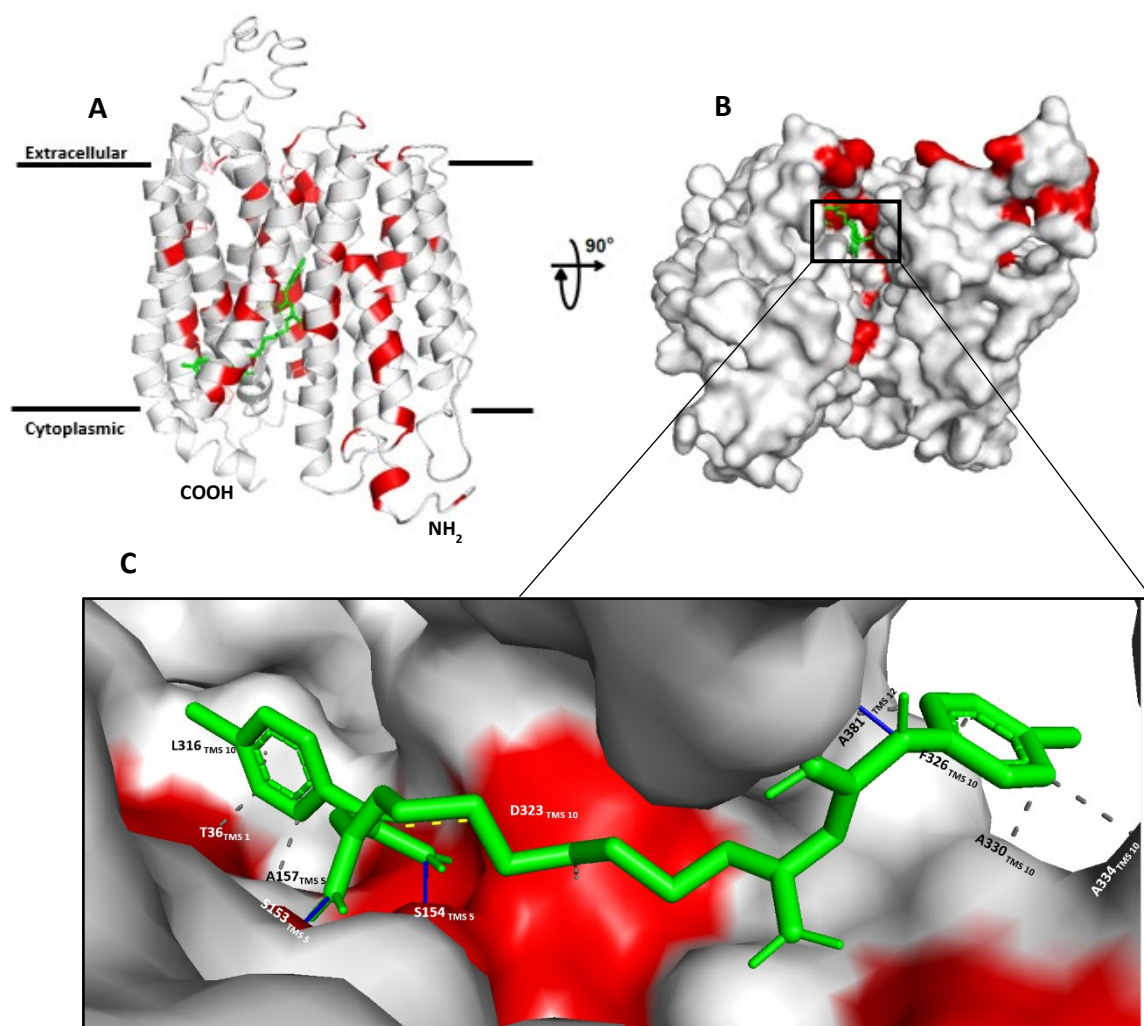


Figure 5.5 Docking of chlorhexidine to QacA.

(A) Best-docked pose of CH (green) into the internal cavity of the QacA model shown as ribbon representation viewed from the side of the membrane. Red highlights in the QacA model are positions of residues identified as playing a role in CH resistance (see Figure 5.4; legend). **(B)** 3D surface view model of QacA-CH docked complex, as seen from the cytoplasm, showing CH in the central transmembrane cavity of QacA in close vicinity of hotspot regions. **(C)** Close-up view of CH within the QacA binding pocket showing their molecular level interactions. Residues directly involved in interactions are labelled (for details of molecular bonds, see Figure 5.6).

identified a binding site for CH localised inside of the central cavity. This binding site is delimited by 10 residues of QacA that are directly involved in the binding of CH. Among those residues, four (T36, S153, S154 and D323) are functionally important belonging to the hotspot region II within the central cavity (Figure 5.4B). Furthermore, the docked complex indicates that binding of CH to QacA takes place through several hydrogen (H) bonds and hydrophobic interactions with specific residues from TMS 1, 5, 10 and 12 (Figure 5.5C). Indeed, CH is bound to QacA within the identified pocket composed of the charged residue D323, polar residues (T36, S153, S154) and a series of hydrophobic residues (A157, L316, F326, A330, A334, and A381).

The type and bond length of the intermolecular contacts within the 5.5 Å distance cut-off established between CH and QacA binding site residues are shown in Figure 5.6. The 5.5 Å threshold often includes all the common non-bonded interactions in protein structures and their complexes (Vangone and Bonvin, 2015; Xue *et al.*, 2016). As can be seen, CH in its binding pocket is stabilised by forming a salt-bridge (4.94 Å) with the residue D323, three H-bonds with S153 (2.33 Å), S154 (3.17 Å) and A381 (3.25 Å), as well as eight hydrophobic interactions of CH (predominantly the aromatic rings) with residues T36 (3.66 Å), A157 (3.73 Å), L316 (3.77 Å), D323 (3.79 Å), F326 (3.67 Å), A330 (3.50 Å), A334 (3.85 Å) and A381 (3.58 Å).

Results of CH docking in this study correlates with those seen in the multidrug transporter SmvA from *Klebsiella pneumoniae*, a DHA2 MFS protein, where the CH binding pocket is delimited by charged and polar residues forming H-bonds (Wand *et al.*, 2019). In addition, a series of hydrophobic residues at the edges of the SmvA

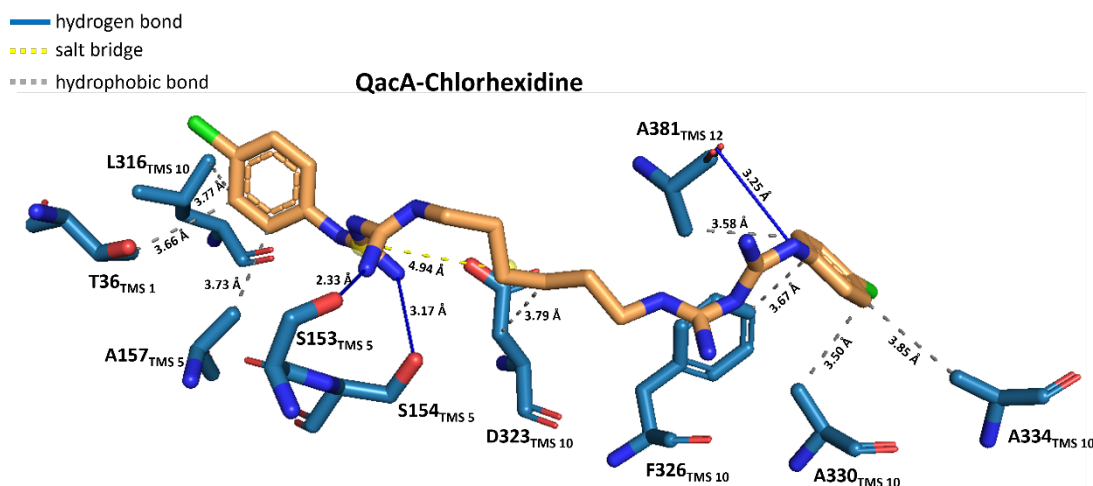


Figure 5.6 Depiction of intermolecular interactions in the binding site of QacA with its substrate chlorhexidine.

Binding site amino acids of QacA with chlorhexidine in the docked pose are shown in blue and orange stick representation, respectively. H-bonds are shown by solid blue lines and hydrophobic interactions by dashed grey lines. The salt bridge is indicated by a dashed yellow line. Calculated bond length is indicated close to the relevant bond. Figure created with PyMol.

binding pocket interact with CH by hydrophobic interactions. Furthermore, the CH-binding pocket in SmvA is composed of residues located in the putative TMS 1, 5, 10 and 12 of SmvA similar to what has been observed in CH binding pocket of QacA in this study.

5.2.5 Hotspot regions in QacA that interact with benzalkonium identified from mutagenesis experiments

BK is a known QAC which is commonly used in many broad-spectrum disinfectant solutions and as a preservative in personal care products. The QacA efflux pump is known to mediate increased resistance to BK in *S. aureus* (see Section 1.12). To determine the hotspot regions in QacA for interactions with BK, functionally-important residues for this substrate were gleaned from mutagenesis studies similar to what has already been explained for identification of CH hotspot regions (Section 5.2.3). Residues identified as playing a role in BK resistance (Table 5.2) were overlaid onto the 3D QacA model (Figure 5.7). This positioning led to the identification of four hotspot regions for BK interactions inside the QacA interior cavity, referred to as regions I, II, III and IV in Figure 5.7C, which appear to be located at different depths in the membrane similarly to CH hotspot regions. These hotspot regions are likely to contribute to binding and transport of BK while this substrate is traveling through the central cavity of QacA.

5.2.6 Identification of the benzalkonium binding pocket in QacA by molecular docking in conjunction with mutagenesis data

To find specific residues within the central cavity of QacA that are involved in binding with BK, this substrate molecule was docked into the 3D model structure of QacA using AutoDock Vina as described in Section 2.13.4. Obtained docking poses for BK

Table 5.2 List of the 48 residues important for benzalkonium resistance as taken from QacA mutational analyses.

Location ^a	Residues ^b
H1	T36
L1-2	L49
H2	L57, W58, Y63, A68
H3	G90, F94, V97
L3-4	A107
H4	I113, R114, L117, G118, G121
L4-5	K140, E141, R142
H5	L146, A147, V148, W149, S150, I155, G156, A157, V158, F159, G160
H6	W173
H9	L296
L9-10	E306
H10	G313, L314, Y315
H11	L343, G346, G353
H12	S387
H13	E407, Y410, D411, G413, G422, L424
L13-14	E452, E453, E460

^a The corresponding location of functionally-important residues for benzalkonium in a H: helix or L: loop of QacA.

^b Important residues that interact with benzalkonium were obtained from mutagenesis studies undertaken and described in this thesis (Chapter 3) as well as those from previous publications and an unpublished mutational dataset in our laboratory (Figure 3.1).

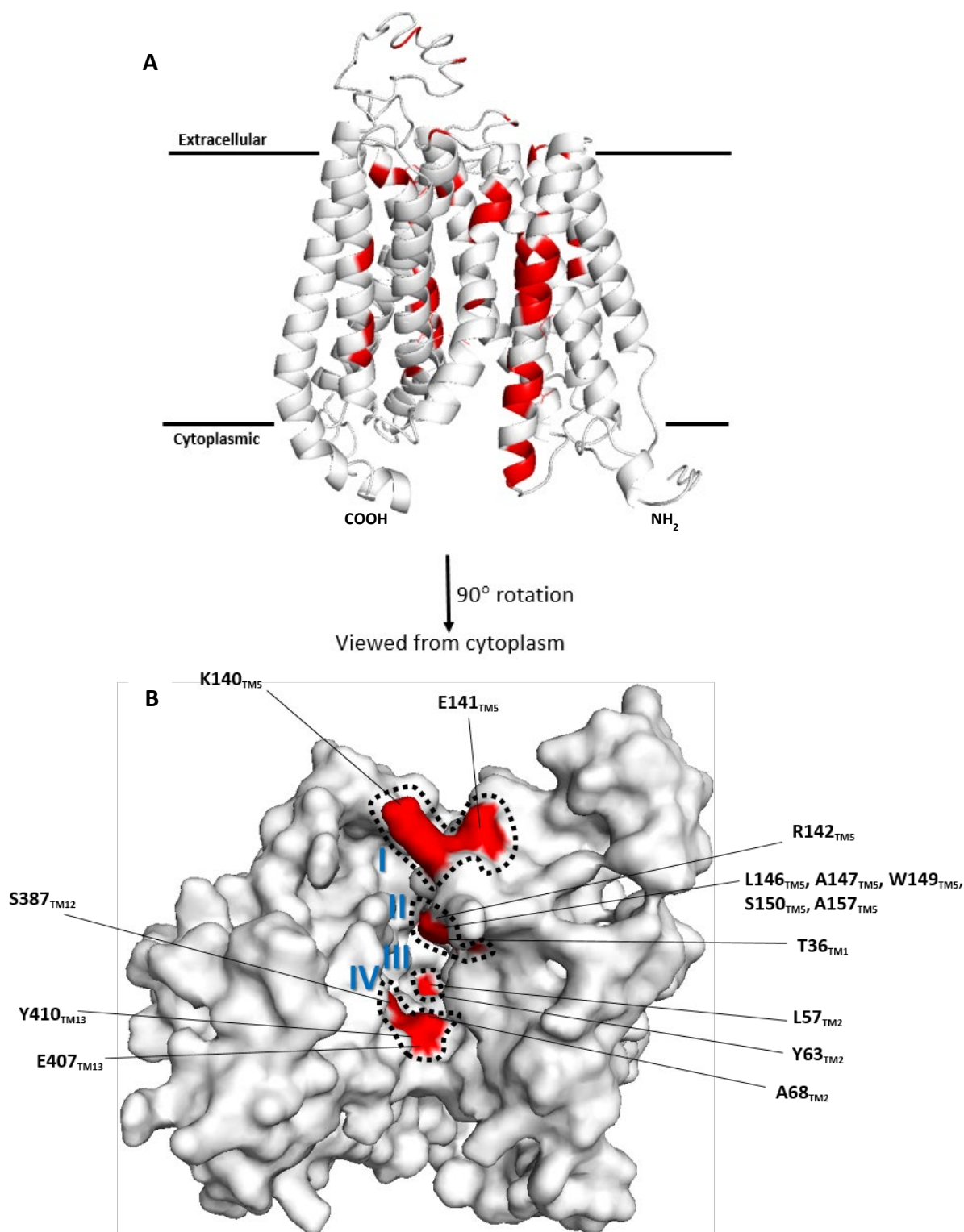


Figure 5.7 Hotspot regions in QacA for interaction with benzalkonium assigned based on extensive mutagenesis studies.

(A) Shown in red are residues identified as important for BK resistance (listed in Table 5.2) overlaid onto the QacA model. **(B)** Surface view model of QacA viewed from the cytoplasm. Residues that are located towards the central transmembrane cavity are labelled. These residues clustered into four hotspot regions (I-IV; blue) as indicated by dashed lines.

had the calculated binding energy values ranging from -5.2 to -4.5 kcal/mol. As the binding energy of the poses were comparable, the best-docked pose was judiciously selected by visual inspection. In the selected docking conformation (-4.6 kcal/mol) BK was suitably oriented within the central cavity of QacA protein.

To ensure the reliability of the BK docking, functional residues for BK identified by mutagenesis studies (Section 5.2.5) were overlaid onto the docking conformation (Figure 5.8A). Interestingly, the predicted position of BK from docking (Figure 5.8B) maps close to hotspot region IV (Figure 5.7). Analysis of the selected docking pose identified a binding site pocket for BK localised inside of the central cavity. The BK molecule is surrounded by hydrophobic residues L67, A68 and I71 in TMS 2 and the polar aromatic residue Y410 in TMS 13. Indeed, BK is bound to QacA within the identified pocket mostly through hydrophobic interactions with the mentioned residues from TMS 2 and 13 (Figure 5.8 C). Among these residues, two (A68 and Y410) are functionally important belonging to the hotspot region IV within the central cavity as depicted in Figure 5.7.

The type and bond length of intermolecular contacts within the 5.5 Å distance cut-off between BK and binding site residues of QacA protein are shown in Figure 5.9. As can be seen, BK in its binding pocket is stabilised predominantly by establishing hydrophobic interactions with residues L67 (3.65 Å), I71 (3.71 Å), A68 (3.75 Å) and Y410 (3.66 Å). In addition, the aromatic ring of BK is oriented parallel to the benzene moiety of the Y410 side chain, resulting in π - π stacking interaction (4.00 Å). The present docking results are consistent with the previous mutational study that indicate that Y410 is part of the QacA drug binding region (Wu *et al.*, 2008).

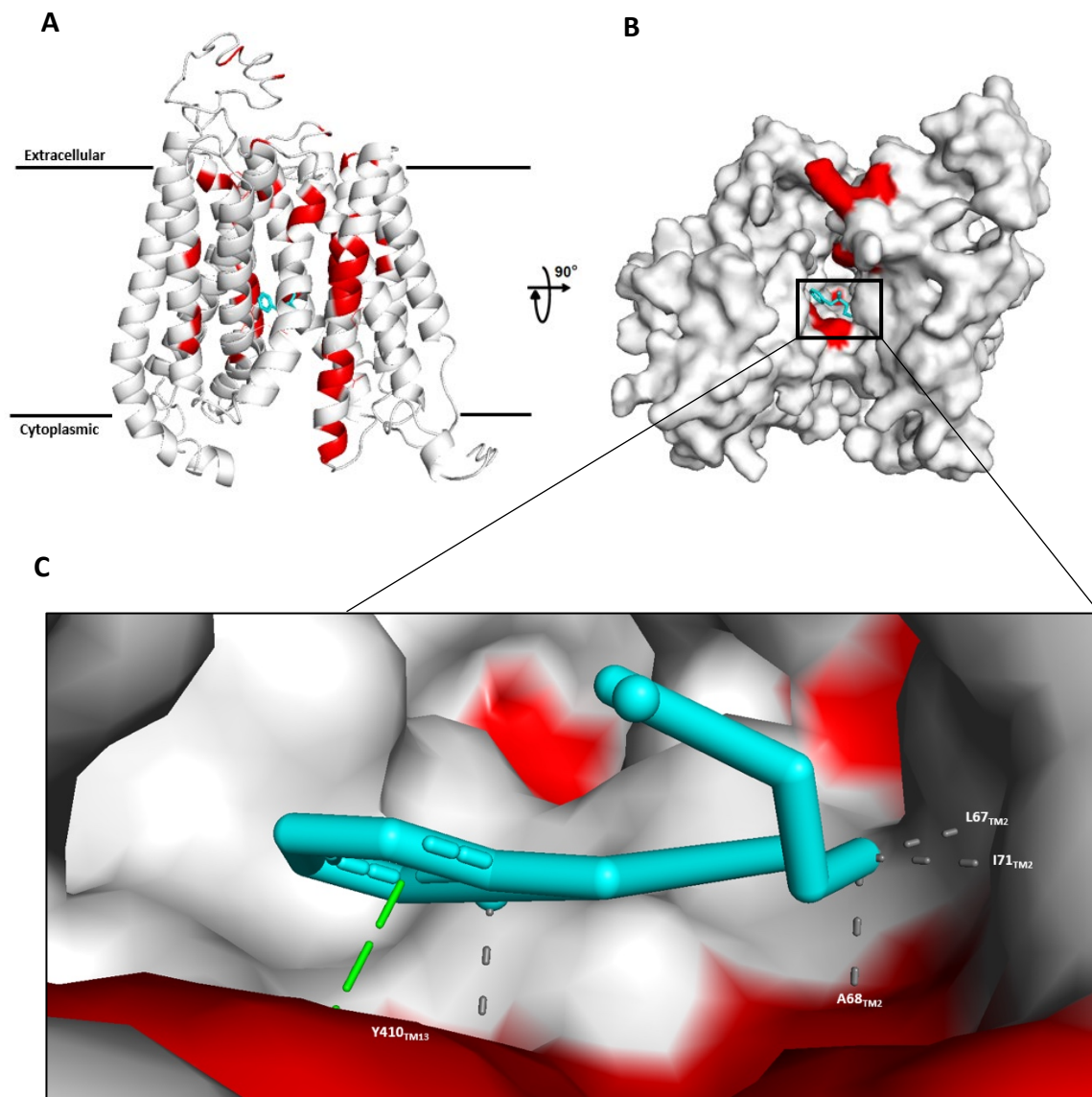


Figure 5.8 Docking of benzalkonium to QacA.

(A) Best-docked pose of BK (cyan) into the central cavity of the QacA model shown as ribbon representation viewed from the side of the membrane. Red highlights in the QacA model are positions of residues identified as playing a role in BK resistance (see Figure 5.7; legend). **(B)** 3D surface view model of QacA-BK docked complex, as seen from the cytoplasm, showing BK docked into the central transmembrane cavity of QacA in close vicinity of hotspot regions. **(C)** Close-up view of BK within the binding pocket of QacA showing their molecular level interactions. Residues directly involved in interactions are labelled (For details of molecular bonds, see Figure 5.9).

- ■ ■ ■ π -stacking interaction
- ■ ■ ■ hydrophobic interaction

QacA-benzalkonium

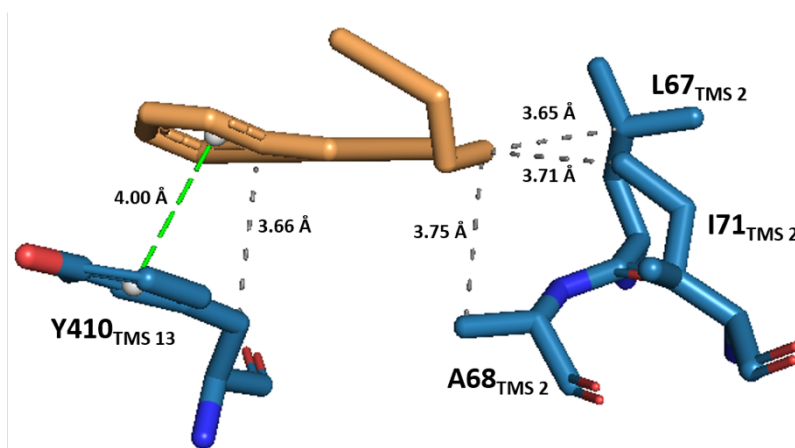


Figure 5.9 Depiction of intermolecular interactions in the binding site of QacA with its substrate benzalkonium.

Binding amino acid residues of QacA and BK in the docked pose are shown in blue and orange stick representation, respectively. Hydrophobic interactions are shown by dashed grey lines. The π -stacking interaction is indicated by dashed green line. Calculated bond length is indicated close to the relevant bond. Figure created with PyMol.

5.2.7 Identification of binding pockets in QacA for ethidium, rhodamine 6G, dequalinium, pentamidine and DAPI by molecular docking

To gain structural insights into the interaction of the transport protein with further substrates of QacA, namely Et, R6G, DQ, PE and DAPI, molecular docking studies were performed using the same docking approach as previously described. These analyses showed that Et, R6G, DQ, and PE bind deeper within the QacA central cavity and this binding is mediated by the residues M35, T36, I39, D61, A157, L294, L316 and A320 for Et; I39, V60, D61, L67, and A320 for R6G; L67, L294, L316, E407 and Y410 for DQ; and S64, L67, A68, L294, L295, S298, L316 and N414 for PE (Figure 5.10A-D). In contrast, DAPI has a shallow binding pocket situated near the entry of central cavity formed by the residues D323, A327, A381 and S382 (Figure 5.10E). The overlap between substrate-binding sites will be discussed in Chapter 6.

Generally, these substrates were observed to make hydrophobic interactions with aromatic (tyrosine) and aliphatic side chains of amino acid residues (alanine, valine, leucine, isoleucine and methionine) as well as forming H-bonds with the polar side chains of residues (threonine, serine, asparagine, aspartic acid and glutamic acid) as typically found in other multidrug transporters such as RND transporters AcrB and AcrD (Ramaswamy *et al.*, 2017) as well as MdfA (Heng *et al.*, 2015; Wu *et al.*, 2020). As can be seen from Figure 5.10, in each substrate-binding site some binding residues, which are highlighted in red, have previously been implicated by mutagenesis studies as part of drug binding region of QacA. This supports the notion that the docking results dovetail with the experimental mutational studies.

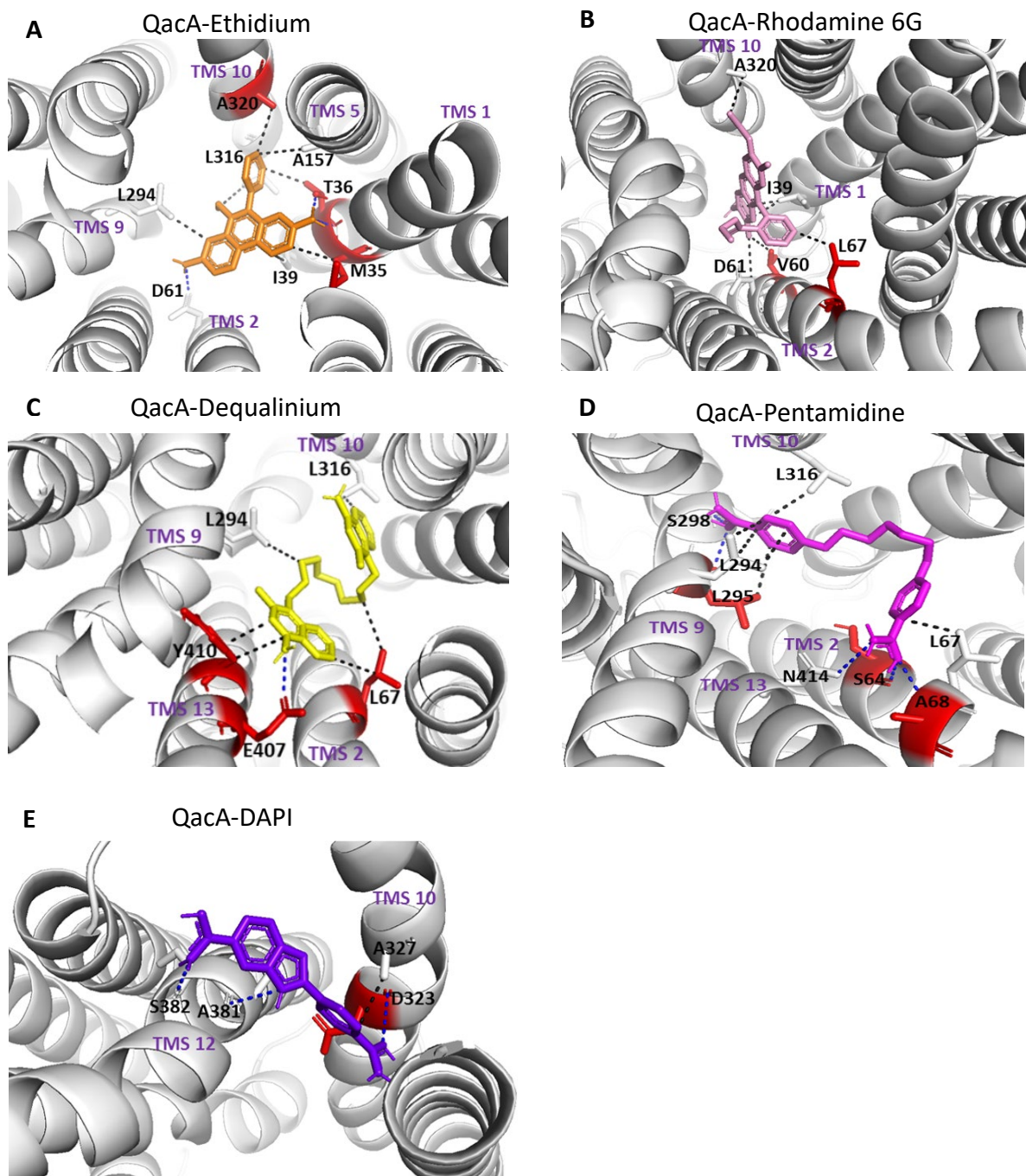


Figure 5.10 Putative substrate-binding sites of QacA for ethidium, rhodamine 6G, dequalinium, pentamidine, and DAPI, identified by molecular docking analysis.

The best-docked pose obtained from the molecular docking of each substrate into the internal cavity of QacA was analysed. Close-up view of the binding sites for **(A)** ethidium; **(B)** rhodamine 6G; **(C)** dequalinium; **(D)** pentamidine; and **(E)** DAPI. QacA is shown as ribbon form and coloured in light grey. Each substrate is depicted in stick style and highlighted in a specific colour (ethidium–orange, rhodamine 6G–pink, dequalinium–yellow, pentamidine–magenta and DAPI–purple). Binding site residues are shown as sticks and labelled in each panel. Residues coloured in red are those that were previously demonstrated to be functionally important in resistance assay for each specific substrate as described in Figure 3.1. Dashed blue lines represent H-bonds, whilst dashed black lines indicate hydrophobic interactions. The labels of TMS involving in the binding are indicated.

According to the underlying principles of docking, lower binding energy (a more negative docking energy) indicates a stronger binding between the ligand and protein (Huang *et al.*, 2018). Binding energies of the best-docked pose between QacA and substrates in this study are given in Table 5.3. As can be seen, CH appears to have the strongest binding with QacA, whilst BK has the weakest binding. The weak binding between QacA and BK could be correlated with its smaller size (Figure 1.5) and/or lower number of intermolecular interactions (Table 5.3). Notably, as can be seen from Table 5.3, among the substrates, R6G and BK did not make any H-bond interactions with the QacA protein.

5.2.8 TMS 7 and TMS 8 constitute a lateral cavity as a second possible binding site for some substrates

TMS 7 and TMS 8 in QacA are equivalent to the additional two TMS in the reported structure of 14-TMS transporters such as the POT family transporters (Solcan *et al.*, 2012; Zhao *et al.*, 2014), EmrB (Yousefian *et al.*, 2020) and NorC (Kumar *et al.*, 2020a) (Section 1.8.1.1). These TMS are inserted between the two six-TMS domains (N- and C-terminal domains) according to the structural arrangement of 14-TMS transporters. The inserted interdomain TMS pair are located on one side of the transmembrane core and they have shorter length compared with other TMS (Zhao *et al.*, 2014).

The overall architecture of the modelled QacA follows the canonical structural fold of MFS transporters as explained in Section 5.2.1. Besides the central cavity, which is the main predicted binding site and transport path for the substrates in MFS transporters (Alegre *et al.*, 2016), the modelled QacA revealed, rather interestingly, that a lateral opening exists at the interface between the interdomain TMS pair (TMS

Table 5.3 Binding energy, number of H-bond and hydrophobic interactions between substrates with QacA predicted by molecular docking.

Substrate compounds	Binding energy (kcal/mol)^a	Number of H-bonds^b	Number of hydrophobic bonds^c
Ethidium	-7.2	3	7
Rhodamine-6G	-7.3	0	6
Benzalkonium	-4.6	0	4
Dequalinium	-6.3	1	6
Chlorhexidine	-7.5	3	8
Pentamidine	-6.0	5	6
DAPI	-6.6	3	1

^a Binding energies of the best-docked pose calculated by AutoDock Vina

^{b,c} Counted from intermolecular interactions between QacA docking complex with cognate substrate in Figure 5.6, Figure 5.9 and Figure 5.10.

7 and TMS 8) and the core of the transporter (TMS 2 and TMS 13) (Figure 5.11 A, B). More intriguingly, the lateral cavity was found by molecular docking experiments in this study to be an additional binding site for QacA substrates (Figure 5.11 C, D, E). Based on this premise, it is tempting to propose that the lateral cavity in QacA is open towards the membrane and may participate as a collateral mechanistic route for catching and expelling the substrates from this environment. This proposition is in accord with the 'membrane vacuum cleaner' model mechanism which was first suggested over 25 years ago for MDR transporters (Bolhuis *et al.*, 1997; Hofmeyr *et al.*, 2002; Lomovskaya and Totrov, 2005). Additionally, it is consonant with earlier fluorimetric transport studies of QacA using trimethylammonium-diphenylhexatriene (TMA-DPH), a substrate that is also a membrane-specific fluorescence probe. QacA was observed to extrude TMA-DPH directly from the inner leaflet of the cytoplasmic membrane (Mitchell *et al.*, 1999). Lipophilic and positively charged antimicrobial molecules can readily intercalate in the lipid bilayer membrane leading to loss of its integrity and ultimately cell death. According to the membrane vacuuming model, MDR transporters are able to catch lipophilic antimicrobials from within the membrane and expel them to the outside. Such a physiological function of MDR transporters is essential for maintenance of membrane integrity and eventually provides protection for the cell (Lomovskaya and Totrov, 2005). The substrate entrance via the inner-membrane has been found in RND-type multidrug exporters particularly AcrAB-TolC, to play a role in taking up hydrophobic drug compounds (Yamaguchi *et al.*, 2015; Murakami *et al.*, 2006), thereby acting as a membrane 'vacuum cleaner'. Moreover, a recent conformational dynamics study of MdfA has suggested that this transporter and supposedly similar multidrug MFS transporters

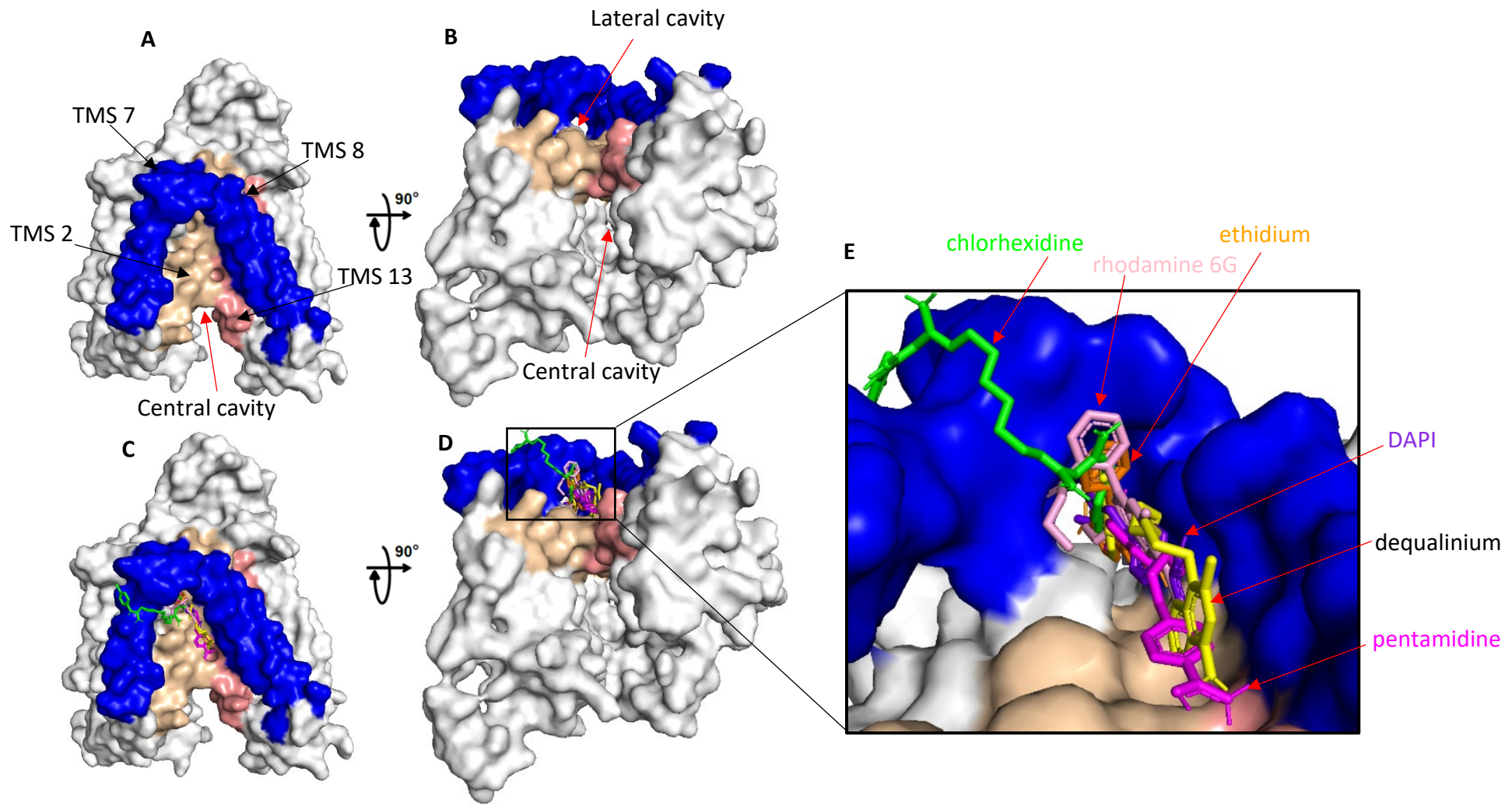


Figure 5.11 Lateral cavity in QacA made up by TMS 7 and TMS 8 as an additional possible substrate-binding site.

(A) Surface view model of QacA showing that TMS 7 and TMS 8 (blue) are separated from the 12-TMS core and located on the side adjacent to TMS 2 (wheat) and TMS 13 (salmon) from the core. **(B)** In addition to a large cavity centrally located in QacA, a somewhat smaller cavity exists laterally between TMS 7, TMS 8, TMS 2 and TMS 13. Structural superimposition of docked substrates in this lateral cavity of QacA shown as **(C)** side view and **(D)** bottom view from the cytoplasmic side of QacA. **(E)** Close-up view of substrates docked into the central cavity of QacA shown in stick representation with same colour scheme as in Figure 5.10.

can recruit lipophilic substrates from the inner leaflet of the membrane through a lateral gate between TMS 5 and TMS 8 (Yardeni et al., 2020).

It has been found that a QacA mutant protein lacking TMS 7 and TMS 8 has protein expression comparable with wild-type QacA, but displays a significant loss of transport activity and binding affinity toward some substrates as compared with the wild-type QacA (Majumder *et al.*, 2019). A similar effect was observed with the 14 TMS tetracycline exporter Tet(L) wherein a TMS 7 and TMS 8 deletion resulted in the loss of tetracycline resistance activity (Jin *et al.*, 2001). Moreover, mutation analyses of H_A and H_B (equivalent to TMS 7 and TMS 8 in QacA) in YbgH, a 14-TMS transporter belonging to the POT family, has implied a hypothetical regulatory role for this interdomain TMS pair (Zhao *et al.*, 2014). In a more recent study, a wide lateral opening was observed in the crystal structure of the staphylococcal MDR exporter NorC in an outward-open conformation. The lateral opening in this 14-TMS transporter was lined by TMS 7 and TMS 8 from one side and TMS 2 and TMS 13 from the helical bundles, thereby suggesting the ability of TMS 7 and TMS 8 to regulate lateral entry and binding of substrates (Kumar *et al.*, 2020a). Taken together, TMS 7 and TMS 8 are essential for normal function of 14 TMS transporters including QacA. This calls for future experimental validation, particularly high-resolution structural information of QacA bound to different substrates and molecular level interactions by MD simulations, to investigate how TMS 7 and 8, that may have been previously overlooked, participate in substrate-binding and the transport mechanism of QacA and similar transporters.

5.3 Conclusion

The QacA efflux pump is a highly promiscuous drug:H⁺ antiporter that confers bacterial resistance to a wide range of cationic antimicrobials via a common antiport mechanism energised by the pmf (Mitchell *et al.*, 1998; Majumder *et al.*, 2019). QacA plays an important role in efflux-mediated resistance of staphylococci to BK and CH which are widely used as antiseptics and disinfectants in health-care and community settings (Addetia *et al.*, 2019; LaBreck *et al.*, 2020). The structure-function insights obtained in this study provide a framework for better understanding the regions of QacA that interact with these biocides. This is an important step toward the ultimate goal of circumventing QacA efflux-mediated antimicrobial resistance by designing novel inhibitors/antimicrobials.

The new structural model of QacA reported here was built based on the I-TASSER homology modelling approach. Indeed, recent studies involving structure modelling for 14-TMS MFS multidrug transporters such as SmvA (Wand *et al.*, 2019), QacA (Majumder *et al.*, 2019) and Rv1410 (Hohl *et al.*, 2019), highlighted the predictive power of I-TASSER constructed models, despite a low sequence similarity to the template structure (sequence identity of ~20% or even less). Notably, the I-TASSER structure prediction pipeline has been shown to reliably build models for targets without close homologous templates by improved modelling algorithms that reassemble the structural fragments from multiple templates (Zhang *et al.*, 2019). Accordingly, the QacA model presented in this work revealed that among the 14-TMS of QacA, TMS 1, 2, 4, 5, 9, 10, 12 and 13 have direct contact with the central cavity region of the protein. This information is consistent with the canonical structural fold of MFS proteins (Harris *et al.*, 2017; Vishwakarma *et al.*, 2018) and provides support

for the accuracy of the constructed model. Therefore, in the absence of a high-resolution structure for QacA transporter, the current QacA structure model provides a framework and guide not only useful for rationalisation of aggregated mutational data set as outlined in previous works and this thesis, but can be also applied for computational prediction of substrate-binding sites and future inhibitor design phase.

Positioning the functionally-important residues for resistance to two of the candidate substrates, CH and BK, onto the 3-D model of QacA, revealed that residues lining the central cavity are proximate to each other and compose “hotspot regions” for substrate interaction sites (Figure 5.4 and Figure 5.7). Such regions could potentially act as essential interaction sites during substrate binding and/or transport through the central cavity. Molecular docking of CH and BK onto the QacA model structure showed that these biocides are able to bind to the central cavity of QacA close to their hotspot regions as identified by mutational studies. Therefore, computational modelling of substrate-binding tied in well with the experimental data in hand, providing confidence that the docking protocol applied is able to be used in a predictive way for gaining structural insights into the interaction between QacA and its substrates.

The molecular docking results for 7 compounds, namely Et, R6G, BK, DQ, CH, PE and DAPI, revealed that distinct substrates interact with QacA differently. This supports the existence of several, separate, but partially overlapping binding sites for different drugs along a large and multifaceted drug-binding pocket in QacA (Hassan *et al.*, 2007a; Majumder *et al.*, 2019). Indeed, such a structural feature is crucial in multidrug recognition and is shared not only by multidrug transporters such as LmrP

(Putman *et al.*, 1999), MexB (Middlemiss and Poole, 2004), MdfA (Wu *et al.*, 2020), P-glycoprotein (Loo *et al.*, 2003) and AcrB (Nakashima *et al.*, 2011), but also by multidrug-binding regulatory proteins such as QacR (Schumacher *et al.*, 2001). The overlapping and non-overlapping substrate-binding sites in QacA identified by docking results will be discussed in detail in Chapter 6.

Importantly, the current docking study found that a small set of H-bonds contribute as part of the intermolecular interactions between QacA and its substrates including Et, DQ, CH, PE and DAPI, but no H-bond was formed between BK and R6G with the contacting residues of QacA. Notably, substrate-binding in MdfA has been described to be often through hydrophobic interactions and rarely through H-bonds (Heng *et al.*, 2015; Wu *et al.*, 2019; Wu *et al.*, 2020). H-bonds have stringent geometric requirements (i.e. specific lengths and directions), which can substantially restrict the capability of MDR transporters to accommodate structurally diverse substrates (Wu *et al.*, 2019). Unlike H-bonds, the predominance of non-specific hydrophobic interactions formed between the drug and MDR transporters, such as MdfA and QacA, is a major contributor to broad substrate specificity of these transporters, such that they are able to recognise and accommodate structurally and chemically different drugs with varying sizes and shapes within a spacious multidrug-binding pocket (Wu *et al.*, 2020). Remarkably, the usage of a low number of H-bonding interactions (typically ≤ 3) appears to encourage a substantial flexibility in the rearrangement required for polyspecific substrate recognition by MDR transporters as opposed to the substrate-specific MFS transporters such as LacY (Kumar *et al.*, 2014) and glucose transporters (Deng *et al.*, 2015), which utilise extensive H-bonding

networks (often of ≥ 8 H-bonds) in selecting and recognising their substrates (Wu *et al.*, 2020).

Of particular note is that the majority of the H-bond interactions in docking complexes are observed to be formed between the substrates and functionally important residues. Therefore, the mutations of these residues likely caused unfavourable modification of the geometry and/or stability of the substrate binding site in a manner counterproductive for substrate transport, taking into account the importance of hydrogen bonds in the stability of protein-substrate binding interactions (Fu *et al.*, 2018).

Some of the functional residues located inside the interior cavity of QacA (Figure 5.4 and Figure 5.7 as examples for CH and BK) were not found to be directly involved in substrate binding based on docking results in this study. The following possibilities can be envisaged about how mutations of such residues were observed to greatly reduce resistance activity while they may not participate in direct binding contact with the substrate. One possibility is that their substitution indirectly impacts the geometry and/or stability of the substrate binding site because they are in close proximity to the binding region according to positioning in the QacA model structure. It is also possible that their replacement could perturb the natural coordination of substrate translocation through the binding cavity or conformational transitions required in the alternating access transport mechanism purportedly to be a general feature of all MFS transporters (Section 1.8.2). Future investigations of QacA dynamics by MD simulations studies could reveal whether and how these residues participate in QacA substrate-binding site(s)/transport mechanism.

In the following, the docking results for some substrates are selectively discussed and compared with available experimental results. A previous study that investigated the importance of tyrosine residues within QacA (Wu *et al.*, 2008) found that Y410 was important for QacA-mediated resistance to most compounds tested, including BK and DQ. Being a non-conserved residue among QacA-related drug efflux transporters, Y410 has been suggested to partake in a QacA-specific binding function. Docking experiments in this study corroborate this postulation by showing that aromatic residue Y410 is part of the QacA binding site for both BK and DQ.

Earlier mutagenesis studies demonstrated that D323 in TMS 10 is causal for the elevated activity of QacA towards the bivalent cations as opposed to QacB that naturally has a substitution of D323A (Paulsen *et al.*, 1996a; Mitchell *et al.*, 1999). Later studies revealed that the D323C heavily compromised DAPI resistance and transport (Xu *et al.*, 2006). This residue has been found to be essential for transport of specific bivalent cations such as DAPI that have two cationic moieties separated by a short linker, via a processive transport mechanism in QacA (Fluman *et al.*, 2014). Docking results presented in this study suggest that D323 is a substrate-binding residue for DAPI and is involved in H-bonding interactions with this substrate. Taken together, D323 serves as the integral constituent of the DAPI binding pocket; it can also be suggested that interaction between DAPI and D323 is via a specific H-bonding and any mutation that changes this H-bond, either by direct removal of the amino acid side-chain, or by indirectly influencing the orientation of this H-bond (S387C in Chapter 4), would alter substrate binding and transport. Conversely, mutations of D323 retained resistance and binding activity against DQ and CH (Fluman *et al.*, 2014; Majumder *et al.*, 2019) but impaired resistance and binding activity towards PE

(Majumder *et al.*, 2019). Docking experiments in this work revealed that D323 is not involved in the DQ and PE binding pocket. This offers an explanation for the unaltered resistance and binding previously observed for D323 mutation in the presence of DQ. However, docking findings contrast with the suggestion that D323 is a recognition site for PE despite the loss of PE binding affinity obtained for D323N (Majumder *et al.*, 2019). The reason for this inconsistency is unknown and awaits confirmation by high-resolution structural determination of QacA bound to PE. In the case of CH, even though D323 was observed in docking to be one of the 10 binding residues that make up the CH binding pocket (Figure 5.6), mutation to D323 did not interrupt the resistance activity towards CH. This indicates that D323 is not a “game changer” in the binding with CH possibly due to hydrophobic interactions between this residue and CH as opposed to its H-bonding observed in DAPI binding pocket.

Molecular docking is a fast and low-cost computational technology which is useful as an initial modelling tool to gain insight into molecular basis of substrate binding. However, molecular docking methods utilise several simplifications that can reduce its accuracy to some extent in comparison to complex algorithms of MD simulations (Chen, 2015; Opperman and Nguyen, 2015; Pantsar and Poso, 2018). For instance, a limitation of the docking process is that it provides only a static snapshot of the putative substrate binding conformation wherein the protein is considered as rigid while a protein intrinsically has significant structural plasticity. Conversely, MD simulations produce dynamic snapshots to simulate protein motions and flexibility of its binding sites at atomic resolution. Thereby, MD simulations would be useful to further explore the real-life binding events. Moreover, docking may be unable to highlight the effects of mutations on the binding conformations but MD simulations

appear to be capable of determining the differences in the substrate binding dynamics as a result of the mutations (Pantsar and Poso, 2018; Torrens-Fontanals *et al.*, 2020). Unfortunately, application of the current MD simulation methods, despite its advantageous aspects and being more realistic than docking, are still limited due to very high computational costs (Lazim *et al.*, 2020).

Overall, the current study on molecular modelling of QacA structure and its binding interaction with substrate compounds builds upon the previous experimental findings and provides new insights into the putative substrate-binding sites of QacA transporter. The results can lay the groundwork for prospective design of specific efflux pump inhibitor against QacA transporter, particularly a high affinity inhibitor that can bind to residues crucial to interaction with antimicrobial substrates.

CHAPTER 6
GENERAL DISCUSSION AND
CONCLUSIONS

The bacterial pathogen *S. aureus* continues to remain a significant public health threat worldwide (Tong *et al.*, 2015). One factor that promotes the continued success of this bacterium is its capacity to readily acquire mobile genetic elements that encode antimicrobial resistance and virulence factors (Baines *et al.*, 2019). This rapid adaptation has largely contributed (and continues to contribute) to the development of resistance to any new antibacterial drug used in treatment of staphylococci infections (Das *et al.*, 2016) and also against vancomycin, an antibiotic of last resort (Gardete and Tomasz, 2014). Alarming, the emergence of MDR *S. aureus* strains and the infections they cause, are increasing in the community setting, with subsequent significant implications in disease management (Lee *et al.*, 2017; Guo *et al.*, 2020). Overuse of antimicrobial agents has hastened the development of resistance to these compounds in pathogens, such as *S. aureus*. Clearly, better antimicrobial stewardship is required globally to minimise resistance threats.

Drug efflux pumps have the ability to extrude a broad range of structurally different toxic compounds such as antibiotics, biocides, heavy metals, and dyes (Blanco *et al.*, 2016; Chitsaz and Brown, 2017). Indeed, drug efflux pumps serve as a frontline defence against antimicrobial compounds decreasing their intracellular concentration, thereby allowing for bacterial survival until other resistance mechanisms can develop (Pidcock, 2006a; Venter, 2019). With a broad-spectrum substrate range and synergistic interplay with other resistance mechanisms, efflux pumps play a crucial role in development of multidrug resistance in *S. aureus*. As such, drug efflux pumps have become very attractive targets for development of EPIs to restore the activity of existing antimicrobials and prevent further emergence and dissemination of resistance (Lowrence *et al.*, 2019).

Bacterial efflux pumps of the MFS family are of great medical significance since they are able to confer antimicrobial resistance in pathogenic bacteria (Section 1.8). In *S. aureus*, a number of MFS efflux pumps such as NorA, QacA, LmrS, MdeA and LmrS have been identified and described in terms of their predicted structure, substrate specificity and contribution to antimicrobial resistance (Section 1.7). Among these, the plasmid-borne QacA efflux pump is widely found in clinical isolates of *S. aureus* (Baines *et al.*, 2019). Classified within the DHA2 family of the MFS, QacA is known as a major drug efflux system imparting increased resistance against clinically important biocides such as BK and CH (LaBreck *et al.*, 2018; Zamudio *et al.*, 2019). Despite the accumulating structural and functional information available for MFS transporters, currently details of recognition, binding and subsequent transport of distinct antimicrobial substrates by DHA2 family transporters remain incomplete. As such, the broad aim of the work described in this thesis was to expand our understanding of how a DHA2 family transporter liaises with its substrates by conducting a range of molecular and biochemical analyses of the QacA multidrug transporter.

Development of EPIs has gained significant traction over the past few years as a strategy to potentiate the efficacy of existing antimicrobial compounds and prevent the emergence of efflux-mediated resistant bacteria in hospitals and community setting (Wang *et al.*, 2016; Sharma *et al.*, 2019). To make progress in design and development of suitable EPIs that can block QacA pump activity, it is imperative to understand the details of the intricate mechanism of how the QacA multidrug efflux protein can interact with different antimicrobials. Efficacious inhibition of disinfectant resistance mediated by QacA could reduce the carriage of *qacA* containing plasmids and concomitant resistance to other antimicrobials carried on

these multiresistance plasmids. This will help eradicate the survival of *qacA* bearing staphylococci that could be present on hospital surfaces such as bed rails, over-bed tables and medical equipment. High-resolution structural data, such as X-ray crystallography and cryo-EM, with and without bound substrate(s) can provide direct and accurate insights into the recognition, binding and transport of substrates by DHA2 multidrug efflux proteins (Schindler *et al.*, 2013b; Schuller *et al.*, 2019; Shoemaker and Ando, 2018; Blair and Piddock, 2016). Many DHA2 proteins have been characterised in pathogenic bacteria, however, unlike the DHA1 family MFS members, there is currently very limited high-resolution structural data available for these transporters. The reason being that determination of high-resolution tertiary structure for DHA2 proteins is inherently more difficult due to their extreme hydrophobicity and defiance to high-level protein overexpression and purification (Hassan *et al.*, 2009; Carpenter *et al.*, 2008; Xu *et al.*, 2006). The presence of two additional TMS in DHA2 proteins may be associated with compounding these difficulties.

Very recently, cryo-EM analysis of the MFS-based tripartite EmrAB-TolC complex from *E. coli* has been published (Yousefian *et al.*, 2020). This study shows the overall architecture of the EmrAB-TolC efflux assembly and the relative arrangement of its components. However, a PDB accession code for the atomic coordinates and the structure factors of the 14-TMS EmrB has not been provided with this study, presumably due to lack of high-quality resolution of the cryo-EM maps. Therefore, its use as a template for QacA could not be explored in this study.

Through structure-function analyses, primarily by cysteine-scanning mutagenesis and chemical labelling techniques, a large number of residues spanning across different

TMS and interconnecting loops in QacA have been studied, as summarised in Table 1.2. From these studies, together with a large unpublished mutational dataset available in our laboratory, the identity of residues important for QacA-mediated resistance against multiple substrates has been achieved (Figure 3.1). Functionally important residues in TMS 10 of QacA (D323 in particular) have indicated the direct involvement of this TMS in forming a pocket that accommodates bivalent substrates (Paulsen *et al.*, 1996a; Brown and Skurray, 2001; Xu *et al.*, 2006). TMS 12 was also predicted to be part of this bivalent pocket based on the finding that acidic residue substitutions of G377 (TMS 12) restored the capacity for bivalent cation resistance in a D323C (TMS 10) QacA mutant protein (Hassan *et al.*, 2007b). Although a number of TMS in QacA have been investigated by detailed functional and structural analyses of all its residues, TMS 12 and its surrounding loop residues, which is recognised as playing a role in resistance, has not. Studies described in Chapter 3 addressed this gap by individually mutating all the previously untargeted residues in this region to cysteine and characterising their functional and structural impacts. These studies led to identification of G361, G379 and S387 as key residues in resistance QacA for selected substrates. The role of these key residues in the substrate-binding and translocation pathway were further investigated in detail by applying the biochemical studies presented in Chapter 4. Molecular structure modelling and docking studies of QacA presented in Chapter 5 supported by mutagenesis data revealed the putative substrate-binding pockets of selected antimicrobials.

This chapter discusses how the findings presented in this thesis have built on the previous structure-function knowledge of QacA. Additionally, structural implications from the QacA model and the architecture of substrate-binding pockets identified by

docking studies backed by mutagenesis data are discussed. These can be the starting point for future studies to probe potential inhibitors for QacA.

6.1 3D model of QacA as a framework for integrating and interpreting mutagenesis data

Knowing the 3D high-resolution structure of an export protein facilitates our understanding of its structural and functional intricacies, the molecular mechanism of multidrug recognition and provides the basis for future design of potent inhibitors to reverse antimicrobial resistance. Providentially, in the current absence of an experimental 3D structure for QacA, efficient and accurate computational approaches are available for the prediction of protein structures. As a step towards this goal, a predictive 3D structure of full-length QacA protein was generated by the I-TASSER server based on its homology to a 14-TMS POT family protein whose structure has already been solved (Section 5.2.1).

Previous structural and functional data from mutagenesis and biochemical studies can be superimposed into hypothetical 3D models to validate their credibility. Such hypothetical 3D models can serve as a framework for formulating the hypotheses relating to functional transport mechanism and predicting substrate binding and transport mechanisms. Interestingly, such models have been reported to be reflective of the high-resolution structures solved as reported in solute transporters such as LacY (Abramson *et al.*, 2003b) and MdfA (Yardeni *et al.*, 2018).

Although structural information for 14-TMS MFS transporters of the DHA2 family is currently lacking, a number of experimentally determined structures are available for 12-TMS MFS transporters of the DHA1 family such as EmrD (Yin *et al.*, 2006), MdfA (Heng *et al.*, 2015; Nagarathinam *et al.*, 2018), LmrP (Debruycker *et al.*, 2020) and 14-

TMS MFS transporters of the POT family such as PepT₅₀₂ (Guettou *et al.*, 2013), GkPOT (Doki *et al.*, 2013), YbgH (Zhao *et al.*, 2014) and YePEPT (Boggavarapu *et al.*, 2015). These experimental high-resolution structures, as well as structural models described for DHA2-family transporters such as SmvA (Wand *et al.*, 2019) and Rv1410 (Hohl *et al.*, 2019), have demonstrated a similar structural core shared by all MFS proteins (Section 1.8.1.1), despite being classified within different families, different substrate specificities, different transport modes and low sequence identity.

The derived model for QacA (Chapter 5) is consistent with the canonical tertiary fold in MFS transporters. Therefore, QacA is also expected to follow the common transport mechanism operating in all MFS transporters known as alternating access (Quistgaard *et al.*, 2016) (Section 1.8.2). This mechanism entails the binding of substrates within the central translocation region, followed by a conformational shift which allows the bound substrates access to the opposite side of the membrane.

6.2 Helix packing of the QacA transporter

Earlier studies on membrane transporters such as LacY (Wang and Kaback, 1999; Wolin and Kaback, 2000) and P-glycoprotein (Loo and Clarke, 1999) extensively used site-directed thiol cross-linking experiments for derivation of helix packing organisation or determination of the proximity of TMS (Green *et al.*, 2001). However, since a 3D model can provide structural details such as the spatial arrangements of TMS, it could be used as an alternative to conventional thiol cross-linking studies in order to deduce the helix packing. Accordingly, the built model for QacA (Section 5.2.1) can illustrate its helix packing. As seen in Figure 6.1, the overall spatial arrangement of the 14 TMS and their relative orientation and proximity can be easily

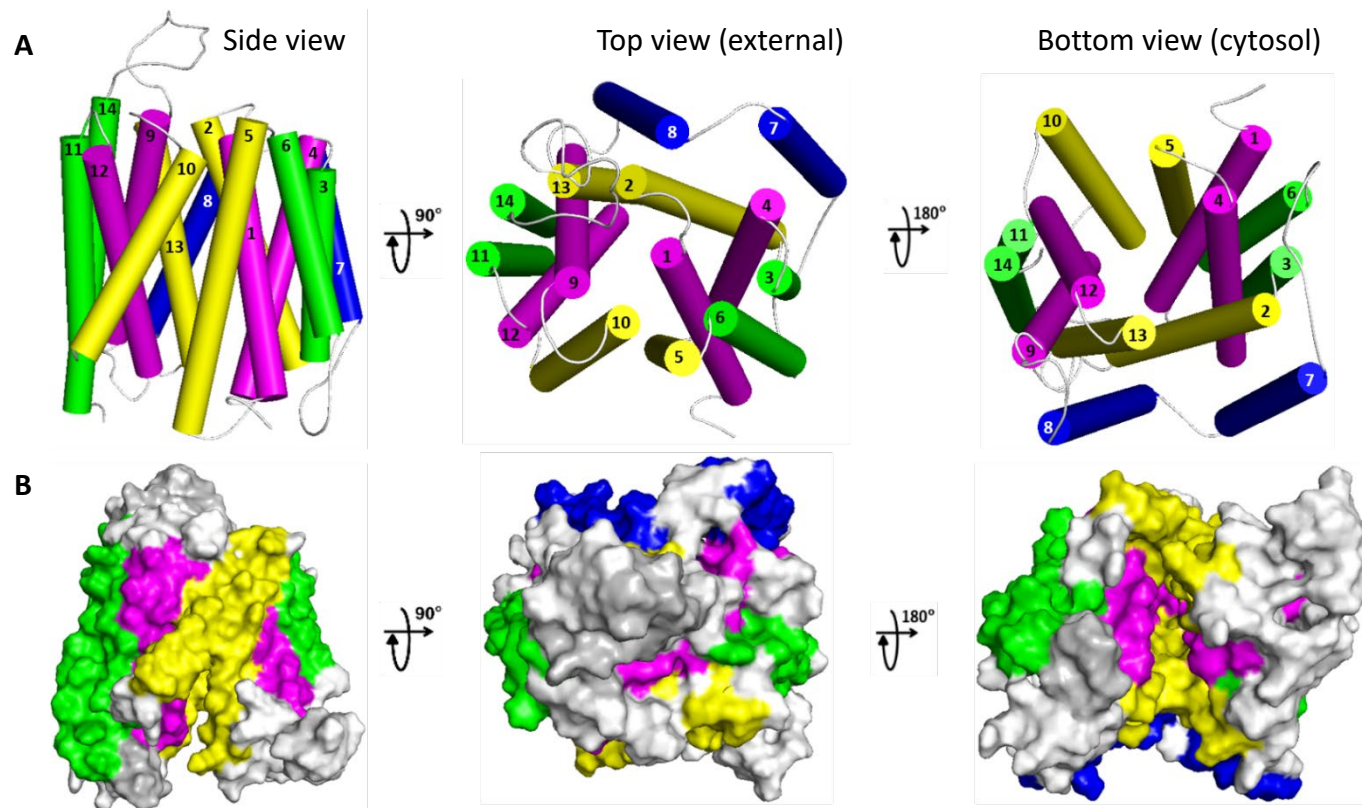


Figure 6.1 Spatial arrangement of 14 TMS in the inward-open model structure of QacA.

TMS are shown as **(A)** cylindrical and **(B)** surface view representation from the side, top and from the bottom of the membrane displaying the relative spatial arrangement of the 14 TMS within the QacA transporter. TMS of QacA are colour-coded according to the common structural features of MFS proteins (Section 1.8.1.1): TMS 1, 4, 9 and 12 (cavity helices), magenta; TMS 2, 5, 10 and 13 (rocker helices), yellow; TMS 3, 6, 11 and 14 (supporting helices), green; TMS 7 and 8, as two additional TMS in 14-TMS MFS proteins, blue.

understood from the QacA model. Based on the common structural features of MFS proteins (Section 1.8.1.1), TMS of QacA are colour-coded here to aid with visualisation: TMS 1, 4, 9 and 12 (cavity helices) are shown in magenta; TMS 2, 5, 10 and 13 (rocker helices) in yellow; TMS 3, 6, 11 and 14 (supporting helices) in green; TMS 7 and 8, as two additional TMS in 14-TMS MFS proteins in blue. As such, TMS 12, which was subject of the mutagenesis and biochemical studies in Chapters 3 and 4, is a cavity-lining helix (Figure 6.1, magenta coloured) and lies adjacent to TMS 9 and 10. TMS 12 together with TMS 1, 2, 4, 5, 9, 10 and 13 surround the QacA central cavity, which is purported to be the main substrate translocation pathway, similar to the central substrate binding pocket of MdfA (Yardeni *et al.*, 2020). It should be reminded that based on the evolution model of 14-TMS MFS proteins (Sections 1.8.1.1 and 3.2.7), TMS 1-6 and TMS 9-14 of the 14-TMS MFS proteins, e.g. QacA, are in similar positions as their corresponding TMS in the 12-TMS MFS proteins, e.g. MdfA, (TMS 1-6 and TMS 7-12, respectively), whereas TMS 7 and 8 connect the N- and C-domains akin to what the long central loop in 12-TMS proteins does.

Similar to what has been performed with MdfA, future experimental investigations by cysteine cross-linking studies (Brodie *et al.*, 2017) and double electron-electron resonance (DEER) analyses (Jeschke, 2012; Yardeni *et al.*, 2019) between the edges of TMS in QacA could be conducted in the absence and presence of various substrates. It should be noted that DEER spectroscopy is a technique that measures distance distributions between spin-labels attached to engineered cysteine residues (Masureel *et al.*, 2014; Martens *et al.*, 2016; Yardeni *et al.*, 2019; Yardeni *et al.*, 2020). DEER studies could be achieved by selecting cysteine mutants from our large body of QacA cysteine mutants (Figure 3.1) and through cloning/constructing cysteine pairs

that located on the intracellular and extracellular sides of the TMS. Such experiments would further test and confirm/refine the static helix packing derived from the QacA model and potentially provide dynamic information about the helices.

6.3 Refinement of QacA topology model

One of the goals in this thesis was to experimentally evaluate the topology of TMS 12 in QacA and to define its precise extents. The putative extents of TMS 12 were predicted in the preliminary QacA topology model (Figure 1.4) based on gene fusions and sequence-based hydropathy predictions (Paulsen *et al.*, 1996; Xu *et al.*, 2006; Hassan *et al.*, 2007). The cysteine-scanning solvent-accessibility experiments for all residues within and around the putative TMS 12 of QacA made it possible to obtain a topological map of TMS 12 and refine its topology accordingly (Section 3.2.6). The extents of the 14 TMS of QacA from the preliminary QacA topology model (Figure 1.4), with those obtained from the computational predictive methods including the Protter (Omasits *et al.*, 2014) (Appendix 6) and PPM web servers (Lomize *et al.*, 2012) (Section 5.2.2), are shown in Table 6.1. The predicted topology obtained from embedding QacA into the membrane (Figure 6.2) using the PPM server was found to better match the solvent-accessibility results of TMS 12 in this thesis and those of other TMS in previous work (M. H. Brown *et al.*, unpublished), indicating a more reliable prediction. Therefore, the initial QacA topology model was refined based on the PPM analysis of QacA model in combination with available solvent-accessibility results. In this way, the finalised 2D membrane topology model for QacA is proposed as presented in Figure 6.3.

It should be noted that some discrepancies (from one residue in TMS 5 up to a maximum of eight residues in the case of TMS 13) are observed between the extents

Table 6.1 Comparison of the predicted extents of TMS regions in QacA.

TMS	Preliminary topology model ^a	Protter ^b	Modelling / PPM ^c	Length (amino acids) ^d
1	24-41	22-43	22-43	22
2	58-76	55-74	56-78	23
3	88-104	86-106	84-103	20
4	113-130	110-131	108-130	23
5	147-164	146-167	146-168	23
6	173-190	173-195	174-193	20
7	208-225	208-226	209-228	20
8	238-255	238-255	235-259	25
9	279-296	276-301	277-301	25
10	310-334	313-334	312-333	22
11	342-360	341-360	339-360	22
12	370-390	366-392	366-390	25
13	411-432	412-432	403-424	22
14	482-499	481-504	478-499	22

^a These extents are taken from the QacA topology model shown in Figure 1.4.

^b Predicted transmembrane topology of QacA by Protter web server is depicted in Appendix 6.

^c Predicted transmembrane topology of QacA by PPM web server as obtained from embedding of the QacA model into the membrane is presented in Figure 6.2.

^d The number of amino acid residues allocated to each TMS based on PPM analysis.

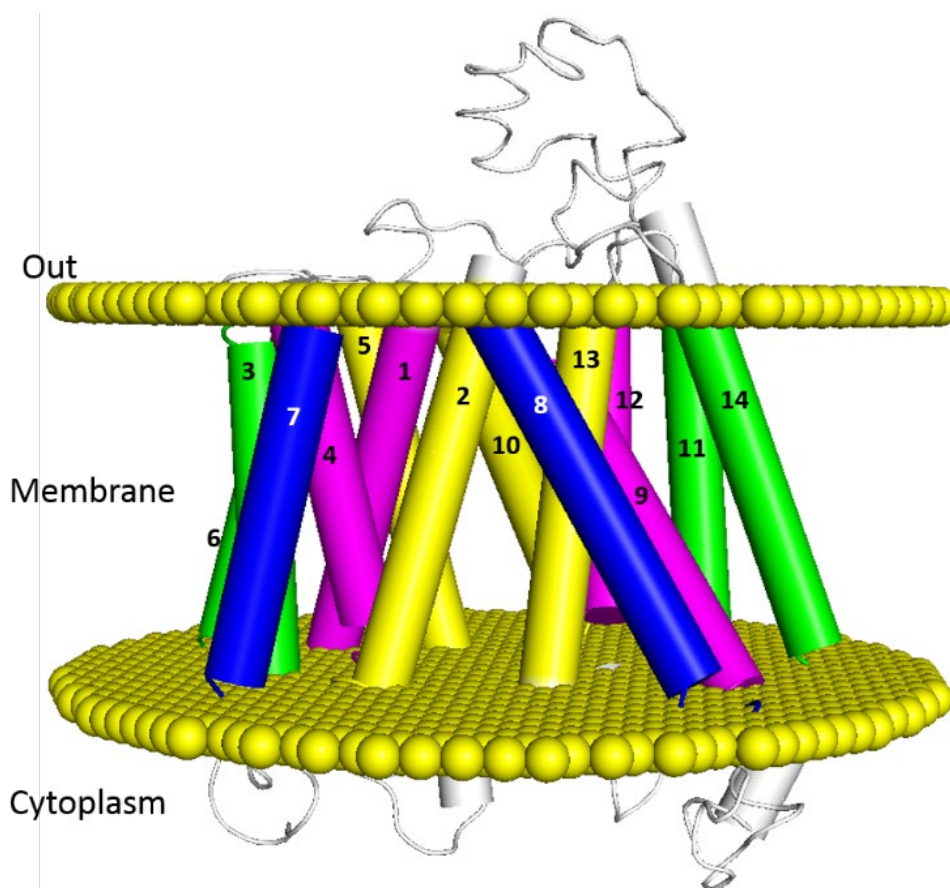


Figure 6.2 QacA embedded into a bilayer membrane.

Shown is the QacA structure model embedded into a membrane bilayer according to the PPM web server (Section 5.2.2). The TMS are displayed as cylindrical representation and are coloured as in Figure 6.1. Both the amino and carboxy termini are in the cytoplasm.

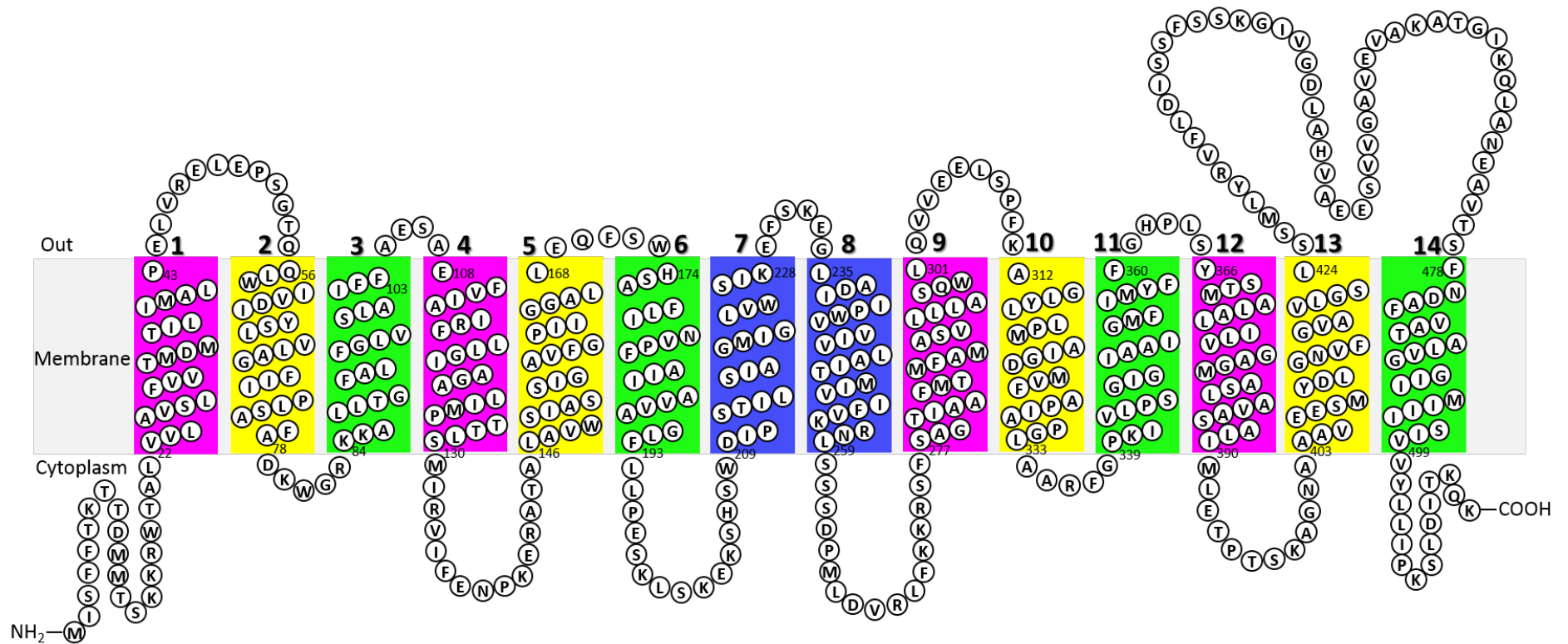


Figure 6.3 Refined 2D QacA topology model.

Finalised membrane topology model for QacA based on the combination of solvent-accessibility studies and predicted extents of TMS by PPM analysis (Table 6.1). The cell membrane is shaded in light grey and TMS (numbered 1-14) are enclosed in boxes coloured in the same colour scheme as Figure 6.1.

of helices predicted by PPM analysis and the allocated boundaries experimentally determined by solvent accessibility studies or sequence-based hydrophathy predictions. Such deviations could be as a result of several reasons: Firstly, lower accuracy of loop-modelling which is quite often reported to be a common problem in homology models, particularly in low-homology loop regions (Feig, 2017; Karami *et al.*, 2018). Further advanced loop-modelling methods could be employed for improving the accuracy of low-homology regions (Haddad *et al.*, 2020). Secondly, since alanine, leucine and lysine residues have high helix-forming tendency (Chakrabarty *et al.*, 1991; Creamer and Rose, 1994), they could be predicted by homology model as part of the TMS especially when they are located at the margin of TMS. However, they are considered to be in the loop due to being solvent accessible. Thirdly, some residues at the beginning or end of the TMS may be partially buried but their side chains are still accessible to FM. Lastly, some residues allocated to be in a loop region may not be accessible to FM because of the tight packing at that position. Conclusive information on helix extremities as well as boundaries between the end of a helix and a succeeding loop awaits future high-resolution structure of QacA.

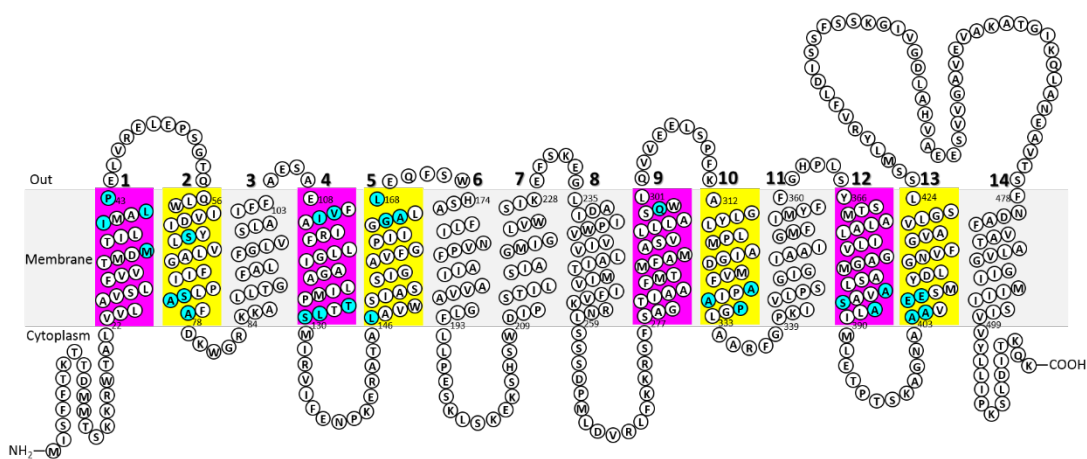
It has been shown that the length of a transmembrane α -helix varies between 12 and 40 residues (Papaloukas *et al.*, 2008). An average TMS is about 20 residues or five helical turns (approximately 3.6 amino acids per turn in an ideal α -helix) which are sufficient to span the 30 Å hydrophobic core of a bacterial membrane bilayer in a straight geometry (Granseth *et al.*, 2005; De Marothy and Elofsson, 2015). The obtained QacA topology model indicates that TMS 8, 9 and 12 are the longest TMS with 25 residues and hence are significantly tilted with respect to the membrane plane.

It should be taken into account that a generalised membrane topology model for QacA in a static system was presented here. In reality, QacA protein is conformationally flexible and membrane bilayers are not uniform in their depth and bilayer arrangement. Therefore, TMS and loop regions may depend on the immediate and local membrane environment of QacA. For example, a longer helix may be accommodated in a thicker membrane or may be tilted in a thinner membrane. Future conformational dynamics study of a QacA structure embedded in a staphylococcal lipid bilayer needs to be conducted to provide more realistic information about QacA membrane embedding in a dynamic system.

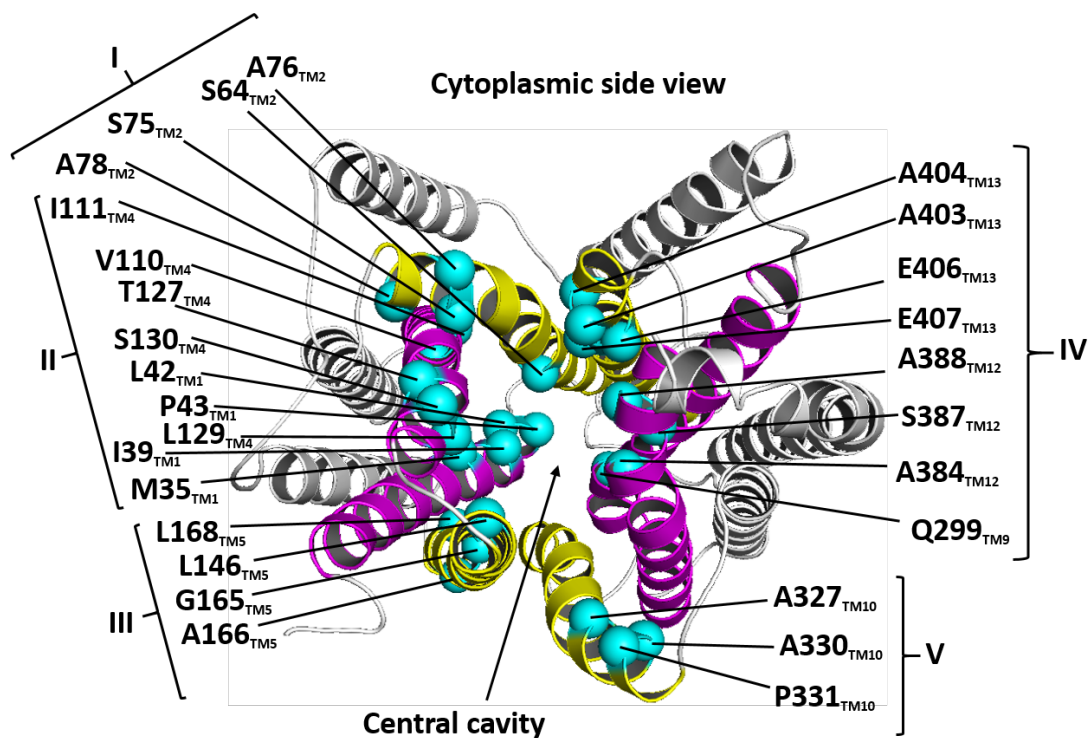
6.4 Solvent-accessible surface areas within the QacA central cavity

The reactivity of specific cysteine-substituted positions in TMS 12 (A384, S387 and A388) with FM (Section 3.2.6) led to the inference that these residues are part of the substrate translocation pathway as they were shown to being highly solvent-accessible. Additionally, a number of cysteine-substituted positions in TMS 10 (Xu *et al.*, 2006) and TMS 1, 2, 4, 5, 9 and 13 (M. H. Brown *et al.*, unpublished) have previously been shown to be solvent accessible (Figure 6.4A) implying that these TMS helices are amphipathic. Conspicuously, the 3D orientation of solvent-accessible residues in the QacA model show they are positioned towards the central cavity of QacA and form the solvent-accessible surface areas within the cavity (Figure 6.4B). Notably, most of the accessible residues, which are near or at the ends of TMS in the 2D topological model (Figure 6.4A), were observed in the homology model to be located in the cytosolic part of the QacA central cavity. Interestingly, the accessible residues in TMS 2, 4 and 5 from the N-terminal domain and TMS 10, 12 and 13 from the C-terminal domain constitute the water-accessible surface areas at the cytoplasmic

A



B



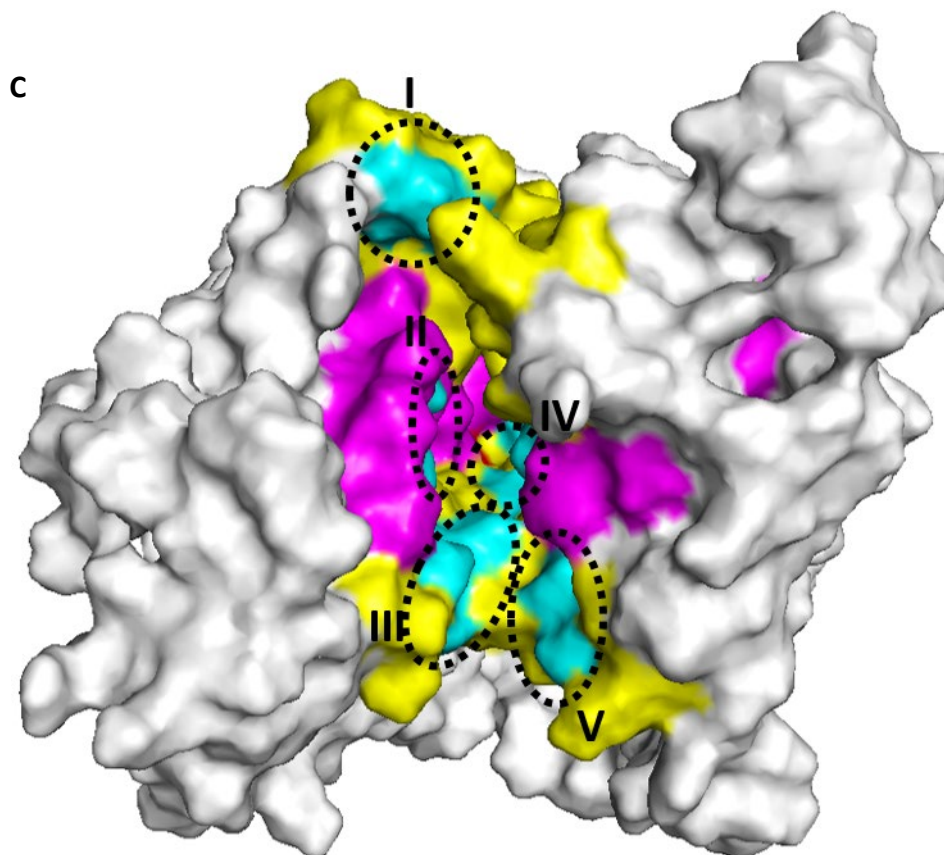


Figure 6.4 Solvent-accessible regions in the QacA central cavity.

(A) 2D QacA topology model with water-accessible residues found within cavity-lining TMS are highlighted in cyan. **(B)** The inward-open conformation QacA model viewed from the cytoplasm with the spatial orientation of water-accessible residues identified in (A) are represented as cyan spheres. **(C)** Surface view of (B) demonstrating accessible residues from TMS 2, 4, 5, 10, 12 and 13 pack against each other to form water-accessible surface areas (I-V; black dashed lines) at the cytoplasmic entrance to the transporter central cavity.

entrance to the central cavity which is believed to be the main substrate-binding and translocation region (Figure 6.4C). Taken together, the findings of solvent accessibility studies suggest that QacA transporter exists preponderantly in the inward-open conformation and its homology model reflects this conformation.

It is worth noting that among the accessible residues found in the QacA internal cavity, alanine residues outnumber other residues by at least twice. This information is in harmony with the reported maximum relative solvent accessibility value for alanine residues in the interior of empirical protein structures (Tien *et al.*, 2013). Among the accessible residues, six residues including M35, I39 (TMS 1), S64 (TMS 2) A327, A330 (TMS 10) and E407 (TMS 13) were found by docking studies (Chapter 5) to be directly involved in substrate binding. Put together, the findings indicate that while the QacA multidrug binding and translocation regions along the central cavity are mostly quite hydrophobic (membrane-embedded or inaccessible to aqueous environment), there exists local water-filled spaces (accessible to aqueous environment) along its whole length. Such hydrophobic/hydrophilic feature of the multidrug binding and translocation regions in QacA could provide a more malleable environment to accommodate structurally different lipophilic and/or amphipathic compounds. This helps to explain the broad range of substrate specificity of this transporter and possibly other multidrug MFS transporters.

A recent study of the MFS DHA1-member LmrP demonstrates that the binding pocket cavity of this multidrug transporter is partially filled with lipid (Debruycker *et al.*, 2020). Such a structural feature is likely to exist within the QacA transporter, which is consistent with the above-mentioned observation that the majority of residues lining the central cavity of QacA are water inaccessible. Future MD simulation studies

with QacA embedded in a mixture of 1-palmitoyl-2-oleoyl phosphatidylcholine (POPC) and 1-palmitoyl 2-oleoyl-phosphatidylglycerol (POPG) lipid bilayer that simulates the staphylococcal membrane could be conducted to explore the insertion/interaction of lipid molecules across the TMS helices. Such studies could address the likelihood that a lipid-filled interior of QacA could play a functional role in transporting substrates. The POPC/POPG membrane bilayer has been suggested to be an ideal model membrane to mimic the lipid composition of the *S. aureus* (Cheng *et al.*, 2011; Carretero *et al.*, 2021).

6.5 Architecture of the QacA multidrug binding site

Docking experiments described in Chapter 5 revealed hypothetical binding sites in QacA for the seven substrates analysed in this thesis, namely Et, R6G, BK, DQ, CH, PE and DAPI. The docking results indicated that these substrates were able to fit and bind within the QacA central cavity which is believed to be the major substrate-binding and translocation region. The combinatorial approach of docking analysis together with the biochemical binding data presented in Chapter 4 provide new and valuable insight into the substrate-binding mode of QacA promoting a better understanding of the architecture of its multidrug binding site. These findings in the context of information determined for other multidrug binding proteins are discussed in the following paragraphs.

The superimposition of docking-based QacA-substrate complexes enable visualisation of the spatial relationship between the whole QacA protein and substrate molecules (Figure 6.5A). This shows that the substrates Et, R6G, BK, DQ and PE bind to QacA in the same general region which is deeply embedded within the QacA central binding site (hereafter termed “inner-binding pocket”) whereas DAPI

binds closer to the mouth of central cavity that cytoplasmic entry of substrates occurs (hereafter termed “outer-binding pocket”).

The inner-binding pocket is delineated by residues from TMS 1, 2, 5, 9, 10 and 13. The substrates Et, R6G, BK, DQ and PE bind to the inner-binding pocket in a spatially close position but through interactions with different residues. As can be seen in Figure 6.5B, the Et and BK binding pockets do not have any overlapping binding residues while other substrates in the inner-binding pocket share between one to three binding residues. Moreover, Et, R6G, BK, DQ have only one distinct binding residue (namely M35, V60, I71 and E407, respectively), while PE has four (S64, L295, S298 and N414).

The outer-binding pocket, which accommodates the complete DAPI molecule and therefore also can be named the “DAPI-binding pocket”, is discrete from the binding sites of Et, R6G, BK, DQ and PE given that it is spatially distant and interacts with a distinct set of amino acid residues (Figure 6.5B). The outer-binding pocket is delineated by residues from TMS 10 and TMS 12, and as mentioned above, is positioned at the mouth of the QacA central cavity.

CH displays a special binding mode wherein one end of the molecule binds in the outer-binding pocket and the other is accommodated in the inner-binding pocket. As such, the CH binding site partially overlaps with both the QacA inner and outer substrate-binding pockets while having its own five distinct, non-overlapping binding site residues (S153 and S154 from TMS 5 and F326, A330 and A334 from TMS 10). Stereochemically, this binding behaviour can be explained considering that CH has

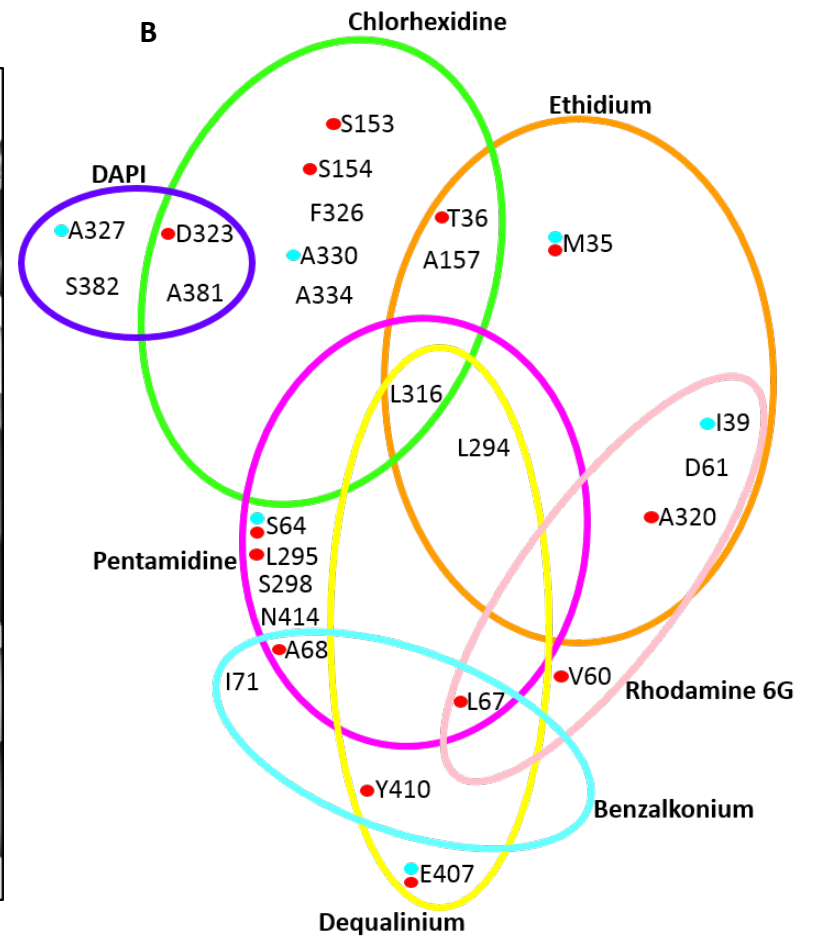
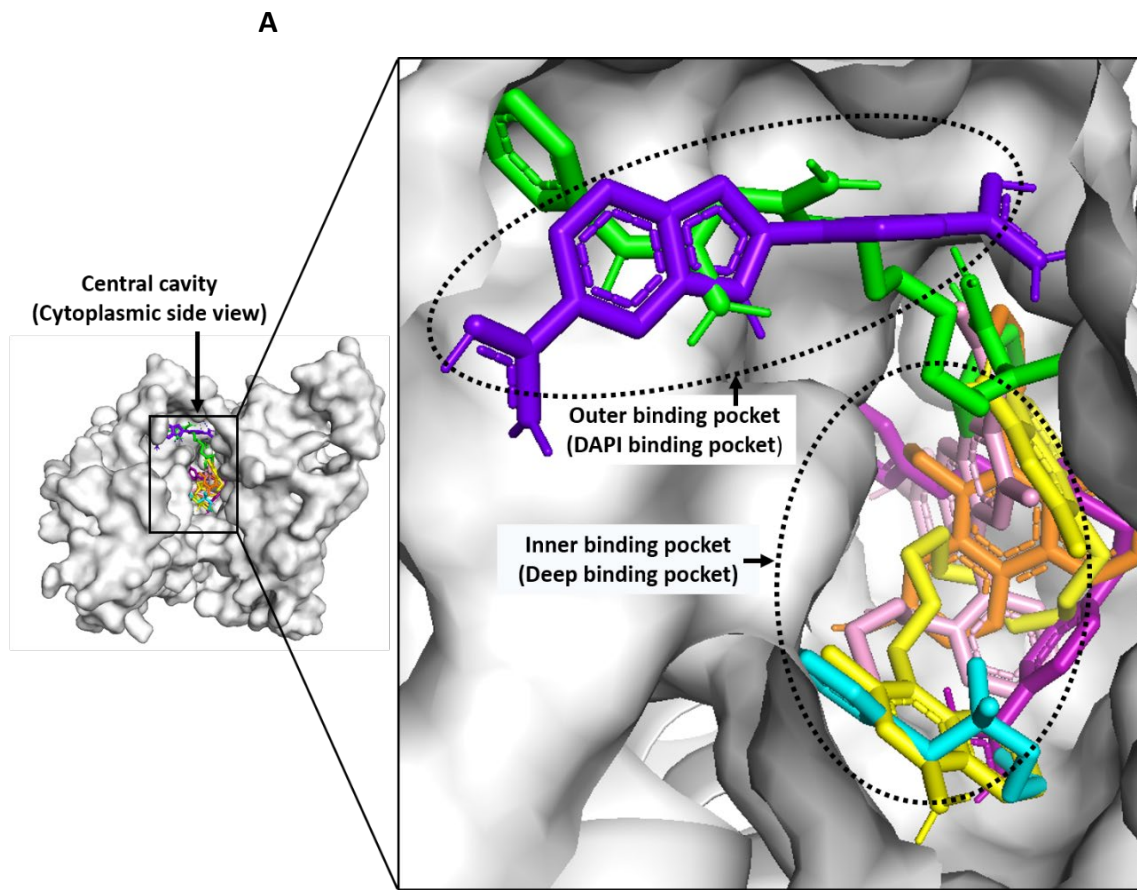


Figure 6.5 Architecture of the expansive central multidrug-binding pocket of QacA.

(A) Overlay of the binding sites of ethidium (orange), rhodamine 6G (pink), benzalkonium (cyan), dequalinium (yellow), chlorhexidine (green), pentamidine (magenta) and DAPI (purple) as obtained by superposition of their best-docked poses, viewed from the cytoplasm. This allows the assignment of two major discrete substrate-binding pockets along the QacA central substrate translocation pathway. The first pocket is located at the mouth of the QacA central cavity (the outer binding pocket) accommodating the complete DAPI molecule (therefore also named “DAPI binding pocket”) and part of the CH molecule. The second pocket is located deep within the QacA central cavity (the inner binding pocket) hosting the complete Et, R6G, BK, DQ, PE molecules as well as part of the CH molecule. **(B)** Venn diagram illustrating the overlap and unique binding residues in the substrate binding sites based on docking. The binding residues identified for each substrate are encircled by the same colour scheme as in (A). Cyan coloured dots indicate the residues that are solvent-accessible (Section 6.4) and red coloured dots are residues that identified as to be functionally important in resistance assays as shown in Figure 3.1.

the longest and unique molecular geometry among the compounds tested (Figure 1.5). A previous docking study of CH bound to a protein reported similar binding behaviour for this compound as seen here, highlighting its stereochemical feature (Cervelli *et al.*, 2013). Furthermore, previously studies with QacR revealed that a substrate can span the length of the multidrug-binding pocket, where DQ could stretch across both the “ethidium” and “rhodamine 6G binding sites” (Peters *et al.*, 2011).

As shown in Figure 6.5B, the cytoplasmic side of TMS 12 constitutes part of the outer-binding pocket of QacA. Intriguingly, experimental evidence to support that the cytoplasmic side of TMS 12 plays a role in substrate binding and translocation of CH and DAPI comes from the biochemical studies described in Chapter 4. It should be reminded that S387 is the only functionally important and solvent accessible residue at the cytoplasmic end of TMS 12 (see Section 3.3) and therefore has been used here as a proxy for discussing the role of this region. The results of substrate preincubation on FM labelling reactivity showed that the QacA S387C mutant protein was allosterically protected from maleimide modification in the presence of CH and DAPI, indicating its juxtaposition to the binding site of these substrates (Section 4.2.3). Moreover, NEM pre-treatment inhibited QacA-mediated DAPI efflux for cells expressing the S387C mutant protein due to a steric clash between the bound bulky maleimide group and DAPI, implying that this position is in close vicinity to the DAPI-binding site and translocation pathway (Section 4.2.4). These findings together with previous results of selected QacA mutants in TMS 10 (Xu *et al.*, 2006) and TMS 12 (Hassan *et al.*, 2007b) provide experimental credence to the notion that these two

TMS constitute the outer or DAPI binding pocket identified by the docking experiments in this thesis.

Overall, docking results of diverse substrates with QacA in this thesis together with mutational and biochemical analyses presented here and elsewhere support the existence of several separate, but linked substrate-binding sites within a voluminous substrate-binding cavity in QacA protein. This is indeed consistent with the known common feature of all the multidrug-binding proteins as they possess spacious and multivalent substrate-binding sites along a substrate translocation trajectory. Such structural organisation imparts the ability to bind promiscuously to structurally and chemically dissimilar substrates of very different sizes and shapes (Shcherbakov *et al.*, 2021).

6.5.1 Comparison of binding sites of QacA with other multidrug-binding proteins

The *E. coli* MdfA efflux pump is one of the most characterised DHA antiporters (Section 1.8.3). MdfA is a close relative of QacA with several common substrates (Fluman *et al.*, 2014). Three crystal structures of MdfA in complex with substrates chloramphenicol (Cm), deoxycholate (Dxc) and n-dodecyl-N,N-dimethylamine-N-oxide (LDAO) revealed the residues involved in substrate binding to the inward-open conformation of the transporter (Heng *et al.*, 2015). These substrates are electroneutral, monoanionic and zwitterionic, respectively. However, it should be noted that the substrate profile of QacA does not include these compounds since QacA substrates are mono- or dicationic compounds and no neutral or anionic compounds have been identified to be substrates of QacA (Section 1.9.3.2). Therefore, due to the lack of crystallographic binding site data of MdfA for a substrate

shared with QacA, it could not be examined whether such a substrate occupies the same geometric position in MdfA structure and QacA model.

A structural alignment (Lu *et al.*, 2016) aided to assign equivalent residues between QacA and MdfA (Figure 6.6). As can be seen, the 12-TMS structural fold of the QacA model aligned quite well with its corresponding TMS in the MdfA crystal structure. TMS 7 and 8, as the additional two TMS located at the side of the core in the 3D model of QacA, did not show any alignment since MdfA is a 12-TMS protein and lacks this extra TMS pair. Interestingly, the majority of the binding site residues of QacA and MdfA could be matched to each other (Table 6.2) because of their similar locations in the structural alignment. Together, these observations indicate the robustness of the QacA model used for docking as well as the docking approach utilised for identification of substrate-binding site residues in QacA. The equivalent substrate-binding residues in the QacA model and MdfA structure are located at approximately the same depth in both the QacA and MdfA TMS 1, 2 and 5 from the N-terminal domain and QacA TMS 9, 10, and 13 (corresponding to MdfA TMS 7, 8, and 11) from the C-terminal domain, implying similarities between QacA and MdfA proteins with respect to the overall architecture (shape and location) of binding pockets.

It has been shown that the binding pocket for minocycline in the MDR efflux transporter AcrB (Murakami *et al.*, 2006) is rich in aromatic amino acid residues (F136, F178, F610, F615, F617 and F628). In addition, the substrate-binding pocket of QacR, in complex with numerous diverse compounds which are also QacA substrates, was revealed to be rich in aromatic (W61, Y92, Y93, Y103, Y123 and F162) and acidic (E57, E58, E90, and E120) residues (Schumacher *et al.*, 2001; Schumacher *et al.*, 2004; Brooks *et al.*, 2007; Peters *et al.*, 2008). However, as seen in Table 6.2, the multidrug

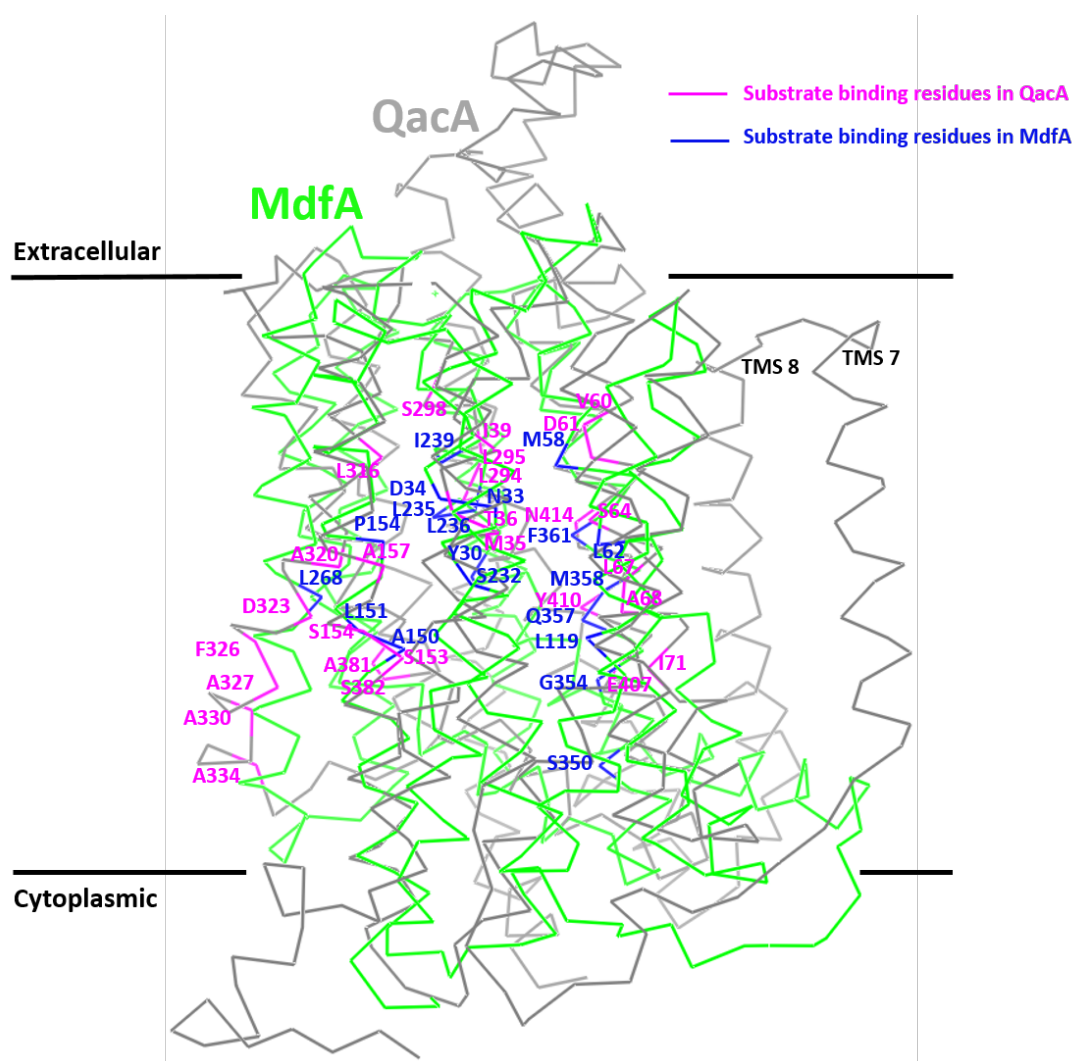


Figure 6.6 Structural alignment of QacA homology model and MdfA structure.

Structural alignment of the QacA model generated in this thesis (Figure 5.1) (grey) and the crystal structure of inward-open conformation of MdfA (PDB: 4ZOW) (green) shows that the structural organisation of the 12-TMS core of QacA closely resembles MdfA. Most of the putative substrate-binding residues identified by docking studies with QacA (magenta) in this thesis are located proximal to the binding residues of MdfA (blue) found by substrate cocrystal structures. This aided the assignment of the corresponding binding residues in MdfA as listed in Table 6.2. The view is from the side of the membrane with the cytoplasmic side of each protein at the bottom. QacA TMS 7 and 8 are located at the side of 12-TMS core and do not show any alignment since MdfA is a 12-TMS transporter and lacks this extra TMS pair.

Table 6.2 Comparison of binding site residues of QacA and MdfA.

Putative substrate-binding residues of QacA ^a								Substrate-binding residues of MdfA ^b				
Et	R6G	BK	DQ	CH	PE	DAPI			Cm	Dxc	LDAO	
✓							M35 _{TMS1}	←→	Y30 _{TMS1}	✓	✓	✓
✓				✓			T36 _{TMS1}	←→	N33 _{TMS1}	✓	✓	✓
✓	✓						I39 _{TMS1}	←→	D34 _{TMS1}	✓	✓	✓
	✓						V60 _{TMS2}	←→	M58 _{TMS2}	✓	✓	✓
✓	✓						D61 _{TMS2}					
					✓		S64 _{TMS2}					
	✓	✓	✓		✓		L67 _{TMS2}	←→	L62 _{TMS2}	✓	✓	✓
		✓			✓		A68 _{TMS2}					
		✓					I71 _{TMS2}					
									L119 _{TMS4}	✓		
				✓			S153 _{TMS5}	←→	A150 _{TMS5}	✓		
				✓			S154 _{TMS5}	←→	L151 _{TMS5}	✓		
✓				✓			A157 _{TMS5}	←→	P154 _{TMS5}		✓	
									S232 _{TMS7}			✓
✓			✓		✓		L294 _{TMS9}	←→	L235 _{TMS7}	✓		
					✓		L295 _{TMS9}	←→	L236 _{TMS7}	✓	✓	✓
					✓		S298 _{TMS9}	←→	I239 _{TMS7}	✓		✓
✓			✓	✓	✓		L316 _{TMS10}					
✓	✓						A320 _{TMS10}					
				✓		✓	D323 _{TMS10}	←→	L268 _{TMS8}	✓		
				✓			F326 _{TMS10}					
						✓	A327 _{TMS10}					
				✓			A330 _{TMS10}					
				✓			A334 _{TMS10}					
				✓		✓	A381 _{TMS12}					
						✓	S382 _{TMS12}					
									S350 _{TMS11}		✓	
			✓				E407 _{TMS13}	←→	G354 _{TMS11}		✓	
		✓	✓				Y410 _{TMS13}	←→	Q357 _{TMS11}		✓	
									M358 _{TMS11}		✓	
					✓		N414 _{TMS13}	←→	F361 _{TMS11}			✓

^a Substrate-binding residues of QacA were identified by docking experiments in this study.

^b Substrate-binding residues of MdfA were determined from the MdfA-Cm complex (PBD: 4ZOW), MdfA-Dxc complex (PBD: 4ZPO) and MdfA-LDAO complex (PBD: 4ZP2) (Heng *et al.*, 2015).

Check mark (✓) in the columns indicates which compound each substrate-binding residue is interacting with.

Et: ethidium; R6G: rhodamine 6G; BK: benzalkonium; DQ: dequalinium; CH: chlorhexidine; PE: pentamidine; Cm: chloramphenicol; Dxc: deoxycholate; LDAO: n-dodecyl-N,N-dimethylamine-N-oxide. The equivalent binding residues in QacA and MdfA, based on the structural alignment in Figure 6.6, are connected by blue double-headed arrows and grey boxes denote residues that do not have an aligned partner.

binding pockets of both QacA and MdfA consist of mainly leucine (hydrophobic) and serine (polar) but also at least one alanine, isoleucine, methionine, phenylalanine, tyrosine, aspartic acid and asparagine are observed. These residues participate in the stabilisation of the substrates mostly through a range of hydrophobic and H-bonding interactions. It is thus conceivable that the presence of multiple aromatic and/or acidic amino acid residues in the substrate-binding pockets is not a common feature of MFS DHA transporters like QacA and MdfA. In QacR, the acidic residues in the binding pocket serve to neutralise the cationic drugs (Schumacher *et al.*, 2004). However, such charge neutralisation of cationic substrates can also be facilitated through long-range electrostatic interactions in MdfA (Wu *et al.*, 2019) and perhaps QacA.

It is known that each distinct substrate favours a specific binding site within the binding pocket based on its molecular physicochemical properties such as shape, size, electrostaticity, amphiphilicity and aromaticity (Guo *et al.*, 2015; Mehla *et al.*, 2021). It is important to keep in mind that different substrates (Et, R6G, BK, DQ, CH, PE and DAPI for QacA versus Cm, Dxc and LDAO for MdfA) have different physicochemical properties. Therefore, some differences in configurations around the binding pockets of QacA and MdfA are expected to accommodate different compounds. This may be the reason that some of the binding residues in QacA could not be assigned to counterparts in MdfA (Table 6.2, residues that are not connected by blue double-headed arrows) in addition to the difference in overall transport protein structure.

6.5.2 Possible structural underpinning for competitive and non-competitive substrate binding in QacA

Previous transport competition studies (Mitchell *et al.*, 1999) showed that BK competitively inhibited QacA-mediated export of Et and suggested that QacA utilises a common binding site region for the recognition of monovalent cationic substrates. In contrast, CH non-competitively inhibited QacA-mediated export of Et suggesting that QacA uses a distinct binding site region for recognition of bivalent cationic substrates. In this work, the architecture of the QacA multidrug binding pocket presented in Figure 6.5, provides important insight into the tenable structural underpinning of the competitive and non-competitive multidrug binding in QacA transporter. Et and BK bind to a spatially close position within the same general region (QacA inner-binding pocket). Therefore, the two substrates would sterically clash with the binding of the other that could lead to their observed competitive binding behaviour. However, Et and CH would simultaneously bind without an allosteric effect because their binding regions are largely located spatially away from each other. This could give rise to their non-competitive binding behaviour. These observations bear some resemblance to the results of simultaneous binding of proflavin and Et in the structure of QacR–proflavin–Et ternary complex (Schumacher *et al.*, 2004). The location of these two substrates in the pocket do not sterically interfere with each other. Therefore, the favourable van der Waals interactions and hydrogen bonds are maintained such that these substrates could be accommodated at the same time.

Future fluorimetric competition studies should be directed to investigate competitive or non-competitive binding situation between Et in the presence of nonfluorescent substrates DQ and PE. In addition, QacA-mediated DAPI export in the presence of BK,

DQ, CH and PE should be examined. This information, as well as a future QacA structure in complex with two different substrates (e.g. Et and CH), could fully elucidate the mechanism of simultaneous recognition and binding of more than one substrate by QacA.

6.6 Functional and structural assessment of identified important residues within and around TMS 12

6.6.1 G361 as a hinge point for the extracellular loop flanking the TMS 12

Longstanding genetic, biochemical and structural lines of evidence have shown that the major substrate binding and translocation region in MFS transporters lie in the centre of the protein formed by α -helical TMS (Quistgaard *et al.*, 2016; Mikros and Diallinas, 2019). TMSs are connected through loops of variable length. Substrate translocation in MFS transporters is elicited by significant reversible conformational alterations. In addition to interactions taking place between substrates and TMS-embedded residues along the binding and translocation trajectory, gating by specific loops at the entrance or exit controls substrate entry to or release from the major binding site of the transporter (Diallinas, 2014; Diallinas, 2016; Mikros and Diallinas, 2019). As such, the synergy between proper functioning of the gates and substrate translocation sites are essential for transporter activity. For example, biochemical and structural data for MFS antiporters LmrP (Masureel *et al.*, 2014; Neuberger and van Veen, 2015), MdfA (Fluman *et al.*, 2009; Fluman *et al.*, 2012) and EmrD (Yin *et al.*, 2006; Ranaweera *et al.*, 2015) have demonstrated that loops on the extracellular side of these transporters are conformationally linked to substrate release from the interior substrate binding cavity. Furthermore, consistent with this line of reasoning, in glucose transporters and related monosaccharide sugar transporters (12-TMS

MFS), TMS 10 (equivalent to TMS 12 in QacA) was found to have a critical role for fine-tuning the substrate binding and gating interactions (Drew *et al.*, 2021) during different conformational states of the rocker-switch alternating-access mechanism (Section 1.8.2). Thus, the extracellular and cytoplasmic loops that connect TMS 12 to TMS 11 and TMS 13, respectively, are likely to be dynamic loops with a gating role during transport of substrates. This calls for future research using MD simulation and DEER studies on QacA to fully elucidate mobility of the TMS and loop regions during the recognition, binding and translocation of a substrate or inhibitor in DHA2-family transporters.

Glycine residues lack a side chain and typically increase the local flexibility in the protein structure. This is particularly important for the normal activity of the MDR transporters that constantly change their conformation to transport a substrate from one side of the membrane to the other (Costa *et al.*, 2019; Andrews *et al.*, 2020). The residue G361, which is located in the extracellular loop 11-12, was found to be functionally important for QacA resistance activity against PE (Section 3.2.3) and DAPI (Section 4.2.1). Taken further, when it was mutated there was a pronounced decrease in the DAPI transport rate (Section 4.2.2) and a higher binding affinity (Section 4.2.5). The former is suggestive of weakened protein dynamics and the latter can be attributed to hindered substrate release. Taking into account all the above-mentioned information together with these results, it is reasonable to presume that G361 may act as a hinge point for efficient motion of the extracellular loop 11-12 which probably relates to the exit of DAPI and PE. Therefore, its mutation would induce rigidity in this gate loop and constrain substrate release leading to decreased MICs.

6.6.2 G379 as an intramembrane conserved glycine residue for TMS 12 helical flexibility

The substitution of G379 in TMS 12 with cysteine displayed an important functional consequence as it caused a significant defect in resistance to all bivalent cations tested (Section 3.2.3). Multiple sequence alignments analysis showed that this glycine residue is highly conserved among related bacterial MFS transporters (Section 3.2.7). Taken further, effects of substrate preincubation on FM labelling reactivity (Section 4.2.3) and NEM pre-treatment on QacA-mediated DAPI efflux (Section 4.2.4) was marginal for G379C, implying that this residue is not directly engaged in substrate-binding and translocation pathway. These experimental results are in agreement with the position of G379 in the QacA model where this residue is oriented away from the central cavity (Figure 6.7). It is thus conceivable that G379 plays a structural role. Indeed, many of intramembrane conserved glycine residues have been ascribed to participate in the helix-helix packing and inter-helical interactions in the structure of multidrug transporters of ABC (e.g., MacAB), RND (e.g., AcrAB), and MFS (e.g., EmrAB) superfamilies (Dong *et al.*, 2012; Zgurskaya *et al.*, 2015).

Taken together, it is likely that G379 in TMS 12 of QacA is structurally important for helical flexibility and inter-helical interactions of TMS 12 required for transport of bivalent substrates, similar to the previously reported G313 in TMS 10 of QacA (Xu *et al.*, 2006). Future DEER experiments and/or MD simulation studies with these glycine mutants could be conducted in the presence of bivalent substrates to provide dynamic information about TMS 12 and 10 in QacA. These TMS are expected to have high mobility during the substrate translocation as shown by spin labelling studies for

corresponding TMS in the EmrD (12-TMS MFS) transporter (Steed *et al.*, 2013). The presence of glycine residues can facilitate such helix flexibility (Baker *et al.*, 2012).

6.6.3 S387 as a kink site in TMS 12

Serine residues are among the polar amino acids which are typically found in protein functional centres (Uversky, 2015; Basile *et al.*, 2019). Serine has a hydroxyl group that can react to form hydrogen bonds with a variety of polar substrates (Faustinella *et al.*, 1991; Burgess and Justice Jr, 1999). Serine residues have been implicated to be important for interactions with cationic substrates in multidrug-binding proteins such as QacR (Schumacher *et al.*, 2001; Murray *et al.*, 2004).

As previously discussed, S387 was found to be both a functionally important and solvent accessible residue in TMS 12 of QacA. Taken further, the effects of substrate preincubation on FM labelling reactivity (Section 4.2.3) and NEM pre-treatment on QacA-mediated DAPI efflux (Section 4.2.4) suggested that this residue is close to the substrate-binding site and translocation pathway of CH and DAPI. These experimental results are consistent with the location of S387 in the QacA model where this residue is oriented towards the central cavity (Figure 6.7). In molecular docking experiments, this residue did not appear to be a binding site residue in the identified QacA substrate-binding pockets (Figure 6.5). However, due to its close proximity to the substrate-binding pocket of CH and DAPI, mutation of S387 could have altered the binding pocket geometry/stability without actually being part of it. Put another way, S387 residue may contribute in providing the correct orientation of the substrate in the binding site during transport.

In transmembrane proteins, serine residues could potentially induce local kinks in

α -helical TMS to enhance regional solvation or dynamics as shown by MD simulations (Hall *et al.*, 2009; Del Val *et al.*, 2012). Notably, TMS 12 is kinked at its cytoplasmic end in the QacA model structure and S387 is located there (Figure 6.7). The serine kink is likely to be critical to facilitate high mobility of TMS 12 during the conformational changes required for substrate transport. This kinking at S387 is likely to be directly influenced by cysteine substitution which leads to weakened protein dynamics as inferred from substantial decrease in DAPI transport rate (Section 4.2.2).

Future MD simulation and DEER studies of QacA with and without substrates will be informative to determine whether/how the dynamic behaviour and conformational changes of wild-type QacA protein are affected upon mutation of functional residues G361, G378 and S387.

6.7 Future research: Towards developing QacA inhibitors

In Chapters 3 and 4, the involvement of TMS 12 in the binding and translocation pathway of QacA was demonstrated through site-directed cysteine-scanning mutagenesis and biochemical studies. Future work could focus on developing and optimising a fluorescent label-free binding assay such as SPR to directly test and compare the binding kinetics and affinity of the wild-type and mutant QacA proteins to the non-fluorescent substrates (BK, DQ, CH and PE). More importantly, setting up the SPR binding assay will benefit prospective research of designing efficient and specific EPIs of QacA. This category of inhibitors often resemble substrates and can bind to the substrate-binding pocket of the efflux pump with tight affinity as opposed to weak affinity binding of antimicrobial substrates. In this way, efficacious inhibition at low concentrations would be achieved, similar to what has been described for

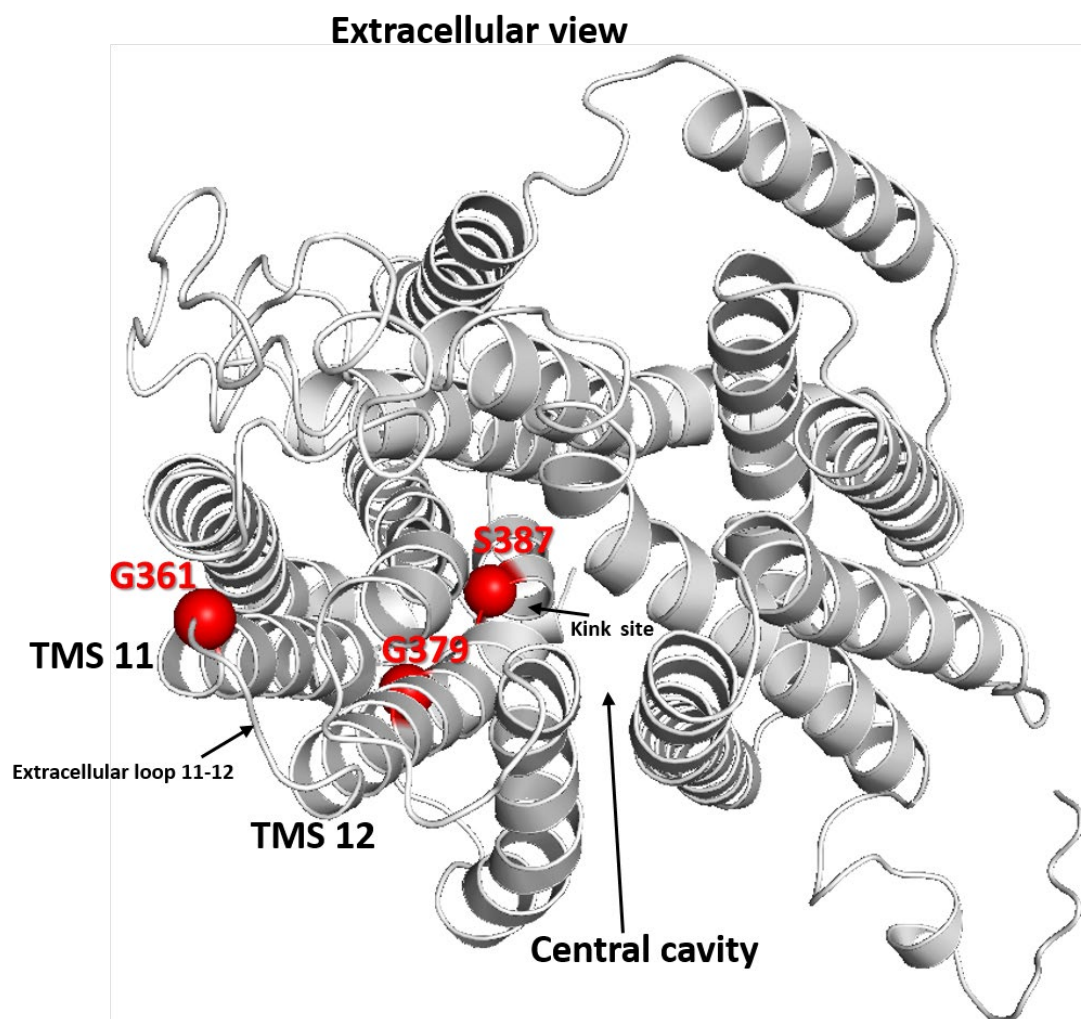


Figure 6.7 Spatial orientation of functionally important residues identified within and around TMS 12.

Residues found to be functionally important in this study are shown as red spheres in the inward-open conformation QacA model viewed from the extracellular side. Within the TMS 12, only S387 is oriented towards the central cavity. The kink site in TMS 12 is labelled.

AcrAB efflux pump (Sjuts *et al.*, 2016; Blanco *et al.*, 2018). Another area of future research should focus on using purified QacA protein (Chapter 4) for solving the X-ray structure of QacA. Such a structure is needed to help us fully understand its interaction with multiple substrates and could be also utilised for structure-based development of EPIs.

Chapter 5 provided a step towards rational design and development of inhibitor compounds for QacA by unravelling the binding modes of substrates as well as the architecture of its substrate-binding pockets. Future research should focus on designing, identifying, and evaluating novel candidate compounds for inhibition of the QacA system. For example, by knowing the binding mode of BK and CH, as commonly used antiseptics and disinfectants, their chemical scaffold can be exploited for designing pharmacophores via medicinal chemistry approaches to prompt tighter binding within the substrate-binding pocket. By this means, EPI properties can be added to the same chemical structure so as to create potent antimicrobial compounds that inhibit their own efflux, as suggested for developing new inhibitors for MexB MDR efflux transporter in *P. aeruginosa* (Mehla *et al.*, 2021).

Several potent EPIs have been identified by screening of natural and synthetic molecules to inhibit *S. aureus* efflux pumps. A notable recent example is thiophene derivatives that promote the inhibition of the NorA efflux pump, potentiating the activity of the antibiotic ciprofloxacin against a NorA-overexpressing strain of *S. aureus*. These EPIs are likely to inhibit by interacting with the binding site of NorA (Baral and Mozafari 2020, Da Cruz *et al.* 2020). However, the lack of high selectivity combined with potential toxicity of current EPIs have hampered progress towards their clinical use (Miethke *et al.*, 2021). Further work is required to gain a detailed

understanding of the precise mechanism of the multidrug binding and transport process, followed by application of this knowledge in structure-guided design of safe and highly selective EPIs.

MDR efflux pumps undergo constant conformational changes during the transport cycle that lead to variations in the accessibility, rearrangement and architecture of the drug binding pocket (Jamshidi *et al.*, 2017; Du *et al.*, 2018). Future MD simulation studies should be directed to deciphering the overall dynamical properties of the QacA structure at the molecular level upon substrate/inhibitor binding as well as probing the dynamic changes in response to mutational effects. Such studies could facilitate the identification of novel inhibitors capable of locking the conformation changing of the transporter (López *et al.*, 2017; Türková and Zdrzil, 2019). In addition, MD simulation studies provide us with a better appreciation of the relationship between QacA protein topology and the membrane lipid bilayer environment, particularly in the light of recent findings which show the presence of embedded lipid within the binding cavity orchestrates the transport cycle (access, binding, and extrusion of substrates) in LmrP and possibly other multidrug transporters (Debruycker *et al.*, 2020).

6.8 Conclusions

The growing emergence of MDR bacteria poses a major threat to public health globally. Among the most serious pathogenic bacteria is *S. aureus*, which is able to cause MDR hospital- or community-acquired infections with an alarming increase in morbidity and mortality worldwide. *S. aureus* employs a number of mechanisms to circumvent the effects of antimicrobials. One of these is the active extrusion of antimicrobial agents by multidrug efflux pumps. QacA is one such protein that confers

resistance to a diverse array of lipophilic cationic antimicrobial compounds, including many widely used antiseptics and disinfectants such as BK and CH. The success in developing new antimicrobials and/or EPIs requires in-depth understanding of bacterial multidrug efflux systems as whole. This highlights the importance of structural and functional analyses of multidrug efflux transporters such as QacA.

The research presented in this thesis has shed light on the role of key amino acid residues within and around TMS 12 of QacA multidrug transporter and advanced our understanding of its structural and functional features in general. Moreover, the QacA structural model presented in this thesis was in excellent agreement with the biochemical experimental data in hand, and provided a useful framework for integration of all the available experimentally identified functionally important residues of QacA in a structural context. This offered a clearer picture of QacA with respect to which residues/regions interact with different antimicrobial substrates during their binding and transport through the protein. Additionally, molecular docking of the substrates with the derived QacA model revealed the mode of substrate-binding to the inward-open conformation of the transporter. The combination of docking and mutational findings provided new insights into the putative architecture of substrate-binding pockets within the expansive central drug binding cavity of QacA transporter.

Collectively, the findings can be used in complementing high-resolution structural data when they are available, and also lay the initial groundwork for future rational structure-based development of specific and efficient antimicrobials and/or EPIs to combat the growing resistance problem caused by QacA and possibly other multidrug MFS transporters.

CHAPTER 7 APPENDICES

7.1 Appendix 1 – The nucleotide and amino acid sequence of QacA

Nucleotide sequence (5'→3') of the *qacA* gene (UniProtKB/Swiss-Prot accession number: P0A0J8) is shown as small black letters while the amino acid (one-letter code) sequence is shown as capital red letters. The QacA protein is consisted of 514 amino acids.

```

atg att tca ttt ttt aca aaa act act gat atg atg aca tca aaa 45
M I S F F T K T T D M M T S K
aaa aga tgg act gca cta gta gta tta gct gtt agt ttg ttt gtt 90
K R W T A L V V L A V S L F V
gtt aca atg gat atg aca ata tta att atg gct tta ccg gaa tta 135
V T M D M T I L I M A L P E L
gta aga gag tta gag cct tct ggt acc caa cag tta tgg ata gtt 180
V R E L E P S G T Q Q L W I V
gat ata tac tct ctt gtt tta gct ggc ttt ata att cca ttg agt 225
D I Y S L V L A G F I I P L S
gcc ttt gct gat aaa tgg gga aga aaa aaa gca tta tta act gga 270
A F A D K W G R K K A L L T G
ttt gct tta ttt ggc ctc gtt tca tta gct ata ttt ttc gca gaa 315
F A L F G L V S L A I F F A E
agt gca gag ttc gta ata gct att cga ttt tta ctt ggt att gca 360
S A E F V I A I R F L L G I A
ggt gct tta ata atg cca act acc ctt tca atg ata aga gta att 405
G A L I M P T T L S M I R V I
ttt gaa aac cct aaa gaa agg gcc act gca tta gct gta tgg tca 450
F E N P K E R A T A L A V W S
atc gct tca tcg ata ggt gct gtt ttt gga cca att atc gga gga 495
I A S S I G A V F G P I I G G
gct tta ctt gag caa ttt tca tgg cac tcg gca ttt tta att aat 540
A L L E Q F S W H S A F L I N
gta ccg ttt gcg ata ata gca gtt gta gca ggt tta ttt tta tta 585
V P F A I I A V V A G L F L L
cca gag tct aag tta tca aaa gaa aag tct cac tcg tgg gat att 630
P E S K L S K E K S H S W D I
cct tct aca att tta tca att gca ggc atg att gga ctg gta tgg 675
P S T I L S I A G M I G L V W
agt atc aaa gaa ttt tca aaa gaa gga cta gca gat att att cca 720
S I K E F S K E G L A D I I P
tgg gtt gta ata gta tta gca att acc atg ata gtg ata ttt gtt 765
W V V I V L A I T M I V I F V
aaa cgt aat tta tca agt tct gat cca atg tta gac gta aga ctt 810
K R N L S S S D P M L D V R L

```

(Continued on next page)

Appendix 1 (continued)

```

ttt aaa aag aga tca ttt tca gct ggt aca att gct gca ttt atg 855
  F  K  K  R  S  F  S  A  G  T  I  A  A  F  M
aca atg ttt gca atg gca tct gtt ttg tta tta gct tca caa tgg 900
  T  M  F  A  M  A  S  V  L  L  L  A  S  Q  W
ctg cag gtt gtg gaa gaa ctt tct cct ttt aaa gct ggc tta tac 945
  L  Q  V  V  E  E  L  S  P  F  K  A  G  L  Y
cta tta cct atg gca ata gga gat atg gtg ttt gca cca att gca 990
  L  L  P  M  A  I  G  D  M  V  F  A  P  I  A
ccc gga tta gcg gcg cga ttt ggg ccc aaa ata gtg tta cct tcc 1035
  P  G  L  A  A  R  F  G  P  K  I  V  L  P  S
gga att gga att gca gcc att ggc atg ttt att atg tat ttc ttt 1080
  G  I  G  I  A  A  I  G  M  F  I  M  Y  F  F
ggt cat cca tta tca tat tct aca atg gct tta gca tta att tta 1125
  G  H  P  L  S  Y  S  T  M  A  L  A  L  I  L
gtt gga gct ggt atg gct tca cta gca gtt gca tct gct cta ata 1170
  V  G  A  G  M  A  S  L  A  V  A  S  A  L  I
atg tta gaa aca cct aca tca aaa gca ggt aat gca gct gct gtt 1215
  M  L  E  T  P  T  S  K  A  G  N  A  A  A  V
gaa gag tct atg tat gac ctt gga aat gtt ttt ggt gta gca gta 1260
  E  E  S  M  Y  D  L  G  N  V  F  G  V  A  V
ctt ggt agc cta tct tct atg ctt tat cgt gta ttt tta gat att 1305
  L  G  S  L  S  S  M  L  Y  R  V  F  L  D  I
tca tct ttt tca tca aaa ggt ata gtt gga gat tta gct cat gta 1350
  S  S  F  S  S  K  G  I  V  G  D  L  A  H  V
gct gaa gaa tct gta gtg ggc gct gtc gaa gta gct aaa gct acg 1095
  A  E  E  S  V  V  G  A  V  E  V  A  K  A  T
ggg ata aaa cag ctt gca aac gag gct gta aca tca ttt aat gat 1440
  G  I  K  Q  L  A  N  E  A  V  T  S  F  N  D
gct ttt gta gca act gct tta gta ggt ggg att atc atg att atc 1485
  A  F  V  A  T  A  L  V  G  G  I  I  M  I  I
att tca ata gtt gtc tat ttg tta att ccc aaa tca ctt gat ata 1530
  I  S  I  V  V  Y  L  L  I  P  K  S  L  D  I
act aaa caa aaa 1542
  T  K  Q  K

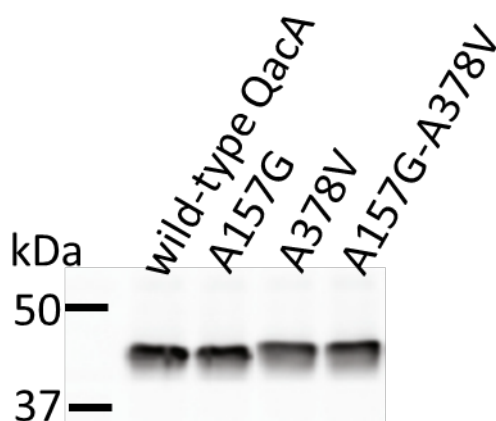
```

7.2 Appendix 2 – AutoDock Vina input configuration file used in docking

```
receptor= protein.pdbqt  
  
ligand= ligand.pdbqt  
  
center_x= 70.901  
  
center_y= 73.681  
  
center_z= 75.257  
  
size_x= 90  
  
size_y= 90  
  
size_z= 90  
  
out= vina_outligand.pdbqt  
  
log= logligand.txt  
  
exhaustiveness= 8
```

* Configuration parameters used in AutoDock Vina throughout the molecular docking studies (Section 2.13.4).

7.3 Appendix 3 – Protein expression, resistance profile and ethidium efflux activity of A157G and A378V substitutions



(A) Western blot analysis of A157G and A378V substitutions. Protein expression was analysed using membrane vesicles isolated from *E. coli* DH5 α expressing wild-type (WT) QacA and mutant derivatives. Equal amounts (100 μ g) of total membrane proteins were loaded onto 10% polyacrylamide gels (Section 2.8.2) and QacA proteins immunologically detected using a rabbit anti-6xHis antibody. Positions of molecular weight markers are indicated and QacA bands are between 37 and 50 kDa.

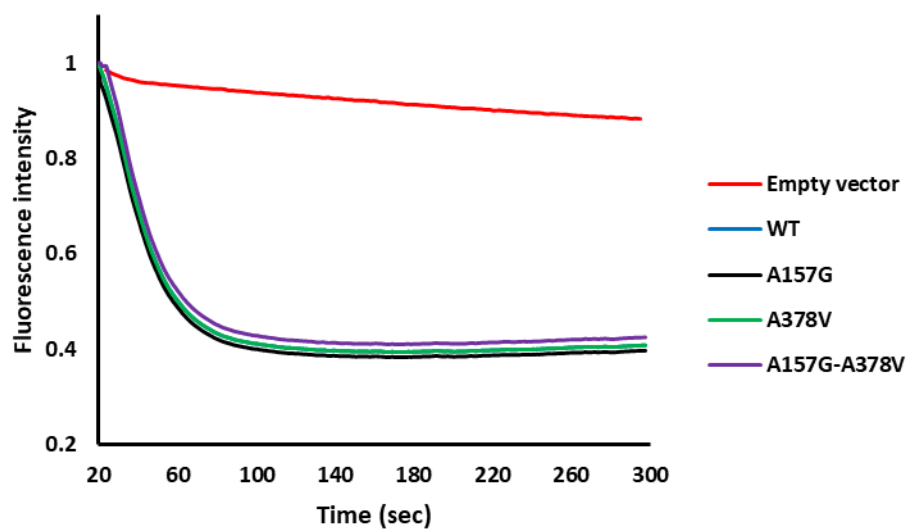
(B) Resistance profile of A157G and A378V substitutions.

Mutation	Relative MICs of QacA mutants ^{a,b}				
	Monovalent substrates			Bivalent substrates	
	Et	R6G	BK	DQ	PE
WT QacA ^c	100 (250)	100 (800)	100 (100)	100 (300)	100 (240)
No QacA	20	30	30	25	35
A157G	103	92	80	100	86
A378V	95	100	100	108	100
A157G-A378V	100	112	100	83	100

^a Numbers indicate relative resistance level of the mutants in comparison to the wild-type QacA (indicative of 100% resistance activity). MIC values determined by a standard agar dilution method, where *E. coli* DH5 α cells expressing wild-type and mutant QacA proteins were grown on LB agar supplemented with different concentrations of individual compounds (Section 2.10). The MIC values of QacA mutants are presented as percentage value relative to wild-type QacA.

^b Et: ethidium; R6G: rhodamine 6G; BK: benzalkonium; DQ: dequalinium; PE: pentamidine.

^c MIC value (μ g mL⁻¹) for wild-type QacA against each substrate is shown in parentheses (first row).

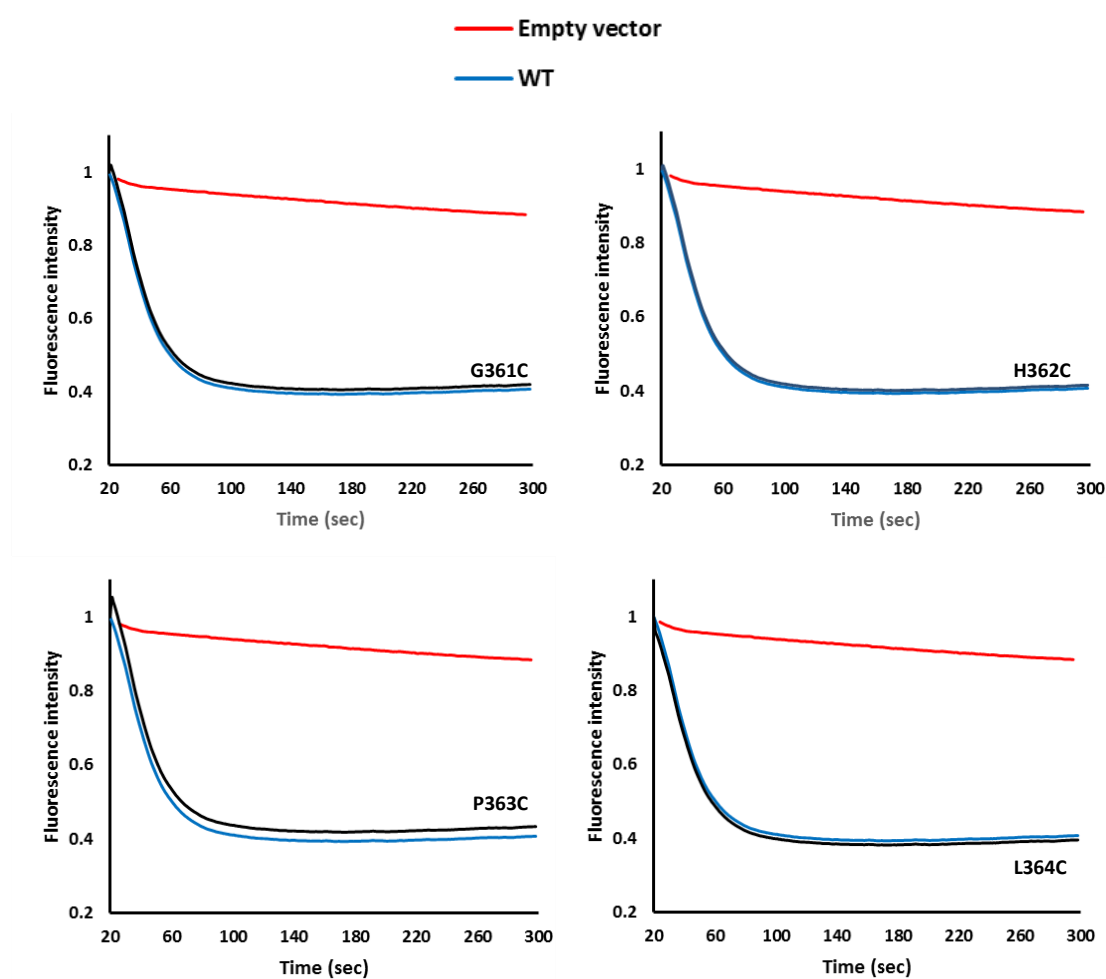


(C) Representative ethidium efflux curves of A157G and A378V substitutions.

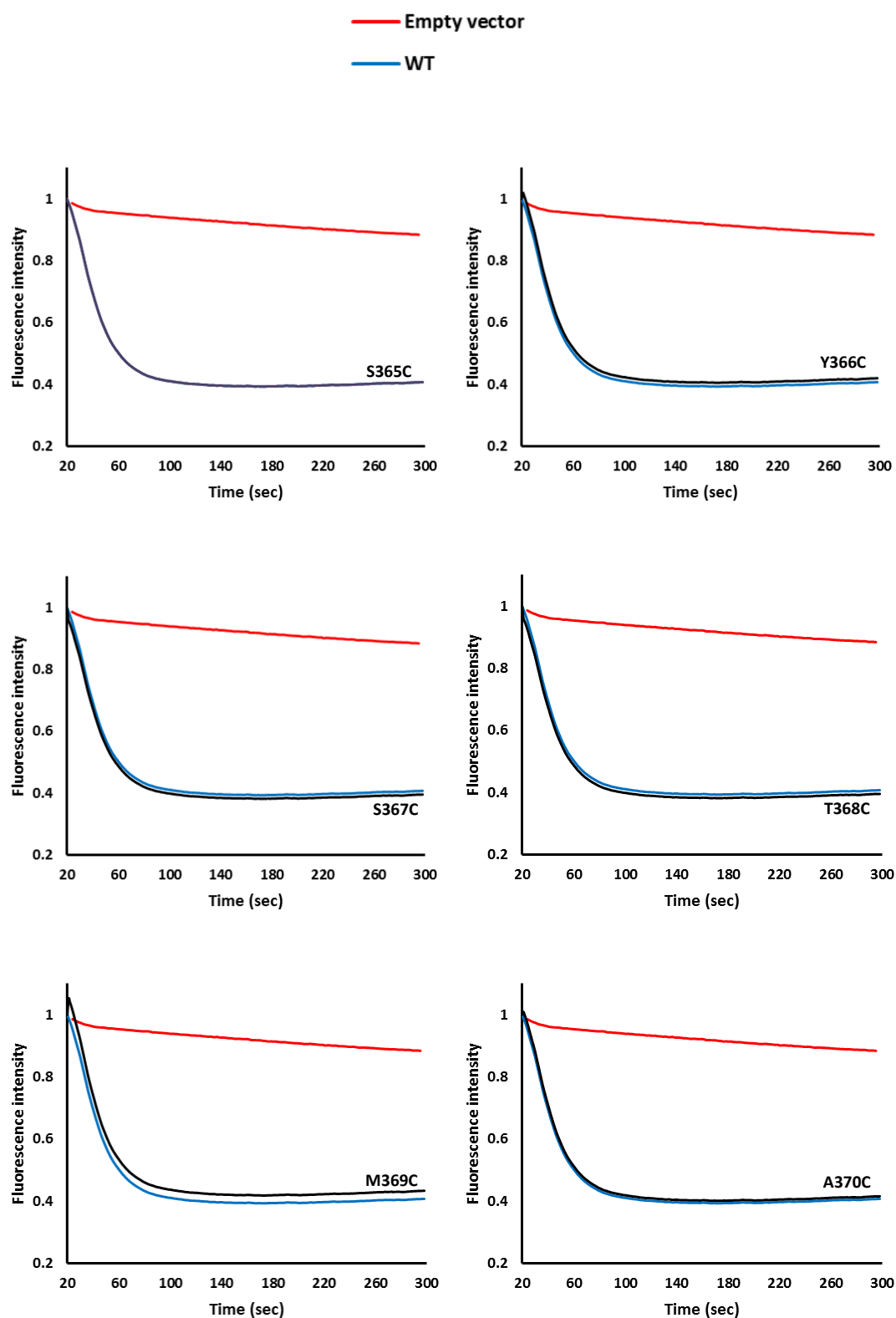
E. coli DH5 α cells carrying the pBluescript II SK (empty vector, red), pSK7201 (wild-type QacA, WT blue) and its derivatives (black) were cultured and loaded with 15 μ M ethidium (Section 2.11). Sodium formate (final concentration, 125 mM) was added at the starting point to energise the energy-starved cells. Ethidium efflux is represented by a rapid decrease in fluorescent intensity as a function of time.

7.4 Appendix 4 – Ethidium efflux curves of QacA mutants obtained in this study

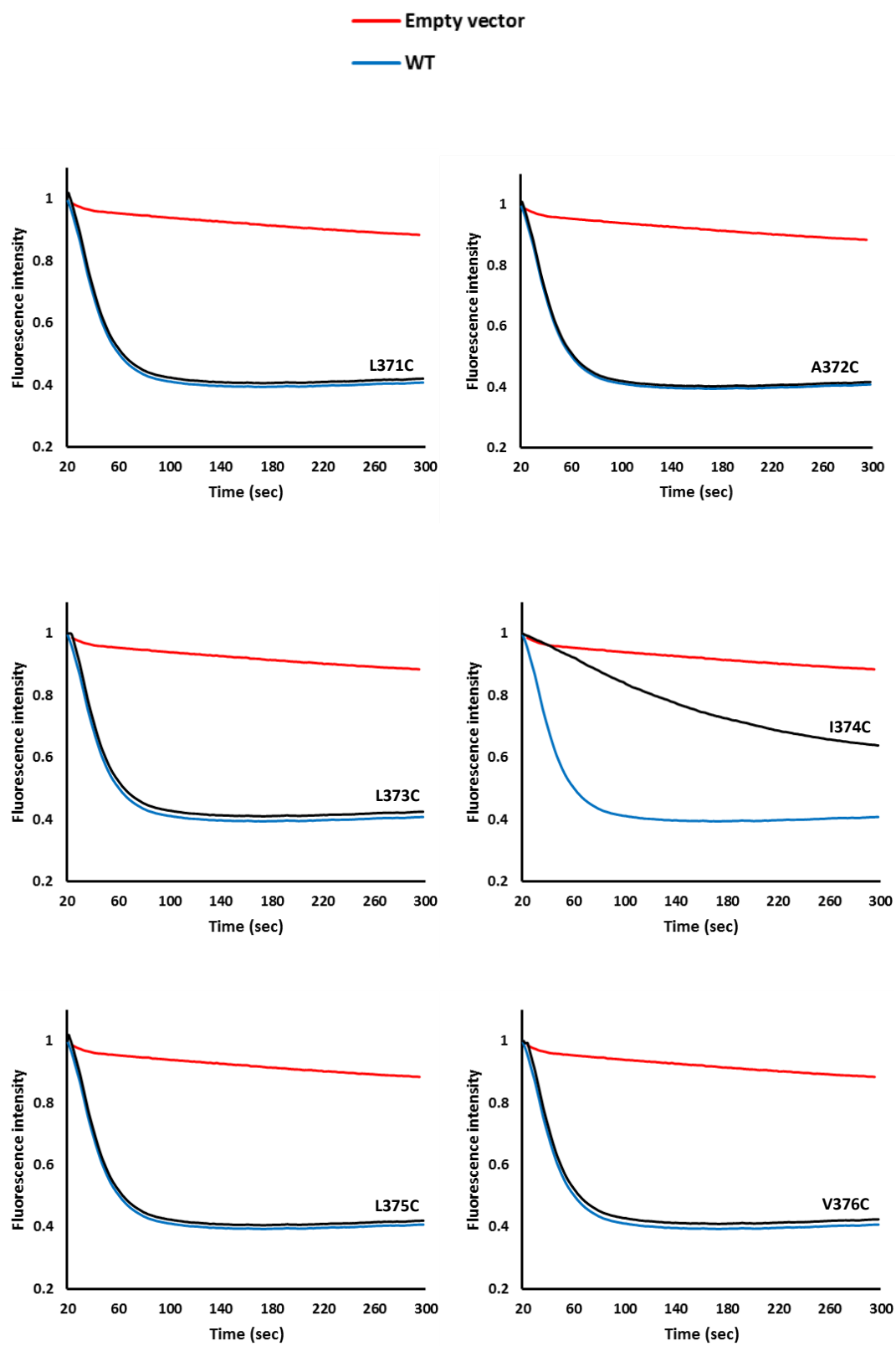
E. coli DH5 α cells carrying the pBluescript II SK (empty vector, red), pSK7201 (wild-type QacA, WT blue) and its derivatives (black) were cultured and loaded with 15 μ M ethidium (Section 2.11). Sodium formate (final concentration, 125 mM) was added at the starting point to energise the energy-starved cells. Ethidium efflux is represented by a rapid decrease in fluorescent intensity as a function of time. Here, representative ethidium efflux curves of WT, empty vector and individual QacA mutants (labelled on each figure) examined in this study are shown.



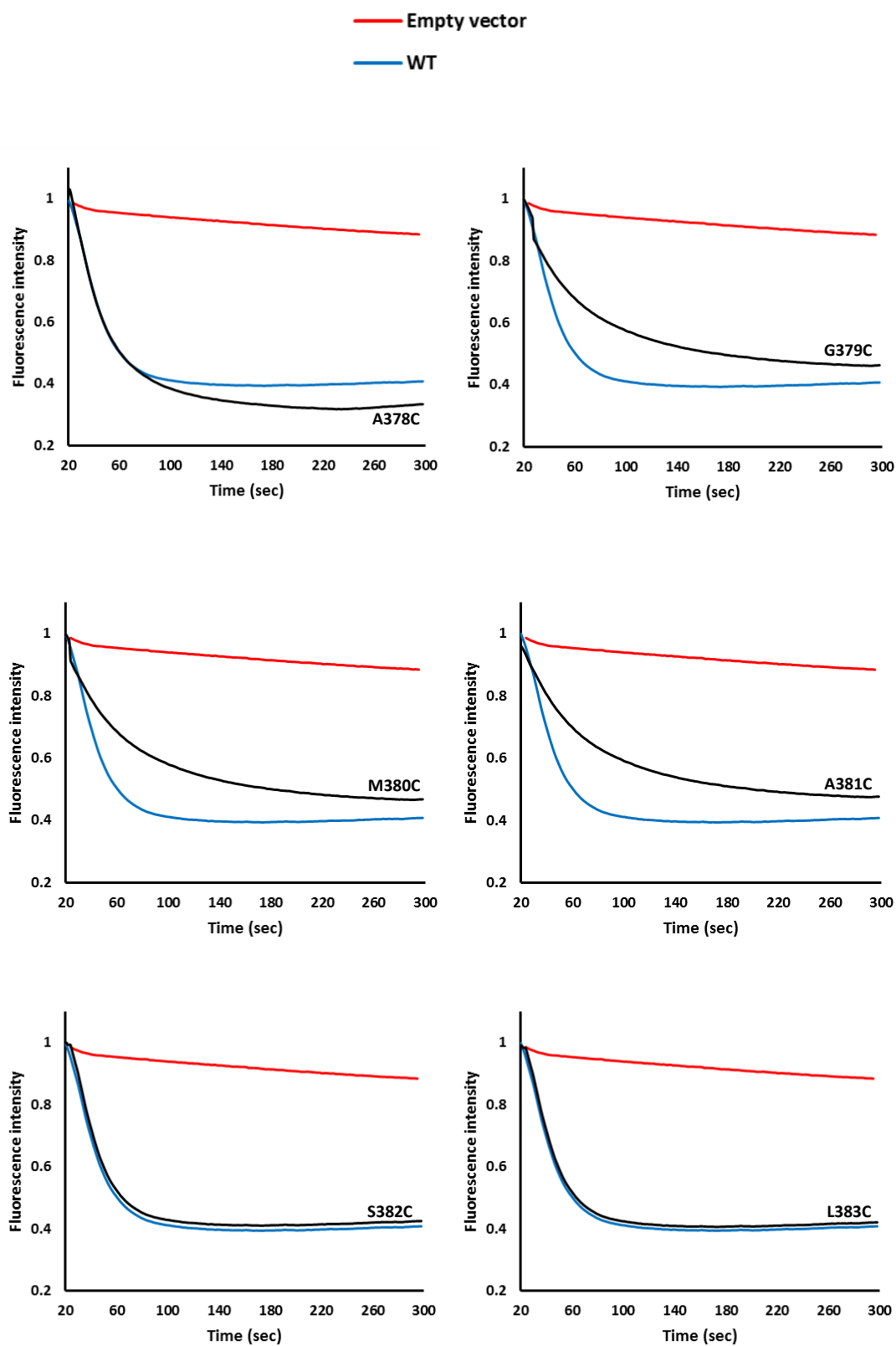
Appendix 4 (continued)



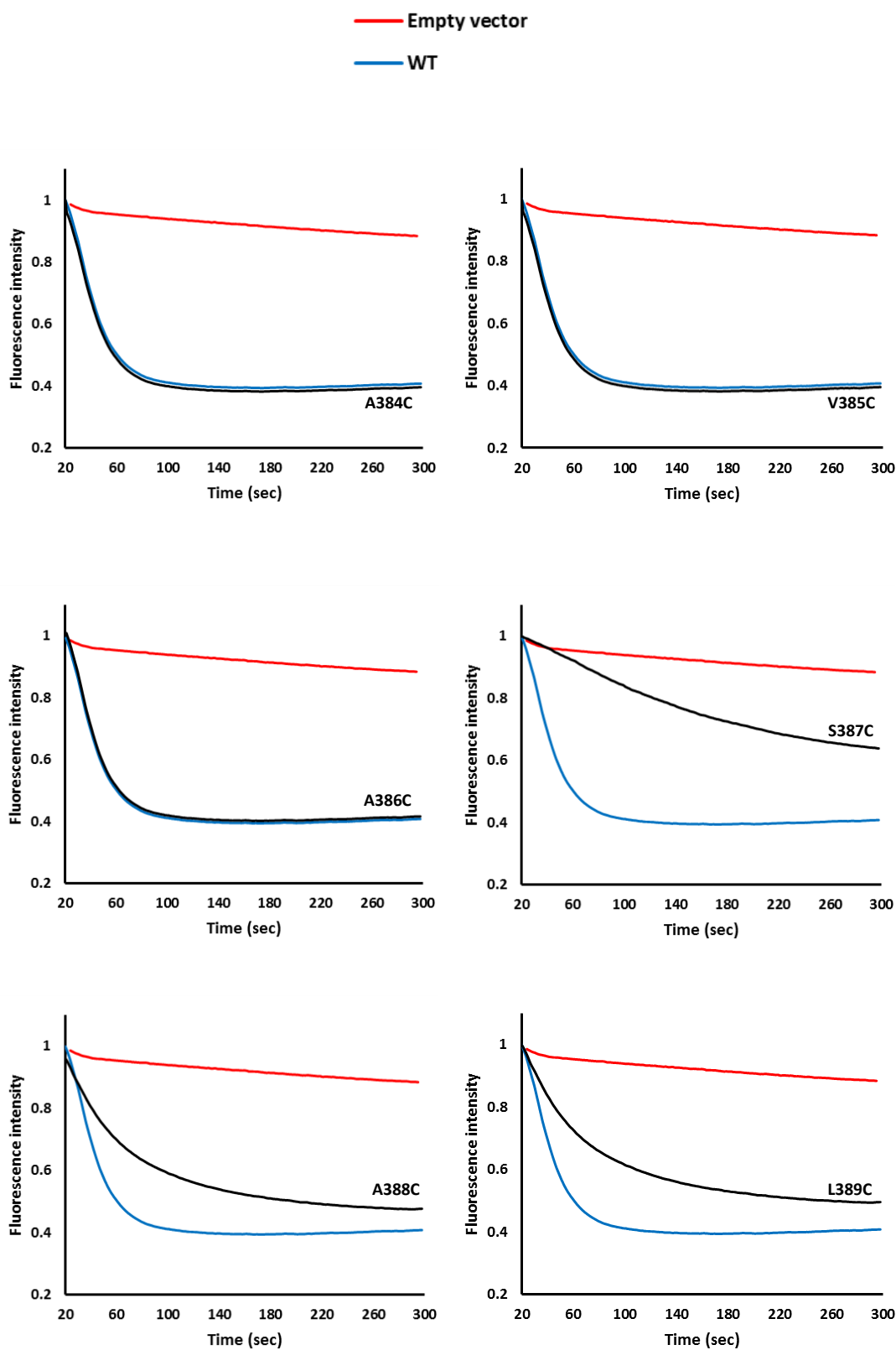
Appendix 4 (continued)



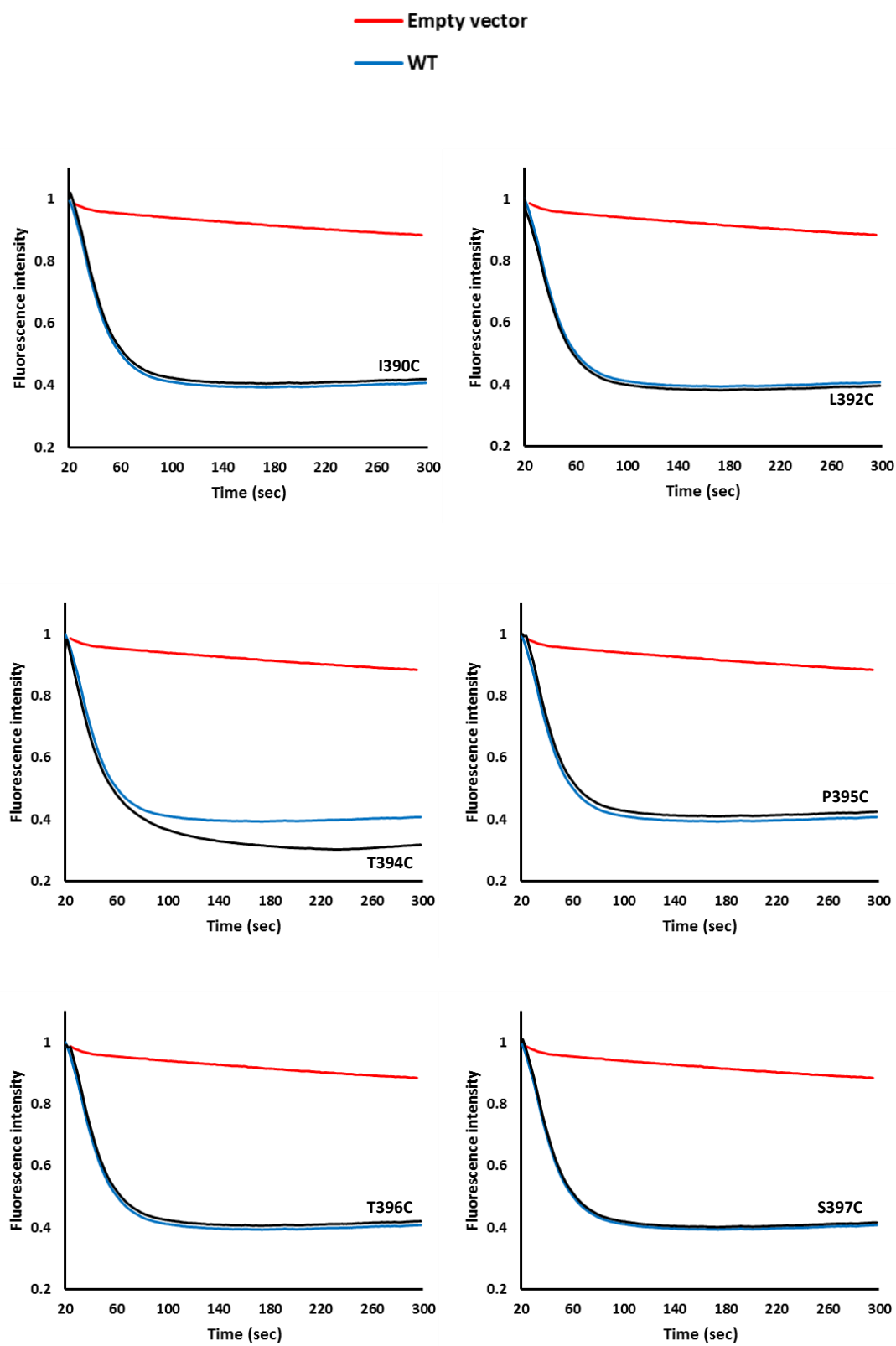
Appendix 4 (continued)



Appendix 4 (continued)



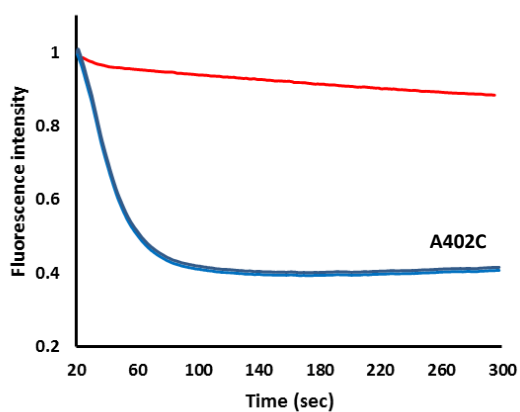
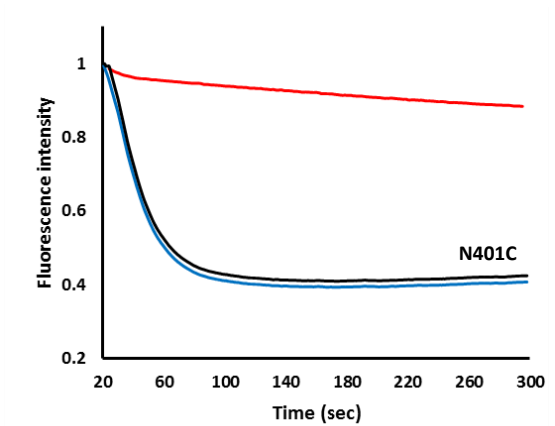
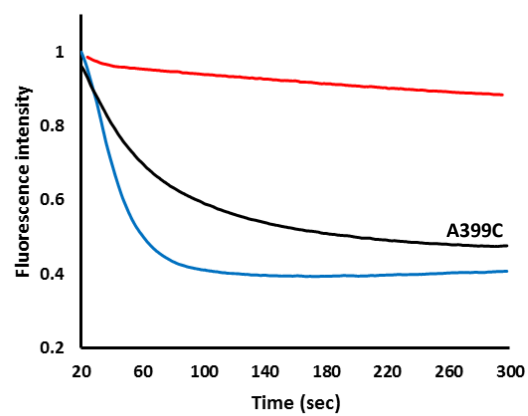
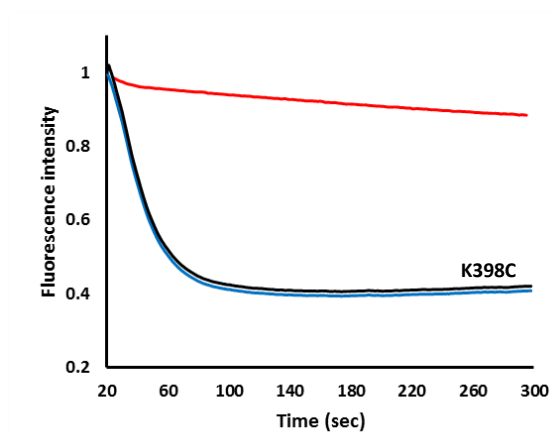
Appendix 4 (continued)



Appendix 4 (continued)

— Empty vector

— WT



7.5 Appendix 5 – Amino acid sequence alignment of QacA with MFS DHA1 and DHA2 family members

Amino acid sequences of representative bacterial DHA1 and DHA2 drug transporters were aligned with QacA using Clustal Omega. Sequences were obtained from the UniProtKB/Swiss-Prot database with the accession numbers presented in Section 2.13.2. Sequence names are shown on the left with their grouping into MFS DHA1 or DHA2 families. Numbers on the left and right refer to the position of the leftmost and rightmost amino acid residues on each line, respectively. The positions of the TMS (1–14) in QacA (as determined in Section 6.3) are indicated by horizontal black bars above the alignment. Dashes indicate gaps. Amino acid residue conservation is shown by blue shading. The percentage of the residues in each column that agree with the consensus residue at a particular alignment position is highlighted as blue hues. Dark blue $\geq 80\%$; medium blue $\geq 60\%$; light blue $\geq 40\%$.

		TMS 7										TMS 8										TMS 9									
DHA2	<i>QacA</i>	208	WDIPSTILSIAGMIGLVWSIKEFSKEG-LADII PWVIVLAI TMI VI	FV	KRNLS	SSSD	PML	DVRL	FKKRS	FSAGT	IAAFMTMFAMASVLL	LASQWL	QVVEEL	SPFKA	-	312															
	<i>LfrA</i>	207	FDPVSI VLSFTTMLPIVWAVKTA AHDG--LSAAAAAFVGVISGAL	FV	RRQRNSAT	PML	DIGL	FKVMP	FTSSILANFLS	IIGL	IGF	IFFISQHL	QLVLGL	SPLTA	-	310															
	<i>KmrA</i>	193	LNLQALVLI AAILMLVFSAKSALKGG-LALWLTALVALGGAAMLTF	FV	IRKQL	SAAR	PMV	DMRL	FTHRI	ILSGVMMAMTAL	ITLV	GFEL	MAQEL	QFVHQKTP	FEA	-	297														
	<i>SmvA</i>	193	LNLGHAVMLIIA ILLLVYSAKTALKGH-LSLWVISFTLLTGALLGL	FV	IRTQL	ATSR	PMI	DMRL	FTHRI	ILSGVMMAMTAMITLV	GFEL	MAQEL	QFVHGL	SPEA	-	297															
	<i>AmvA</i>	193	INLQALVLVVA ILSLIYSIKSAMYN--FSVLTVMFVVGISTLIH	FV	RSQKRATT	PMI	DLEL	FKHPV	ISTSIVMAVVS	MIALV	GFEL	LSQEL	QFVHGF	SPLQA	-	295															
	<i>MdrM</i>	200	L DVLGVIMSTVGFGLL L GFSNAGDHD-WLTKWVAGFI I LGLVVLGI	FV	IRYQTSNKA	PLL	NFRV	FKYPT	FALTTA	ISFFVVMGLF	GGML	LLP	IFLQ	TVRGF	SPL	-	304														
	<i>LmrS</i>	199	L DKRSVMYSTIGFGLMLYAFSSAGDLG-FTSPIVIGALILSMV I IYL	FV	IRRFNIT	NALLNLRV	FKNRT	FALCT	ISSMI	IMMSMV	GPALL	IPLYV	QNSLS	SALLS	-	303															
	<i>MdrT</i>	207	IDFLSIVMSSIGFGAL L YGFSSAGNDG-WGDTTVITMLIVGVV IAL	FV	WRQLVIDN	PML	ELHV	FKYPV	FSLSV	ILGSIVTMAMI	GAE	IVL	PLYI	QIRGES	ALQS	-	311														
	<i>FarB</i>	200	TDYVGLT LMMVIGALQMM LDRGKELDWFASGEIITLGI TALVCLSY	FV	WELGEKY	PIV	DLSL	FKDRN	FTVGA	IATSLGFMVY	MGTL	LLP	LVLQ	TNLGY	TSAWA	-	305														
	<i>NorB</i>	201	FDIKGLV L L VIMLLTLN I LITKGS ELG-VTSLFFITLLA I AIGSFSL	FV	LEKRATN	PLI	DFKL	FKNKAY	TGATASNFL	-LNGVAGT	IVANTFV	QRGLG	YSSLQA	-	304																
<i>NorC</i>	197	FDVAGLIVLVVMLLS LNVVITKGAALG-YTSLWFFGLI AIVIVAFFI	FV	LNVEK	KVDN	PLI	DFKL	FENKPY	TGATISNFL	-LNGVAGT	IVANTFV	QQGLG	YALQA	-	300																
<i>VceB</i>	206	IDKVG LALVVVVAALQLMLDEGKDHDFESSRIVFLAVI AVIGFIA	FV	LWELTERN	PVV	DLKV	FRHRG	YSISLVT	LSLAFGAFFS	ISVVT	P	LWLQ	IYMG	YATIS	-	311															
<i>TetA(L)</i>	199	IDMAGIILMSAGIVFFMLF-----TTSYRFSFLIISILAFFI	FV	QHIRKAQD	PVD	PEL	GKNVFF	VIGTLC	CGGLIFGTVA	GFVSMV	PYMMK	DVHHL	STAAIG	-	295																
<i>EmrB</i>	201	IDAVGLALLVIGIGSLQIM LDRGKELDWFSSQEI I LTVVAVVA ICF	FV	WELTDDN	PIV	DLSL	FKSRN	FTIGCLC	ISLAYMLY	FGA	IVL	P	QLLQ	EVYGY	-	306															
<i>TetA(K)</i>	199	L D I V G I V L M S I S I C F M L F ----- T T N Y N W T F L I L F T I F F V I	FV	IKHIS	RVSN	PV	INPKL	GKNIP	FMLG	LSGGL	IFS	VAGF	ISMV	PYMMK	TIYH	-	295														
<i>Tet38</i>	196	LDFVGLILVATIATVMLF-----ITNFNLYMIGALIAIIV	FV	LYIKNAQR	PLVNK	SFF	QNKRY	ASFLF	IVFV	MYA	IQL	GYI	FTFP	I	-	291															
<i>MdeA</i>	194	IDFISVIFSVLGFGLLYGTSSISEKG-FDNPV L V L S M I G G V V L V A L	FV	LRQYRLST	PLL	NAFV	FKNKQ	FTVGI	IIMGVT	MVSMI	GSET	ILP	IFVQ	NLLHRS	-	298															
<i>Bmr</i>	192	IKGQKTGFKRIFA-----PMYFIAFLIILISSFGLASFESL	FV	FALFV	DHKG	FTASDI	-	243																							
<i>MdfA</i>	203	L L K E L G R D Y K L V ----- L K N G R F V A G A L A G F V S L P L L A W I A Q S P I I I T G E O L S S Y E Y	-	-	-	-	-	-	-	-	-	-	-	-	-	257															
<i>TetA(B)</i>	190	DTEVG VETQSNV-----YITL F K T M P I L L I Y F S A Q L I G Q I P A T V W V L F T E N R F G W N S M M V G	-	-	-	-	-	-	-	-	-	-	-	-	-	247															
<i>TetA(C)</i>	192	MPLRAFNPVSSFR-----WARGMTIVAALMTVFFIMQLVGGVPAALWVIFGEDRFRWSATMIG	-	-	-	-	-	-	-	-	-	-	-	-	-	249															
<i>CmlA</i>	201	LQWSQLL LPVKCL-----NFWLYTLLCYAAGMGSFFVFFSIA PGLMMGRQVGLS	-	-	-	-	-	-	-	-	-	-	-	-	-	251															
<i>EmrD</i>	189	V D A P R T R L L T S Y K ----- T L F G N S G F N C Y L L M I G G L A G I A A F E A C S G V L M G A V L G S S M T V	-	-	-	-	-	-	-	-	-	-	-	-	-	245															
<i>MdtM</i>	199	FSAKSVLRDFRNV-----FCNRLFLFGAATISLSYIPMMSWVAVSPVILIDAGSLTTSQF	-	-	-	-	-	-	-	-	-	-	-	-	-	253															
<i>NorA</i>	189	QKLEPQL LTKINW-----KVFIATPVILTLVLSFGLSAFETLYSLYTDKVNYS	-	-	-	-	-	-	-	-	-	-	-	-	-	240															
<i>LmrP</i>	199	EKAENIFQAYKTVLQDKTY-----MIFMGANIATTFIIMQFDNPLPVHLSNSFKITFWGFEIYQGRML	-	-	-	-	-	-	-	-	-	-	-	-	-	262															

		TMS 10										TMS 11										TMS 12										TMS 13										
DHA2	<i>QacA</i>	313	GLYLLPMAIGDMVFAP IAPGLAARFGPKIVLPSGIGIAAIGMFIMY--FFGHPLSYSTMALALILVGA	GMA	-SLAVASAL	IMLETPTS	KAGNA	AAVEES	SMYDLGNV	F	416																															
	<i>LfrA</i>	311	GLVTLPGAVVSMIAGLAVVKA AKRFAPDTLMVYGLV FVAVGFLMIL--LFRHNLTVAAIIASFVVLEL	CV	GV	SQTVS	NDTIV	ASVPA	AKSGA	ASAVSET	AYELG	AVV	415																													
	<i>KmrA</i>	298	GIFMLPVMVASGFSGPIAGLLVSRLLGLREVATGGM LLSA F S F L G L A ---L T D F S T Q Q W L A W G L M T L L	G	FS	VASALL	ASSA	IMAA	APKEK	AAAGA	IETMAYEL	G	400																													
	<i>SmvA</i>	298	GVFMLPVMVASGFSGPIAGV LVSRLGLRLVATGGMALSALSFGYGLA---MTDFSTQQWQAWGLM L L	G	FS	ASALL	ASTSA	IMAA	APKEK	AAAGA	IETMAYEL	G	400																													
	<i>AmvA</i>	296	AMFII PFMIAISLGGPLAGICLNK WGLRRVSSLGILV SALS WLGLA ---QLNFSTDHFLAWTCMVFL	G	FS	IEI	ALL	ASTAA	IMSS	VPPQK	ASAGA	IEGMAYEL	G	398																												
	<i>MdrM</i>	305	GLVLLPGALVTA ILSPTVGMVDFRFGAKYLSLVGLIIMAGSTFMFT--NLDESTTLTFLIIVQTI R S A	G	MAM	VMP	LQTA	ALNSL	PLKL	ASHG	SAMFNT	MRQVA	G	409																												
	<i>LmrS</i>	304	GLVIMPGA IIVANGIMSVFTGKFYDYGPRPLIYTGFTLITITIMLC--FLATDTSYTLIVVYAIRMF	SV	SLL	MMP	INT	GINS	L	NEE	ISHG	TAIMN	FGRVMA	G	408																											
	<i>MdrT</i>	312	GLLLLPGA IIMGIMSPITGIIFDKIGAKWLTITGV TILTIGTIPFM--FLTMDTPLWYIVVYAVRFF	G	I	S	MAM	P	V	S	T	A	G	M	N	L	P	N	H	L	I	N	H	G	S	A	V	N	N	T	I	R	Q	I	A	G	S	I	416			
	<i>FarB</i>	306	GLAAAPVGLIPVFLSPLIGRFGNKIDMRLLV TASFLTFAFTFYWR--DFYADMDIGNV IWPQFQQGV	G	V	A	M	F	F	L	P	L	T	I	T	L	S	H	M	K	G	G	Q	I	A	A	G	S	L	S	N	F	L	R	V	L	M	G	V	410		
	<i>NorB</i>	305	GSLSITYLVMVIMIRVGEKLLQTLGCKKPMIIGTVLIVGECLISLTLFPEILYVICCIIGLFFGL	GL	G	I	Y	A	T	P	S	T	D	T	A	I	A	N	A	P	L	E	K	V	G	V	A	A	G	I	Y	K	M	A	S	A	L	G	G	A	411	
<i>NorC</i>	301	GYLSITYLIMVLLMIRVGEKLLQKMGSKRPM L L G T F I V I G I A L I S L V F L P G I F Y I S C V V G Y L C F G L	GL	G	I	Y	A	T	P	S	T	D	T	A	I	S	N	A	P	L	D	K	V	G	V	A	S	G	I	Y	K	M	A	S	S	L	G	G	A	407		
<i>VceB</i>	312	GHATASMGILAVFLAPIVANLSSKFDPRPFVFA GVMWLGLWTFMRG--FNTVDMTFSQISWPLFFQGI	G	M	P	L	F	V	P	L	T	A	I	A	L	G	S	V	K	P	H	E	M	E	S	A	G	L	M	N	F	I	R	T	L	S	G	A	416			
<i>TetA(L)</i>	296	SGIIFPGTMSVIFGPIAGLLVDRKGS LYVLTIGSALLSSGFLIAA--FFIDAAPWIMTIIVIFVFG	GL	S	F	T	K	T	V	I	S	T	V	S	S	L	K	E	K	E	A	G	A	G	A	S	L	L	N	F	T	S	F	L	S	E	G	T	399			
<i>EmrB</i>	307	GLASAPVGIIPVILSPIIGRFAHKLD MRRLVTF SFIMYAVCFYWRAY--TFEPGMDFGASAWPQFIQ	G	F	A	V	A	C	F	F	M	P	L	T	I	T	L	S	G	L	P	P	E	R	L	A	A	A	S	S	L	S	N	F	T	R	T	L	A	G	410	
<i>TetA(K)</i>	296	NSVIFPGTMSVIFGPIAGLLVDRKGS LYVLTIGSLSISISFLTIA--FFVEFSMWLTFMFIFVMG	GL	S	F	T	K	T	V	I	S	K	I	V	S	S	L	S	E	E	V	A	S	G	M	S	L	L	N	F	T	S	F	L	S	E	G	T	399			
<i>Tet38</i>	292	SLLLVPGYIIVAVIVGALS KIGEYLNKQAIITAILALSLILPA--FATGNHISIFVISMIFFA	G	S	F	A	L	M	P	A	L	L	N	E	A	I	K	T	I	D	L	N	M	T	G	V	A	I	G	F	N	L	I	N	V	A	S	394				
<i>MdeA</i>	299	GLTLLPGA IVMAFMSMTSGALYEKFGPRNLALVGM AIVVITAYFV--VMDEQSTSTIMLATVYAIRMV	G	I	A	L	G	L	I	P	V	M	T	H	M	N	Q	L	K	P	E	M	N	A	H	G	S	S	M	T	N	T	V	Q	I	A	G	S	I	403		
<i>Bmr</i>	244	AIMITGGAIVGAIQTQVLFDRFTRWFGIHLIRYSLILSTLSVFL--TTVSHSYVA ILLVTVTVF	G	F	D	L	M	R	P	A	V	T	T	Y	L	S	K	I	A	G	N	E	Q	G	F	A	G	M	S	M	F	T	S	I	G	N	V	F	G	346		
<i>MdfA</i>	258	GLLQVPIFGAL IAGNLLARLTSRRTVRSLLIMGGWPIMIGLLVA AATVSSHAYLWMTAGLSIYAF	G	I	G	L	A	N	A	G	L	V	R	L	T	L	F	A	S	D	M	S	K	G	T	V	A	A	M	-	G	M	L	Q	M	L	I	F	V	363		
<i>TetA(B)</i>	248	FSLAGLGLLHVSVFQAFVAGRIATKVG EKTA VLLGFIADSSAFFLA-----FISEGWLVFPVLLILA	G	G	I	A	L	P	A	L	Q	G	V	M	S	I	Q	T	K	S	H	Q	Q	G	A	L	Q	G	L	L	V	S	L	T	N	A	T	G	V	I	348	
<i>TetA(C)</i>	250	LSLAVFGLHALAQAFVGPATKRFGEKQAI IAGMAADALGVYLLA-----FATRGMWAFPIMLLAS	G	G	I	G	M	P	A	L	Q	A	M	L	S	R	Q	V	D	D	H	Q	G	L	Q	G	S	L	A	A	L	T	S	L	T	S	I	T	G	351		
<i>CmlA</i>	252	SLLFATVAIAMVFTARFMRV I PKWSPSVLRMGMGCL IAGAVLLAITE I W A L Q S V L G F I A P M W L V G I	G	V	A	T	A	V	S	V	A	P	N	G	A	L	R	G	F	D	H	V	A	G	T	V	T	A	V	F	C	L	G	G	V	L	L	G	S	I	358	
<i>EmrD</i>	246	SILFILPIPAAFFGAWFAGRPNKR FSTLMWQSVICCLLAGL LMWIP--DWFGVMNVWTLVPAALFFF	G	A	G	M	L	F	L	A	T	S	G	A	M	E	P	F	P	F	L	A	G	T	A	G	A	L	V	G	G	L	Q	N	I	G	S	V	L	350		
<i>MdtM</i>	254	AWTQV PVFVGAIVANAIVFDFKDPTEPRFIWRAPV IQLVLSLL I VGNLLSPHVWLSVLTGSLYAF	G	I	G	L	I	F	P	T	L	F	R	F	T	L	F	S	N	K	L	P	K	G	T	V	A	S	L	-	N	M	V	L	M	V	M	S	359			
<i>NorA</i>	241	SIAITGGGIFGALFQIYVDFKFMK YFSELTFIAWSLLYSVVVLLI--VFANGYVSIMLISFVVFI	G	F	D	M	I	R	P	A	I	T	N	F	S	N	I	A	G	E	R	G	G	F	A	G	L	N	S	T	F	T	S	M	G	N	F	I	G	343		
<i>LmrP</i>	263	TIYLI LACVLVLLMTTLNRLTKDWSHQKGF I W G S L F M A I G M I F S F -----L T T T F T P I F I A G I V Y T L	G	E	I	V	Y	T	P	S	V	Q	T	L	G	A	D	L	M	N	P	E	K	I	G	S	Y	N	G	V	A	A	I	K	M	P	I	A	S	I	L	364

TMS 13

TMS 14

Gene	Accession	Sequence	Position
<i>QacA</i>	417	GVAVLGSLSSMLYRVFLDISSFSSKGI VGD LAHVAAEESVVGAVEVAKATGIKQLANEAVTSFNDAFVATALVGGIIMIIISIVVYLLIPKS--LDITKQK----	514
<i>LfrA</i>	416	GTATLGTIFTAFYRSNVDVPAGLTPEQTGAAAESIGGAAAVAADLPAATA-TQLLDSARAAFDSGIAPTAVIAAMLVLA AAAAVVGVAFRR-----	504
<i>KmrA</i>	401	GLGIALFGLILTRSYSASIALPSGLSGAMAQQAASSIGEAVLSQALPAGVA-QALMAAAKTAFIQAHSLVLATAGVLLLLLAAGIWRSLATV--AKPQSAL---	499
<i>SmvA</i>	401	GLGIAIFGLLLLSRFSASIRLPAGLEAQEIRASSSMGEAVQLANSLPPTQG-QAILDAARHAFIWSHSVALSSAGSMLLLLAVGMWFSLAKA--QRR-----	495
<i>AmvA</i>	399	CLGVAIFGLMLSWFYRSRIILPAELPSNLEKASISIGETMQLASNLNENPLG-GQLIVVAQQAQAFSYAHSWVLTLSAICFFLLTVFVWFSPFKK--VN-----	492
<i>MdrM</i>	410	GTAALITVMSKSAASFATKLG-----PADVIG-KTKTDIANHVLIHGIETAFVAGILSVVACVLA LFIQKNRSAMDP IVTKTEKA-	489
<i>LmrS</i>	409	GTALMVTLM SFGAKIFLS-----TSPSH-LTATEIKQQSIAIGVDISFAFVAVLVMAAYVIALFIREPKE-IESNRRKF----	480
<i>MdrT</i>	417	GTAVLITVLTNTVTKDNMPGKA-----LMATDP-ASFAQKAQDASLDGMRAAFMVA AIFAAIGMILSLFLKTKK--QEP IVKEYTK--	493
<i>FarB</i>	411	GVSVVSTLWERREALHHTRF AEHITPYSATLHETA AHL SQQGISDGGQTLG-IINNTITQQGFIIGSNEIFLAGSILFIVLPIVWLAKPPF--HSGGGGH-----	507
<i>NorB</i>	412	GVALSGAVYAI-----VSNMTNIYTGAMIALWLNAGMGILSFVILLLLVPKQNDTQ--L-----	463
<i>NorC</i>	408	GVAISGAVYAG-----AVAATSIHTGAMIALWVNVLMGIMAFI AILFAIPNDDKRV--KDAK-----	462
<i>VceB</i>	417	ATSMINTSWEHETRYVHAELAGLTDKAGVAAQAMQSS---GMSAEQTRS-AMDWILQNQSVMVATNQLFIVIALIFVFAACMIWFAPKPK--QAVDTSAVH---	511
<i>TetA(L)</i>	400	GIAIVGGLLSIGFLDHR-----LLPIDVDHSTYLYSNMLILFAGIIVICWLVI LN VYKRSRR--HG-----	458
<i>EmrB</i>	411	SIGTSITTTMWTNRESMHHAQLTESVNPFPNPAQAMYSQLEGLGMTQQQASG-WIAQQITNQGLIISANEIFWMSAGIFLVLLGLVWFAPKPPF--GAGGGGGGAH	512
<i>TetA(K)</i>	400	GIAIVGGLLSLQLINRK-----LVLEFINYSSGVYSNILVAMA ILLCCLLTIIVFKRSEK--QFE-----	459
<i>Tet38</i>	395	VGIAIAAALIDFKALN-----FPGNDALSSHFGIILILGLMSIVGLVLFVILNRWTQSEK-----	450
<i>MdeA</i>	404	GTAALITILSHASKNFSP TMSD-----YNGMNKI-DMMNQIKVD TMLHGYHAGFLFALLITVVSFFCSFMLQGGK--KEVDSRQ-----	479
<i>Bmr</i>	347	PIIG-----GMLFDIDVNYPFYFATVTLAIGI ALTI AWKAP AHLKAST-----	389
<i>MdfA</i>	364	GIEISKHAWLNGGNG-----LFNLFNLVNGILWLSLMVIFLKDKQMGN SHEG-----	410
<i>TetA(B)</i>	349	GPLLF AVI-----YNHSLPIWDGWIWII GLAFYCI ILLSMTFMLTPQAQGSK--QETSA-----	401
<i>TetA(C)</i>	352	PLIVTAI-----YAASASTWNGLAWIVGAALYLVCLPALRRGAWSRATST-----	396
<i>CmlA</i>	359	CTLII SLLPRNTAWP-----VVVYCLTLATVVVLGLSCVSRVKGSRGQGEHDVVALQSAES--TSNPNR-----	419
<i>EmrD</i>	351	ASLS-----AML PQTGGGSLGLLMTLMGLLIVLCWLPLATRMSHQGGQPV-----	394
<i>MdtM</i>	360	SVEIGRWLWFNGGRL-----PFHLLAVVAGVIVVFTLAGLLNRVYRQHQA AELVEEQ-----	410
<i>NorA</i>	344	PLIAG-----ALFDVHIEAPIYMAIGVSLAGVVIVLIEKQHRAKLKEQNM-----	388
<i>LmrP</i>	365	AGLLV-----SISPMIKAIGVSLVLAALTEVLA IILVVLVAVNRHQKTKLN-----	408

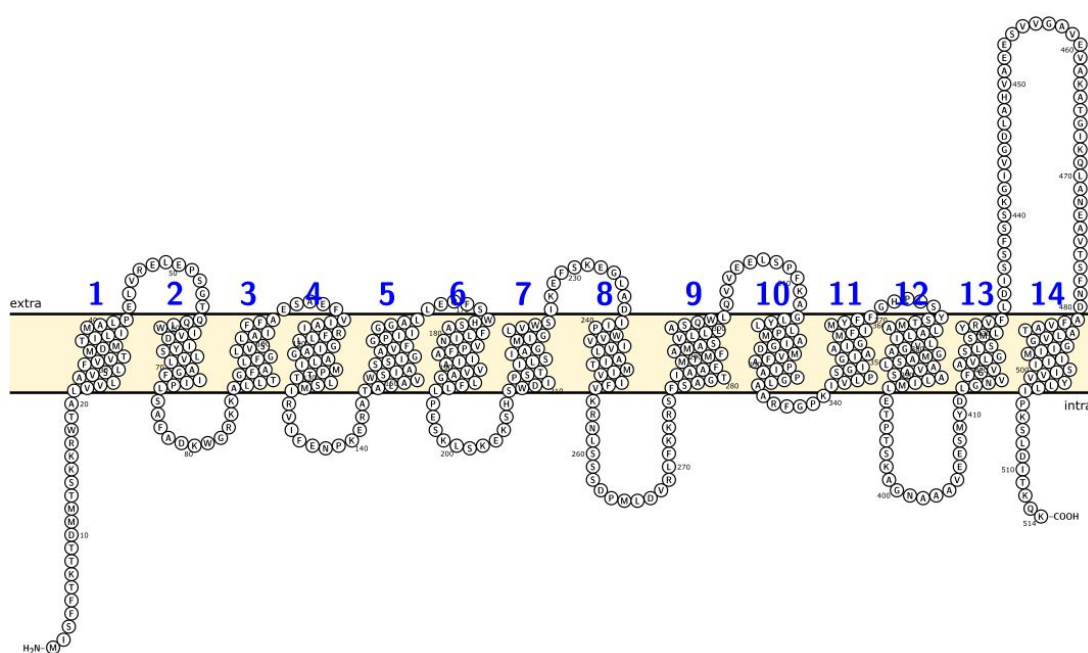
DHA2

DHA1

7.6 Appendix 6 – QacA topology generated by Protter webserver

The topology of QacA (UniProtKB/Swiss-Prot accession number: POA0J8) was predicted using the Protter web-based application, freely available open source at

<https://wlab.ethz.ch/protter/start/>



7.7 Appendix 7 – Codes and chemical properties of the 20 standard amino acids found in proteins

Amino acid	One-letter code	Three-letter code	Chemical property
Alanine	A	Ala	Hydrophobic
Arginine	R	Arg	Basic
Asparagine	N	Asn	Polar
Aspartic acid	D	Asp	Acidic
Cysteine	C	Cys	Sulphydryl group
Glutamine	Q	Gln	Polar
Glutamic acid	E	Glu	Acidic
Glycine	G	Gly	No side-chain
Histidine	H	His	Basic
Isoleucine	I	Ile	Hydrophobic
Leucine	L	Leu	Hydrophobic
Lysine	K	Lys	Basic
Methionine	M	Met	Hydrophobic
Phenylalanine	F	Phe	Aromatic
Proline	P	Pro	Imino acid
Serine	S	Ser	Polar
Threonine	T	Thr	Polar
Tryptophan	W	Trp	Aromatic
Tyrosine	Y	Tyr	Aromatic
Valine	V	Val	Hydrophobic

7.8 Appendix 8 – List of abbreviations

~	Approximately
%	Percent
µg	Microgram
µL	Microlitre
µM	Micromolar
Å	Angstrom
6xHis-tag	Tag encoding six consecutive histidine residues
ABC	(Adenosine triphosphate) binding cassette
AbgT	p-aminobenzoyl-glutamate transporter
AGRF	Australian Genome Research Facility
AMR	Antimicrobial resistance
ATP	Adenosine triphosphate
BCA	bicinchoninic acid
BK	Benzalkonium
bp	Base pair
BSA	Bovine serum albumin
°C	Degrees Celsius
CA-MRSA	Community acquired methicillin-resistant <i>S. aureus</i>
CCCP	Carbonyl-cyanide m-chlorophenyl hydrazone
CD	Circular dichroism
CH	Chlorhexidine
Cm	Chloramphenicol
CM	Cytoplasmic membrane
C-terminus	Carboxy-terminus
Cryo-EM	Electron cryomicroscopy
ds DNA	Double-stranded DNA

DAPI	4',6-diamidino-2-phenylindole
DC	Detergent compatible
DDM	<i>n</i> -dodecyl- β -d-maltopyranoside
DEER	Double electron-electron resonance
dH ₂ O	Distilled water
DHA1	Drug/H ⁺ antiporter 1 family
DHA2	Drug/H ⁺ antiporter 2 family
DiOC ₃	3',3'-dipropylloxycarbocyanine
DMSO	Dimethyl sulfoxide
DNA	Deoxyribonucleic acid
dNTP	2'-deoxynucleotide 5'-triphosphate
DQ	Dequalinium
Dxc	Deoxycholate
EDTA	Ethylenediaminetetra-acetic acid
EM	Electron microscopy
EPI	Efflux pump inhibitor
Et	Ethidium
FIC	Fractional inhibitory concentration
FP	Fluorescence polarisation
FM	Fluorescein-5-maleimide
FU S ⁻¹	Fluorescence units per second
<i>g</i>	Centrifugal force
H ⁺	Proton
HEPES	N-2-hydroxyethylpiperazine-N-ethanesulfonic acid
IMP	Inner membrane protein
ICU	Intensive care unit
IPTG	Isopropyl- β -D-thiogalactopyranoside
ITC	Isothermal titration calorimetry

kb	Kilo base
kDa	Kilo dalton
K_m	Michaelis-Menten constant
K_D	Dissociation constant
L	Litre
LB	Luria-Bertani
LDAO	n-dodecyl-N,N-dimethylamine-N-oxide
M	Molar
MATE	Multidrug and toxic compound extrusion
MD	Molecular dynamics
MDR	Multidrug resistant
MFP	Membrane fusion protein
MFS	Major facilitator superfamily
mg	Milligram
MGE	Mobile genetic elements
MHA	Muller-Hinton agar
MHB	Muller-Hinton broth
MIC	Minimum inhibitory concentration
min	Minute
mL	Millilitre
mM	Millimolar
MOPS	4-morpholinepropanesulfonic acid
mPEG-Mal	methoxypolyethylene glycol maleimide
MRSA	Methicillin-resistant <i>Staphylococcus aureus</i>
MST	Microscale thermophoresis
MW	Molecular weight
Na ⁺	Sodium
NaCl	Sodium chloride

NEM	N-ethylmaleimide
Ni-NTA	Nickel-nitrilotriacetic acid
NMR	Nuclear magnetic resonance
nt	Nucleotide
N-terminal	Amino-terminal
OD	Optical density
OMP	Outer membrane protein
PACE	Proteobacterial antimicrobial compound efflux
PAGE	Polyacrylamide gel electrophoresis
PBP	Penicillin-binding protein
PCR	Polymerase chain reaction
PE	Pentamidine
PEG-Mal	polyethylene glycol-maleimide
PDB	Protein data bank
P-gp	P-glycoprotein
pmf	proton motive force
pmol	Picomole
POPC	1-palmitoyl-2-oleoyl phosphatidylcholine
POPG	1-palmitoyl 2-oleoyl-phosphatidylglycerol
psi	Pounds per square inch
PVDF	Polyvinylidene difluoride
QACs	Quaternary ammonium compounds
R6G	Rhodamine 6G
RMSD	Root mean square deviation
RND	Resistance-nodulation division
rpm	Revolutions per minute
SD	Standard deviation

SDS-PAGE	Sodium dodecyl sulphate-polyacrylamide gel electrophoresis
SEM	Standard error of the mean
SLC	Human solute carrier
SMA	Styrene maleic acid
SMALPs	Styrene maleic acid lipid particles
SMR	Small multidrug resistance
SPR	Surface plasmon resonance
ss DNA	Single-stranded DNA
TAE	Tris-base acetic acid ethylenediaminetetraacetic acid
TBS	Tris-buffered saline
Tet	Tetracycline
TTBS	Tween tris-buffered saline
TCDB	Transporter classification database
TEMED	<i>N,N,N', N'</i> -tetramethylethylene diamine
TMA-DPH	1-(4-trimethylammoniumphenyl)-6-phenyl-1,3,5-hexatriene
TMS	Transmembrane spanning (or segment)
Tris-HCl	Tris-hydromethylaminomethane-hydrogen chloride
U	Units
UV	Ultraviolet
V	Volt
v/v	Volume/volume
V_{\max}	Maximal transport rate
w/v	Weight/volume
WT	Wild-type
WHO	World Health Organisation

7.9 Appendix 9 – Conference contributions and publications

Conference presentations:

Abolfazl Dashtbani Roozbehani and Melissa H Brown. Staphylococcal multidrug efflux pump QacA: identification of functionally-important residues in helix 12.

Australian Society for Microbiology Annual Scientific Meeting 2019, Adelaide, South Australia (oral presentation)

Abolfazl Dashtbani Roozbehani and Melissa H Brown. Structure and function of the staphylococcal multidrug efflux pump QacA: the importance of helix 12. BacPath 2019, Western Australia (poster presentation)

Abolfazl Dashtbani Roozbehani and Melissa H Brown. Role played by QacA multidrug efflux pump in antimicrobial resistance. Gordon Research Conference on Multi-Drug Efflux Systems 2019, Italy-Barga (poster presentation)

Abolfazl Dashtbani Roozbehani and Melissa H Brown. Functional analysis of QacA multidrug efflux pump. Australian Society for Microbiology (ASM) student award 2018, Adelaide, South Australia (oral presentation)

Abolfazl Dashtbani Roozbehani and Melissa H Brown. Functional importance of transmembrane helix 12 of QacA multidrug efflux pump from *Staphylococcus aureus*. 3rd Annual College of Science and Engineering HDR conference at Flinders University 2017, Adelaide, South Australia (oral presentation)

Manuscripts:

Dashtbani-Roozbehani A, Chitsaz M, Brown M.H. Deciphering the roles of residues within and around transmembrane segment 12 of staphylococcal multidrug efflux protein QacA (Manuscript in preparation)

Dashtbani-Roozbehani A, Chitsaz M, Brown M.H. Hotspot regions of QacA involved in resistance to biocides benzalkonium chloride and chlorhexidine (Manuscript in preparation)

Dashtbani-Roozbehani A, Chitsaz M, Brown M.H. Identification of putative substrate-binding pockets of QacA using molecular docking and mutagenesis studies (Manuscript in preparation)

Dashtbani-Roozbehani A and Brown M.H. Efflux pump mediated antimicrobial resistance by staphylococci in health-related environments: challenges and the quest for inhibition (Manuscript in preparation)

CHAPTER 8 REFERENCES

- ABRAMSON, J., SMIRNOVA, I., KASHO, V., VERNER, G., IWATA, S. and KABACK, H. R.** (2003a). The lactose permease of *Escherichia coli*: overall structure, the sugar-binding site and the alternating access model for transport. *FEBS Letters* **555**: 96-101.
- ABRAMSON, J., SMIRNOVA, I., KASHO, V., VERNER, G., KABACK, H. R. and IWATA, S.** (2003b). Structure and mechanism of the lactose permease of *Escherichia coli*. *Science* **301**: 610-615.
- ADDETIA, A., GRENINGER, A. L., ADLER, A., YUAN, S., MAKHSOUS, N., QIN, X. and ZERR, D. M.** (2019). A novel, widespread *qacA* allele results in reduced chlorhexidine susceptibility in *Staphylococcus epidermidis*. *Antimicrobial Agents and Chemotherapy* **63**: e02607-18.
- ADLER, J. and BIBI, E.** (2002). Membrane topology of the multidrug transporter MdfA: complementary gene fusion studies reveal a nonessential C-terminal domain. *Journal of Bacteriology* **184**: 3313-3320.
- ADLER, J. and BIBI, E.** (2004). Determinants of substrate recognition by the *Escherichia coli* multidrug transporter MdfA identified on both sides of the membrane. *The Journal of Biological Chemistry* **279**: 8957-8965.
- ADLER, J. and BIBI, E.** (2005). Promiscuity in the geometry of electrostatic interactions between the *Escherichia coli* multidrug resistance transporter MdfA and cationic substrates. *The Journal of Biological Chemistry* **280**: 2721-2729.
- AGOSTINO, J. W., FERGUSON, J. K., EASTWOOD, K. and KIRK, M. D.** (2017). The increasing importance of community-acquired methicillin-resistant *Staphylococcus aureus* infections. *The Medical Journal of Australia* **207**: 388-393.
- AKABAS, M. H.** (2015). Cysteine modification: probing channel structure, function and conformational change. *Advances in Experimental Medicine and Biology* **869**: 25-54.
- AKBAL-DELIBAS, B., POMPLUN, M. and HASPEL, N.** (2015). Accurate prediction of docked protein structure similarity. *Journal of Computational Biology* **22**: 892-904.
- ALAV, I., SUTTON, J. M. and RAHMAN, K. M.** (2018). Role of bacterial efflux pumps in biofilm formation. *The Journal of Antimicrobial Chemotherapy* **73**: 2003-2020.
- ALEGRE, K. O., PAUL, S., LABARBUTA, P. and LAW, C. J.** (2016). Insight into determinants of substrate binding and transport in a multidrug efflux protein. *Scientific Reports* **6**: 22833.

- ALEXEYEV, M. F., ROBERTS, R. A., DAUGHERTY, R. M., AUDIA, J. P. and WINKLER, H. H.** (2004). Cysteine-scanning mutagenesis and thiol modification of the *Rickettsia prowazekii* ATP/ADP translocase: evidence that transmembrane regions I and II, but not III, are structural components of the aqueous translocation channel. *Biochemistry* **43**: 6995-7002.
- ALFORD, R. F., LEMAN, J. K., WEITZNER, B. D., DURAN, A. M., TILLEY, D. C., ELAZAR, A. and GRAY, J. J.** (2015). An integrated framework advancing membrane protein modeling and design. *PLOS Computational Biology* **11**: e1004398.
- ALLIGNET, J. and EL SOLH, N.** (1997). Characterization of a new staphylococcal gene, *vgaB*, encoding a putative ABC transporter conferring resistance to streptogramin A and related compounds. *Gene* **202**: 133-138.
- ALLIGNET, J., LONCLE, V. and EL SOHL, N.** (1992). Sequence of a staphylococcal plasmid gene, *vga*, encoding a putative ATP-binding protein involved in resistance to virginiamycin A-like antibiotics. *Gene* **117**: 45-51.
- ALMATAR, M., ALBARRI, O., MAKKY, E. A. and KÖKSAL, F.** (2020). Efflux pump inhibitors: new updates. *Pharmacological Reports* **73**: 1-16.
- ALMEIDA, J. G., PRETO, A. J., KOUKOS, P. I., BONVIN, A. M. and MOREIRA, I. S.** (2017). Membrane proteins structures: A review on computational modeling tools. *Biochimica et Biophysica Acta-Biomembranes* **1859**: 2021-2039.
- ALNASERI, H., ARSIC, B., SCHNEIDER, J. E., KAISER, J. C., SCINOCCA, Z. C., HEINRICHS, D. E. and MCGAVIN, M. J.** (2015). Inducible expression of a resistance-nodulation-division-type efflux pump in *Staphylococcus aureus* provides resistance to linoleic and arachidonic acids. *Journal of Bacteriology* **197**: 1893-1905.
- ANDERSEN, J. L., HE, G.-X., KAKARLA, P., KC, R., KUMAR, S., LAKRA, W. S., MUKHERJEE, M. M., RANAWEERA, I., SHRESTHA, U. and TRAN, T.** (2015). Multidrug efflux pumps from Enterobacteriaceae, *Vibrio cholerae* and *Staphylococcus aureus* bacterial food pathogens. *International Journal of Environmental Research and Public Health* **12**: 1487-1547.
- ANDREWS, B., ZHANG, S., SCHWEITZER-STENNER, R. and URBANC, B.** (2020). Glycine in water favors the Polyproline II state. *Biomolecules* **10**: 1121.
- ANES, J., MCCUSKER, M. P., FANNING, S. and MARTINS, M.** (2015). The ins and outs of RND efflux pumps in *Escherichia coli*. *Frontiers in Microbiology* **6**: 587.
- ANGELOW, S. and YU, A. S.** (2009). Structure-function studies of claudin extracellular domains by cysteine-scanning mutagenesis. *The Journal of Biological Chemistry* **284**: 29205-29217.
- ATZORI, A., MALLOCI, G., PRAJAPATI, J. D., BASCIU, A., BOSIN, A., KLEINEKATHÖFER, U., DREIER, J. R., VARGIU, A. V. and RUGGERONE, P.** (2019a). Molecular interactions of cephalosporins with the deep binding pocket of the RND transporter AcrB. *Journal of Physical Chemistry B* **123**: 4625-4635.

- ATZORI, A., MALVIYA, V. N., MALLOCI, G., DREIER, J., POS, K. M., VARGIU, A. V. and RUGGERONE, P.** (2019b). Identification and characterization of carbapenem binding sites within the RND-transporter AcrB. *Biochimica et Biophysica Acta-Biomembranes* **1861**: 62-74.
- AUER, M., KIM, M. J., LEMIEUX, M. J., VILLA, A., SONG, J., LI, X. D. and WANG, D. N.** (2001). High-yield expression and functional analysis of *Escherichia coli* glycerol-3-phosphate transporter. *Biochemistry* **40**: 6628-35.
- BAGNOLI, F., RAPPUOLI, R. and GRANDI, G.** (2018). *Staphylococcus aureus*: Microbiology, pathology, immunology, therapy and prophylaxis (Springer International Publishing).
- BAI, X., MORAES, T. F. and REITHMEIER, R. A.** (2017). Structural biology of solute carrier (SLC) membrane transport proteins. *Molecular Membrane Biology* **34**: 1-32.
- BAINES, S. L., JENSEN, S. O., FIRTH, N., DA SILVA, A. G., SEEMANN, T., CARTER, G. P., WILLIAMSON, D. A., HOWDEN, B. P. and STINEAR, T. P.** (2019). Remodeling of pSK1 family plasmids and enhanced chlorhexidine tolerance in a dominant hospital lineage of methicillin-resistant *Staphylococcus aureus*. *Antimicrobial Agents and Chemotherapy* **63**: e02356-18.
- BAKER, J., WRIGHT, S. H. and TAMA, F.** (2012). Simulations of substrate transport in the multidrug transporter EmrD. *Proteins* **80**: 1620-1632.
- BANCHS, C., POULOS, S., NIMJAREANSUK, W. S., JOO, Y. E. and FAHAM, S.** (2014). Substrate binding to the multidrug transporter MepA. *Biochimica et Biophysica Acta-Biomembranes* **1838**: 2539-2546.
- BARAL, B. and MOZAFARI, M.** (2020). Strategic moves of “superbugs” against available chemical scaffolds: signaling, regulation, and challenges. *ACS Pharmacology and Translational Science* **3**: 373-400.
- BASILE, W., SALVATORE, M., BASSOT, C. and ELOFSSON, A.** (2019). Why do eukaryotic proteins contain more intrinsically disordered regions? *PLoS Computational Biology* **15**: e1007186.
- BASS, R. B., BUTLER, S. L., CHERVITZ, S. A., GLOOR, S. L. and FALKE, J. J.** (2007). Use of site-directed cysteine and disulfide chemistry to probe protein structure and dynamics: applications to soluble and transmembrane receptors of bacterial chemotaxis. *Methods in Enzymology* **423**: 25-51.
- BAY, D. C., ROMMENS, K. L. and TURNER, R. J.** (2008). Small multidrug resistance proteins: a multidrug transporter family that continues to grow. *Biochimica et Biophysica Acta* **1778**: 1814-1838.
- BAY, D. C. and TURNER, R. J.** (2016). Small multidrug resistance efflux pumps. Li XZ., Elkins C., Zgurskaya H. (eds) “Efflux-Mediated Antimicrobial Resistance in Bacteria” (Adis, Cham), pp 45-71.

- BAYER, A. S., CHENG, D., YEAMAN, M. R., COREY, G. R., MCCLELLAND, R. S., HARREL, L. J. and FOWLER, V. G., JR.** (1998). *In vitro* resistance to thrombin-induced platelet microbicidal protein among clinical bacteremic isolates of *Staphylococcus aureus* correlates with an endovascular infectious source. *Antimicrobial Agents and Chemotherapy* **42**: 3169-3172.
- BAYER, A. S., KUPFERWASSER, L., BROWN, M. H., SKURRAY, R. A., GRKOVIC, S., JONES, T., MUKHOPADHAY, K. and YEAMAN, M.** (2006). Low-level resistance of *Staphylococcus aureus* to thrombin-induced platelet microbicidal protein 1 *in vitro* associated with *qacA* gene carriage is independent of multidrug efflux pump activity. *Antimicrobial Agents and Chemotherapy* **50**: 2448-2454.
- BAYER, A. S., PRASAD, R., CHANDRA, J., KOUL, A., SMRITI, M., VARMA, A., SKURRAY, R. A., FIRTH, N., BROWN, M. H. and KOO, S.-P.** (2000). *In vitro* resistance of *Staphylococcus aureus* to thrombin-induced platelet microbicidal protein is associated with alterations in cytoplasmic membrane fluidity. *Infection and Immunity* **68**: 3548-3553.
- BECKER, K., HEILMANN, C. and PETERS, G.** (2014). Coagulase-negative staphylococci. *Clinical Microbiology Reviews* **27**: 870-926.
- BELARDINELLI, J. M., YAZIDI, A., YANG, L., FABRE, L., LI, W., JACQUES, B., ANGALA, S. K., ROUILLER, I., ZGURSKAYA, H. I., SYGUSCH, J. and JACKSON, M.** (2016). Structure-function profile of MmpL3, the essential mycolic acid transporter from *Mycobacterium tuberculosis*. *ACS Infectious Diseases* **2**: 702-713.
- BERG, T., FIRTH, N., APISIRIDEJ, S., HETTIARATCHI, A., LEELAPORN, A. and SKURRAY, R. A.** (1998). Complete nucleotide sequence of pSK41: evolution of staphylococcal conjugative multiresistance plasmids. *Journal of Bacteriology* **180**: 4350-4359.
- BIAN, F., YUE, S., PENG, Z., ZHANG, X., CHEN, G., YU, J., XUAN, N. and BI, Y.** (2015). A comprehensive alanine-scanning mutagenesis study reveals roles for salt bridges in the structure and activity of *Pseudomonas aeruginosa* elastase. *PLoS One* **10**: e0121108.
- BIASINI, M., BIENERT, S., WATERHOUSE, A., ARNOLD, K., STUDER, G., SCHMIDT, T., KIEFER, F., CASSARINO, T. G., BERTONI, M. and BORDOLI, L.** (2014). SWISS-MODEL: modelling protein tertiary and quaternary structure using evolutionary information. *Nucleic Acids Research* **42**: W252-W258.
- BIBI, E., ADLER, J., LEWINSON, O. and EDGAR, R.** (2001). MdfA, an interesting model protein for studying multidrug transport. *Journal of Molecular Microbiology and Biotechnology* **3**: 171-177.
- BIRCH, J., CHERUVARA, H., GAMAGE, N., HARRISON, P. J., LITHGO, R. and QUIGLEY, A.** (2020). Changes in membrane protein structural biology. *Biology* **9**: 401.
- BIRUKOU, I., SEO, S. M., SCHINDLER, B. D., KAATZ, G. W. and BRENNAN, R. G.** (2014). Structural mechanism of transcription regulation of the *Staphylococcus*

aureus multidrug efflux operon *mepRA* by the MarR family repressor MepR. *Nucleic Acids Research* **42**: 2774-2788.

- BISCHOFF, M., BAUER, J., PREIKSCHAT, P., SCHWAIGER, K., MOLLE, G. and HOLZEL, C.** (2012). First detection of the antiseptic resistance gene *qacA/B* in *Enterococcus faecalis*. *Microbial Drug Resistance* **18**: 7-12.
- BISIGNANO, P., LEE, M. A., GEORGE, A., ZUCKERMAN, D. M., GRABE, M. and ROSENBERG, J. M.** (2020). A kinetic mechanism for enhanced selectivity of membrane transport. *PLoS Computational Biology* **16**: e1007789.
- BJORLAND, J., STEINUM, T., SUNDE, M., WAAGE, S. and HEIR, E.** (2003). Novel plasmid-borne gene *qacJ* mediates resistance to quaternary ammonium compounds in equine *Staphylococcus aureus*, *Staphylococcus simulans*, and *Staphylococcus intermedius*. *Antimicrobial Agents and Chemotherapy* **47**: 3046-3052.
- BLAIR, J. M. and PIDDOCK, L. J.** (2016). How to measure export via bacterial multidrug resistance efflux pumps. *mBio* **7**: e00840-16.
- BLAIR, J. M., WEBBER, M. A., BAYLAY, A. J., OGBOLU, D. O. and PIDDOCK, L. J.** (2015). Molecular mechanisms of antibiotic resistance. *Nature Reviews Microbiology* **13**: 42-51.
- BLANCO, P., HERNANDO-AMADO, S., REALES-CALDERON, J. A., CORONA, F., LIRA, F., ALCALDE-RICO, M., BERNARDINI, A., SANCHEZ, M. B. and MARTINEZ, J. L.** (2016). Bacterial multidrug efflux pumps: much more than antibiotic resistance determinants. *Microorganisms* **4**: 14.
- BLANCO, P., SANZ-GARCÍA, F., HERNANDO-AMADO, S., MARTÍNEZ, J. L. and ALCALDE-RICO, M.** (2018). The development of efflux pump inhibitors to treat Gram-negative infections. *Expert Opinion on Drug Discovery* **13**: 919-931.
- BOGDANOV, M., MILEYKOVSKAYA, E. and DOWHAN, W.** (2008). Lipids in the assembly of membrane proteins and organization of protein supercomplexes: implications for lipid-linked disorders. Quinn P.J., Wang X. (eds) "Lipids in Health and Disease. Subcellular Biochemistry" (Springer, Dordrecht), pp. 197-239.
- BOGDANOV, M., ZHANG, W., XIE, J. and DOWHAN, W.** (2005). Transmembrane protein topology mapping by the substituted cysteine accessibility method (SCAM(TM)): application to lipid-specific membrane protein topogenesis. *Methods* **36**: 148-171.
- BOGGAVARAPU, R., JECKELMANN, J.-M., HARDER, D., UCURUM, Z. and FOTIADIS, D.** (2015). Role of electrostatic interactions for ligand recognition and specificity of peptide transporters. *BMC Biology* **13**: 58.
- BOLHUIS, H., VAN VEEN, H. W., POOLMAN, B., DRIESSEN, A. J. and KONINGS, W. N.** (1997). Mechanisms of multidrug transporters. *FEMS Microbiology Reviews* **21**: 55-84.

- BREDA, A., VALADARES, N. F., DE SOUZA, O. N. and GARRATT, R. C.** (2007). Protein structure, modelling and applications. "Bioinformatics in tropical disease research: A practical and case-study approach" (National Center for Biotechnology Information, USA).
- BRIAUD, P., CAMUS, L., BASTIEN, S., DOLÉANS-JORDHEIM, A., VANDENESCH, F. and MOREAU, K.** (2019). Coexistence with *Pseudomonas aeruginosa* alters *Staphylococcus aureus* transcriptome, antibiotic resistance and internalization into epithelial cells. *Scientific Reports* **9**: 1-14.
- BRINCAT, J. P., CAROSATI, E., SABATINI, S., MANFRONI, G., FRAVOLINI, A., RAYGADA, J. L., PATEL, D., KAATZ, G. W. and CRUCIANI, G.** (2011). Discovery of novel inhibitors of the NorA multidrug transporter of *Staphylococcus aureus*. *Journal of Medicinal Chemistry* **54**: 354-365.
- BRODIE, N. I., POPOV, K. I., PETROTCHENKO, E. V., DOKHOLYAN, N. V. and BORCHERS, C. H.** (2017). Solving protein structures using short-distance cross-linking constraints as a guide for discrete molecular dynamics simulations. *Science Advances* **3**: e1700479.
- BROOKS, B. E., PIRO, K. M. and BRENNAN, R. G.** (2007). Multidrug-binding transcription factor QacR binds the bivalent aromatic diamidines DB75 and DB359 in multiple positions. *Journal of the American Chemical Society* **129**: 8389-8395.
- BROWN, A. F., LEECH, J. M., ROGERS, T. R. and MCLOUGHLIN, R. M.** (2014). *Staphylococcus aureus* colonization: modulation of host immune response and impact on human vaccine design. *Frontiers in Immunology* **4**: 507.
- BROWN, C. J., TRIEBER, C. and OVERDUIN, M.** (2021). Structural biology of endogenous membrane protein assemblies in native nanodiscs. *Current Opinion in Structural Biology* **69**: 70-77.
- BROWN, M. H. and SKURRAY, R. A.** (2001). Staphylococcal multidrug efflux protein QacA. *Journal of Molecular Microbiology and Biotechnology* **3**: 163-70.
- BUFFET-BATAILLON, S., TATTEVIN, P., BONNAURE-MALLET, M. and JOLIVET-GOUGEON, A.** (2012). Emergence of resistance to antibacterial agents: the role of quaternary ammonium compounds—a critical review. *International Journal of Antimicrobial Agents* **39**: 381-389.
- BUKOWSKI, M., PIWOWARCZYK, R., MADRY, A., ZAGORSKI-PRZYBYLO, R., HYDZIK, M. and WLADYKA, B.** (2019). Prevalence of antibiotic and heavy metal resistance determinants and virulence-related genetic elements in plasmids of *Staphylococcus aureus*. *Frontiers in Microbiology* **10**: 805.
- BUONERBA, F., LEPRI, S., GORACCI, L., SCHINDLER, B. D., SEO, S. M., KAATZ, G. W. and CRUCIANI, G.** (2017). Improved potency of indole-based NorA efflux pump inhibitors: from serendipity toward rational design and development. *Journal of Medicinal Chemistry* **60**: 517-523.

- BURGESS, K. S. D. and JUSTICE JR, J. B.** (1999). Effects of serine mutations in transmembrane domain 7 of the human norepinephrine transporter on substrate binding and transport. *Journal of Neurochemistry* **73**: 656-664.
- CALABRESE, A. N., JACKSON, S. M., JONES, L. N., BECKSTEIN, O., HEINKEL, F., GSPONER, J., SHARPLES, D., SANS, M., KOKKINIDOU, M., PEARSON, A. R., RADFORD, S. E., ASHCROFT, A. E. and HENDERSON, P. J. F.** (2017). Topological dissection of the membrane transport protein Mhp1 derived from cysteine accessibility and mass spectrometry. *Analytical Chemistry* **89**: 8844-8852.
- CARNALLY, S. M., EDWARDSON, J. M. and BARRERA, N. P.** (2011). Imaging the spatial orientation of subunits within membrane receptors by atomic force microscopy. Braga P., Ricci D. (eds) "Atomic Force Microscopy in Biomedical Research". Methods in Molecular Biology (Methods and Protocols), vol 736. (Humana Press), pp.47-60.
- CARPENTER, E. P., BEIS, K., CAMERON, A. D. and IWATA, S.** (2008). Overcoming the challenges of membrane protein crystallography. *Current Opinion in Structural Biology* **18**: 581-6.
- CARRETERO, G. P. B., SARAIVA, G. K. V., RODRIGUES, M. A., KIYOTA, S., BEMQUERER, M. P., CHAIMOVICH, H. and CUCCOVIA, I. M.** (2021). Naphthalimide-containing BP100 leads to higher model membranes interactions and antimicrobial activity. *Biomolecules* **11**: 542.
- CASARES, D., ESCRIBÁ, P. V. and ROSSELLÓ, C. A.** (2019). Membrane lipid composition: effect on membrane and organelle structure, function and compartmentalization and therapeutic avenues. *International Journal of Molecular Sciences* **20**: 2167.
- CERVELLI, M., POLTICELLI, F., FIORUCCI, L., ANGELUCCI, E., FEDERICO, R. and MARIOTTINI, P.** (2013). Inhibition of acetyl polyamine and spermine oxidases by the polyamine analogue chlorhexidine. *Journal of Enzyme Inhibition and Medicinal Chemistry* **28**: 463-467.
- CHAKRABARTTY, A., SCHELLMAN, J. A. and BALDWIN, R. L.** (1991). Large differences in the helix propensities of alanine and glycine. *Nature* **351**: 586-588.
- CHAMBERS, H. F. and DELEO, F. R.** (2009). Waves of resistance: *Staphylococcus aureus* in the antibiotic era. *Nature Reviews Microbiology* **7**: 629-41.
- CHEN, A., MAJDINASAB, E. J., FIORI, M. C., LIANG, H. and ALTENBERG, G. A.** (2020). Polymer-encased nanodiscs and polymer nanodiscs: new platforms for membrane protein research and applications. *Frontiers in Bioengineering and Biotechnology* **8**: 598450.
- CHEN, P.-C. and HENNIG, J.** (2018). The role of small-angle scattering in structure-based screening applications. *Biophysical Reviews* **10**: 1295-1310.
- CHEN, Y.-C.** (2015). Beware of docking! *Trends in Pharmacological Sciences* **36**: 78-95.

- CHENG, J. T., HALE, J. D., ELLIOTT, M., HANCOCK, R. E. and STRAUS, S. K.** (2011). The importance of bacterial membrane composition in the structure and function of aurein 2.2 and selected variants. *Biochimica et Biophysica Acta-Biomembranes* **1808**: 622-633.
- CHESNEAU, O., LIGERET, H., HOSAN-AGHAIE, N., MORVAN, A. and DASSA, E.** (2005). Molecular analysis of resistance to streptogramin A compounds conferred by the Vga proteins of staphylococci. *Antimicrobial Agents and Chemotherapy* **49**: 973-980.
- CHITSAZ, M. and BROWN, M. H.** (2017). The role played by drug efflux pumps in bacterial multidrug resistance. *Essays in Biochemistry* **61**: 127-139.
- CHOO, E. J.** (2017). Community-associated methicillin-resistant *Staphylococcus aureus* in nosocomial infections. *Infection and Chemotherapy* **49**: 158-159.
- CHOO, E. J. and CHAMBERS, H. F.** (2016). Treatment of methicillin-resistant *Staphylococcus aureus* bacteremia. *Infection and Chemotherapy* **48**: 267-273.
- CHOY, B. C., CATER, R. J., MANCIA, F. and PRYOR JR, E. E.** (2020). A 10-year meta-analysis of membrane protein structural biology: detergents, membrane mimetics, and structure determination techniques. *Biochimica et Biophysica Acta-Biomembranes* **1863**: 183533.
- CIEPLIK, F., JAKUBOVICS, N. S., BUCHALLA, W., MAISCH, T., HELMWIG, E. and AL-AHMAD, A.** (2019). Resistance toward chlorhexidine in oral bacteria—Is there cause for concern? *Frontiers in Microbiology* **10**: 587.
- CLAY, A. T., LU, P. and SHAROM, F. J.** (2015). Interaction of the P-glycoprotein multidrug transporter with sterols. *Biochemistry* **54**: 6586-97.
- CLEMENCON, B., LUSCHER, B. P. and HEDIGER, M. A.** (2018). Establishment of a novel microscale thermophoresis ligand-binding assay for characterization of SLC solute carriers using oligopeptide transporter PepT1 (SLC15 family) as a model system. *Journal of Pharmacological and Toxicological Methods* **92**: 67-76.
- COLLIGNON, P.** (2015). Antibiotic resistance: are we all doomed? *Internal Medicine Journal* **45**: 1109-1115.
- COSTA, L. M., DE MACEDO, E. V., OLIVEIRA, F. A., FERREIRA, J. H., GUTIERREZ, S. J., PELAEZ, W. J., LIMA, F. C., DE SIQUEIRA JUNIOR, J. P., COUTINHO, H. D., KAATZ, G. W., DE FREITAS, R. M. and BARRETO, H. M.** (2016). Inhibition of the NorA efflux pump of *Staphylococcus aureus* by synthetic riparins. *Journal of Applied Microbiology* **121**: 1312-1322.
- COSTA, S. S., SOBKOWIAK, B., PARREIRA, R., EDGEWORTH, J. D., VIVEIROS, M., CLARK, T. G. and COUTO, I.** (2019). Genetic diversity of *norA*, coding for a main efflux pump of *Staphylococcus aureus*. *Frontiers in Genetics* **9**: 710.

- COSTA, S. S., VIVEIROS, M., AMARAL, L. and COUTO, I.** (2013). Multidrug efflux pumps in *Staphylococcus aureus*: an update. *The Open Microbiology Journal* **7**: 59-71.
- CREAMER, T. P. and ROSE, G. D.** (1994). α -Helix-forming propensities in peptides and proteins. *Proteins: Structure, Function, and Bioinformatics* **19**: 85-97.
- DA CRUZ, R. M., ZELLI, R., BENSCHAIN, S., DA CRUZ, R. M., SIQUEIRA-JÚNIOR, J. P., DÉCOUT, J., MINGEOT-LECLERCQ, M.P. and MENDONÇA-JUNIOR, F. J.** (2020). Synthesis and evaluation of 2-aminothiophene derivatives as *Staphylococcus aureus* efflux pump inhibitors. *ChemMedChem* **15**: 716-725.
- DANG, S., SUN, L., HUANG, Y., LU, F., LIU, Y., GONG, H., WANG, J. and YAN, N.** (2010). Structure of a fucose transporter in an outward-open conformation. *Nature* **467**: 734-738.
- DANIEL, H., SPANIER, B., KOTTRA, G. and WEITZ, D.** (2006). From bacteria to man: archaic proton-dependent peptide transporters at work. *Physiology* **21**: 93-102.
- DARZYNKIEWICZ, Z. M., GREEN, A. T., ABDALI, N., HAZEL, A., FULTON, R. L., KIMBALL, J., GRZYCZYNSKI, Z., GUMBART, J. C., PARKS, J. M. and SMITH, J. C.** (2019). Identification of binding sites for efflux pump inhibitors of the AcrAB-TolC component AcrA. *Biophysical Journal* **116**: 648-658.
- DAS, S., DASGUPTA, A. and CHOPRA, S.** (2016). Drug repurposing: a new front in the war against *Staphylococcus aureus*. *Future Microbiology* **11**: 1091-1099.
- DAURY, L., ORANGE, F., TAVEAU, J. C., VERCHERE, A., MONLEZUN, L., GOUNOU, C., MARREDDY, R. K., PICARD, M., BROUTIN, I., POS, K. M. and LAMBERT, O.** (2016). Tripartite assembly of RND multidrug efflux pumps. *Nature Communications* **7**: 10731.
- DAVID, M. Z. and DAUM, R. S.** (2010). Community-associated methicillin-resistant *Staphylococcus aureus*: epidemiology and clinical consequences of an emerging epidemic. *Clinical Microbiology Reviews* **23**: 616-687.
- DAWSON, R. J. and LOCHER, K. P.** (2006). Structure of a bacterial multidrug ABC transporter. *Nature* **443**: 180-185.
- DAWSON, R. J. and LOCHER, K. P.** (2007). Structure of the multidrug ABC transporter Sav1866 from *Staphylococcus aureus* in complex with AMP-PNP. *FEBS Letters* **581**: 935-938.
- DE KRAKER, M. E., STEWARDSON, A. J. and HARBARTH, S.** (2016). Will 10 million people die a year due to antimicrobial resistance by 2050? *PLoS Medicine* **13**: e1002184.
- DE MAROTHY, M. T. and ELOFSSON, A.** (2015). Marginally hydrophobic transmembrane α -helices shaping membrane protein folding. *Protein Science* **24**: 1057-1074.

- DE MORAIS OLIVEIRA-TINTINO, C. D., TINTINO, S. R., MUNIZ, D. F., DOS SANTOS BARBOSA, C. R., PEREIRA, R. L. S., BEGNINI, I. M., REBELO, R. A., DA SILVA, L. E., MIRESKI, S. L. and NASATO, M. C.** (2021). Chemical synthesis, molecular docking and MepA efflux pump inhibitory effect by 1, 8-naphthyridines sulfonamides. *European Journal of Pharmaceutical Sciences* **160**: 105753.
- DE SIENA, B., CAMPOLATTANO, N., D'ABROSCA, G., RUSSO, L., CANTILLON, D., MARASCO, R., MUSCARIELLO, L., WADDELL, S. J. and SACCO, M.** (2020). Characterization of the mycobacterial MSMEG-3762/63 efflux pump in *Mycobacterium smegmatis* drug efflux. *Frontiers in Microbiology* **11**: 575828.
- DEACON, L. J., BILLONES, H., GALYEAN, A. A., DONALDSON, T., PENNACCHIO, A., IOZZINO, L., D'AURIA, S. and DATTELBAUM, J. D.** (2014). Tryptophan-scanning mutagenesis of the ligand binding pocket in *Thermotoga maritima* arginine-binding protein. *Biochimie* **99**: 208-214.
- DEBRUYCKER, V., HUTCHIN, A., MASUREEL, M., FICICI, E., MARTENS, C., LEGRAND, P., STEIN, R. A., MCHAOURAB, H. S., FARALDO-GÓMEZ, J. D. and REMAUT, H.** (2020). An embedded lipid in the multidrug transporter LmrP suggests a mechanism for polyspecificity. *Nature Structural and Molecular biology* **27**: 829-835.
- DEL VAL, C., WHITE, S. H. and BONDAR, A.-N.** (2012). Ser/Thr motifs in transmembrane proteins: conservation patterns and effects on local protein structure and dynamics. *The Journal of Membrane Biology* **245**: 717-730.
- DELEO, F. R., OTTO, M., KREISWIRTH, B. N. and CHAMBERS, H. F.** (2010). Community-associated methicillin-resistant *Staphylococcus aureus*. *Lancet* **375**: 1557-1568.
- DENG, D., SUN, P., YAN, C., KE, M., JIANG, X., XIONG, L., REN, W., HIRATA, K., YAMAMOTO, M. and FAN, S.** (2015). Molecular basis of ligand recognition and transport by glucose transporters. *Nature* **526**: 391-396.
- DEPRIEST, A., PHELAN, P. and MARTHA SKERRETT, I.** (2011). Tryptophan scanning mutagenesis of the first transmembrane domain of the innexin Shaking-B(Lethal). *Biophysical Journal* **101**: 2408-2416.
- DIALLINAS, G.** (2014). Understanding transporter specificity and the discrete appearance of channel-like gating domains in transporters. *Frontiers in Pharmacology* **5**: 207.
- DIALLINAS, G.** (2016). Dissection of transporter function: from genetics to structure. *Trends in Genetics* **32**: 576-590.
- DING, Y., ONODERA, Y., LEE, J. C. and HOOPER, D. C.** (2008). NorB, an efflux pump in *Staphylococcus aureus* strain MW2, contributes to bacterial fitness in abscesses. *Journal of Bacteriology* **190**: 7123-7129.
- DO VALE, B. C. M., NOGUEIRA, A. G., CIDRAL, T. A., LOPES, M. C. S. and DE MELO, M. C. N.** (2019). Decreased susceptibility to chlorhexidine and distribution of

qacA/B genes among coagulase-negative Staphylococcus clinical samples. *BMC Infectious Diseases* **19**: 1-5.

DOKHOLYAN, N. V. (2020). Experimentally-driven protein structure modeling. *Journal of Proteomics* **220**: 103777.

DOKI, S., KATO, H. E., SOLCAN, N., IWAKI, M., KOYAMA, M., HATTORI, M., IWASE, N., TSUKAZAKI, T., SUGITA, Y. and KANDORI, H. (2013). Structural basis for dynamic mechanism of proton-coupled symport by the peptide transporter POT. *Proceedings of the National Academy of Sciences of the United States of America* **110**: 11343-11348.

DONG, H., SHARMA, M., ZHOU, H.-X. and CROSS, T. A. (2012). Glycines: role in α -helical membrane protein structures and a potential indicator of native conformation. *Biochemistry* **51**: 4779-4789.

DREW, D., NORTH, R. A., NAGARATHINAM, K. and TANABE, M. (2021). Structures and general transport mechanisms by the Major Facilitator Superfamily (MFS). *Chemical Reviews* **121**: 5289–5335.

DU, D., WANG-KAN, X., NEUBERGER, A., VAN VEEN, H. W., POS, K. M., PIDDOCK, L. J. V. and LUISI, B. F. (2018). Multidrug efflux pumps: structure, function and regulation. *Nature Reviews Microbiology* **16**: 523-539.

DURÃES, F., PINTO, M. and SOUSA, E. (2018). Medicinal chemistry updates on bacterial efflux pump modulators. *Current Medicinal Chemistry* **25**: 6030-6069.

EARLS, M. R., KINNEVEY, P. M., BRENNAN, G. I., LAZARIS, A., SKALLY, M., O'CONNELL, B., HUMPHREYS, H., SHORE, A. C. and COLEMAN, D. C. (2017). The recent emergence in hospitals of multidrug-resistant community-associated sequence type 1 and spa type t127 methicillin-resistant *Staphylococcus aureus* investigated by whole-genome sequencing: Implications for screening. *PLoS One* **12**: e0175542.

EBBENSGAARD, A. E., LØBNER-OLESEN, A. and FRIMODT-MØLLER, J. (2020). The role of efflux pumps in the transition from low-level to clinical antibiotic resistance. *Antibiotics* **9**: 855.

EDGAR, R. and BIBI, E. (1997). MdfA, an *Escherichia coli* multidrug resistance protein with an extraordinarily broad spectrum of drug recognition. *Journal of Bacteriology* **179**: 2274-2280.

ETHAYATHULLA, A. S., YOUSEF, M. S., AMIN, A., LEBLANC, G., KABACK, H. R. and GUAN, L. (2014). Structure-based mechanism for Na⁺/melibiose symport by MelB. *Nature Communications* **5**: 3009.

ETO, K. Y., FIRTH, N., DAVIS, A. M., KWONG, S. M., KRYSIAK, M., LEE, Y. T., O'BRIEN, F. G., GRUBB, W. B., COOMBS, G. W. and BOND, C. S. (2019). Evolution of a 72-kilobase cointegrant, conjugative multiresistance plasmid in community-

associated methicillin-resistant *Staphylococcus aureus* isolates from the early 1990s. *Antimicrobial Agents and Chemotherapy* **63**: e01560-19.

EXNER, M., BHATTACHARYA, S., CHRISTIANSEN, B., GEBEL, J., GORONCY-BERMES, P., HARTEMANN, P., HEEG, P., ILSCHNER, C., KRAMER, A., LARSON, E., MERKENS, W., MIELKE, M., OLTMANN, P., ROSS, B., ROTTER, M., SCHMITHAUSEN, R. M., SONNTAG, H. G. and TRAUTMANN, M. (2017). Antibiotic resistance: what is so special about multidrug-resistant Gram-negative bacteria? *GMS hygiene and Infection Control* **12**: Doc05.

FANG, R., SUN, Y., DAI, W., ZHENG, X., TIAN, X., ZHANG, X., WANG, C., CAO, J. and ZHOU, T. (2020). Mutations in the MepRAB efflux system contribute to the *in vitro* development of tigecycline resistance in *Staphylococcus aureus*. *Journal of Global Antimicrobial Resistance* **22**: 631-636.

FAUSTINELLA, F., SMITH, L. C., SEMENKOVICH, C. and CHAN, L. (1991). Structural and functional roles of highly conserved serines in human lipoprotein lipase. Evidence that serine 132 is essential for enzyme catalysis. *The Journal of Biological Chemistry* **266**: 9481-9485.

FEIG, M. (2017). Computational protein structure refinement: almost there, yet still so far to go. *Wiley Interdisciplinary Reviews: Computational Molecular Science* **7**: e1307.

FELICETTI, T., CANNALIRE, R., BURALI, M. S., MASSARI, S., MANFRONI, G., BARRECA, M. L., TABARRINI, O., SCHINDLER, B. D., SABATINI, S., KAATZ, G. W. and CECCHETTI, V. (2017). Searching for novel inhibitors of the *S. aureus* NorA efflux pump: synthesis and biological evaluation of the 3-phenyl-1,4-benzothiazine Analogues. *ChemMedChem* **12**: 1293-1302.

FELICETTI, T., CANNALIRE, R., NIZI, M. G., TABARRINI, O., MASSARI, S., BARRECA, M. L., MANFRONI, G., SCHINDLER, B. D., CECCHETTI, V. and KAATZ, G. W. (2018). Studies on 2-phenylquinoline *Staphylococcus aureus* NorA efflux pump inhibitors: new insights on the C-6 position. *European Journal of Medicinal Chemistry* **155**: 428-433.

FIORI, M. C., ZHENG, W., KAMILAR, E., SIMIYU, G., ALTENBERG, G. A. and LIANG, H. (2020). Extraction and reconstitution of membrane proteins into lipid nanodiscs encased by zwitterionic styrene-maleic amide copolymers. *Scientific Reports* **10**: 9940.

FIRTH, N., RIDGWAY, K. P., BYRNE, M. E., FINK, P. D., JOHNSON, L., PAULSEN, I. T. and SKURRAY, R. A. (1993). Analysis of a transfer region from the staphylococcal conjugative plasmid pSK41. *Gene* **136**: 13-25.

FISHER, E., ZHAO, Y., RICHARDSON, R., JANIK, M., BUELL, A. K., AIGBIRHIO, F. I. and TOTH, G. (2017). Detection and characterization of small molecule interactions with fibrillar protein aggregates using microscale thermophoresis. *ACS Chemical Neuroscience* **8**: 2088-2095.

- FISHOVITZ, J., HERMOSO, J. A., CHANG, M. and MOBASHERY, S.** (2014). Penicillin-binding protein 2a of methicillin-resistant *Staphylococcus aureus*. *International Union of Biochemistry and Molecular Biology life* **66**: 572-577.
- FLOYD, J. L., SMITH, K. P., KUMAR, S. H., FLOYD, J. T. and VARELA, M. F.** (2010). LmrS is a multidrug efflux pump of the major facilitator superfamily from *Staphylococcus aureus*. *Antimicrobial Agents and Chemotherapy* **54**: 5406-5412.
- FLUMAN, N., ADLER, J., ROTENBERG, S. A., BROWN, M. H. and BIBI, E.** (2014). Export of a single drug molecule in two transport cycles by a multidrug efflux pump. *Nature Communications* **5**: 4615.
- FLUMAN, N. and BIBI, E.** (2009). Bacterial multidrug transport through the lens of the major facilitator superfamily. *Biochimica et Biophysica Acta* **1794**: 738-747.
- FLUMAN, N., COHEN-KARNI, D., WEISS, T. and BIBI, E.** (2009). A promiscuous conformational switch in the secondary multidrug transporter MdfA. *The Journal of Biological Chemistry* **284**: 32296-32304.
- FLUMAN, N., RYAN, C. M., WHITELEGGE, J. P. and BIBI, E.** (2012). Dissection of mechanistic principles of a secondary multidrug efflux protein. *Molecular Cell* **47**: 777-787.
- FORMAN, M. E., FLETCHER, M. H., JENNINGS, M. C., DUGGAN, S. M., MINBIOLE, K. P. and WUEST, W. M.** (2016). Structure–resistance relationships: interrogating antiseptic resistance in bacteria with multicationic quaternary ammonium dyes. *ChemMedChem* **11**: 958-962.
- FOSTER, T. J.** (2017). Antibiotic resistance in *Staphylococcus aureus*. current status and future prospects. *FEMS Microbiology Reviews* **41**: 430-449.
- FRIERI, M., KUMAR, K. and BOUTIN, A.** (2017). Antibiotic resistance. *Journal of Infection and Public Health* **10**: 369-378.
- FU, Y., ZHAO, J. and CHEN, Z.** (2018). Insights into the molecular mechanisms of protein-ligand interactions by molecular docking and molecular dynamics simulation: a case of oligopeptide binding protein. *Computational and Mathematical Methods in Medicine* **2018**: 3502514.
- FU, Z., MA, Y., CHEN, C., GUO, Y., HU, F., LIU, Y., XU, X. and WANG, M.** (2016). Prevalence of fosfomycin resistance and mutations in *murA*, *glpT*, and *uhpT* in methicillin-resistant *Staphylococcus aureus* strains isolated from blood and cerebrospinal fluid samples. *Frontiers in Microbiology* **6**: 1544.
- GARDETE, S. and TOMASZ, A.** (2014). Mechanisms of vancomycin resistance in *Staphylococcus aureus*. *The Journal of Clinical Investigation* **124**: 2836-2840.
- GAROY, E. Y., GEBREAB, Y. B., ACHILA, O. O., TEKESTE, D. G., KESETE, R., GHIRMAY, R., KIFLAY, R. and TESFU, T.** (2019). Methicillin-resistant *Staphylococcus aureus* (MRSA): prevalence and antimicrobial sensitivity pattern among

patients-a multicenter study in Asmara, Eritrea. *Canadian Journal of Infectious Diseases and Medical Microbiology* **2019**: 8321834.

GEBEL, J., EXNER, M., FRENCH, G., CHARTIER, Y., CHRISTIANSEN, B., GEMEIN, S., GORONCY-BERMES, P., HARTEMANN, P., HEUDORF, U., KRAMER, A., MAILLARD, J. Y., OLTMANN, P., ROTTER, M. and SONNTAG, H. G. (2013). The role of surface disinfection in infection prevention. *GMS Hygiene and Infection Control* **8**: Doc10.

GILLESPIE, M. T., MAY, J. W. and SKURRAY, R. A. (1986). Plasmid-encoded resistance to acriflavine and quaternary ammonium compounds in methicillin-resistant *Staphylococcus aureus*. *FEMS Microbiology Letters* **34**: 47-51.

GINN, S. L., BROWN, M. H. and SKURRAY, R. A. (1997). Membrane topology of the metal-tetracycline/H⁺ antiporter TetA(K) from *Staphylococcus aureus*. *Journal of Bacteriology* **179**: 3786-3789.

GINN, S. L., BROWN, M. H. and SKURRAY, R. A. (2000). The TetA(K) tetracycline/H⁺ antiporter from *Staphylococcus aureus*: mutagenesis and functional analysis of motif C. *Journal of Bacteriology* **182**: 1492-1498.

GRANSETH, E., VON HEIJNE, G. and ELOFSSON, A. (2005). A study of the membrane-water interface region of membrane proteins. *Journal of Molecular Biology* **346**: 377-385.

GRAY, V. E., HAUSE, R. J. and FOWLER, D. M. (2017). Analysis of large-scale mutagenesis data to assess the impact of single amino acid substitutions. *Genetics* **207**: 53-61.

GREEN, N. S., REISLER, E. and HOUK, K. (2001). Quantitative evaluation of the lengths of homobifunctional protein cross-linking reagents used as molecular rulers. *Protein Science* **10**: 1293-1304.

GREEN, R. and ROGERS, E. J. (2013). Transformation of chemically competent *E. coli*. *Methods in Enzymology* **529**: 329-36.

GREENE, N. P., PORCELLI, I., BUCHANAN, G., HICKS, M. G., SCHERMANN, S. M., PALMER, T. and BERKS, B. C. (2007). Cysteine scanning mutagenesis and disulfide mapping studies of the TatA component of the bacterial twin arginine translocase. *The Journal of Biological Chemistry* **282**: 23937-23945.

GRIFFITH, J. K., BAKER, M. E., ROUCH, D. A., PAGE, M. G., SKURRAY, R. A., PAULSEN, I. T., CHATER, K. F., BALDWIN, S. A. and HENDERSON, P. J. (1992). Membrane transport proteins: implications of sequence comparisons. *Current Opinion in Cell Biology* **4**: 684-695.

GRINIUS, L. L. and GOLDBERG, E. B. (1994). Bacterial multidrug resistance is due to a single membrane protein which functions as a drug pump. *The Journal of Biological Chemistry* **269**: 29998-30004.

- GRKOVIC, S., BROWN, M. H., ROBERTS, N. J., PAULSEN, I. T. and SKURRAY, R. A.** (1998). QacR is a repressor protein that regulates expression of the *Staphylococcus aureus* multidrug efflux pump QacA. *The Journal of Biological Chemistry* **273**: 18665-18673.
- GRKOVIC, S., BROWN, M. H., SCHUMACHER, M. A., BRENNAN, R. G. and SKURRAY, R. A.** (2001). The staphylococcal QacR multidrug regulator binds a correctly spaced operator as a pair of dimers. *Journal of Bacteriology* **183**: 7102-7109.
- GRKOVIC, S., HARDIE, K. M., BROWN, M. H. and SKURRAY, R. A.** (2003). Interactions of the QacR multidrug-binding protein with structurally diverse ligands: implications for the evolution of the binding pocket. *Biochemistry* **42**: 15226-15236.
- GUAY, G. G., KHAN, S. A. and ROTHSTEIN, D. M.** (1993). The *tet(K)* gene of plasmid pT181 of *Staphylococcus aureus* encodes an efflux protein that contains 14 transmembrane helices. *Plasmid* **30**: 163-166.
- GUAY, G. G. and ROTHSTEIN, D. M.** (1993). Expression of the *tetK* gene from *Staphylococcus aureus* in *Escherichia coli*: comparison of substrate specificities of TetA (B), TetA (C), and TetK efflux proteins. *Antimicrobial Agents and Chemotherapy* **37**: 191-198.
- GUETTOU, F., QUISTGAARD, E. M., TRESAUGUES, L., MOBERG, P., JEGERSCHÖLD, C., ZHU, L., JONG, A. J. O., NORDLUND, P. and LÖW, C.** (2013). Structural insights into substrate recognition in proton-dependent oligopeptide transporters. *EMBO Reports* **14**: 804-810.
- GULISTAN, T., AHMAD, S. and AZAM, S. S.** (2020). Conformational transition of *Acinetobacter baumannii* KdsC enzyme and the role of magnesium in binding: an insight from comparative molecular dynamics simulation and its implications in novel antibiotics design. *Journal of Molecular Graphics and Modelling* **99**: 107625.
- GUO, Y., SONG, G., SUN, M., WANG, J. and WANG, Y.** (2020). Prevalence and therapies of antibiotic-resistance in *Staphylococcus aureus*. *Frontiers in Cellular and Infection Microbiology* **10**: 107.
- GUO, Z., LI, B., CHENG, L.-T., ZHOU, S., MCCAMMON, J. A. and CHE, J.** (2015). Identification of protein–ligand binding sites by the level-set variational implicit-solvent approach. *Journal of Chemical Theory and Computation* **11**: 753-765.
- GUZMAN, L. M., BELIN, D., CARSON, M. J. and BECKWITH, J.** (1995). Tight regulation, modulation, and high-level expression by vectors containing the arabinose P_{BAD} promoter. *Journal of Bacteriology* **177**: 4121-4130.
- HAABER, J., PENADES, J. R. and INGMER, H.** (2017). Transfer of antibiotic resistance in *Staphylococcus aureus*. *Trends in Microbiology* **25**: 893-905.

- HADDAD, Y., ADAM, V. and HEGER, Z.** (2020). Ten quick tips for homology modeling of high-resolution protein 3D structures. *PLOS Computational Biology* **16**: e1007449.
- HALL, S. E., ROBERTS, K. and VAIDEHI, N.** (2009). Position of helical kinks in membrane protein crystal structures and the accuracy of computational prediction. *Journal of Molecular Graphics and Modelling* **27**: 944-950.
- HAMPTON, T.** (2013). Report reveals scope of US antibiotic resistance threat. *Journal of the American Medical Association* **310**: 1661-1663.
- HANAHAH, D.** (1983). Studies on transformation of *Escherichia coli* with plasmids. *Journal of Molecular Biology* **166**: 557-580.
- HANDZLIK, J., MATYS, A. and KIEC-KONONOWICZ, K.** (2013). Recent advances in multi-drug resistance (MDR) efflux pump inhibitors of Gram-positive bacteria *S. aureus*. *Antibiotics* **2**: 28-45.
- HARDY, K., SUNNUCKS, K., GIL, H., SHABIR, S., TRAMPARI, E., HAWKEY, P. and WEBBER, M.** (2018). Increased usage of antiseptics is associated with reduced susceptibility in clinical isolates of *Staphylococcus aureus*. *mBio* **9**: e00894-18.
- HARRIS, N. J., FINDLAY, H. E., SANDERS, M. R., KEDZIERSKI, M., DOS SANTOS, Á. and BOOTH, P. J.** (2017). Comparative stability of major facilitator superfamily transport proteins. *European Biophysics Journal* **46**: 655-663.
- HASSAN, K. A., GALEA, M., WU, J., MITCHELL, B. A., SKURRAY, R. A. and BROWN, M. H.** (2006a). Functional effects of intramembranous proline substitutions in the staphylococcal multidrug transporter QacA. *FEMS Microbiology Letters* **263**: 76-85.
- HASSAN, K. A., NAIDU, V., EDGERTON, J. R., METTRICK, K. A., LIU, Q., FAHMY, L., LI, L., JACKSON, S. M., AHMAD, I. and SHARPLES, D.** (2019). Short-chain diamines are the physiological substrates of PACE family efflux pumps. *Proceedings of the National Academy of Sciences of the United States of America* **116**: 18015-18020.
- HASSAN, K. A., ROBINSON, K. L., SMITH, A. N., GIBSON, J. H., SKURRAY, R. A. and BROWN, M. H.** (2006b). Glycine-rich transmembrane helix 10 in the staphylococcal tetracycline transporter TetA (K) lines a solvent-accessible channel. *Biochemistry* **45**: 15661-15669.
- HASSAN, K. A., SKURRAY, R. A. and BROWN, M. H.** (2007a). Active export proteins mediating drug resistance in staphylococci. *Journal of Molecular Microbiology and Biotechnology* **12**: 180-196.
- HASSAN, K. A., SKURRAY, R. A. and BROWN, M. H.** (2007b). Transmembrane helix 12 of the *Staphylococcus aureus* multidrug transporter QacA lines the bivalent cationic drug binding pocket. *Journal of Bacteriology* **189**: 9131-9134.

- HASSAN, K. A., SOUHANI, T., SKURRAY, R. A. and BROWN, M. H.** (2008). Analysis of tryptophan residues in the staphylococcal multidrug transporter QacA reveals long-distance functional associations of residues on opposite sides of the membrane. *Journal of Bacteriology* **190**: 2441-2449.
- HASSAN, K. A., XU, Z., WATKINS, R. E., BRENNAN, R. G., SKURRAY, R. A. and BROWN, M. H.** (2009). Optimized production and analysis of the staphylococcal multidrug efflux protein QacA. *Protein Expression and Purification* **64**: 118-124.
- HASSANZADEH, S., POURMAND, M. R., MASHHADI, R. and GHAZVINI, K.** (2020). Epidemiology of efflux pumps genes mediating resistance among *Staphylococcus aureus*; a systematic review. *Microbial Pathogenesis* **139**: 103850.
- HASSOUN, A., LINDEN, P. K. and FRIEDMAN, B.** (2017). Incidence, prevalence, and management of MRSA bacteremia across patient populations-a review of recent developments in MRSA management and treatment. *Critical Care* **21**: 211.
- HENDERSON, P. J., MAHER, C., ELBOURNE, L. D., EIJKELKAMP, B. A., PAULSEN, I. T. and HASSAN, K. A.** (2021). Physiological functions of bacterial “multidrug” efflux pumps. *Chemical Reviews* **121**: 5417–5478.
- HENG, J., ZHAO, Y., LIU, M., LIU, Y., FAN, J., WANG, X., ZHAO, Y. and ZHANG, X. C.** (2015). Substrate-bound structure of the *E. coli* multidrug resistance transporter MdfA. *Cell Research* **25**: 1060-1073.
- HOFMEYR, J.-H., ROHWER, J., SNOEP, J., WESTERHOFF, H. and KONINGS, W.** (2002). How to distinguish between the vacuum cleaner and flippase mechanisms of the LmrA multi-drug transporter in *Lactococcus lactis*. *Molecular Biology Reports* **29**: 107-112.
- HOHL, M., REMM, S., ESKANDARIAN, H. A., DAL MOLIN, M., ARNOLD, F. M., HÜRLIMANN, L. M., KRÜGEL, A., FANTNER, G. E., SANDER, P. and SEEGER, M. A.** (2019). Increased drug permeability of a stiffened mycobacterial outer membrane in cells lacking MFS transporter Rv1410 and lipoprotein LprG. *Molecular Microbiology* **111**: 1263-1282.
- HOLDSWORTH, S. R. and LAW, C. J.** (2013). The major facilitator superfamily transporter MdtM contributes to the intrinsic resistance of *Escherichia coli* to quaternary ammonium compounds. *The Journal of Antimicrobial Chemotherapy* **68**: 831-839.
- HONG, S. I., LEE, Y. M., PARK, K. H., RYU, B. H., HONG, K. W., KIM, S., BAE, I. G. and CHO, O. H.** (2019). Clinical and molecular characteristics of *qacA*- and *qacB*-positive methicillin-resistant *Staphylococcus aureus* causing bloodstream infections. *Antimicrobial Agents and Chemotherapy* **63**: e02157-18.

- HOOPER, D. C. and JACOBY, G. A.** (2015). Mechanisms of drug resistance: quinolone resistance. *Annals of the New York Academy of Sciences* **1354**: 12.
- HORNER, C., MAWER, D. and WILCOX, M.** (2012). Reduced susceptibility to chlorhexidine in staphylococci: Is it increasing and does it matter? *The Journal of Antimicrobial Chemotherapy* **67**: 2547-2559.
- HUANG, H., ZHANG, G., ZHOU, Y., LIN, C., CHEN, S., LIN, Y., MAI, S. and HUANG, Z.** (2018). Reverse screening methods to search for the protein targets of chemopreventive compounds. *Frontiers in Chemistry* **6**: 138.
- HUANG, J., O'TOOLE, P. W., SHEN, W., AMRINE-MADSEN, H., JIANG, X., LOBO, N., PALMER, L. M., VOELKER, L., FAN, F., GWYNN, M. N. and MCDEVITT, D.** (2004). Novel chromosomally encoded multidrug efflux transporter MdeA in *Staphylococcus aureus*. *Antimicrobial Agents and Chemotherapy* **48**: 909-917.
- HUANG, Y., LEMIEUX, M. J., SONG, J., AUER, M. and WANG, D. N.** (2003). Structure and mechanism of the glycerol-3-phosphate transporter from *Escherichia coli*. *Science* **301**: 616-620.
- HUANG, Y., MENG, L., NIE, Q., ZHOU, Y., CHEN, L., YANG, S., FUNG, Y. M. E., LI, X., HUANG, C. and CAO, Y.** (2020). Selection of DNA-encoded chemical libraries against endogenous membrane proteins on live cells. *Nature Chemistry* **13**: 77-88.
- HUET, A. A., RAYGADA, J. L., MENDIRATTA, K., SEO, S. M. and KAATZ, G. W.** (2008). Multidrug efflux pump overexpression in *Staphylococcus aureus* after single and multiple *in vitro* exposures to biocides and dyes. *Microbiology* **154**: 3144-3153.
- HUGHES, D. and ANDERSSON, D. I.** (2015). Evolutionary consequences of drug resistance: shared principles across diverse targets and organisms. *Nature Reviews Genetics* **16**: 459-471.
- HUSAIN, F., BIKHCHANDANI, M. and NIKAIDO, H.** (2011). Vestibules are part of the substrate path in the multidrug efflux transporter AcrB of *Escherichia coli*. *Journal of Bacteriology* **193**: 5847-5849.
- HUSAIN, F. and NIKAIDO, H.** (2010). Substrate path in the AcrB multidrug efflux pump of *Escherichia coli*. *Molecular Microbiology* **78**: 320-330.
- IANCU, C. V., ZAMOON, J., WOO, S. B., ALESHIN, A. and CHOE, J. Y.** (2013). Crystal structure of a glucose/H⁺ symporter and its mechanism of action. *Proceedings of the National Academy of Sciences of the United States of America* **110**: 17862-17867.
- JAMROZY, D., COLL, F., MATHER, A. E., HARRIS, S. R., HARRISON, E. M., MACGOWAN, A., KARAS, A., ELSTON, T., ESTEE TOROK, M., PARKHILL, J. and PEACOCK, S. J.** (2017). Evolution of mobile genetic element composition in an epidemic methicillin-resistant *Staphylococcus aureus*: temporal changes correlated with frequent loss and gain events. *BMC Genomics* **18**: 684.

- JAMSHIDI, S., SUTTON, J. M. and RAHMAN, K. M.** (2017). Computational study reveals the molecular mechanism of the interaction between the efflux inhibitor PA β N and the AdeB transporter from *Acinetobacter baumannii*. *ACS Omega* **2**: 3002-3016.
- JANG, S.** (2016). Multidrug efflux pumps in *Staphylococcus aureus* and their clinical implications. *Journal of Microbiology* **54**: 1-8.
- JENNINGS, M. C., BUTTARO, B. A., MINBIOLE, K. P. and WUEST, W. M.** (2015a). Bioorganic investigation of multicationic antimicrobials to combat QAC-resistant *Staphylococcus aureus*. *ACS Infectious Diseases* **1**: 304-309.
- JENNINGS, M. C., MINBIOLE, K. P. and WUEST, W. M.** (2015b). Quaternary ammonium compounds: an antimicrobial mainstay and platform for innovation to address bacterial resistance. *ACS Infectious Diseases* **1**: 288-303.
- JERABEK-WILLEMSEN, M., ANDRE, T., WANNER, R., ROTH, H. M., DUHR, S., BAASKE, P. and BREITSPRECHER, D.** (2014). MicroScale thermophoresis: interaction analysis and beyond. *Journal of Molecular Structure* **1077**: 101-113.
- JERABEK-WILLEMSEN, M., WIENKEN, C. J., BRAUN, D., BAASKE, P. and DUHR, S.** (2011). Molecular interaction studies using microscale thermophoresis. *Assay and Drug Development Technologies* **9**: 342-353.
- JESCHKE, G.** (2012). DEER distance measurements on proteins. *Annual Review of Physical Chemistry* **63**: 419-446.
- JESSEN-MARSHALL, A. E., PAUL, N. J. and BROOKER, R. J.** (1995). The conserved motif, GXXX (D/E)(R/K) XG [X](R/K)(R/K), in hydrophilic loop 2/3 of the lactose permease. *The Journal of Biological Chemistry* **270**: 16251-16257.
- JIANG, D., ZHAO, Y., WANG, X., FAN, J., HENG, J., LIU, X., FENG, W., KANG, X., HUANG, B., LIU, J. and ZHANG, X. C.** (2013). Structure of the YajR transporter suggests a transport mechanism based on the conserved motif A. *Proceedings of the National Academy of Sciences of the United States of America* **110**: 14664-14669.
- JIANG, L. H.** (2013). Cysteine-based cross-linking approach to study inter-domain interactions in ion channels. *Methods in Molecular Biology* **998**: 267-276.
- JIN, J., GUFFANTI, A. A., BECHHOFFER, D. H. and KRULWICH, T. A.** (2002). Tet (L) and tet (K) tetracycline-divalent metal/H⁺ antiporters: characterization of multiple catalytic modes and a mutagenesis approach to differences in their efflux substrate and coupling ion preferences. *Journal of Bacteriology* **184**: 4722-4732.
- JIN, J., GUFFANTI, A. A., BECK, C. and KRULWICH, T. A.** (2001). Twelve-transmembrane-segment (TMS) version (Δ TMS VII-VIII) of the 14-TMS Tet(L) antibiotic resistance protein retains monovalent cation transport modes but lacks tetracycline efflux capacity. *Journal of Bacteriology* **183**: 2667-2671.

- JONES, P. M. and GEORGE, A. M.** (2015). The nucleotide-free state of the multidrug resistance ABC transporter LmrA: sulfhydryl cross-linking supports a constant contact, head-to-tail configuration of the nucleotide-binding domains. *PLoS One* **10**: e0131505.
- KAATZ, G. W., DEMARCO, C. E. and SEO, S. M.** (2006). MepR, a repressor of the *Staphylococcus aureus* MATE family multidrug efflux pump MepA, is a substrate-responsive regulatory protein. *Antimicrobial Agents and Chemotherapy* **50**: 1276-1281.
- KAATZ, G. W., MCALEESE, F. and SEO, S. M.** (2005). Multidrug resistance in *Staphylococcus aureus* due to overexpression of a novel multidrug and toxin extrusion (MATE) transport protein. *Antimicrobial Agents and Chemotherapy* **49**: 1857-1864.
- KABACK, H. R., SAHIN-TOTH, M. and WEINGLASS, A. B.** (2001). The kamikaze approach to membrane transport. *Nature Reviews Molecular Cell Biology* **2**: 610-620.
- KAMPF, G.** (2016). Acquired resistance to chlorhexidine—is it time to establish an ‘antiseptic stewardship’ initiative? *The Journal of Hospital Infection* **94**: 213-227.
- KAPOOR, K., REHAN, M., KAUSHIKI, A., PASRIJA, R., LYNN, A. M. and PRASAD, R.** (2009). Rational mutational analysis of a multidrug MFS transporter CaMdr1p of *Candida albicans* by employing a membrane environment based computational approach. *PLoS Computational Biology* **5**. e1000624.
- KARAMI, Y., GUYON, F., DE VRIES, S. and TUFFÉRY, P.** (2018). DaReUS-Loop: accurate loop modeling using fragments from remote or unrelated proteins. *Scientific Reports* **8**: 1-12.
- KASAHARA, M., SHIMODA, E. and MAEDA, M.** (1996). Transmembrane segment 10 is important for substrate recognition in Ga12 and Hxt2 sugar transporters in the yeast *Saccharomyces cerevisiae*. *FEBS Letters* **389**: 174-178.
- KASAHARA, T. and KASAHARA, M.** (1998). Tryptophan 388 in putative transmembrane segment 10 of the rat glucose transporter Glut1 is essential for glucose transport. *The Journal of Biological Chemistry* **273**: 29113-29117.
- KEHRENBURG, C. and SCHWARZ, S.** (2005). Florfenicol-chloramphenicol exporter gene *fxA* is part of the novel transposon Tn558. *Antimicrobial Agents and Chemotherapy* **49**: 813-815.
- KELLEY, L. A., MEZULIS, S., YATES, C. M., WASS, M. N. and STERNBERG, M. J.** (2015). The Phyre2 web portal for protein modeling, prediction and analysis. *Nature Protocols* **10**: 845-858.
- KIM, G., WEISS, S. J. and LEVINE, R. L.** (2014). Methionine oxidation and reduction in proteins. *Biochimica et Biophysica Acta* **1840**: 901-915.

- KIMURA-SOMEYA, T., IWAKI, S. and YAMAGUCHI, A.** (1998). Site-directed chemical modification of cysteine-scanning mutants as to transmembrane segment II and its flanking regions of the Tn10-encoded metal-tetracycline/H⁺ antiporter reveals a transmembrane water-filled channel. *The Journal of Biological Chemistry* **273**: 32806-32811.
- KIMURA, T., NAKATANI, M., KAWABE, T. and YAMAGUCHI, A.** (1998). Roles of conserved arginine residues in the metal- tetracycline/H⁺ antiporter of *Escherichia coli*. *Biochemistry* **37**: 5475-5480.
- KINANA, A. D., VARGIU, A. V. and NIKAIDO, H.** (2016). Effect of site-directed mutations in multidrug efflux pump AcrB examined by quantitative efflux assays. *Biochemical and Biophysical Research Communications* **480**: 552-557.
- KOEHLER LEMAN, J., ULMSCHNEIDER, M. B. and GRAY, J. J.** (2015). Computational modeling of membrane proteins. *Proteins: Structure, Function, and Bioinformatics* **83**: 1-24.
- KOHLER, C., PROCTOR, R. A., BAYER, A. S., YEAMAN, M. R., LALK, M., ENGELMANN, S. and MISHRA, N. N.** (2019). Proteomic and membrane lipid correlates of reduced host defense peptide susceptibility in a *snoD* mutant of *Staphylococcus aureus*. *Antibiotics* **8**: 169.
- KONG, E. F., JOHNSON, J. K. and JABRA-RIZK, M. A.** (2016). Community-associated methicillin-resistant *Staphylococcus aureus*: an enemy amidst us. *PLoS Pathogens* **12**: e1005837.
- KONG, K. F., SCHNEPER, L. and MATHEE, K.** (2010). Beta-lactam antibiotics: from antibiosis to resistance and bacteriology. *Acta Pathologica, Microbiologica, et Immunologica Scandinavica*: **118**: 1-36.
- KOURTESI, C., BALL, A. R., HUANG, Y. Y., JACHAK, S. M., VERA, D. M., KHONDKAR, P., GIBBONS, S., HAMBLIN, M. R. and TEGOS, G. P.** (2013). Microbial efflux systems and inhibitors: approaches to drug discovery and the challenge of clinical implementation. *The Open Microbiology Journal* **7**: 34-52.
- KRISHNAMOORTHY, G., TIKHONOVA, E. B., DHAMDHERE, G. and ZGURSKAYA, H. I.** (2013). On the role of TolC in multidrug efflux: the function and assembly of AcrAB-TolC tolerate significant depletion of intracellular TolC protein. *Molecular Microbiology* **87**: 982-997.
- KROEGER, J. K., HASSAN, K., VÖRÖS, A., SIMM, R., SAIDIJAM, M., BETTANEY, K. E., BECHTHOLD, A., PAULSEN, I. T., HENDERSON, P. and KOLSTØ, A.-B.** (2015). *Bacillus cereus* efflux protein BC3310-a multidrug transporter of the unknown major facilitator family, UMF-2. *Frontiers in Microbiology* **6**: 1063.
- KRULWICH, T. A., JIN, J., GUFFANTI, A. A. and BECHHOFFER, D. H.** (2001). Functions of tetracycline efflux proteins that do not involve tetracycline. *Journal of Molecular Microbiology and Biotechnology* **3**: 237-246.

- KUMAR, A. and SCHWEIZER, H. P.** (2005). Bacterial resistance to antibiotics: active efflux and reduced uptake. *Advanced Drug Delivery Reviews* **57**: 1486-1513.
- KUMAR, H., KASHO, V., SMIRNOVA, I., FINER-MOORE, J. S., KABACK, H. R. and STROUD, R. M.** (2014). Structure of sugar-bound LacY. *Proceedings of the National Academy of Sciences of the United States of America* **111**: 1784-1788.
- KUMAR, S., ATHREYA, A., GULATI, A., NAIR, R. M. and PENMATSA, A.** (2020a). Structural basis of inhibition of a putative drug efflux transporter NorC, through a single-domain camelid antibody. *bioRxiv* DOI: 10.1101/2020.10.21.349639.
- KUMAR, S., MAHENDRAN, I., ATHREYA, A., RANJAN, R. and PENMATSA, A.** (2020b). Isolation and structural characterization of a Zn²⁺-bound single-domain antibody against NorC, a putative multidrug efflux transporter in bacteria. *The Journal of Biological Chemistry* **295**: 55-68.
- KUPFERWASSER, L. I., SKURRAY, R. A., BROWN, M. H., FIRTH, N., YEAMAN, M. R. and BAYER, A. S.** (1999). Plasmid-mediated resistance to thrombin-induced platelet microbicidal protein in staphylococci: role of the *qacA* locus. *Antimicrobial Agents and Chemotherapy* **43**: 2395-2399.
- LABRECK, P. T., BOCHI-LAYEC, A. C., STANBRO, J., DABBAH-KRANCHER, G., SIMONS, M. P. and MERRELL, D. S.** (2020). Systematic analysis of efflux pump-mediated antiseptic resistance in *Staphylococcus aureus* suggests a need for greater antiseptic stewardship. *mSphere* **5**: e00959-19.
- LABRECK, P. T., RICE, G. K., PASKEY, A. C., ELASSAL, E. M., CER, R. Z., LAW, N. N., SCHLETT, C. D., BENNETT, J. W., MILLAR, E. V. and ELLIS, M. W.** (2018). Conjugative transfer of a novel staphylococcal plasmid encoding the biocide resistance gene, *qacA*. *Frontiers in Microbiology* **9**: 2664.
- LAGANOWSKY, A., READING, E., ALLISON, T. M., ULMSCHNEIDER, M. B., DEGIACOMI, M. T., BALDWIN, A. J. and ROBINSON, C. V.** (2014). Membrane proteins bind lipids selectively to modulate their structure and function. *Nature* **510**: 172-175.
- LAMUT, A., PETERLIN MAŠIČ, L., KIKELJ, D. and TOMAŠIČ, T.** (2019). Efflux pump inhibitors of clinically relevant multidrug resistant bacteria. *Medicinal Research Reviews* **39**: 2460-2504.
- LANDREH, M. and ROBINSON, C. V.** (2015). A new window into the molecular physiology of membrane proteins. *The Journal of Physiology* **593**: 355-362.
- LAW, C. J., MALONEY, P. C. and WANG, D.-N.** (2008). Ins and outs of major facilitator superfamily antiporters. *Annual Review of Microbiology* **62**: 289-305.
- LAXMINARAYAN, R.** (2014). Antibiotic effectiveness: balancing conservation against innovation. *Science* **345**: 1299-1301.

- LAZIM, R., SUH, D. and CHOI, S.** (2020). Advances in molecular dynamics simulations and enhanced sampling methods for the study of protein systems. *International Journal of Molecular Sciences* **21**: 6339.
- LE BOUTER, A., LECLERCQ, R. and CATTOIR, V.** (2011). Molecular basis of resistance to macrolides, lincosamides and streptogramins in *Staphylococcus saprophyticus* clinical isolates. *International Journal of Antimicrobial Agents* **37**: 118-123.
- LEA, W. A. and SIMEONOV, A.** (2011). Fluorescence polarization assays in small molecule screening. *Expert Opinion on Drug Discovery* **6**: 17-32.
- LEANO, J. B., BATARNI, S., ERIKSEN, J., JUGE, N., PAK, J. E., KIMURA-SOMEYA, T., ROBLES-COLMENARES, Y., MORIYAMA, Y., STROUD, R. M. and EDWARDS, R. H.** (2019). Structures suggest a mechanism for energy coupling by a family of organic anion transporters. *PLoS Biology* **17**: e3000260.
- LEE, G. C., DALLAS, S. D., WANG, Y., OLSEN, R. J., LAWSON, K. A., WILSON, J. and FREI, C. R.** (2017). Emerging multidrug resistance in community-associated *Staphylococcus aureus* involved in skin and soft tissue infections and nasal colonization. *The Journal of Antimicrobial Chemotherapy* **72**: 2461-2468.
- LEE, J., IWASAKI, T., OHTANI, S., MATSUI, H., NEJIMA, R., MORI, Y., KAGAYA, F., YAGI, A., YOSHIMURA, A. and HANAOKI, H.** (2020). Benzalkonium chloride resistance in *Staphylococcus epidermidis* on the ocular surface of glaucoma patients under long-term administration of eye drops. *Translational Vision Science and Technology* **9**: 9.
- LEE, J., SANDS, Z. A. and BIGGIN, P. C.** (2016). A numbering system for MFS transporter proteins. *Frontiers in Molecular Biosciences* **3**: 21.
- LEELAPORN, A., FIRTH, N., PAULSEN, I. T., HETTIARATCHI, A. and SKURRAY, R. A.** (1995). Multidrug resistance plasmid pSK108 from coagulase-negative staphylococci; relationships to *Staphylococcus aureus qacC* plasmids. *Plasmid* **34**: 62-67.
- LEELAPORN, A., PAULSEN, I. T., TENNENT, J. M., LITTLEJOHN, T. G. and SKURRAY, R. A.** (1994). Multidrug resistance to antiseptics and disinfectants in coagulase-negative staphylococci. *Journal of Medical Microbiology* **40**: 214-220.
- LEKSHMI, M., AMMINI, P., JONES ADJEI, L. M. S., SHRESTHA, U., KUMAR, S. and VARELA, M. F.** (2018). Modulation of antimicrobial efflux pumps of the major facilitator superfamily in *Staphylococcus aureus*. *American Institute of Mathematical Sciences Microbiology* **4**: 1-18.
- LEMIEUX, M. J. and OVERDUIN, M.** (2020). Structure and function of proteins in membranes and nanodiscs. *Biochimica et Biophysica Acta-Biomembranes* **1863**: 183445.
- LEWINSON, O., ADLER, J., POELARENDS, G. J., MAZURKIEWICZ, P., DRIESSEN, A. J. and BIBI, E.** (2003). The *Escherichia coli* multidrug transporter MdfA catalyzes

both electrogenic and electroneutral transport reactions. *Proceedings of the National Academy of Sciences of the United States of America* **100**: 1667-1672.

- LEWINSON, O. and BIBI, E.** (2001). Evidence for simultaneous binding of dissimilar substrates by the *Escherichia coli* multidrug transporter MdfA. *Biochemistry* **40**: 12612-12618.
- LEWIS, K.** (2020). The science of antibiotic discovery. *Cell* **181**: 29-45.
- LI, B. and WEBSTER, T. J.** (2018). Bacteria antibiotic resistance: new challenges and opportunities for implant-associated orthopedic infections. *Journal of Orthopaedic Research* **36**: 22-32.
- LI, X. Z., PLESIAT, P. and NIKAIDO, H.** (2015). The challenge of efflux-mediated antibiotic resistance in Gram-negative bacteria. *Clinical Microbiology Reviews* **28**: 337-418.
- LI, X. Z., ZHANG, L. and NIKAIDO, H.** (2004). Efflux pump-mediated intrinsic drug resistance in *Mycobacterium smegmatis*. *Antimicrobial Agents and Chemotherapy* **48**: 2415-2423.
- LIN, Y.-H., LIN, S.-Y., LI, G.-S., WENG, S.-E., TZENG, S.-L., HSIAO, Y.-H. and HU, N.-J.** (2019). Site-directed alkylation detected by in-gel fluorescence (SDAf) to determine the topology map and probe the solvent accessibility of membrane proteins. *Scientific Reports* **9**: 1-9.
- LITTLEJOHN, T. G., DIBERARDINO, D., MESSEROTTI, L. J., SPIERS, S. J. and SKURRAY, R. A.** (1991). Structure and evolution of a family of genes encoding antiseptic and disinfectant resistance in *Staphylococcus aureus*. *Gene* **101**: 59-66.
- LITTLEJOHN, T. G., PAULSEN, I. T., GILLESPIE, M. T., TENNENT, J. M., MIDGLEY, M., JONES, I. G., PUREWAL, A. S. and SKURRAY, R. A.** (1992). Substrate specificity and energetics of antiseptic and disinfectant resistance in *Staphylococcus aureus*. *FEMS Microbiology Letters* **74**: 259-265.
- LIU, Q., HASSAN, K. A., ASHWOOD, H. E., GAMAGE, H., LI, L., MABBUTT, B. C. and PAULSEN, I. T.** (2018). Regulation of the *acel* multidrug efflux pump gene in *Acinetobacter baumannii*. *The Journal of Antimicrobial Chemotherapy* **73**: 1492-1500.
- LIVNAT LEVANON, N., VIGONSKY, E. and LEWINSON, O.** (2014). Real time measurements of membrane protein: receptor interactions using Surface Plasmon Resonance (SPR). *Journal of Visualized Experiments* **93**: e51937.
- LOMIZE, A. L., POGOZHEVA, I. D., LOMIZE, M. A. and MOSBERG, H. I.** (2006a). Positioning of proteins in membranes: a computational approach. *Protein Science* **15**: 1318-1333.
- LOMIZE, M. A., LOMIZE, A. L., POGOZHEVA, I. D. and MOSBERG, H. I.** (2006b). OPM: orientations of proteins in membranes database. *Bioinformatics* **22**: 623-625.

- LOMIZE, M. A., POGOZHEVA, I. D., JOO, H., MOSBERG, H. I. and LOMIZE, A. L.** (2012). OPM database and PPM web server: resources for positioning of proteins in membranes. *Nucleic Acids Research* **40**: D370-D376.
- LOMOVSKAYA, O. and TOTROV, M.** (2005). Vacuuming the periplasm. *Journal of Bacteriology* **187**: 1879-1883.
- LONG, S. B., TAO, X., CAMPBELL, E. B. and MACKINNON, R.** (2007). Atomic structure of a voltage-dependent K⁺ channel in a lipid membrane-like environment. *Nature* **450**: 376-82.
- LOO, T. W., BARTLETT, M. C. and CLARKE, D. M.** (2003). Simultaneous binding of two different drugs in the binding pocket of the human multidrug resistance P-glycoprotein. *The Journal of Biological Chemistry* **278**: 39706-39710.
- LOO, T. W. and CLARKE, D. M.** (1999). Determining the structure and mechanism of the human multidrug resistance P-glycoprotein using cysteine-scanning mutagenesis and thiol-modification techniques. *Biochimica et Biophysica Acta-Biomembranes* **1461**: 315-325.
- LOO, T. W. and CLARKE, D. M.** (2000). Identification of residues within the drug-binding domain of the human multidrug resistance P-glycoprotein by cysteine-scanning mutagenesis and reaction with dibromobimane. *The Journal of Biological Chemistry* **275**: 39272-39278.
- LÓPEZ, C. A., TRAVERS, T., POS, K. M., ZGURSKAYA, H. I. and GNANAKARAN, S.** (2017). Dynamics of intact MexAB-OprM efflux pump: focusing on the MexA-OprM interface. *Scientific Reports* **7**: 1-17.
- LOWRENCE, R. C., SUBRAMANIAPILLAI, S. G., ULAGANATHAN, V. and NAGARAJAN, S.** (2019). Tackling drug resistance with efflux pump inhibitors: from bacteria to cancerous cells. *Critical Reviews in Microbiology* **45**: 334-353.
- LU, J., XU, G., ZHANG, S. and LU, B.** (2016). An effective sequence-alignment-free superpositioning of pairwise or multiple structures with missing data. *Algorithms for Molecular Biology* **11**: 1-10.
- LY, K., BARTHO, J. D., EICHER, T., POS, K. M. and MITRA, A. K.** (2014). A novel packing arrangement of AcrB in the lipid bilayer membrane. *FEBS Letters* **588**: 4776-4783.
- LYON, B. R. and SKURRAY, R.** (1987). Antimicrobial resistance of *Staphylococcus aureus*: genetic basis. *Microbiological Reviews* **51**: 88-134.
- MA, J., LEI, H.-T., REYES, F. E., SANCHEZ-MARTINEZ, S., SARHAN, M. F., HATTNE, J. and GONEN, T.** (2019). Structural basis for substrate binding and specificity of a sodium–alanine symporter AgcS. *Proceedings of the National Academy of Sciences of the United States of America* **116**: 2086-2090.

- MACINTYRE, C. R. and BUI, C. M.** (2017). Pandemics, public health emergencies and antimicrobial resistance-putting the threat in an epidemiologic and risk analysis context. *Archives of Public Health* **75**: 1-6.
- MADEJ, M. G., DANG, S., YAN, N. and KABACK, H. R.** (2013). Evolutionary mix-and-match with MFS transporters. *Proceedings of the National Academy of Sciences of the United States of America* **110**: 5870-5874.
- MAGIORAKOS, A. P., SRINIVASAN, A., CAREY, R. B., CARMELI, Y., FALAGAS, M. E., GISKE, C. G., HARBARTH, S., HINDLER, J. F., KAHLMETER, G., OLSSON-LILJEQUIST, B., PATERSON, D. L., RICE, L. B., STELLING, J., STRUELENS, M. J., VATOPOULOS, A., WEBER, J. T. and MONNET, D. L.** (2012). Multidrug-resistant, extensively drug-resistant and pandrug-resistant bacteria: an international expert proposal for interim standard definitions for acquired resistance. *Clinical Microbiology and Infection* **18**: 268-281.
- MAHONEY, A. R., SAFAEE, M. M., WUEST, W. M. and FURST, A. L.** (2021). The silent pandemic: emergent antibiotic resistances following the global response to SARS-CoV-2. *iScience* **24**: 102304.
- MAJUMDER, P., KHARE, S., ATHREYA, A., HUSSAIN, N., GULATI, A. and PENMATSA, A.** (2019). Dissection of protonation sites for antibacterial recognition and transport in QacA, a multi-drug efflux transporter. *Journal of Molecular Biology* **431**: 2163-2179.
- MALACHOWA, N. and DELEO, F. R.** (2010). Mobile genetic elements of *Staphylococcus aureus*. *Cellular and Molecular Life Sciences* **67**: 3057-3071.
- MAO, W., WARREN, M. S., BLACK, D. S., SATOU, T., MURATA, T., NISHINO, T., GOTOH, N. and LOMOVSKAYA, O.** (2002). On the mechanism of substrate specificity by resistance nodulation division (RND)-type multidrug resistance pumps: the large periplasmic loops of MexD from *Pseudomonas aeruginosa* are involved in substrate recognition. *Molecular Microbiology* **46**: 889-901.
- MARRINK, S. J., CORRADI, V., SOUZA, P. C., INGÓLFSSON, H. I., TIELEMAN, D. P. and SANSOM, M. S.** (2019). Computational modeling of realistic cell membranes. *Chemical Reviews* **119**: 6184-6226.
- MARTENS, C., STEIN, R. A., MASUREEL, M., ROTH, A., MISHRA, S., DAWALIBY, R., KONIJNENBERG, A., SOBOTT, F., GOVAERTS, C. and MCHAOURAB, H. S.** (2016). Lipids modulate the conformational dynamics of a secondary multidrug transporter. *Nature Structural and Molecular Biology* **23**: 744-751.
- MARTENS, E. and DEMAÏN, A. L.** (2017). The antibiotic resistance crisis, with a focus on the United States. *The Journal of Antibiotics* **70**: 520-526.
- MASUREEL, M., MARTENS, C., STEIN, R. A., MISHRA, S., RUYSSCHAERT, J.-M., MCHAOURAB, H. S. and GOVAERTS, C.** (2014). Protonation drives the conformational switch in the multidrug transporter LmrP. *Nature Chemical Biology* **10**: 149-155.

- MAYER, S., BOOS, M., BEYER, A., FLUIT, A. C. and SCHMITZ, F. J.** (2001). Distribution of the antiseptic resistance genes *qacA*, *qacB* and *qacC* in 497 methicillin-resistant and -susceptible European isolates of *Staphylococcus aureus*. *The Journal of Antimicrobial Chemotherapy* **47**: 896-897.
- MCALEESE, F., PETERSEN, P., RUZIN, A., DUNMAN, P. M., MURPHY, E., PROJAN, S. J. and BRADFORD, P. A.** (2005). A novel MATE family efflux pump contributes to the reduced susceptibility of laboratory-derived *Staphylococcus aureus* mutants to tigecycline. *Antimicrobial Agents and Chemotherapy* **49**: 1865-1871.
- MCDONALD, M., DOUGALL, A., HOLT, D., HUYGENS, F., OPPEDISANO, F., GIFFARD, P. M., INMAN-BAMBER, J., STEPHENS, A. J., TOWERS, R., CARAPETIS, J. R. and CURRIE, B. J.** (2006). Use of a single-nucleotide polymorphism genotyping system to demonstrate the unique epidemiology of methicillin-resistant *Staphylococcus aureus* in remote aboriginal communities. *Journal of Clinical Microbiology* **44**: 3720-3727.
- MCDUGAL, L. K., FOSHEIM, G. E., NICHOLSON, A., BULENS, S. N., LIMBAGO, B. M., SHEARER, J. E., SUMMERS, A. O. and PATEL, J. B.** (2010). Emergence of resistance among USA300 methicillin-resistant *Staphylococcus aureus* isolates causing invasive disease in the United States. *Antimicrobial Agents and Chemotherapy* **54**: 3804-3811.
- MCGUINNESS, W. A., MALACHOWA, N. and DELEO, F. R.** (2017). Vancomycin resistance in *Staphylococcus aureus*. *The Yale Journal of Biology and Medicine* **90**: 269-281.
- MEHLA, J., MALLOCI, G., MANSBACH, R., LÓPEZ, C. A., TSIVKOVSKI, R., HAYNES, K., LEUS, I. V., GRINDSTAFF, S. B., CASCELLA, R. H. and D’CUNHA, N.** (2021). Predictive rules of efflux inhibition and avoidance in *Pseudomonas aeruginosa*. *mBio* **12**: e02785-20.
- MELANDER, R. J. and MELANDER, C.** (2017). The challenge of overcoming antibiotic resistance: an adjuvant approach? *ACS Infectious Diseases* **3**: 559-563.
- MIDDLEMISS, J. K. and POOLE, K.** (2004). Differential impact of MexB mutations on substrate selectivity of the MexAB-OprM multidrug efflux pump of *Pseudomonas aeruginosa*. *Journal of Bacteriology* **186**: 1258-1269.
- MIETHKE, M., PIERONI, M., WEBER, T., BRÖNSTRUP, M., HAMMANN, P., HALBY, L., ARIMONDO, P. B., GLASER, P., AIGLE B., and BODE, H. B.** (2021). Towards the sustainable discovery and development of new antibiotics. *Nature Reviews Chemistry* 1-24.
- MIKROS, E. and DIALLINAS, G.** (2019). Tales of tails in transporters. *Open Biology* **9**: 190083.

- MIRAGAIA, M.** (2018). Factors contributing to the evolution of *mecA*-mediated beta-lactam resistance in Staphylococci: update and new insights from whole genome sequencing (WGS). *Frontiers in Microbiology* **9**: 2723.
- MITCHELL, B. A., BROWN, M. H. and SKURRAY, R. A.** (1998). QacA multidrug efflux pump from *Staphylococcus aureus*: comparative analysis of resistance to diamidines, biguanidines, and guanylhydrazones. *Antimicrobial Agents and Chemotherapy* **42**: 475-477.
- MITCHELL, B. A., PAULSEN, I. T., BROWN, M. H. and SKURRAY, R. A.** (1999). Bioenergetics of the staphylococcal multidrug export protein QacA. identification of distinct binding sites for monovalent and divalent cations. *The Journal of Biological Chemistry* **274**: 3541-3548.
- MITCHELL, M. A., IANNETTA, A. A., JENNINGS, M. C., FLETCHER, M. H., WUEST, W. M. and MINBIOLE, K. P.** (2015). Scaffold-hopping of multicationic amphiphiles yields three new classes of antimicrobials. *ChemBioChem* **16**: 2299-2303.
- MORAES, I., EVANS, G., SANCHEZ-WEATHERBY, J., NEWSTEAD, S. and STEWART, P. D. S.** (2014). Membrane protein structure determination—the next generation. *Biochimica et Biophysica Acta-Biomembranes* **1838**: 78-87.
- MORRIS, G. M., HUEY, R., LINDSTROM, W., SANNER, M. F., BELEW, R. K., GOODSSELL, D. S. and OLSON, A. J.** (2009). AutoDock4 and AutoDockTools4: Automated docking with selective receptor flexibility. *Journal of Computational Chemistry* **30**: 2785-2791.
- MOWLA, R., WANG, Y., MA, S. and VENTER, H.** (2018). Kinetic analysis of the inhibition of the drug efflux protein AcrB using surface plasmon resonance. *Biochimica et Biophysica Acta* **1860**: 878-886.
- MUECKLER, M. and MAKEPEACE, C.** (2009). Model of the exofacial substrate-binding site and helical folding of the human Glut1 glucose transporter based on scanning mutagenesis. *Biochemistry* **48**: 5934-5942.
- MULDER, I., SIEMENS, J., SENTEK, V., AMELUNG, W., SMALLA, K. and JECHALKE, S.** (2018). Quaternary ammonium compounds in soil: implications for antibiotic resistance development. *Reviews in Environmental Science and Bio/Technology* **17**: 159-185.
- MULLER, M. P., JIANG, T., SUN, C., LIHAN, M., PANT, S., MAHINTHICHAICHAN, P., TRIFAN, A. and TAJKHORSHID, E.** (2019). Characterization of lipid-protein interactions and lipid-mediated modulation of membrane protein function through molecular simulation. *Chemical Reviews* **119**: 6086-6161.
- MUNITA, J. M. and ARIAS, C. A.** (2016). Mechanisms of antibiotic resistance. "Virulence Mechanisms of Bacterial Pathogens, 5th Edition" (American Society for Microbiology).

- MURAKAMI, S., NAKASHIMA, R., YAMASHITA, E., MATSUMOTO, T. and YAMAGUCHI, A.** (2006). Crystal structures of a multidrug transporter reveal a functionally rotating mechanism. *Nature* **443**: 173-179.
- MURRAY, D. S., SCHUMACHER, M. A. and BRENNAN, R. G.** (2004). Crystal structures of QacR-diamidine complexes reveal additional multidrug-binding modes and a novel mechanism of drug charge neutralization. *The Journal of Biological Chemistry* **279**: 14365-14371.
- NAGARATHINAM, K., NAKADA-NAKURA, Y., PARTHIER, C., TERADA, T., JUGE, N., JAENECKE, F., LIU, K., HOTTA, Y., MIYAJI, T., OMOTE, H., IWATA, S., NOMURA, N., STUBBS, M. T. and TANABE, M.** (2018). Outward open conformation of a Major Facilitator Superfamily multidrug/H⁺ antiporter provides insights into switching mechanism. *Nature Communications* **9**: 4005.
- NAIR, A. V., SINGH, H., RATURI, S., NEUBERGER, A., TONG, Z., DING, N., AGBOH, K. and VAN VEEN, H. W.** (2016). Relocation of active site carboxylates in major facilitator superfamily multidrug transporter LmrP reveals plasticity in proton interactions. *Scientific Reports* **6**: 38052.
- NAKASHIMA, R., SAKURAI, K., YAMASAKI, S., HAYASHI, K., NAGATA, C., HOSHINO, K., ONODERA, Y., NISHINO, K. and YAMAGUCHI, A.** (2013). Structural basis for the inhibition of bacterial multidrug exporters. *Nature* **500**: 102-106.
- NAKASHIMA, R., SAKURAI, K., YAMASAKI, S., NISHINO, K. and YAMAGUCHI, A.** (2011). Structures of the multidrug exporter AcrB reveal a proximal multisite drug-binding pocket. *Nature* **480**: 565-569.
- NARUI, K., NOGUCHI, N., WAKASUGI, K. and SASATSU, M.** (2002). Cloning and characterization of a novel chromosomal drug efflux gene in *Staphylococcus aureus*. *Biological and Pharmaceutical Bulletin* **25**: 1533-1536.
- NAVA, A. R., MAURICIO, N., SANCA, A. J. and DOMINGUEZ, D. C.** (2020). Evidence of calcium signaling and modulation of the LmrS multidrug resistant efflux pump activity by Ca²⁺ ions in *S. aureus*. *Frontiers in Microbiology* **11**: 573388.
- NAWROCKI, K. L., CRISPELL, E. K. and MCBRIDE, S. M.** (2014). Antimicrobial peptide resistance mechanisms of Gram-positive bacteria. *Antibiotics* **3**: 461-492.
- NEUBERGER, A. and VAN VEEN, H. W.** (2015). Hoechst 33342 is a hidden “Janus” amongst substrates for the multidrug efflux pump LmrP. *PloS One* **10**: e0141991.
- NEWSTEAD, S., DREW, D., CAMERON, A. D., POSTIS, V. L., XIA, X., FOWLER, P. W., INGRAM, J. C., CARPENTER, E. P., SANSOM, M. S. and MCPHERSON, M. J.** (2011). Crystal structure of a prokaryotic homologue of the mammalian oligopeptide-proton symporters, PepT1 and PepT2. *EMBO Journal* **30**: 417-426.

- NEYFAKH, A. A.** (1992). The multidrug efflux transporter of *Bacillus subtilis* is a structural and functional homolog of the Staphylococcus NorA protein. *Antimicrobial Agents and Chemotherapy* **36**: 484-485.
- NEYFAKH, A. A., BORSCH, C. and KAATZ, G.** (1993). Fluoroquinolone resistance protein NorA of *Staphylococcus aureus* is a multidrug efflux transporter. *Antimicrobial Agents and Chemotherapy* **37**: 128-129.
- NG, J. W., HOLT, D. C., LILLIEBRIDGE, R. A., STEPHENS, A. J., HUYGENS, F., TONG, S. Y., CURRIE, B. J. and GIFFARD, P. M.** (2009). Phylogenetically distinct *Staphylococcus aureus* lineage prevalent among indigenous communities in northern Australia. *Journal of Clinical Microbiology* **47**: 2295-2300.
- NIE, Y., ERMOLOVA, N. and KABACK, H. R.** (2007). Site-directed alkylation of LacY: effect of the proton electrochemical gradient. *Journal of Molecular Biology* **374**: 356-364.
- NIKAIDO, H.** (2009). Multidrug resistance in bacteria. *Annual Review of Biochemistry* **78**: 119-146.
- NIKAIDO, H.** (2011). Structure and mechanism of RND-type multidrug efflux pumps. *Advances in Enzymology and Related Areas of Molecular Biology* **77**: 1-60.
- NIKOLAEV, D. M., SHYROV, A. A., PANOV, M. S., JAMAL, A., CHAKCHIR, O. B., KOICHEMIROVSKY, V. A., OLIVUCCI, M. and RYAZANTSEV, M. N.** (2018). A comparative study of modern homology modeling algorithms for rhodopsin structure prediction. *ACS Omega* **3**: 7555-7566.
- OMASITS, U., AHRENS, C. H., MÜLLER, S. and WOLLSCHIED, B.** (2014). Protter: interactive protein feature visualization and integration with experimental proteomic data. *Bioinformatics* **30**: 884-886.
- OMOTE, H., HIASA, M., MATSUMOTO, T., OTSUKA, M. and MORIYAMA, Y.** (2006). The MATE proteins as fundamental transporters of metabolic and xenobiotic organic cations. *Trends in Pharmacological Sciences* **27**: 587-593.
- OPPERMAN, T. J. and NGUYEN, S. T.** (2015). Recent advances toward a molecular mechanism of efflux pump inhibition. *Frontiers in Microbiology* **6**: 421.
- OTTO, M.** (2010). Staphylococcus colonization of the skin and antimicrobial peptides. *Expert Review of Dermatology* **5**: 183-195.
- PALAZZOTTI, D., BISSARO, M., BOLCATO, G., ASTOLFI, A., FELICETTI, T., SABATINI, S., STURLESE, M., CECCHETTI, V., BARRECA, M. L. and MORO, S.** (2019). Deciphering the molecular recognition mechanism of multidrug resistance *Staphylococcus aureus* NorA efflux pump using a supervised molecular dynamics approach. *International Journal of Molecular Sciences* **20**: 4041.
- PANTOSTI, A., SANCHINI, A. and MONACO, M.** (2007). Mechanisms of antibiotic resistance in *Staphylococcus aureus*. *Future Microbiology* **2**: 323-334.

- PANTSAR, T. and POSO, A.** (2018). Binding affinity via docking: fact and fiction. *Molecules* **23**: 1899.
- PAPALOUKAS, C., GRANSETH, E., VIKLUND, H. and ELOFSSON, A.** (2008). Estimating the length of transmembrane helices using Z-coordinate predictions. *Protein Science* **17**: 271-278.
- PASCUAL, J. M., WANG, D., YANG, R., SHI, L., YANG, H. and DARRYL, C.** (2008). Structural signatures and membrane helix 4 in GLUT1 inferences from human blood-brain glucose transport mutants. *The Journal of Biological Chemistry* **283**: 16732-16742.
- PASQUA, M., GROSSI, M., ZENNARO, A., FANELLI, G., MICHELI, G., BARRAS, F., COLONNA, B. and PROSEDA, G.** (2019). The varied role of efflux pumps of the MFS family in the interplay of bacteria with animal and plant cells. *Microorganisms* **7**: 285.
- PATEL, N., EXELL, J. C., JARDINE, E., OMBLER, B., FINGER, L. D., CIANI, B. and GRASBY, J. A.** (2013). Proline scanning mutagenesis reveals a role for the flap endonuclease-1 helical cap in substrate unpairing. *The Journal of Biological Chemistry* **288**: 34239-34248.
- PAUL, D., CHAKRABORTY, R. and MANDAL, S. M.** (2019). Biocides and health-care agents are more than just antibiotics: inducing cross to co-resistance in microbes. *Cotoxicology and Environmental Safety* **174**: 601-610.
- PAULSEN, I. T., BROWN, M. H., DUNSTAN, S. J. and SKURRAY, R. A.** (1995). Molecular characterization of the staphylococcal multidrug resistance export protein QacC. *Journal of Bacteriology* **177**: 2827-2833.
- PAULSEN, I. T., BROWN, M. H., LITTLEJOHN, T. G., MITCHELL, B. A. and SKURRAY, R. A.** (1996a). Multidrug resistance proteins QacA and QacB from *Staphylococcus aureus*: membrane topology and identification of residues involved in substrate specificity. *Proceedings of the National Academy of Sciences of the United States of America* **93**: 3630-3635.
- PAULSEN, I. T., BROWN, M. H. and SKURRAY, R. A.** (1996b). Proton-dependent multidrug efflux systems. *Microbiological Reviews* **60**: 575-608.
- PAULSEN, I. T., BROWN, M. H. and SKURRAY, R. A.** (1998). Characterization of the earliest known *Staphylococcus aureus* plasmid encoding a multidrug efflux system. *Journal of Bacteriology* **180**: 3477-3479.
- PAULSEN, I. T. and SKURRAY, R. A.** (1993). Topology, structure and evolution of two families of proteins involved in antibiotic and antiseptic resistance in eukaryotes and prokaryotes—an analysis. *Gene* **124**: 1-11.
- PAULSEN, I. T., SKURRAY, R. A., TAM, R., SAIER JR, M. H., TURNER, R. J., WEINER, J. H., GOLDBERG, E. B. and GRINIUS, L. L.** (1996c). The SMR family: a novel family of multidrug efflux proteins involved with the efflux of lipophilic drugs. *Molecular Microbiology* **19**: 1167-1175.

- PEACOCK, S. J. and PATERSON, G. K.** (2015). Mechanisms of methicillin resistance in *Staphylococcus aureus*. *Annual Review of Biochemistry* **84**: 577-601.
- PEDERSEN, B. P., KUMAR, H., WAIGHT, A. B., RISENMAY, A. J., ROE-ZURZ, Z., CHAU, B. H., SCHLESSINGER, A., BONOMI, M., HARRIES, W. and SALI, A.** (2013). Crystal structure of a eukaryotic phosphate transporter. *Nature* **496**: 533-536.
- PEREIRA, B. M. P. and TAGKOPOULOS, I.** (2019). Benzalkonium chlorides: uses, regulatory status, and microbial resistance. *Applied and Environmental Microbiology* **85**: e00377-19.
- PEREIRA, J. C., CAFFARENA, E. R. and DOS SANTOS, C. N.** (2016). Boosting docking-based virtual screening with deep learning. *Journal of Chemical Information and Modeling* **56**: 2495-2506.
- PETERS, K. M., BROOKS, B. E., SCHUMACHER, M. A., SKURRAY, R. A., BRENNAN, R. G. and BROWN, M. H.** (2011). A single acidic residue can guide binding site selection but does not govern QacR cationic-drug affinity. *PLoS One* **6**: e15974.
- PETERS, K. M., SCHUMAN, J. T., SKURRAY, R. A., BROWN, M. H., BRENNAN, R. G. and SCHUMACHER, M. A.** (2008). QacR-cation recognition is mediated by a redundancy of residues capable of charge neutralization. *Biochemistry* **47**: 8122-8129.
- PETTERSEN, E. F., GODDARD, T. D., HUANG, C. C., COUCH, G. S., GREENBLATT, D. M., MENG, E. C. and FERRIN, T. E.** (2004). UCSF Chimera—a visualization system for exploratory research and analysis. *Journal of Computational Chemistry* **25**: 1605-1612.
- PIDDOCK, L. J.** (2006a). Clinically relevant chromosomally encoded multidrug resistance efflux pumps in bacteria. *Clinical Microbiology Reviews* **19**: 382-402.
- PIDDOCK, L. J.** (2006b). Multidrug-resistance efflux pumps - not just for resistance. *Nature Reviews Microbiology* **4**: 629-636.
- POGET, S. F., HARRIS, R., CAHILL, S. M. and GIRVIN, M. E.** (2010). ¹H, ¹³C, ¹⁵N backbone NMR assignments of the *Staphylococcus aureus* small multidrug-resistance pump (Smr) in a functionally active conformation. *Biomolecular NMR assignments* **4**: 139-142.
- POLYAK, S. W., MOWLA, R. and VENTER, H.** (2020). Measuring small molecule binding to *Escherichia coli* AcrB by surface plasmon resonance. Labrou N. (eds) "Targeting Enzymes for Pharmaceutical Development. Methods in Molecular Biology" (Humana, New York), pp.119-130.
- POOLE, K.** (2002). Mechanisms of bacterial biocide and antibiotic resistance. *Journal of Applied Microbiology* **92 Suppl**: 55s-64s.
- POOLE, K.** (2004). Efflux-mediated multiresistance in Gram-negative bacteria. *Clinical Microbiology and Infection* **10**: 12-26.

- POOLE, K.** (2007). Efflux pumps as antimicrobial resistance mechanisms. *Annals of Medicine* **39**: 162-176.
- PRAX, M., LEE, C. Y. and BERTRAM, R.** (2013). An update on the molecular genetics toolbox for staphylococci. *Microbiology* **159**: 421-435.
- PURSLOW, J. A., KHATIWADA, B., BAYRO, M. J. and VENDITTI, V.** (2020). NMR methods for structural characterization of protein-protein complexes. *Frontiers in Molecular Biosciences* **7**: 9.
- PUTMAN, M., KOOLE, L. A., VAN VEEN, H. W. and KONINGS, W. N.** (1999). The secondary multidrug transporter LmrP contains multiple drug interaction sites. *Biochemistry* **38**: 13900-13905.
- PUTMAN, M., VAN VEEN, H. W. and KONINGS, W. N.** (2000). Molecular properties of bacterial multidrug transporters. *Microbiology and Molecular Biology Reviews* **64**: 672-693.
- QUICK, M., LOO, D. D. and WRIGHT, E. M.** (2001). Neutralization of a conserved amino acid residue in the human Na⁺/glucose transporter (hSGLT1) generates a glucose-gated H⁺ channel. *The Journal of Biological Chemistry* **276**: 1728-1734.
- QUISTGAARD, E. M., LÖW, C., GUETTOU, F. and NORDLUND, P.** (2016). Understanding transport by the major facilitator superfamily (MFS): structures pave the way. *Nature Reviews Molecular cell biology* **17**: 123-132.
- QUISTGAARD, E. M., LOW, C., MOBERG, P., TRESAUGUES, L. and NORDLUND, P.** (2013). Structural basis for substrate transport in the GLUT-homology family of monosaccharide transporters. *Nature Structural and Molecular Biology* **20**: 766-768.
- QUISTGAARD, E. M., MARTINEZ MOLLEDO, M. and LÖW, C.** (2017). Structure determination of a major facilitator peptide transporter: inward facing PepT_{St} from *Streptococcus thermophilus* crystallized in space group P3₁21. *PloS one* **12**: e0173126.
- QURESHI, N. K., YIN, S. and BOYLE-VAVRA, S.** (2014). The role of the Staphylococcal VraTSR regulatory system on vancomycin resistance and *vanA* operon expression in vancomycin-resistant *Staphylococcus aureus*. *PloS One* **9**: e85873.
- RADCHENKO, M., NIE, R. and LU, M.** (2016). Disulfide cross-linking of a multidrug and toxic compound extrusion transporter impacts multidrug efflux. *The Journal of Biological Chemistry* **291**: 9818-9826.
- RAJABI, S., SHIVAEI, A., KHOSRAVI, M. A., ESHAGHI, M., SHAHBAZI, S. and HOSSEINI, F.** (2020). Evaluation of multidrug efflux pump expression in clinical isolates of *Staphylococcus aureus*. *Gene Reports* **18**: 100537.

- RAJARATHNAM, K. and ROSGEN, J.** (2014). Isothermal titration calorimetry of membrane proteins - progress and challenges. *Biochimica et Biophysica Acta* **1838**: 69-77.
- RAMASWAMY, V. K., VARGIU, A. V., MALLOCI, G., DREIER, J. and RUGGERONE, P.** (2017). Molecular rationale behind the differential substrate specificity of bacterial RND multi-drug transporters. *Scientific Reports* **7**: 8075.
- RANAWEERA, I., SHRESTHA, U., RANJANA, K., KAKARLA, P., WILLMON, T. M., HERNANDEZ, A. J., MUKHERJEE, M. M., BARR, S. R. and VARELA, M. F.** (2015). Structural comparison of bacterial multidrug efflux pumps of the major facilitator superfamily. *Trends in Cell and Molecular Biology* **10**: 131-140.
- REDDY, V. S., SHLYKOV, M. A., CASTILLO, R., SUN, E. I. and SAIER, M. H., JR.** (2012). The major facilitator superfamily (MFS) revisited. *The FEBS Journal* **279**: 2022-2035.
- REES, D. C., JOHNSON, E. and LEWINSON, O.** (2009). ABC transporters: the power to change. *Nature Reviews Molecular Cell Biology* **10**: 218-227.
- REINHARD, A. and NURNBERGER, T.** (2017). Steady-state and kinetics-based affinity determination in effector-effector target interactions. *Methods in Molecular Biology* **1578**: 81-108.
- RENNER, L. D., ZAN, J., HU, L. I., MARTINEZ, M., RESTO, P. J., SIEGEL, A. C., TORRES, C., HALL, S. B., SLEZAK, T. R., NGUYEN, T. H. and WEIBEL, D. B.** (2017). Detection of ESKAPE bacterial pathogens at the point of care using isothermal DNA-based assays in a portable degas-actuated microfluidic diagnostic assay platform. *Applied and Environmental Microbiology* **83**: e02449-16.
- REYNOLDS, E., ROSS, J. I. and COVE, J. H.** (2003). Msr(A) and related macrolide/streptogramin resistance determinants: incomplete transporters? *International Journal of Antimicrobial Agents* **22**: 228-236.
- ROTHNIE, A., STORM, J., CAMPBELL, J., LINTON, K. J., KERR, I. D. and CALLAGHAN, R.** (2004). The topography of transmembrane segment six is altered during the catalytic cycle of P-glycoprotein. *The Journal of Biological Chemistry* **279**: 34913-34921.
- ROUCH, D. A., CRAM, D. S., DIBERARDINO, D., LITTLEJOHN, T. G. and SKURRAY, R. A.** (1990). Efflux-mediated antiseptic resistance gene *qacA* from *Staphylococcus aureus*: common ancestry with tetracycline- and sugar-transport proteins. *Molecular Microbiology* **4**: 2051-2062.
- ROY, A., KUCUKURAL, A. and ZHANG, Y.** (2010). I-TASSER: a unified platform for automated protein structure and function prediction. *Nature Protocols* **5**: 725-738.
- SAHU, I. D. and LORIGAN, G. A.** (2018). Site-directed spin labeling EPR for studying membrane proteins. *BioMed Research International* **2018**: 3248289.

- SAIER JR, M. H., REDDY, V. S., MORENO-HAGELSIEB, G., HENDARGO, K. J., ZHANG, Y., IDDAMSETTY, V., LAM, K. J. K., TIAN, N., RUSSUM, S. and WANG, J.** (2021). The Transporter Classification Database (TCDB): 2021 update. *Nucleic Acids Research* **49**: D461-D467.
- SAIER, M. H., JR.** (2003). Tracing pathways of transport protein evolution. *Molecular Microbiology* **48**: 1145-1156.
- SAIER, M. H., JR., REDDY, V. S., TAMANG, D. G. and VASTERMARK, A.** (2014). The transporter classification database. *Nucleic Acids Research* **42**: D251- D258.
- SAMBROOK, J. and RUSSELL, D. W.** (2006). "Storage of bacterial cultures growing in liquid media", (Cold Spring Harbor Laboratory Press, Cold Spring Harbor, New York), pdb.prot4452.
- SANTAJIT, S. and INDRAWATTANA, N.** (2016). Mechanisms of antimicrobial resistance in ESKAPE pathogens. *BioMed Research International* **2016**: 2475067.
- SARGISON, F. A. and FITZGERALD, J. R.** (2020). Advances in transposon mutagenesis of *Staphylococcus aureus*: insights into pathogenesis and antimicrobial resistance. *Trends in Microbiology* **29**: 282-285.
- SARKAR, P., YARLAGADDA, V., GHOSH, C. and HALDAR, J.** (2017). A review on cell wall synthesis inhibitors with an emphasis on glycopeptide antibiotics. *MedChemComm* **8**: 516-533.
- SASATSU, M., SHIMA, K., SHIBATA, Y. and KONO, M.** (1989). Nucleotide sequence of a gene that encodes resistance to ethidium bromide from a transferable plasmid in *Staphylococcus aureus*. *Nucleic Acids Research* **17**: 10103.
- SCALLAN, E., HOEKSTRA, R. M., ANGULO, F. J., TAUXE, R. V., WIDDOWSON, M.-A., ROY, S. L., JONES, J. L. and GRIFFIN, P. M.** (2011). Foodborne illness acquired in the United States—major pathogens. *Emerging Infectious Diseases* **17**: 7-15.
- SCHAEDLER, T. A. and VAN VEEN, H. W.** (2010). A flexible cation binding site in the multidrug major facilitator superfamily transporter LmrP is associated with variable proton coupling. *The FASEB Journal* **24**: 3653-3661.
- SCHERF, J. R., DOS SANTOS, C. R. B., DE FREITAS, T. S., ROCHA, J. E., MACÊDO, N. S., LIMA, J. N. M., COUTINHO, H. D. M. and DA CUNHA, F. A. B.** (2020). Effect of terpinolene against the resistant *Staphylococcus aureus* strain, carrier of the efflux pump QacC and β -lactamase gene, and its toxicity in the *Drosophila melanogaster* model. *Microbial Pathogenesis* **149**: 104528.
- SCHILCHER, K. and HORSWILL, A. R.** (2020). Staphylococcal biofilm development: structure, regulation, and treatment strategies. *Microbiology and Molecular Biology Reviews* **84**: e00026-19.

- SCHINDLER, B. D., JACINTO, P. and KAATZ, G. W.** (2013a). Inhibition of drug efflux pumps in *Staphylococcus aureus*: current status of potentiating existing antibiotics. *Future Microbiology* **8**: 491-507.
- SCHINDLER, B. D. and KAATZ, G. W.** (2016). Multidrug efflux pumps of Gram-positive bacteria. *Drug Resistance Updates* **27**: 1-13.
- SCHINDLER, B. D., PATEL, D., SEO, S. M. and KAATZ, G. W.** (2013b). Mutagenesis and modeling to predict structural and functional characteristics of the *Staphylococcus aureus* MepA multidrug efflux pump. *Journal of Bacteriology* **195**: 523-533.
- SCHITO, G. C.** (2006). The importance of the development of antibiotic resistance in *Staphylococcus aureus*. *Clinical Microbiology and Infection* **12 Suppl 1**: 3-8.
- SCHLESSINGER, A., WELCH, M. A., VAN VLIJMEN, H., KORZEKWA, K., SWAAN, P. W. and MATSSON, P.** (2018). Molecular modeling of drug–transporter interactions—an International Transporter Consortium perspective. *Clinical Pharmacology and Therapeutics* **104**: 818-835.
- SCHRADER-FISCHER, G. and BERGER-BACHI, B.** (2001). The AbcA transporter of *Staphylococcus aureus* affects cell autolysis. *Antimicrobial Agents and Chemotherapy* **45**: 407-412.
- SCHULLER, J. M., BIRRELL, J. A., TANAKA, H., KONUMA, T., WULFHORST, H., COX, N., SCHULLER, S. K., THIEMANN, J., LUBITZ, W. and SÉTIF, P.** (2019). Structural adaptations of photosynthetic complex I enable ferredoxin-dependent electron transfer. *Science* **363**: 257-260.
- SCHUMACHER, M. A., MILLER, M. C. and BRENNAN, R. G.** (2004). Structural mechanism of the simultaneous binding of two drugs to a multidrug-binding protein. *EMBO Journal* **23**: 2923-2930.
- SCHUMACHER, M. A., MILLER, M. C., GRKOVIC, S., BROWN, M. H., SKURRAY, R. A. and BRENNAN, R. G.** (2001). Structural mechanisms of QacR induction and multidrug recognition. *Science* **294**: 2158-2163.
- SCHUMACHER, M. A., MILLER, M. C., GRKOVIC, S., BROWN, M. H., SKURRAY, R. A. and BRENNAN, R. G.** (2002). Structural basis for cooperative DNA binding by two dimers of the multidrug-binding protein QacR. *EMBO Journal* **21**: 1210-1218.
- SEIDEL, S. A., DIJKMAN, P. M., LEA, W. A., VAN DEN BOGAART, G., JERABEK-WILLEMSSEN, M., LAZIC, A., JOSEPH, J. S., SRINIVASAN, P., BAASKE, P., SIMEONOV, A., KATRITCH, I., MELO, F. A., LADBURY, J. E., SCHREIBER, G., WATTS, A., BRAUN, D. and DUHR, S.** (2013). Microscale thermophoresis quantifies biomolecular interactions under previously challenging conditions. *Methods* **59**: 301-315.
- SENN, L., CLERC, O., ZANETTI, G., BASSET, P., PROD'HOM, G., GORDON, N. C., SHEPPARD, A. E., CROOK, D. W., JAMES, R., THORPE, H. A., FEIL, E. J. and**

- BLANC, D. S.** (2016). The stealthy superbug: the role of asymptomatic enteric carriage in maintaining a long-term hospital outbreak of ST228 methicillin-resistant *Staphylococcus aureus*. *mBio* **7**: e02039-15.
- SEUKEP, A. J., KUETE, V., NAHAR, L., SARKER, S. D. and GUO, M.** (2020). Plant-derived secondary metabolites as the main source of efflux pump inhibitors and methods for identification. *Journal of Pharmaceutical Analysis* **10**: 277-290.
- SHARMA, A., GUPTA, V. K. and PATHANIA, R.** (2019). Efflux pump inhibitors for bacterial pathogens: from bench to bedside. *Indian Journal of Medical Research* **149**: 129-145.
- SHAROM, F. J.** (2014). Complex interplay between the P-glycoprotein multidrug efflux pump and the membrane: Its role in modulating protein function. *Frontiers in Oncology* **4**: 41.
- SHATSKY, M., NUSSINOV, R. and WOLFSON, H. J.** (2008). Algorithms for multiple protein structure alignment and structure-derived multiple sequence alignment. Zaki M.J., Bystroff C. (eds) "Protein Structure Prediction. Methods in Molecular Biology" (Humana Press), pp. 125-146.
- SHCHERBAKOV, A. A., HISAO, G., MANDALA, V. S., THOMAS, N. E., SOLTANI, M., SALTER, E., DAVIS, J. H., HENZLER-WILDMAN, K. A. and HONG, M.** (2021). Structure and dynamics of the drug-bound bacterial transporter EmrE in lipid bilayers. *Nature Communications* **12**: 1-13.
- SHENG, W. H., WANG, J. T., LAUDERDALE, T. L., WENG, C. M., CHEN, D. and CHANG, S. C.** (2009). Epidemiology and susceptibilities of methicillin-resistant *Staphylococcus aureus* in Taiwan: emphasis on chlorhexidine susceptibility. *Diagnostic Microbiology and Infectious Disease* **63**: 309-313.
- SHI, Y.** (2013). Common folds and transport mechanisms of secondary active transporters. *Annual Review of Biophysics* **42**: 51-72.
- SHOEMAKER, S. C. and ANDO, N.** (2018). X-rays in the cryo-electron microscopy era: structural biology's dynamic future. *Biochemistry* **57**: 277-285.
- SHORT, F. L., LIU, Q., ASHWOOD, H. E., NAIDU, V., LI, L., MABBUTT, B. C., HASSAN, K. A. and PAULSEN, I. T.** (2020). Spermidine and spermine are the natural substrates of the *Acinetobacter baumannii* AmvA multidrug efflux pump. *bioRxiv* DOI: 10.1101/2020.10.02.324624.
- SIEVERS, F., WILM, A., DINEEN, D., GIBSON, T. J., KARPLUS, K., LI, W., LOPEZ, R., MCWILLIAM, H., REMMERT, M. and SÖDING, J.** (2011). Fast, scalable generation of high-quality protein multiple sequence alignments using Clustal Omega. *Molecular Systems Biology* **7**: 539.
- SIGAL, N., VARDY, E., MOLSHANSKI-MOR, S., EITAN, A., PILPEL, Y., SCHULDINER, S. and BIBI, E.** (2005). 3D model of the *Escherichia coli* multidrug transporter

MdfA reveals an essential membrane-embedded positive charge. *Biochemistry* **44**: 14870-14880.

SILTBERG-LIBERLES, J., GRAHNEN, J. A. and LIBERLES, D. A. (2011). The evolution of protein structures and structural ensembles under functional constraint. *Genes* **2**: 748-762.

SINGH, S., KALIA, N. P., JOSHI, P., KUMAR, A., SHARMA, P. R., KUMAR, A., BHARATE, S. B. and KHAN, I. A. (2017). Boeravinone B, a novel dual inhibitor of NorA bacterial efflux pump of *Staphylococcus aureus* and human P-glycoprotein, reduces the biofilm formation and intracellular invasion of bacteria. *Frontiers in Microbiology* **8**: 1868.

SIRIJATUPHAT, R., SRIPANIDKULCHAI, K., BOONYASIRI, A., RATTANAUMPAWAN, P., SUPAPUENG, O., KIRATISIN, P. and THAMLIKITKUL, V. (2018). Implementation of global antimicrobial resistance surveillance system (GLASS) in patients with bacteremia. *PLoS One* **13**: e0190132.

SJUTS, H., VARGIU, A. V., KWASNY, S. M., NGUYEN, S. T., KIM, H.-S., DING, X., ORNIK, A. R., RUGGERONE, P., BOWLIN, T. L. and NIKAIDO, H. (2016). Molecular basis for inhibition of AcrB multidrug efflux pump by novel and powerful pyranopyridine derivatives. *Proceedings of the National Academy of Sciences of the United States of America* **113**: 3509-3514.

SMITH, K., GEMMELL, C. G. and HUNTER, I. S. (2008). The association between biocide tolerance and the presence or absence of *qac* genes among hospital-acquired and community-acquired MRSA isolates. *The Journal of Antimicrobial Chemotherapy* **61**: 78-84.

SNELL, S. B., GILL, A. L., HAIDARIS, C. G., FOSTER, T. H., BARAN, T. M. and GILL, S. R. (2021). *Staphylococcus aureus* tolerance and genomic response to photodynamic inactivation. *MSphere* **6**: e00762-20.

SOLCAN, N., KWOK, J., FOWLER, P. W., CAMERON, A. D., DREW, D., IWATA, S. and NEWSTEAD, S. (2012). Alternating access mechanism in the POT family of oligopeptide transporters. *EMBO Journal* **31**: 3411-3421.

SPAULDING, A. R., SALGADO-PABON, W., KOHLER, P. L., HORSWILL, A. R., LEUNG, D. Y. and SCHLIEVERT, P. M. (2013). Staphylococcal and streptococcal superantigen exotoxins. *Clinical Microbiology Reviews* **26**: 422-447.

STARACE, D. M. and BEZANILLA, F. (2001). Histidine scanning mutagenesis of basic residues of the S4 segment of the shaker K⁺ channel. *The Journal of General Physiology* **117**: 469-490.

STARON, P., FORCHHAMMER, K. and MALDENER, I. (2014). Structure-function analysis of the ATP-driven glycolipid efflux pump DevBCA reveals complex organization with TolC/HgdD. *FEBS Letters* **588**: 395-400.

STEED, P. R., ZOU, P., TRONE, K. E. and MCHAOUB, H. S. (2013). Structure and pH-induced structural rearrangements of the putative multidrug efflux pump

EmrD in liposomes probed by site-directed spin labeling. *Biochemistry* **52**: 7964-7974.

STIERAND, K. and RAREY, M. (2010). PoseView--molecular interaction patterns at a glance. *Journal of Cheminformatics* **2**: 50.

STOFFREGEN, M. C., SCHWER, M. M., RENSCHLER, F. A. and WIESNER, S. (2012). Methionine scanning as an NMR tool for detecting and analyzing biomolecular interaction surfaces. *Structure* **20**: 573-581.

SU, Y. W. and WANG, W. (2018). Surface plasmon resonance sensing: from purified biomolecules to intact cells. *Analytical and Bioanalytical Chemistry* **410**: 3943-3951.

SUN, J., DENG, Z. AND YAN, A. (2014). Bacterial multidrug efflux pumps: mechanisms, physiology and pharmacological exploitations. *Biochemical and Biophysical Research Communications* **453**: 254-267.

TAKATSUKA, Y. and NIKAIDO, H. (2006). Threonine-978 in the transmembrane segment of the multidrug efflux pump AcrB of *Escherichia coli* is crucial for drug transport as a probable component of the proton relay network. *Journal of Bacteriology* **188**: 7284-7289.

TAMURA, N., KONISHI, S., IWAKI, S., KIMURA-SOMEYA, T., NADA, S. and YAMAGUCHI, A. (2001). Complete cysteine-scanning mutagenesis and site-directed chemical modification of the Tn10-encoded metal-tetracycline/H⁺ antiporter. *The Journal of Biological Chemistry* **276**: 20330-20339.

TANABE, M., SZAKONYI, G., BROWN, K. A., HENDERSON, P. J., NIELD, J. and BYRNE, B. (2009). The multidrug resistance efflux complex, EmrAB from *Escherichia coli* forms a dimer *in vitro*. *Biochemical and Biophysical Research Communications* **380**: 338-342.

TANAKA, Y., HIPOLITO, C. J., MATURANA, A. D., ITO, K., KURODA, T., HIGUCHI, T., KATOH, T., KATO, H. E., HATTORI, M., KUMAZAKI, K., TSUKAZAKI, T., ISHITANI, R., SUGA, H. and NUREKI, O. (2013). Structural basis for the drug extrusion mechanism by a MATE multidrug transporter. *Nature* **496**: 247-251.

TANG, Q. and FENTON, A. W. (2017). Whole-protein alanine-scanning mutagenesis of allostery: a large percentage of a protein can contribute to mechanism. *Human Mutation* **38**: 1132-1143.

TEIXEIRA, C. F., PEREIRA, T. B., MIYAZAKI, N. H. and VILLAS BOAS, M. H. (2010). Widespread distribution of *qacA/B* gene among coagulase-negative *Staphylococcus spp.* in Rio de Janeiro, Brazil. *The Journal of Hospital Infection* **75**: 333-334.

TENNENT, J. M., LYON, B. R., GILLESPIE, M. T., MAY, J. W. and SKURRAY, R. A. (1985). Cloning and expression of *Staphylococcus aureus* plasmid-mediated quaternary ammonium resistance in *Escherichia coli*. *Antimicrobial Agents and Chemotherapy* **27**: 79-83.

- THURLOW, B., DAVIS, J. H., LEONG, V., MORAES, T. F., WILLIAMSON, J. R. and ORTEGA, J.** (2016). Binding properties of YjeQ (RsgA), RbfA, RimM and Era to assembly intermediates of the 30S subunit. *Nucleic Acids Research* **44**: 9918-9932.
- TIEN, M. Z., MEYER, A. G., SYDYKOVA, D. K., SPIELMAN, S. J. and WILKE, C. O.** (2013). Maximum allowed solvent accessibilities of residues in proteins. *PLoS One* **8**: e80635.
- TIROSH, O., SIGAL, N., GELMAN, A., SAHAR, N., FLUMAN, N., SIEMION, S. and BIBI, E.** (2012). Manipulating the drug/proton antiport stoichiometry of the secondary multidrug transporter MdfA. *Proceedings of the National Academy of Sciences of the United States of America* **109**: 12473-12478.
- TONG, S. Y., DAVIS, J. S., EICHENBERGER, E., HOLLAND, T. L. and FOWLER, V. G., JR.** (2015). *Staphylococcus aureus* infections: epidemiology, pathophysiology, clinical manifestations, and management. *Clinical Microbiology Reviews* **28**: 603-661.
- TORRENS-FONTANALS, M., STEPNIEWSKI, T. M., ARANDA-GARCÍA, D., MORALES-PASTOR, A., MEDEL-LACRUZ, B. and SELENT, J.** (2020). How do molecular dynamics data complement static structural data of GPCRs. *International Journal of Molecular Sciences* **21**: 5933.
- TOUATI, A., BELLIL, Z., BARACHE, D. and MAIRI, A.** (2021). Fitness cost of antibiotic resistance in *Staphylococcus aureus*: a systematic review. *Microbial Drug Resistance*.
- Trahey, M., Li, M. J., Kwon, H., Woodahl, E. L., McClary, W. D. and Atkins, W. M.** (2015). Applications of lipid nanodiscs for the study of membrane proteins by surface plasmon resonance. *Current Protocols in Protein Science* **81**: 29.13.21-29.13.16.
- TROTT, O. and OLSON, A. J.** (2010). AutoDock Vina: improving the speed and accuracy of docking with a new scoring function, efficient optimization, and multithreading. *Journal of Computational Chemistry* **31**: 455-461.
- TRUONG-BOLDUC, Q., BOLDUC, G., MEDEIROS, H., VYAS, J., WANG, Y. and HOOPER, D.** (2015). Role of the Tet38 efflux pump in *Staphylococcus aureus* internalization and survival in epithelial cells. *Infection and Immunity* **83**: 4362-4372.
- TRUONG-BOLDUC, Q., DUNMAN, P., STRAHILEVITZ, J., PROJAN, S. and HOOPER, D.** (2005). MgrA is a multiple regulator of two new efflux pumps in *Staphylococcus aureus*. *Journal of Bacteriology* **187**: 2395-2405.
- TRUONG-BOLDUC, Q., WANG, Y. and HOOPER, D.** (2018). Tet38 efflux pump contributes to fosfomycin resistance in *Staphylococcus aureus*. *Antimicrobial Agents and Chemotherapy* **62**: e00927-18.

- TRUONG-BOLDUC, Q., WANG, Y. and HOOPER, D.** (2019). Tet38 of *Staphylococcus aureus* binds to host cell receptor complex CD36–Toll-like receptor 2 and protects from teichoic acid synthesis inhibitors tunicamycin and Congo red. *Infection and Immunity* **87**: e00194-19.
- TRUONG-BOLDUC, Q., WANG, Y. and HOOPER, D.** (2021). *Staphylococcus aureus* Tet38 efflux pump structural modeling and roles of essential residues in drug efflux and host cell internalization. *Infection and Immunity* **89**: e00811-20.
- TRUONG-BOLDUC, Q. C. and HOOPER, D. C.** (2010). Phosphorylation of MgrA and its effect on expression of the NorA and NorB efflux pumps of *Staphylococcus aureus*. *Journal of Bacteriology* **192**: 2525-2534.
- TRUONG-BOLDUC, Q. C., HSING, L. C., VILLET, R., BOLDUC, G. R., ESTABROOKS, Z., TAGUEZEM, G. F. and HOOPER, D. C.** (2012). Reduced aeration affects the expression of the NorB efflux pump of *Staphylococcus aureus* by posttranslational modification of MgrA. *Journal of Bacteriology* **194**: 1823-1834.
- TRUONG-BOLDUC, Q. C., STRAHILEVITZ, J. and HOOPER, D. C.** (2006). NorC, a new efflux pump regulated by MgrA of *Staphylococcus aureus*. *Antimicrobial Agents and Chemotherapy* **50**: 1104-1107.
- TRUONG-BOLDUC, Q. C., VILLET, R. A., ESTABROOKS, Z. A. and HOOPER, D. C.** (2014). Native efflux pumps contribute resistance to antimicrobials of skin and the ability of *Staphylococcus aureus* to colonize skin. *The Journal of Infectious Diseases* **209**: 1485-1493.
- TŮRKOVÁ, A. and ZDRAZIL, B.** (2019). Current advances in studying clinically relevant transporters of the solute carrier (SLC) family by connecting computational modeling and data science. *Computational and Structural Biotechnology Journal* **17**: 390-405.
- UEHARA, Y., SASAKI, T., BABA, T., LU, Y., IMAJO, E., SATO, Y., TANNO, S., FURUICHI, M., KAWADA, M. and HIRAMATSU, K.** (2019). Regional outbreak of community-associated methicillin-resistant *Staphylococcus aureus* ST834 in Japanese children. *BMC Infectious Diseases* **19**: 35.
- UVERSKY, V. N.** (2015). The intrinsic disorder alphabet. III. Dual personality of serine. *Intrinsically Disordered Proteins* **3**: e1027032.
- VALI, L., DAVIES, S. E., LAI, L. L., DAVE, J. and AMYES, S. G.** (2008). Frequency of biocide resistance genes, antibiotic resistance and the effect of chlorhexidine exposure on clinical methicillin-resistant *Staphylococcus aureus* isolates. *The Journal of Antimicrobial Chemotherapy* **61**: 524-532.
- VAN GEEST, M. and LOLKEMA, J. S.** (2000). Membrane topology and insertion of membrane proteins: search for topogenic signals. *Microbiology and Molecular Biology Reviews* **64**: 13-33.

- VANGONE, A. and BONVIN, A. M.** (2015). Contacts-based prediction of binding affinity in protein–protein complexes. *elife* **4**: e07454.
- VARDY, E., ARKIN, I. T., GOTTSCHALK, K. E., KABACK, H. R. and SCHULDINER, S.** (2004). Structural conservation in the major facilitator superfamily as revealed by comparative modeling. *Protein Science* **13**: 1832-40.
- VARELA, M. F., ANDERSEN, J. L., RANJANA, K., KUMAR, S., SANFORD, L. M. and HERNANDEZ, A. J.** (2017). Bacterial resistance mechanisms and inhibitors of multidrug efflux pumps belonging to the major facilitator superfamily of solute transport systems. "Frontiers in Anti-Infective Drug Discovery" (Bentham Science Publishers), pp.109-131.
- VARELA, M. F., SANSOM, C. E. and GRIFFITH, J. K.** (1995). Mutational analysis and molecular modelling of an amino acid sequence motif conserved in antiporters but not symporters in a transporter superfamily. *Molecular Membrane Biology* **12**: 313-319.
- VELAMAKANNI, S., YAO, Y., GUTMANN, D. A. and VAN VEEN, H. W.** (2008). Multidrug transport by the ABC transporter Sav1866 from *Staphylococcus aureus*. *Biochemistry* **47**: 9300-9308.
- VÉNIEN-BRYAN, C., LI, Z., VUILLARD, L. and BOUTIN, J. A.** (2017). Cryo-electron microscopy and X-ray crystallography: complementary approaches to structural biology and drug discovery. *Acta Crystallographica Section F Structural Biology Communications* **73**: 174-183.
- VENKO, K., CHOUDHURY, A. R. and NOVIČ, M.** (2017). Computational approaches for revealing the structure of membrane transporters: case study on bilitranslocase. *Computational and Structural Biotechnology Journal* **15**: 232-242.
- VENTER, H.** (2019). Reversing resistance to counter antimicrobial resistance in the World Health Organisation's critical priority of most dangerous pathogens. *Bioscience Reports* **39**: BSR20180474.
- VENTER, H., HENNINGSEN, M. L. and BEGG, S. L.** (2017). Antimicrobial resistance in healthcare, agriculture and the environment: the biochemistry behind the headlines. *Essays in Biochemistry* **61**: 1-10.
- VIJAYAKUMAR, R. and SANDLE, T.** (2019). A review on biocide reduced susceptibility due to plasmid-borne antiseptic-resistant genes—special notes on pharmaceutical environmental isolates. *Journal of Applied Microbiology* **126**: 1011-1022.
- VILLET, R. A., TRUONG-BOLDUC, Q. C., WANG, Y., ESTABROOKS, Z., MEDEIROS, H. and HOOPER, D. C.** (2014). Regulation of expression of *abcA* and its response to environmental conditions. *Journal of Bacteriology* **196**: 1532-1539.
- VIMBERG, V., CAVANAGH, J. P., NOVOTNA, M., LENART, J., NGOC, B. N. T., VESELA, J., PAIN, M., KOBERSKA, M. and NOVOTNA, G. B.** (2020). Ribosome-mediated

attenuation of *vga (A)* expression is shaped by the antibiotic resistance specificity of Vga (A) protein variants. *Antimicrobial Agents and Chemotherapy* **64**: e00666-20.

- VISHWAKARMA, P., BANERJEE, A., PASRIJA, R., PRASAD, R. and LYNN, A. M.** (2018). Phylogenetic and conservation analyses of MFS transporters. *3 Biotech* **8**: 462.
- VIVIAN, D. and POLLI, J. E.** (2014). Mechanistic interpretation of conventional Michaelis–Menten parameters in a transporter system. *European Journal of Pharmaceutical Sciences* **64**: 44-52.
- WAND, M. E., JAMSHIDI, S., BOCK, L. J., RAHMAN, K. M. and SUTTON, J. M.** (2019). SmvA is an important efflux pump for cationic biocides in *Klebsiella pneumoniae* and other Enterobacteriaceae. *Scientific Reports* **9**: 1-11.
- WANG, C., CAI, P., ZHAN, Q., MI, Z., HUANG, Z. and CHEN, G.** (2008a). Distribution of antiseptic-resistance genes *qacA/B* in clinical isolates of methicillin-resistant *Staphylococcus aureus* in China. *The Journal of Hospital Infection* **69**: 393-394.
- WANG, F., ZHOU, H., OLADEMEHIN, O. P., KIM, S. J. and TAO, P.** (2018). Insights into key interactions between vancomycin and bacterial cell wall structures. *ACS Omega* **3**: 37-45.
- WANG, J., JIAO, H., MENG, J., QIAO, M., DU, H., HE, M., MING, K., LIU, J., WANG, D. and WU, Y.** (2019). Baicalin inhibits biofilm formation and the quorum-sensing system by regulating the MsrA drug efflux pump in *Staphylococcus saprophyticus*. *Frontiers in Microbiology* **10**: 2800.
- WANG, J., XUE, J., DONG, X., YU, Q., BAKER, S. N., WANG, M. and HUANG, H.** (2020a). Antimicrobial properties of benzalkonium chloride derived polymerizable deep eutectic solvent. *International Journal of Pharmaceutics* **575**: 119005.
- WANG, J. T., SHENG, W. H., WANG, J. L., CHEN, D., CHEN, M. L., CHEN, Y. C. and CHANG, S. C.** (2008b). Longitudinal analysis of chlorhexidine susceptibilities of nosocomial methicillin-resistant *Staphylococcus aureus* isolates at a teaching hospital in Taiwan. *The Journal of Antimicrobial Chemotherapy* **62**: 514-517.
- WANG, Q. and KABACK, H. R.** (1999). Location of helix III in the lactose permease of *Escherichia coli* as determined by site-directed thiol cross-linking. *Biochemistry* **38**: 16777-16782.
- WANG, S. C., DAVEJAN, P., HENDARGO, K. J., JAVADI-RAZAZ, I., CHOU, A., YEE, D. C., GHAZI, F., LAM, K. J. K., CONN, A. M. and MADRIGAL, A.** (2020b). Expansion of the Major Facilitator Superfamily (MFS) to include novel transporters as well as transmembrane-acting enzymes. *Biochimica et Biophysica Acta-Biomembranes* **1862**: 183277.
- WANG, W., GUFFANTI, A. A., WEI, Y., ITO, M. and KRULWICH, T. A.** (2000). Two types of *Bacillus subtilis tetA(L)* deletion strains reveal the physiological importance

of TetA (L) in K⁺ acquisition as well as in Na⁺, alkali, and tetracycline resistance. *Journal of Bacteriology* **182**: 2088-2095.

WANG, Y., VENTER, H. and MA, S. (2016). Efflux pump inhibitors: a novel approach to combat efflux-mediated drug resistance in bacteria. *Current Drug Targets* **17**: 702-719.

WASSENAAR, T. M., USSERY, D., NIELSEN, L. N. and INGMER, H. (2015). Review and phylogenetic analysis of *qac* genes that reduce susceptibility to quaternary ammonium compounds in *Staphylococcus* species. *European Journal of Microbiology and Immunology* **5**: 44-61.

WASSENAAR, T. M., USSERY, D. W. and INGMER, H. (2016). The *qacC* gene has recently spread between rolling circle plasmids of *Staphylococcus*, indicative of a novel gene transfer mechanism. *Frontiers in Microbiology* **7**: 1528.

WEBBER, M. A. and PIDDOCK, L. J. (2003). The importance of efflux pumps in bacterial antibiotic resistance. *The Journal of Antimicrobial Chemotherapy* **51**: 9-11.

WEBER, D. J., RUTALA, W. A. and SICKBERT-BENNETT, E. E. (2019). Use of germicides in health care settings—is there a relationship between germicide use and antimicrobial resistance: a concise review. *American Journal of Infection Control* **47**: A106-A109.

WEIDENMAIER, C., GOERKE, C. and WOLZ, C. (2012). *Staphylococcus aureus* determinants for nasal colonization. *Trends in Microbiology* **20**: 243-250.

WEIGEL, L. M., CLEWELL, D. B., GILL, S. R., CLARK, N. C., MCDUGAL, L. K., FLANNAGAN, S. E., KOLONAY, J. F., SHETTY, J., KILLGORE, G. E. and TENOVER, F. C. (2003). Genetic analysis of a high-level vancomycin-resistant isolate of *Staphylococcus aureus*. *Science* **302**: 1569-1571.

WEINGLASS, A. B., SMIRNOVA, I. N. and KABACK, H. R. (2001). Engineering conformational flexibility in the lactose permease of *Escherichia coli*: use of glycine-scanning mutagenesis to rescue mutant Glu325-->Asp. *Biochemistry* **40**: 769-776.

WEINSTEIN, J. Y., ELAZAR, A. and FLEISHMAN, S. J. (2019). A lipophilicity-based energy function for membrane-protein modelling and design. *PLOS Computational Biology* **15**: e1007318.

WELCH, A., AWAH, C. U., JING, S. H., VAN VEEN, H. W. and VENTER, H. (2010). Promiscuous partnering and independent activity of MexB, the multidrug transporter protein from *Pseudomonas aeruginosa*. *Biochemical Journal* **430**: 355-364.

WERNLI, D., JORGENSEN, P. S., MOREL, C. M., CARROLL, S., HARBARTH, S., LEVRAT, N. and PITTET, D. (2017). Mapping global policy discourse on antimicrobial resistance. *BMJ Global Health* **2**: e000378.

- WHO** (2018). Antibiotic resistance: fact sheets (Accessed: 5 Feb 2018). <http://www.who.int/mediacentre/factsheets/antibiotic-resistance/en/>.
- WIENKEN, C. J., BAASKE, P., ROTHBAUER, U., BRAUN, D. and DUHR, S.** (2010). Protein-binding assays in biological liquids using microscale thermophoresis. *Nature Communications* **1**: 100.
- WOLIN, C. D. and KABACK, H. R.** (2000). Thiol cross-linking of transmembrane domains IV and V in the lactose permease of *Escherichia coli*. *Biochemistry* **39**: 6130-6135.
- WRIGHT, G. D.** (2016). Antibiotic adjuvants: rescuing antibiotics from resistance. *Trends in Microbiology* **24**: 862-871.
- WU, D., LU, R., CHEN, Y., QIU, J., DENG, C. and TAN, Q.** (2016). Study of cross-resistance mediated by antibiotics, chlorhexidine and *Rhizoma coptidis* in *Staphylococcus aureus*. *Journal of Global Antimicrobial Resistance* **7**: 61-66.
- WU, H. H., SYMERSKY, J. and LU, M.** (2019). Structure of an engineered multidrug transporter MdfA reveals the molecular basis for substrate recognition. *Communications Biology* **2**: 210.
- WU, H. H., SYMERSKY, J. and LU, M.** (2020). Structure and mechanism of a redesigned multidrug transporter from the Major Facilitator Superfamily. *Scientific Reports* **10**: 3949.
- WU, J., HASSAN, K. A., SKURRAY, R. A. and BROWN, M. H.** (2008). Functional analyses reveal an important role for tyrosine residues in the staphylococcal multidrug efflux protein QacA. *BMC Microbiology* **8**: 147.
- XIA, J., GAO, J. and TANG, W.** (2016). Nosocomial infection and its molecular mechanisms of antibiotic resistance. *Bioscience Trends* **10**: 14-21.
- XU, D. and ZHANG, Y.** (2011). Improving the physical realism and structural accuracy of protein models by a two-step atomic-level energy minimization. *Biophysical Journal* **101**: 2525-2534.
- XU, Z., O'ROURKE, B. A., SKURRAY, R. A. and BROWN, M. H.** (2006). Role of transmembrane segment 10 in efflux mediated by the staphylococcal multidrug transport protein QacA. *The Journal of Biological Chemistry* **281**: 792-799.
- XUE, L. C., RODRIGUES, J. P., KASTRITIS, P. L., BONVIN, A. M. and VANGONE, A.** (2016). PRODIGY: a web server for predicting the binding affinity of protein-protein complexes. *Bioinformatics* **32**: 3676-3678.
- YAFFE, D., RADESTOCK, S., SHUSTER, Y., FORREST, L. R. and SCHULDINER, S.** (2013). Identification of molecular hinge points mediating alternating access in the vesicular monoamine transporter VMAT2. *Proceedings of the National Academy of Sciences of the United States of America* **110**: E1332-E1341.

- YAMADA, Y., HIDEKA, K., SHIOTA, S., KURODA, T. and TSUCHIYA, T.** (2006a). Gene cloning and characterization of SdrM, a chromosomally-encoded multidrug efflux pump, from *Staphylococcus aureus*. *Biological and Pharmaceutical Bulletin* **29**: 554-556.
- YAMADA, Y., SHIOTA, S., MIZUSHIMA, T., KURODA, T. and TSUCHIYA, T.** (2006b). Functional gene cloning and characterization of MdeA, a multidrug efflux pump from *Staphylococcus aureus*. *Biological and Pharmaceutical bulletin* **29**: 801-804.
- YAMAGUCHI, A., NAKASHIMA, R. and SAKURAI, K.** (2015). Structural basis of RND-type multidrug exporters. *Frontiers in Microbiology* **6**: 327.
- YAMAGUCHI, A., SOMEYA, Y. and SAWAI, T.** (1992). Metal-tetracycline/H⁺ antiporter of *Escherichia coli* encoded by transposon Tn10. The role of a conserved sequence motif, GXXXXRXGRR, in a putative cytoplasmic loop between helices 2 and 3. *The Journal of Biological Chemistry* **267**: 19155-19162.
- YAN, H., HUANG, W., YAN, C., GONG, X., JIANG, S., ZHAO, Y., WANG, J. and SHI, Y.** (2013). Structure and mechanism of a nitrate transporter. *Cell Reports* **3**: 716-723.
- YAN, N.** (2013). Structural advances for the major facilitator superfamily (MFS) transporters. *Trends in Biochemical Sciences* **38**: 151-159.
- YAN, N.** (2015). Structural biology of the major facilitator superfamily transporters. *Annual Review of Biophysics* **44**: 257-283.
- YANG, J., YAN, R., ROY, A., XU, D., POISSON, J. and ZHANG, Y.** (2015). The I-TASSER Suite: protein structure and function prediction. *Nature Methods* **12**: 7-8.
- YANG, J. and ZHANG, Y.** (2015). Protein structure and function prediction using I-TASSER. *Current Protocols in Bioinformatics* **52**: 5.8.1-5.8.15.
- YARDENI, E. H., BAHRENBURG, T., STEIN, R. A., MISHRA, S., ZOMOT, E., GRAHAM, B., TUCK, K. L., HUBER, T., BIBI, E. and MCHAOURAB, H. S.** (2019). Probing the solution structure of the *E. coli* multidrug transporter MdfA using DEER distance measurements with nitroxide and Gd (III) spin labels. *Scientific Reports* **9**: 1-14.
- YARDENI, E. H., MISHRA, S., STEIN, R. A., BIBI, E. and MCHAOURAB, H. S.** (2020). The multidrug transporter MdfA deviates from the canonical model of alternating access of MFS Transporters. *Journal of Molecular Biology* **432**: 5665-5680.
- YARDENI, E. H., ZOMOT, E. and BIBI, E.** (2018). The fascinating but mysterious mechanistic aspects of multidrug transport by MdfA from *Escherichia coli*. *Research in Microbiology* **169**: 455-460.
- YEAMAN, M. R., TANG, Y. Q., SHEN, A. J., BAYER, A. S. and SELSTED, M. E.** (1997). Purification and *in vitro* activities of rabbit platelet microbicidal proteins. *Infection and Immunity* **65**: 1023-1031.

- YEN, P. and PAPIN, J. A.** (2017). History of antibiotic adaptation influences microbial evolutionary dynamics during subsequent treatment. *PLoS Biology* **15**: e2001586.
- YIN, Y., HE, X., SZEWCZYK, P., NGUYEN, T. and CHANG, G.** (2006). Structure of the multidrug transporter EmrD from *Escherichia coli*. *Science* **312**: 741-744.
- YOSHIDA, H., BOGAKI, M., NAKAMURA, S., UBUKATA, K. and KONNO, M.** (1990). Nucleotide sequence and characterization of the *Staphylococcus aureus* *norA* gene, which confers resistance to quinolones. *Journal of Bacteriology* **172**: 6942-6949.
- YOUSEFIAN, N., ORNIK-CHA, A., POUSSARD, S., DECOSSAS, M., BERBON, M., DAURY, L., TAVEAU, J.-C., DUPUY, J.-W., ĐORĐEVIĆ-MARQUARDT, S. and LAMBERT, O.** (2020). Structural characterization of the EmrAB-TolC efflux complex from *E. coli*. *Biochimica et Biophysica Acta-Biomembranes* **1863**: 183488.
- YU, J. L., GRINIUS, L. and HOOPER, D. C.** (2002). NorA functions as a multidrug efflux protein in both cytoplasmic membrane vesicles and reconstituted proteoliposomes. *Journal of Bacteriology* **184**: 1370-1377.
- YU, K., YANG, G. and LABAHN, J.** (2017). High-efficient production and biophysical characterisation of nicastrin and its interaction with APPC100. *Scientific Reports* **7**: 44297.
- ZAKI, M. E. S., BASTAWY, S. and MONTASSER, K.** (2019). Molecular study of resistance of *Staphylococcus aureus* to antiseptic quaternary ammonium compounds. *Journal of Global Antimicrobial Resistance* **17**: 94-97.
- ZAMUDIO, R., OGGIONI, M. R., GOULD, I. M. and HIJAZI, K.** (2019). Time for biocide stewardship? *Nature Microbiology* **4**: 732-733.
- ZGURSKAYA, H. I., WEEKS, J. W., NTREH, A. T., NICKELS, L. M. and WOLLOSCHECK, D.** (2015). Mechanism of coupling drug transport reactions located in two different membranes. *Frontiers in Microbiology* **6**: 100.
- ZHANG, C., LANE, L., OMENN, G. S. and ZHANG, Y.** (2019). Blinded testing of function annotation for uPE1 proteins by I-TASSER/cofactor pipeline using the 2018–2019 additions to nextprot and the cfa3 challenge. *Journal of Proteome Research* **18**: 4154-4166.
- ZHANG, M., O'DONOGHUE, M. M., ITO, T., HIRAMATSU, K. and BOOST, M. V.** (2011). Prevalence of antiseptic-resistance genes in *Staphylococcus aureus* and coagulase-negative staphylococci colonising nurses and the general population in Hong Kong. *The Journal of Hospital Infection* **78**: 113-117.
- ZHANG, X. C., ZHAO, Y., HENG, J. and JIANG, D.** (2015). Energy coupling mechanisms of MFS transporters. *Protein Science* **24**: 1560-1579.

- ZHANG, Y.** (2008). I-TASSER server for protein 3D structure prediction. *BMC Bioinformatics* **9**: 40.
- ZHAO, Y., MAO, G., LIU, M., ZHANG, L., WANG, X. and ZHANG, X. C.** (2014). Crystal structure of the *E. coli* peptide transporter YbgH. *Structure* **22**: 1152-1160.
- ZHENG, G., FILIPPELLI, G. and SALAMOVA, A.** (2020). Indoor exposure to commonly used disinfectants during the COVID-19 pandemic. *Environmental Science and Technology Letters* **7**: 760-765.
- ZHENG, H., WISEDCHAI SRI, G. and GONEN, T.** (2013). Crystal structure of a nitrate/nitrite exchanger. *Nature* **497**: 647-651.
- ZHU, Q. and CASEY, J. R.** (2007). Topology of transmembrane proteins by scanning cysteine accessibility mutagenesis methodology. *Methods* **41**: 439-450.
- ZIMMERMANN, S., TUCHSCHERR, L., RODEL, J., LOFFLER, B. and BOHNERT, J. A.** (2017). Optimized efflux assay for the NorA multidrug efflux pump in *Staphylococcus aureus*. *Journal of Microbiological Methods* **142**: 39-40.
- ZOMOT, E., YARDENI, E. H., VARGIU, A. V., TAM, H. K., MALLOCI, G., RAMASWAMY, V. K., PERACH, M., RUGGERONE, P., POS, K. M. and BIBI, E.** (2018). A new critical conformational determinant of multidrug efflux by an MFS transporter. *Journal of Molecular Biology* **430**: 1368-1385.